# Energy conservation in anaerobic *Prevotella bryantii* and *Prevotella bivia*: the role of membrane bound electron transfer complexes

**Dissertation to obtain the doctoral degree of Natural Science (Dr. rer. nat)**

Faculty of Natural Sciences

University of Hohenheim

Institute of Biology

submitted by

Lena Schleicher

from Stuttgart

-2022-

| | |
|---|---|
| Dean: | Prof. Dr. Uwe Beifuss |
| 1. Reviewer: | Prof. Dr. Julia Fritz-Steuber |
| 2. Reviewer: | Prof. Dr. Jana Seifert |
| Oral examination: | 10.05.2022 |

# Abstract

Members of the family *Prevotellaceae* are Gram-negative, obligate anaerobic bacteria found in animal and human microbiomes, where they participate in the degradation of carbohydrates and peptides. Some *Prevotella* species are also opportunistic pathogens. In this study, growth requirements and central catabolic reactions of two different *Prevotella* strains were characterized.

First, the energy conservation by *Prevotella bryantii* was analyzed (Chapter 3). *P. bryantii* is a dominant species in the ruminal microbiome. It was demonstrated, that *P. bryantii* ferments glucose mainly to acetate and succinate. Furthermore, enzymatic and biochemical studies revealed that *P. bryantii* membranes harbor fully functional $Na^+$ -translocating NADH:quinone oxidoreductase (NQR) and quinol:fumarate reductase (QFR). It was shown, that electron transfer between these two enzymes occurs in native membranes. The enzymatic activities increased significantly by anoxic membrane preparations (Chapter 2). Electron transfer in membrane vesicles was coupled to the build-up of a sodium motive force (SMF) in *P. bryantii*. A respiratory chain composed of NQR and QFR in *P. bryantii* was proposed, which links succinate formation to NADH oxidation and SMF formation. Thus, *P. bryantii* does not rely solely on substrate-level phosphorylation for energy conservation, but gains additional energy utilizing the $Na^+$-pump, NQR. This increases the overall yield of ATP per consumed glucose molecule. By gel electrophoresis and size exclusion chromatography, the existence of a supercomplex composed of NQR and QFR in *P. bryantii* membranes was demonstrated, which operates as sodium-translocating NADH:fumarate oxidoreductase. The understanding of the catabolic reactions in the rumen by the ruminal microbiota is important for the optimal nutrition of the ruminant. Our results indicate that *P. bryantii* plays an important role in the ruminal microbiota. *P. bryantii* extrudes mainly acetate and succinate as fermentative end-products into the rumen. The latter can be used by

other organisms of the ruminal microbiome to metabolize propionate, which is an important nutrient for the ruminant since it enters the pathway of gluconeogenesis, yielding glucose.

*Prevotella bivia* is considered to act as causative agent of human bacterial vaginosis (BV). Growth of *P. bivia* on glucose was dependent on $CO_2$ and resulted in the production of succinate, malate and acetate (Chapter 4). With the help of optical spectroscopy and enzymatic measurements, the presence and activity of NQR and QFR in *P. bivia* were demonstrated. Electron transfer in membrane vesicles of *P. bivia* resulted in the build-up of a SMF. Similar to *P. bryantii*, *P. bivia* operates NQR and QFR for energy conservation in its membrane, resulting in succinate formation and SMF generation. *P. bivia* also exhibits high L-asparaginase and aspartate ammonia lyase activities *in vitro*, catalyzing the conversion of L-asparagine to fumarate and $NH_4^+$. These results were confirmed *in vivo* by growth experiments (Chapter 4). Additional L-asparagine in the growth medium led to an elevated production of $NH_4^+$ and succinate from fumarate obtained during degradation of L-asparagine. At the same time an inhibitory effect of $NH_4^+$ on growth of *P. bivia* was observed. It is proposed, that amino acid degradation by *P. bivia* in microbial consortia associated with BV depends on the consumption of ammonium by *Gardnerella vaginalis*, another typical pathogen found in BV. At the same time, *G. vaginalis* could provide L-asparagine to *P. bivia*, strengthening their symbiotic relationship and triggering BV.

# Zusammenfassung

Mitglieder der Familie *Prevotellaceae* sind Gram-negative, obligat anaerobe Bakterien, die in tierischen und menschlichen Mikrobiomen vorkommen. Dort sind sie am Abbau von Kohlenhydraten und Peptiden beteiligt. Einige *Prevotella* Spezies sind auch opportunistische Krankheitserreger. In dieser Studie wurden zwei *Prevotella* Stämme hinsichtlich ihrer Wachstumsbedingungen und der zentralen katabolischen Reaktionen charakterisiert.

Zuerst wurde die Energiekonservierung von *Prevotella bryantii* untersucht (Kapitel 3), eine vorherrschende Spezies im Mikrobiom des Pansens. Es wurde gezeigt, dass *P. bryantii* Glukose hauptsächlich zu Acetat und Succinat fermentiert. Außerdem zeigten enzymatische und biochemische Studien, dass Membranen von *P. bryantii* funktionsfähige $Na^+$ -translozierende NADH:Chinon Oxidoreduktase (NQR) und Chinol:Fumarat Reduktase (QFR) besitzen. Es wurde gezeigt, dass zwischen diesen beiden Enzymen Elektronentransport in nativen Membranen stattfindet. Die enzymatischen Aktivitäten konnten signifikant durch anoxische Membranpräparation gesteigert werden (Kapitel 2). Dieser Elektronentransport in nativen Membranen ist an den Aufbau eines elektrochemischen Natriumgradienten in *P. bryantii* gekoppelt. Diese Ergebnisse führen zu der begründeten Hypothese, dass eine Atmungskette bestehend aus NQR und QFR unter Oxidation von NADH und Bildung von Succinat zur Erzeugung eines elektrochemischen Natriumgradienten in *P. bryantii* beiträgt. Folglich beruht die Energiekonservierung von *P. bryantii* nicht ausschließlich auf Substratkettenphosphorylierung, denn durch die Nutzung der $Na^+$ -Pumpe, NQR, wird zusätzlich Energie generiert. Dadurch erhöht sich die Ausbeute an ATP pro konsumiertem Glukosemolekül. Durch Gel-Elektrophorese und Größenausschluss-Chromatographie wurde ein Superkomplexes (bestehend aus NQR und QFR) nachgewiesen, welcher als Natrium-translozierende NADH:Fumarat Oxidoreduktase

arbeitet. Das Verständnis für die katabolen Reaktionen des Mikrobioms im Pansen ist wichtig für die optimale Ernährung des Wiederkäuers. Unsere Ergebnisse lassen vermuten, dass *P. bryantii* eine wichtige Rolle im Pansenmikrobiom spielt. *P. bryantii* gibt vor allem Acetat und Succinat als fermentative Endprodukte in den Pansen ab. Diese Fermentationsprodukte werden von anderen Organismen des Pansenmikrobioms benutzt, um Propionat zu bilden. Dies ist ein wichtiger Nährstoff für den Wiederkäuer, da Propionat in der Glukoneogenese verwendet wird.

Man nimmt an, dass *Prevotella bivia* ein Krankheitserreger der bakteriellen Vaginose (BV) ist. Das Wachstum von *P. bivia* auf Glukose war $CO_2$-abhängig und führte zur Produktion von Succinat und Acetat (Kapitel 4). Mit Hilfe von optischer Spektroskopie und enzymatischen Messungen konnte die Anwesenheit und Aktivität der NQR und QFR in der Membran von *P. bivia* nachgewiesen werden. Der Elektronentransport in Membranvesikeln von *P. bivia* führte zu dem Aufbau eines elektrochemischen Natriumgradienten. Folglich sind in *P. bivia*, ähnlich zur Situation in *P. bryantii*, die NQR und QFR an der Energiekonservierung beteiligt, wobei Succinat und Acetat gebildet werden. Des Weiteren zeigt *P. bivia* hohe L-Asparaginase und Aspartat-Ammonium-Lyase Aktivitäten *in vitro*, was zur Umwandlung von Asparagin zu Fumarat und $NH_4^+$ führt. Diese Ergebnisse wurden in Wachstumsexperimenten *in vivo* bestätigt (Kapitel 4). Zusätzliches L-Asparagin im Wachstumsmedium führte zu einer erhöhten Produktion von $NH_4^+$ und Succinat. Dieses Succinat wurde aus Fumarat gebildet, welches durch den Abbau von L-Asparagin entstand. Gleichzeitig wurde ein inhibitorischer Effekt von $NH_4^+$ auf das Wachstum von *P. bivia* beobachtet. Die Studien legen den Schluss nahe, dass der Aminosäureabbau durch *P. bivia* in dem mikrobiellen Konsortium einer BV nur durch *Gardnerella vaginalis* ermöglicht wird, der das durch *P. bivia* freigesetzte Ammonium kontinuierlich verwendet. Gleichzeitig stellt *G. vaginalis* L-Asparagin für *P. bivia* bereit und stärkt so ihre symbiontische Beziehung, die maßgeblich für die Ausbildung der BV ist.

# Contents

# Chapter 1 – General introduction

## 1.1 The chemiosmotic theory: from proton gradients to ATP

The chemiosmotic theory postulated in 1961 by Mitchell describes the formation of the energy currency of any cell, adenosine triphosphate (ATP), by the accumulation of protons in the periplasmic outer membrane space of mitochondria (1). Here, respiratory enzymes of the electron transport chain establish a transmembrane electrochemical ion gradient coupled to exergonic electron flow. This electrochemical potential fuels the ATP synthase, generating ATP inside the mitochondria, which is exported to the cytoplasmic compartment.

### 1.1.1 High-energy compounds as energy providers of the cells

Generation of energy is the essential process in all living organisms of the three kingdoms of life: archaea, bacteria and eukaryotes. The ultimate aim here is the generation of high-energy compounds like pyro phosphates, enol phosphates, acyl phosphates, thio esters and guanidio phosphates (phosphagenes) by chemical reactions (2) (table 1.1). The Gibbs energy change (ΔG) describes the free energy, which is actually available in a closed system to perform work (at constant temperature and pressure) (equation 1.1):

$$\Delta G = \Delta H - T * \Delta S \qquad (1.1)$$

Thus, ΔG predicts if a reaction proceeds, because it combines the change in entropy (ΔS, the degree of disorder resulting from a reaction), changes in enthalpy (ΔH, heat that is released or absorbed during a reaction) and the absolute temperature (T) (3). Reactions with $\Delta G < 0$ are exergonic and occur spontaneously (sometimes a catalyst is required to overcome the activation barrier). In contrast, reactions with $\Delta G > 0$ are endergonic. They will proceed unless further energy is provided to the system. $\Delta G^{0'}$ describes this free energy change under standard conditions (reactant/product concentration of 1 mol/L, 1 atm of pressure, pH 7.0, 25°C). Thus, $\Delta G^{0'}$ can be used to predict the occurrence of a reaction under these total hypothetical standard conditions, which mostly do not represent the physiological

conditions. The substrate and product ratios are critical for the capacity of the reactants. When a reaction A ⇌ B is at equilibrium the free energy change is zero, no matter how energy rich the compounds are. Therefore, to predict if a reaction can take place, the actual product and substrate concentrations have to be considered (equation 1.2):

$$\Delta G = \Delta G^{0\prime} + R * T * \ln \frac{[B]}{[A]} \qquad (1.2)$$

Where R is the gas constant (8.3 J $K^{-1}$ $mol^{-1}$), T the absolute temperature (298 K), B the product and A the substrate concentration.

Hydrolysis of high-energy compounds is used in the cell to drive energetically unfavorable but essential reactions. ATP, a representative of pyro phosphates, is the most important energy carrier in the cell. Due to two phosphoanhydride bonds in the triphosphate unit, hydrolysis of ATP results in adenosine diphosphate (ADP), inorganic phosphate ($P_i$) and the release of a large amount of energy (-30.5 kJ/mol) (table 1.1).

**Table 1.1** Classes of high-energy compounds with examples and structural formulas (anions) are shown. High-energy bonds are highlighted in red. Example reactions are presented with the corresponding standard free energy (2). Structures are from ChemSpider (4) (http://www.chemspider.com/; 23.09.2021) and were adapted with ChemSketch (5) (Version 2021.1.1).

| **Class** | **Examples** | **Reactions** | **$\Delta G^{0'}$ [kJ/mol]** |
|---|---|---|---|
| Pyro phosphates | ATP 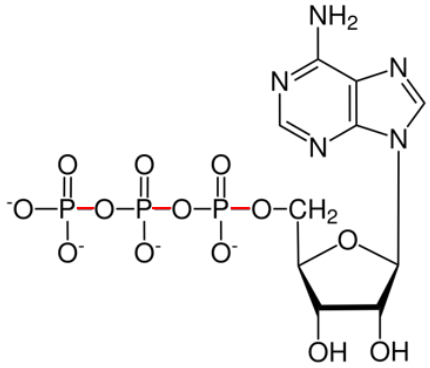 | ATP → ADP + $P_i$ | -30.5 |
| Acyl phosphates | 1,3-Bisphosphoglycerate 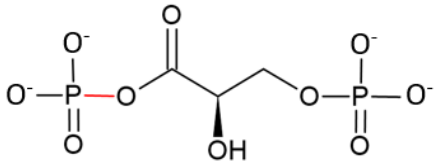 | 1,3-Bisphosphoglycerate → 3-Phosphoglycerat + $P_i$ | -49.4 |

| | | | |
|---|---|---|---|
| Enol phosphates | Phosphoenolpyruvate 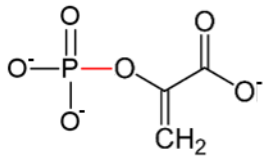 | Phosphoenolpyruvate → Pyruvate + $P_i$ | -61.9 |
| Thio esters | Acetyl CoA 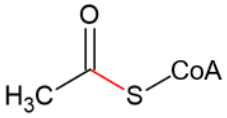 | Acetyl CoA → Acetate + CoA | -31.5 |
| Guanidio phosphates | Phosphocreatine 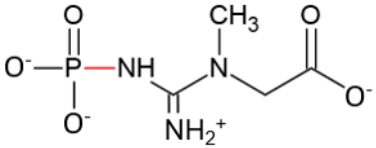 | Phosphocreatine → Creatine + $P_i$ | -43.1 |

This energy is used to perform different kind of work, like mechanical work (movement), chemical work (biosynthesis) or osmotic work (electrochemical gradient, active transport) (6, 7). Furthermore, ATP hydrolysis can be used to energize low-energy compounds and ADP can be re-energized by receiving a phosphoryl group ($-PO_3^{2-}$) (1, 7). Alternatively, ATP can be hydrolyzed to adenosine monophosphate (AMP) and pyrophosphate ($PP_i$) with $\Delta G^{0'}$ = -49.5 kJ/mol. The $\Delta G^{0'}$ of pyrophosphate hydrolysis to two $P_i$ is -61.9 kJ/mol. The conversion of ATP to ADP or AMP and *vice versa* is the foundation of energy exchange reactions, and links catabolism and anabolism in all living cells (8).

In the facultative anaerobic model organism *Escherichia coli*, ATP may be synthesized by substrate-level phosphorylation (SLP) or oxidative phosphorylation (9). During SLP, a phosphoryl group of a high-energy compound is transferred to ADP by a kinase. *E. coli* possesses three kinases for SLP and two of them catalyze essential reactions during glycolysis. The first one, 3-phosphogycerate kinase, transfers the phosphoryl group from 1,3-bisphosphoglycerate to ADP, resulting in 3-phosphoglycerate and ATP (10, 11). This is a highly exergonic reaction and the main driving force for glycolysis. The second one, pyruvate kinase, catalyzes the conversion of phosphoenolpyruvate to pyruvate, coupled to the synthesis of ATP (12). This is a crucial step in glycolysis because under physiological conditions this reaction is irreversible and the product pyruvate is involved in several essential cellular processes. During mixed acid fermentation in *E. coli*, the acetate kinase converts acetyl phosphate and ADP into acetate and ATP (13). Another important enzyme for SLP in *E. coli* is the succinyl-CoA synthetase, participating in the oxidative TCA cycle under aerobic conditions. It cleaves succinyl-CoA and uses the released energy to transfer $P_i$ to ADP resulting in succinate, CoA and ATP (14). The reducing equivalents (e.g. NADH) and succinate, generated during glycolysis and in the TCA cycle, are used further for energy conservation with the respiratory chain. This kind of SLP is an exception, because normally SLP for ATP synthesis occurs under anaerobic conditions during fermentation. In general,

during fermentation the main branch for ATP synthesis is the degradation of glucose to pyruvate, but also additional fermentative branches can be involved. Anaerobically, pyruvate is not oxidized further in the TCA cycle and the oxidative phosphorylation by the respiratory chain is not functioning. This is accompanied by the problem, that the reduced NADH, generated during glycolysis, is not re-oxidized to $NAD^+$ by respiratory enzymes. To maintain a carbon and redox balance, the organism has to produce and extrude fermentative products with e.g. additional fermentative branches and pyruvate as substrate. Thus, the ATP yield is very small with 2 molecules of ATP per 1 molecule of glucose during glycolysis (3). In contrast, during oxidative phosphorylation 26 molecules ATP are generated per glucose molecule (15, 16), which is achieved by electron transfer.

During oxidative phosphorylation, electrons are transferred in several redox-reactions from one redox carrier to another. A redox-reaction combines the oxidation of one substrate (electron donor) and the reduction of another substrate (electron acceptor). The electron acceptor gains one or more electrons and by changes in the pK value it may also gain one or more protons (17). The redox potential $\Delta E$ describes the tendency of a substance to lose or gain electrons. The standard redox potential $\Delta E^{0'}$, also called midpoint potential, describes the redox potential under standard conditions (substrate concentration of 1 M, 1 atm, pH 7.0, 25°C) (table 1.2). With decreasing redox potential, the tendency to donate electrons increases and with increasing redox potential the tendency to accept electrons increases. Due to its very positive midpoint potential (+0.82 V), oxygen is the most effective electron acceptor in nature. It is also possible to calculate the free energy released by a redox reaction because $\Delta E^{0'}$ is directly related to $\Delta G^{0'}$ (equation 1.3):

$$\Delta G^{0\prime} = -n * F * \Delta E_h \qquad (1.3)$$

Where n is the number of transferred electrons, F the Faraday constant (95.5 kJ $V^{-1}$ $mol^{-1}$) and $\Delta E_h$ the difference in the redox potential between the electron donor and acceptor (17).

**Table 1.2** Midpoint potentials of intrinsic redox carriers utilized in various respiratory microorganisms. Typical redox couples are listed in order of their redox potential. n: number of transferred electrons; m: number of taken protons; *: representative $\Delta E^{0'}$ for flavins (18). The redox potential of proteins associated with flavins strongly depends on the protein environment. Table is adapted from (17).

| **Redox couple (ox. / red.)** | **m** | **n** | **$\Delta E^{0'}$ [V]** |
|---|---|---|---|
| Ferredoxin ($Fe^{3+}/Fe^{2+}$) | 0 | 1 | -0.45 |
| $NAD^+$, $H^+$/NADH | 1 | 2 | -0.32 |
| Flavin nucleotides | 0 | 1 | -0.19* |
| Menaquinone/Menaquinol | 2 | 2 | -0.07 |
| Ubiquinone/Ubiquinol | 2 | 2 | +0.10 |
| Cytochrome *c* ($Fe^{3+}/Fe^{2+}$) | 0 | 1 | +0,22 |
| $^1/_2$ $O_2$, 2 $H^+/H_2O$ | 2 | 2 | +0.82 |

### 1.1.2 The aerobic respiratory chain of *Escherichia coli*

The respiratory chain of *E. coli* is the most studied bacterial respiratory system and by now, many insights into structure, kinetics and transcriptional regulation were gained. In general, the enzymes involved in respiration are located in the inner bacterial membrane. Under aerobic conditions, two nicotinamide adenine dinucleotide (NADH) dehydrogenases, NDH-I (or Nuo complex) and NDH-II, are expressed (19, 20), which feed electrons from NADH into the respiratory chain. Furthermore, two terminal quinol oxidases, quinol oxidase *$bo_3$* and *bd*, are expressed under aerobic conditions (21–23), transferring the electrons to the terminal electron acceptor oxygen as last step of the respiratory chain. These two complexes possess *c*-type cytochromes, which can directly oxidize ubiquinol. Quinones, especially ubiquinone-8 (UQ-8), in the *E. coli* membrane mediate the transfer of electrons between the NADH dehydrogenases and the quinol oxidases (24). It is important that the electrons are transferred stepwise in several, consecutive redox-reactions from NADH to $O_2$, otherwise a huge amount of energy would be released at once ($\Delta G^{0'} \sim$ -220 kJ/mol) and the cell wouldn't

be able to use it efficiently. Therefore, many respiratory enzymes have the property to use the energy released by these redox-reactions to transport protons across the membrane dielectric from the cytoplasm into the periplasm, resulting in a proton motive force (PMF). In this process, the semipermeable membrane plays a key role. It serves as chemical and physical barrier, whereas cytoplasm, periplasm and the extracellular space are separated from each other. Furthermore, due to the membrane composition, ions and other charged species cannot cross the membrane on their own. Consequently, uphill transport of protons leads to the generation of a membrane potential ΔΨ (electrically negative inside and positive outside) and to a gradient of protons (ΔpH) (alkaline inside and acidic outside) (1, 25). These two potentials are the main components of the PMF (equation 1.4):

$$\mathrm{PMF} = -\Delta\Psi + \frac{2.3\ \mathrm{R} * \mathrm{T}}{\mathrm{F}} * \Delta\mathrm{pH} \qquad [\ \mathrm{V}\ ] \qquad (1.4)$$

Where F is the Faraday constant (95.5 kJ $V^{-1}$ $mol^{-1}$), R the gas constant (8.3 J $K^{-1}$ $mol^{-1}$) and T the absolute temperature (298 K) (26).

Thus, the downhill transport of the protons can be used to perform different kind of work, like driving the ATP synthase for ATP synthesis. Furthermore, ATPases can catalyze the opposite reaction. Here, ATP hydrolysis is directly used to generate a transmembrane $H^+$ gradient. In the *E. coli* aerobic respiratory chain, the enzymes NDH-I and quinol oxidase *bo*$_3$ are both proton pumps. It is suggested, that NDH-I translocates 4 protons per NADH oxidized. This stoichiometry was studied mostly in the mitochondrial Complex I, which is very similar to *E. coli* NDH-I (27, 28). NDH-II reduces UQ-8 without PMF generation (29). The quinol oxidase *bo*$_3$ pumps with a stoichiometry of 2 $H^+$/2 $e^-$ and causes an overall charge movement of 4 $H^+$/2 $e^-$ (17, 21). The quinol oxidase *bd* catalyzes charge separation across the membrane by reduction of $O_2$, but it is not a proton pump (30) (fig. 1.1). The generated PMF is used mainly to synthesize ATP by the $F_1F_0$-ATP synthase. This membrane embedded protein complex couples the reversible synthesis of ATP to the downhill transport of protons

of the PMF (31). This type of ATP synthase harbors a hydrophobic part ($F_0$), which is mainly composed of the c-ring, and a soluble part ($F_1$). The number of c-subunits in the c-ring, which varies between species, determines the $H^+$/ATP ratio. In *E. coli*, the preferred number of c-subunits is 10 (32), meaning that 10 $H^+$ are needed for one rotation cycle of the $F_0$ subunit and per cycle 3 ATP molecules are released. Considering that 8 $H^+$ are transferred across the membrane per oxidized NADH, 2.4 molecules ATP can be synthesized. Theoretically, complete oxidation of 1 mol glucose in *E. coli* leads to the net generation of 2 mol ATP by SLP, and 10 mol NADH by glycolysis and TCA cycle. 10 mol NADH is used by oxidative phosphorylation to generate 24 mol ATP. In sum, *E. coli* generates theoretically 26 mol ATP out of 1 mol glucose (15, 16).

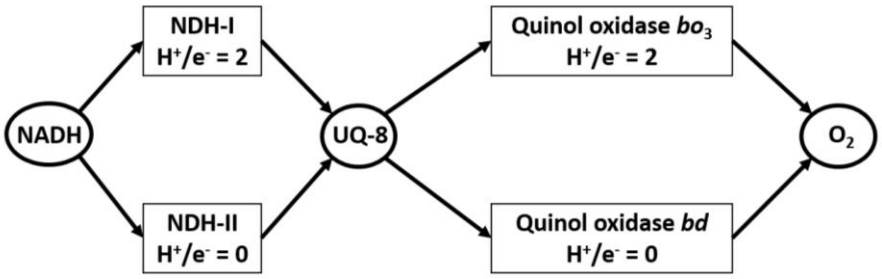


**Figure 1.1** Scheme of the *E. coli* respiratory chain. NADH represents the electron donor. NDH-I and NDH-II oxidize NADH and transfer the electrons to ubiquinone-8 (UQ-8). From UQ-8, the electrons can be transferred to oxygen by the quinol oxidase *bo*$_3$ or by the quinol oxidase *bd*. The number of protons released into the periplasm per electron is indicated ($H^+/e^-$). Figure was adapted from (9).

### 1.1.3 Supramolecular assemblies of respiratory protein complexes

Not only the catalytic activity of different respiratory enzymes influences the efficiency of the respiratory chain, but also the arrangement of these enzymes. Three different models have been proposed, explaining the possible organization of the respiratory chain: the "fluid-state model" (33), the "solid-state model" (34), the "plasticity model" (35) and the "compartmented model" (36). The first theory postulates that respiratory enzymes diffuse freely and independently in the membrane and by random collision, electron transfer occurs

(fig. 1.2, panel A). Here, the possibility of permanent assemblies or transient aggregations formed by the respiratory components is rejected and considered to be unnecessary. The second model assumes that the respiratory enzymes are attached in supramolecular structures, also called supercomplexes (fig. 1.2, panel B). Here, the substrate is channeled directly from one enzyme to the next, allowing a more efficient transport of electrons. The plasticity model, which seems to be the most likely situation in nature, combines the other two models, assuming a dynamic organization of the respiratory enzymes as a network of individual complexes and different associated supercomplexes (fig. 1.2, panel C). Recent cryo-electron microscopic studies revealed that on tightly curved cristae edges of mitochondria, ATP synthase dimers can be observed, whereas the proton pumps of the electron transfer chain, especially Complex I, are located in the adjacent membrane regions (36). This is considered to be the "compartmented model" (fig. 1.2, panel D).

In general, the presence of supercomplexes in prokaryotes is not unusual, since they are widely distributed in the natural kingdom (37), although their functional relevance is not understood so far. The best studied supercomplex is the respirasome of mitochondria (38–43), composed typically of the respiratory enzymes Complex I (NADH dehydrogenase), homo dimeric Complex III (cytochrome *c* reductase) and Complex IV (cytochrome *c* oxidase), and the mobile carriers $Q/QH_2$ and cytochrome *c* (44). Even though the function of these enzymes as respiratory chain does not need physical linkage, biochemical and *in vivo* studies revealed an association of these complexes in the native membrane (43). The advantage of substrate channeling in supercomplexes is highly discussed but several studies refuted this hypothesis, e.g. for the respirasome. It was demonstrated that the respirasome does not enhance catalysis by quinone channeling and that $Q/QH_2$ can diffuse freely in and out of the supercomplex (40). This finding was supported by structural analysis, because no confining protein structure or physical channels were identified, which could guide diffusion of the electron carriers $Q/QH_2$ and cytochrome *c* (37, 44). Nevertheless, supercomplex

formation is advantageous because the enzymes stay in close proximity and favorable orientation, avoiding the loss of the electron carriers and resulting in a facilitated and accelerated electron transfer. This also avoids or limits non-specific contacts between different membrane bound proteins. Supercomplex formation is also suspected to be a strategy of the cell to maintain extremely high protein concentration and, simultaneously, avoid nucleation and aggregation (39, 43). Furthermore, the highly specialized arrangement of ATP synthases in mitochondrial cristae optimize ATP synthesis by creating a directional proton flow along the membrane surface (36).

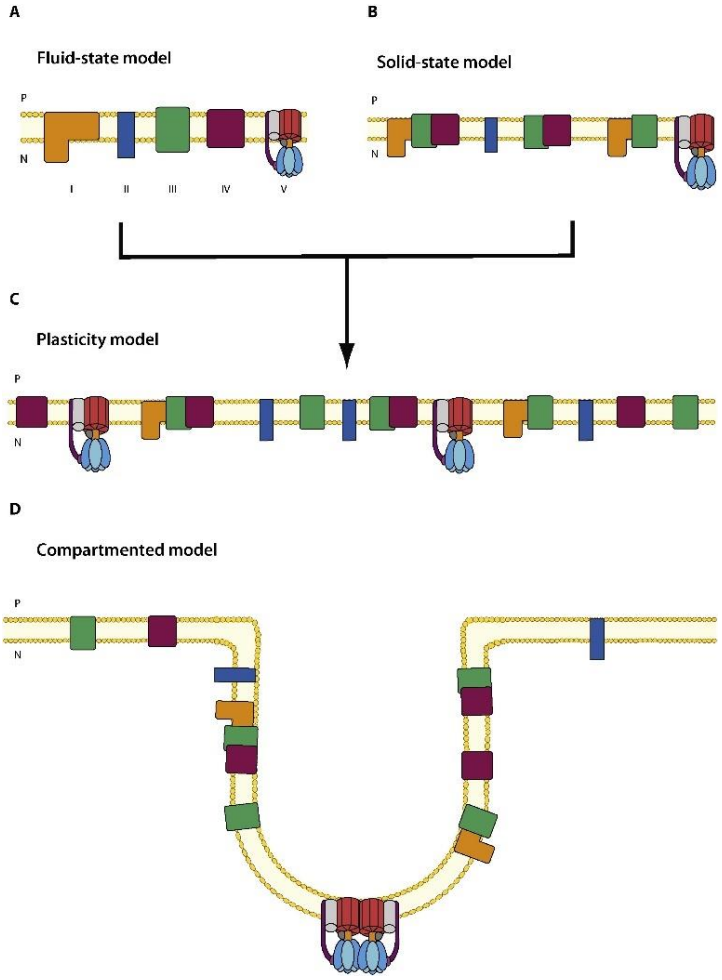


**Figure 1.2** Different organization models of the mitochondrial respiratory chain, which is composed of Complex I (orange), Complex II (blue), Complex III (green), Complex IV (magenta) and Complex V (ATPase structure). A: fluid-state model, in which respiratory enzymes diffuse freely and independently in the membrane and by random collision, electron transfer occurs. B: the solid-state model describes the organization of the complexes in supramolecular assemblies (supercomplexes). C: the plasticity model, which describes the most likely situation in the cell, unites the other two models. Here, a dynamic organization of the respiratory enzymes in different kinds of supercomplexes and individual complexes is assumed. D: the compartmented model describes the specialized molecular organization of cristae membranes in mitochondria. ATP synthases form dimers at the cristae edges, and enzymes of the electron transfer chain reside the adjacent membrane regions. Figure was obtained from (41).

## 1.2 The sodium translocating NADH:quinone oxidoreductase (NQR): $Na^+$ as alternative coupling cation

Steuber and co-workers demonstrated in 2000 that the *E. coli* NDH-I is not solely a proton pump. In contrast, it was shown that it also catalyzes NADH-dependent $Na^+$ -translocation across the bacterial membrane dielectric. With the sodium sensitive *E. coli* strain EP432 growth studies and biochemical studies with inverted membrane vesicles were conducted. Here, an increasing $Na^+$ translocating activity by membrane vesicles was observed together with an increasing synthesis of NDH-I and an increasing $Na^+$ tolerance during growth. Furthermore, this $Na^+$ -translocating activity could be inhibited by a specific NDH-I inhibitor and respiration-driven translocation of $Na^+$ in inverted vesicles was diminished in the NDH-I-deficient *E. coli* strain ANN021 (45). It was also shown in previous studies that the NDH-I from *Klebsiella pneumoniae*, closely related to *E. coli* NDH-I, rather pumps $Na^+$ than $H^+$ (46), generating a sodium motive force (SMF). In general, the sodium ion specificity of respiratory complexes is more widespread than it has been suspected in the past. Due to SMF consumers in the cell like $Na^+$-dependent ATP synthases (e.g. in *Propionigenium modestum* (47)), $Na^+$-dependent membrane transporters for the uptake of several essential substrates or $Na^+$-dependent flagellum movement (48), sodium gradients are also essential to a variety of bacteria. Organisms like *E. coli* can also use a SMF for ATP generation although the ATP synthase is driven by a PMF, due to $Na^+/H^+$ antiporters. These membrane embedded enzymes can convert a SMF into a PMF and *vice versa* (49). The ability to store and generate energy with a SMF can be essential for bacteria. Especially halophilic bacteria and bacteria living under alkaline conditions depend on sodium as coupling ion in the respiration (26). In alkaline environments it becomes difficult for the organism to maintain a PMF, because $[H^+]_{out} << [H^+]_{in}$ diminishes the proton gradient but the electrochemical sodium gradient is not affected (50). Here, sodium gradients are more suitable for energy conservation and

storaging than proton gradients. For these organisms antiporters converting PMF into SMF are essential. Another type of bacteria, which benefit from a SMF instead of a PMF are thermophilic bacteria, because at elevated temperatures the proton leakage of the bacterial membrane increases, which would also lead to a diminished $H^+$ gradient (51). The pathogenic, facultative anaerobic bacterium *Vibrio cholerae* is one example for an organism, which utilizes both, SMF and PMF in different habitats. During its life cycle, it encounters a wide range of pH and salinity. Therefore, *V. cholerae* possesses a large variety of $Na^+/H^+$ antiporters and a primary $Na^+$ pump as first part of the respiratory chain, the $Na^+$-translocating NADH:quinone oxidoreductase (NQR), which is essential for *V. cholerae* growth at low osmolarity in alkaline environments (52).

### 1.2.1 Structure and function of the NQR

The NQR of the model organism *V. cholerae* is a respiratory, membrane protein complex composed of six subunits (NqrABCDEF), embedded into the inner bacterial membrane (fig. 1.3, panel A). This enzyme acts as electron input module in the respiratory chain not only in *V. cholerae*, the causative agent of cholera, but also in other marine bacteria and many other human pathogens. As first part of the respiratory chain, this enzyme oxidizes NADH followed by the reduction of UQ-8. Furthermore, it is a primary $Na^+$ pump, translocating sodium ions across the membrane dielectric and leading to the generation of a SMF. The NQR has a compact shape with dimensions of about 90 Å x 140 Å x 52 Å (53) and an overall molecular mass of approximately 220 kDa (NqrA: 48.6 kDa, NqrB: 45.3 kDa, NqrC: 27.6 kDa, NqrD: 22.8 kDa, NqrE: 21.4 kDa and NqrF: 45.1 kDa) (50). The NQR subunits are not related to any NDH-I subunit (50) and they also harbor a different set of cofactors, which transfer the electrons through the complex. The known redox centers are: one non-covalently bound flavin adenine dinucleotide (FAD) in NqrF, two covalently attached flavin mononucleotides (FMN) in NqrB and NqrC, one non-covalently bound riboflavin (RF) in

NqrB, one [2Fe-2S] clusters in NqrF, a Fe site between NqrD/NqrE, and a proposed UQ-8 binding site in NqrA (53) (fig. 1.3, panel B). The subunit NqrF represents the entry side of the electrons from NADH into the complex, thus catalyzing the NADH dehydrogenase reaction. NqrF is composed of two hydrophilic domains, the N-terminal [2Fe-2S] domain and the C-terminal FAD-binding domain, and it is anchored into the NQR complex by one single transmembrane helix (53). It catalyzes the transfer of the electrons from NADH to FAD and from there to the [2Fe-2S] center (54). FAD transiently forms a neutral flavosemiquinone to enable the electron transfer between the hydride donor NADH and the one-electron acceptor [2Fe-2S]. From the iron sulfur cluster, the electrons are transferred to the Fe site formed by Cys ligands from the hydrophobic subunits NqrD and NqrE. From this Fe site, electrons are transferred further to the FMN of the hydrophilic, periplasmic subunit NqrC, followed by the reduction of the FMN in subunit NqrB. Interestingly, NqrB shares a high structural resemblance with urea and ammonium transporter from prokaryotes and eukaryotes (50). Like these transporters, NqrB possesses central helices, forming a membrane-spanning channel, but in contrast to urea and ammonium transporter the channel in NqrB is narrowed in the center. This results in two half-channels, one open to the cytoplasm and one to the periplasm. Thus, NqrB is suspected to form the $Na^+$ channel for $Na^+$ translocation through the NQR. Furthermore, the opening of this channel is most likely coupled to the change of redox state of the FMN in NqrB and therefore, FMN reduction seems to be the trigger for $Na^+$ translocation (53, 55). However, from the FMN the electrons are transferred further to a RF, also harbored by the NqrB, followed by the ultimate electron transfer step, leading to the reduction of UQ-8 to $UQH_2$-8 in NqrA (56).

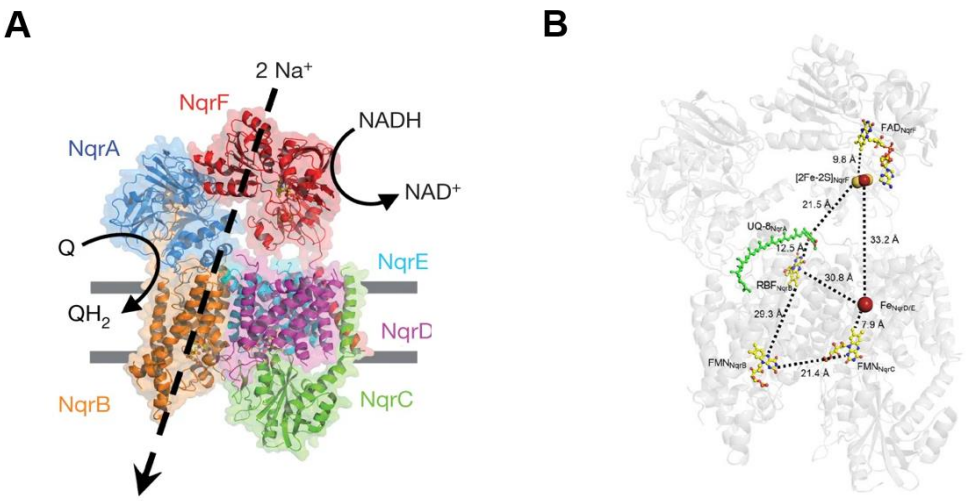


**Figure 1.3** Overall structure of the $Na^+$ NQR from *V. cholerae*. A: The NQR is composed of six subunits: NqrA (blue), NqrB (orange), NqrC (green), NqrD (magenta), NqrE (cyan), NqrF (red). NqrA contains no transmembrane helix, while NqrB, NqrD and NqrE are integral membrane proteins. NqrF and NqrC are cytoplasmic/periplasmic and anchored with one single transmembrane helix into the membrane. The membrane is indicated by grey lines, whereas the top represents the cytoplasm and the bottom the periplasm. NADH is oxidized at NqrF and UQ is reduced most probably at NqrA (53). B: Arrangement of the redox cofactors in the $Na^+$ NQR of *V. cholerae*. Edge to edge distances of the cofactors are indicated by dotted lines given in Ångstrom. Subunits of NQR are shown in transparent grey. Cofactors are shown in color in ball-and-stick type or as van der Waals spheres. Carbon atoms for flavins are shown in yellow and for ubiquinone-8 (UQ-8) in green. In the flavin structures, nitrogen atoms are depicted in blue and oxygen atoms in red. Fe is indicated as dark red sphere and the sulfur as yellow sphere (50).

Based on the 3D structure (53), the proposed electron transfer pathway in the NQR is summarized as follows (fig. 1.3, panel B):

$NADH \rightarrow FAD_{NqrF} \rightarrow [2Fe\text{-}2S]_{NqrF} \rightarrow Fe_{NqrD/E} \rightarrow FMN_{NqrC} \rightarrow FMN_{NqrB} \rightarrow RF_{NqrB} \rightarrow UQ\text{-}8_{NqrA}$

The 3D structure of the NQR allows determination of distances between the different redox cofactors. Interestingly, several of them were too distant to permit fast electron transfer, which was observed in kinetic studies of the NQR (55, 57). This led to the proposal of conformational changes of the NQR driven by the redox events. The largest distance was observed between the [2Fe-2S] center in NqrF and the Fe site in NqrD/E with 33.2 Å (edge-to-edge distance), but only distances below 15 Å enable fast electron transfer between redox

centers through protein medium (53, 58). This distance can be shortened by a rotational movement of the NqrF [2Fe-2S] domain towards the membrane, performed by flexible linkers between the [2Fe-2S] domain and the FAD-binding domain of NqrF (53). Further conformational changes of the NQR are suggested during $Na^+$ -translocating. In the model of Steuber and co-workers from 2014 (fig. 1.4), $Na^+$ binds in the cytoplasmic half-channel of NqrB, which is most likely triggered by the conformational change in NqrF during electron transfer. The reduction of FMN in NqrB leads to the occlusion of $Na^+$ in NqrB and the following reduction of the riboflavin results in the release of the $Na^+$ into the second half-channel, releasing the sodium ion into the periplasm. The reduction of quinone might be necessary for $Na^+$ release. In this way, the NQR pumps two sodium ions from the cytoplasm into the periplasm per oxidized NADH (50).

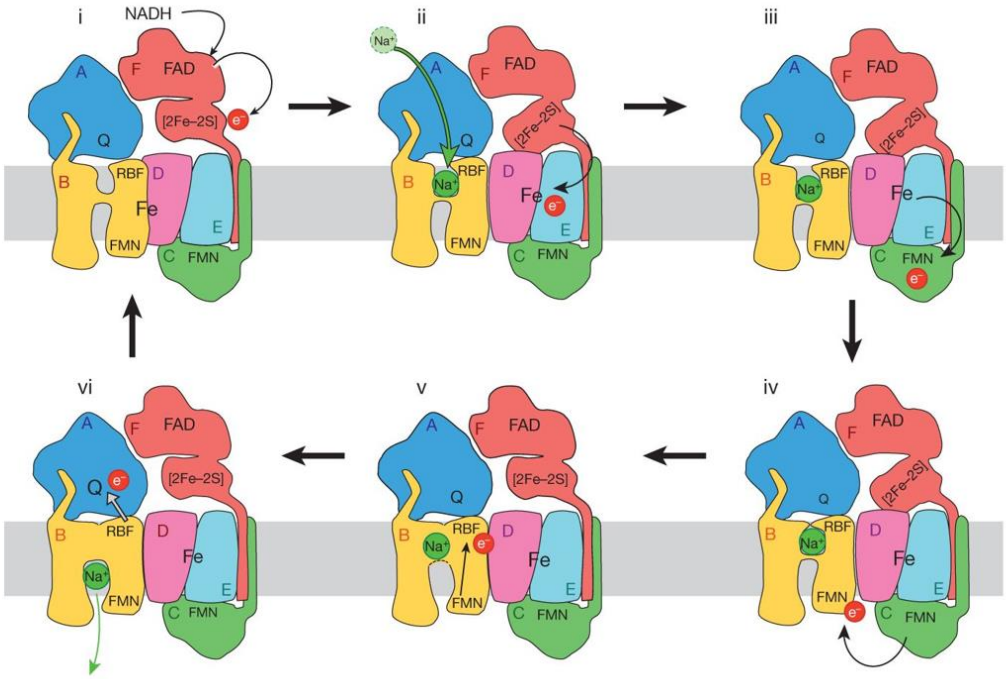


**Figure 1.4** Model for coupling of electron transfer and $Na^+$ translocation in $Na^+$ NQR of *V. cholerae*. NADH is oxidized at the FAD of NqrF, which mediates a single electron transfer to the [2Fe-2S] cluster (i). A conformational change in the NqrF subunits permits electron transfer from [2Fe-2S] to the Fe site between NqrD/NqrE, triggering $Na^+$ binding to the cytoplasmic half-channel of NqrB (ii). After reduction of NqrC FMN (iii), the electrons are transferred further to the FMN of NqrB (iv). The reduction of NqrB FMN triggers the occlusion of $Na^+$ in NqrB. Further electron transfer to the riboflavin leads to the opening of the second half-channel (v), leading $Na^+$ into the periplasm (vi). The reduction of UQ might be necessary for this. NqrA (blue), NqrB (orange), NqrC (green), NqrD (magenta), NqrE (cyan), NqrF (red). The membrane is indicated in grey. Top, cytoplasmic side; bottom, periplasmic side (53).

### 1.2.2 Electron carriers of the NQR

As mentioned previously, the NQR harbors several redox cofactors, which are essential for the catalytic activity of the NQR. In the following sections, these cofactors are introduced in greater detail.

Nicotinamide adenine dinucleotide

NADH is a redox active molecule involved in a variety of cellular processes in all living cells. NADH is an important electron donor in the cell, because it operates at a negative midpoint potential of -0.32 V. Very frequently, NADH acts as the first electron donor in respiratory chains (26). One molecule NADH is composed of two nucleotides connected by their phosphate groups (fig. 1.5, panel A). The C1 of each ribose moiety is attached to an adenine or a nicotinamide, respectively. NADH exists in two redox states, oxidized ($NAD^+$) and reduced (NADH). Reduction of $NAD^+$ is accompanied by the transfer of two electrons and one $H^+$ to the nicotinamide. Due to their chemical structure, NADH and $NAD^+$ have characteristic and different UV/VIS spectra, enabling quantification and monitoring of enzymatic conversion of these substances spectrophotometrically. NADH exhibits two maxima at 340 nm and 260 nm (fig. 1.5, panel B) (59). The maximum at 260 nm is caused by the adenine moiety, which is also present in $NAD^+$. Therefore, the UV/VIS spectrum of $NAD^+$ also exhibits a maximum at 260 nm but with a lower intensity compared to the 260 nm maximum of NADH. In contrast, a strong absorbance at 340 nm occurs in the UV/VIS spectrum of NADH, caused by the reduced nicotinamide moiety, which is not present in $NAD^+$. Thus, the conversion of NADH to $NAD^+$ and *vice versa* can be monitored at 340 nm spectrophotometrically. The concentration of NADH is determined with the Lambert-Beer law (equation 1.5):

$$E = \varepsilon * c * d \qquad (1.5)$$

Where E is the extinction, ε the extinction coefficient, c the molar concentration and d the

path length. In the absence of optical scattering, the extinction (E) equals the absorbance (A). The extinction coefficient for NADH at 340 nm is $\varepsilon_{340} = 6.22\ mM^{-1}\ cm^{-1}$ (26).

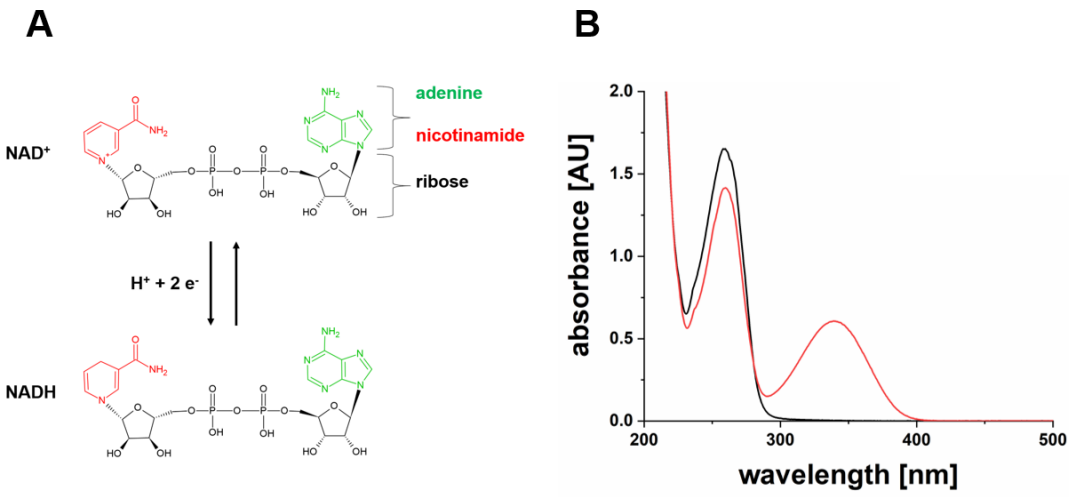


**Figure 1.5** Properties of NADH and $NAD^+$. A: Chemical structures of NADH and $NAD^+$. NADH is composed of two nucleotides connected by a phosphoanhydride bond. The C1 of each ribose moiety is attached to an adenine (green) or a nicotinamide (red), respectively. Reduction of $NAD^+$ requires two electrons and one $H^+$. Structures are from ChemSpider (4) (http://www.chemspider.com/; 23.09.2021) and were adapted with ChemSketch (5) (Version 2021.1.1). B: Absorbance spectra of 100 µM NADH (red) and $NAD^+$ (black). NADH exhibits two maxima at 260 nm and 340 nm. $NAD^+$ exhibits one maximum at 260 nm with higher intensity compared to the peak of NADH.

## Flavins

Flavins are ubiquitous organic substances in nature and play an important role in cellular processes. Three main types of flavins are defined: Riboflavin (RF), flavin mononucleotide (FMN) and flavin adenine dinucleotide (FAD). FMNs and FADs are derivatives of RF, with a characteristic isoalloxazine ring system linked to a ribityl side chain (fig. 1.6, panel A). Note that FMN and FAD do not represent nucleotides since they do not have a glycosidic bond between the ribose and the isoalloxazine ring (60). The isoalloxazine moiety has the ability to participate in one-electron or two-electron transfer reactions and therefore flavin molecules can have three redox states: oxidized, one-electron reduced (semiquinone) and two-electron reduced (hydroquinone) (61, 62). The semiquinone can be protonated (neutral, blue color) or monodeprotonated (anionic, red color). Complete reduction of flavins requires two electrons and two protons, which can be transferred stepwise or simultaneously.

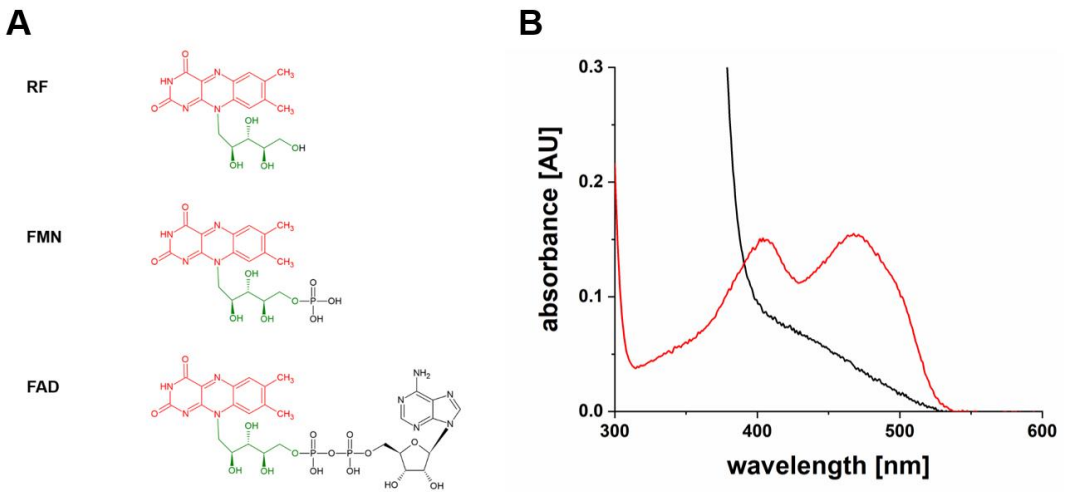


**Figure 1.6** Properties of flavins. A: Chemical structure of riboflavin (RF), flavin mononucleotide (FMN) and flavin adenine dinucleotide (FAD). FMN and FAD are derivatives of RF and have a characteristic isoalloxazine ring system (red) and ribityl side chain (green) (61, 63). Structures are from ChemSpider (4) (http://www.chemspider.com/; 23.09.2021) and were adapted with ChemSketch (5) (Version 2021.1.1)**.** B: VIS absorbance spectrum of the purified NqrF-FAD domain (25 µg) of *V. cholerae* in its oxidized (red) and reduced (black) state. The oxidized FAD (red) exhibits two prominent peaks at 405 and 467 nm.

The isoalloxazine ring system absorbs light in the range from 300 – 500 nm, resulting in a yellow coloring of the flavins (62). Oxidized flavins exhibit maxima at around 445 nm, 375 nm, 265 nm and 220 nm (61, 64). Reduction of flavins can be monitored by the change in absorbance at 445 nm, because reduced flavins exhibit a much lower absorbance at this wavelength than oxidized flavins (fig.1.6, panel B). Correspondingly, extinction coefficient at 445 nm decreases from to oxidized (riboflavin: 12.2 $mM^{-1}$ $cm^{-1}$; FMN: 12.2 $mM^{-1}$ $cm^{-1}$, FAD: 11.3 $mM^{-1}$ $cm^{-1}$) to the reduced state (riboflavin: 0.78 $mM^{-1}$ $cm^{-1}$; FMN: 0.87 $mM^{-1}$ $cm^{-1}$, FAD: 0.98 $mM^{-1}$ $cm^{-1}$) (65).

Flavoproteins are proteins containing flavins as prosthetic group, catalyzing a wide range of different and essential reactions in the cell. Here, the isoalloxazine ring system is the reactive part of the flavin and the ribityl side chain modulates the interaction in a binding site of the protein (63). For a two-electron reduction the midpoint potential is about -0.2 V but can vary between –0.4 V and +0.06 V, depending on the protein environment (66). Due to their flexibility in the number of transferred electrons, flavins represent the perfect linkage

between one- and two-electron redox systems. This is the reason, why all known NADH dehydrogenases have a flavin as primary redox cofactor, which accepts the hydride from NADH (26). The NQR of *V. cholerae* contains not only one flavin cofactor as primary redox center, but four flavin cofactors in the whole complex. Typically, flavins are not covalently bound to the protein, but like in the NQR, flavins can be covalently attached (67). Here, three types can be distinguished according to the type of linkage: flavin linked with a 8α-methyl group to a tyrosine, histidine or cysteine residue of the protein, FMN linked with the C6 atom of the isoalloxazine ring system to a cysteine residue of the protein. A third mode of covalent attachment found in the NQR is the linkage of a flavin *via* a phosphodiester with a threonine or serine residue of the protein (65, 68, 69). This was demonstrated for the covalently bound FMNs of NqrC and NqrB, the membrane bound subunits of the NQR. According to a comparative sequence-structure study of 32 FAD- binding proteins done by Dym and Eisenberg in 2001, non-covalently FAD bonds are mainly formed by hydrogen bonds from the diphosphate moiety to highly conserved protein motives. Less specific binding by the isoalloxazine ring system and the adenine ring to less conserved protein motives are suspected to assist in FAD coordination and stabilization (70). Depending on this protein environment, the absorbance spectrum of the flavin can vary. The purified NqrF-FAD domain of *V. cholerae* exhibits two prominent peaks at 405 and 467 nm in its VIS absorbance spectrum (fig. 1.6, panel B).

Upon reduction of flavins under oxic conditions, harmful reactive oxygen species like superoxide $O_2^-$ or $H_2O_2$ may be formed. This has been shown for FMN in mitochondrial Complex I (71) and for the covalently bound FAD in NqrF of the *V. cholerae* NQR (72). These reactive oxygen species have noxious effects on the cell, like DNA double strain breaks (73) or inactivation of iron-sulfur clusters (74). For fast degradation of such reactive oxygen species, many organism express specific enzymes, like superoxide dismutases (75) or catalases (76).

## Iron-sulfur clusters

Next to organic electron carriers, also metal containing redox cofactors like iron-sulfur clusters are participating in a variety of essential processes in eukaryotes and prokaryotes. It is suggested that FeS clusters were among the very first catalysts of biochemical reactions (77). These clusters are characterized by non-heme iron ions linked to inorganic sulfur and/or organic sulfur (78). FeS clusters have a preference for thiolate ligation and therefore, cysteinyl sulfur is the most frequent ligation partner but interactions with other amino acid residues or atoms and molecules were also observed (79). Proteins containing exclusively iron-sulfur centers are called ferredoxins or rubredoxins. The latter type contains one iron ion ligated to four organic sulfur residues ([1Fe] or [1Fe-0S]) (fig. 1.7, panel A). Here, the iron atom is in its $Fe^{3+}$ state and can undergo transient reduction to $Fe^{2+}$ (78) with midpoint redox potentials in rubredoxins ranging from - 0.1 V to + 0.2 V (77). Among ferredoxins, three main types are distinguished by the number of iron and inorganic sulfur atoms: [2Fe - 2S], [3Fe – 2S] and [4Fe – 4S]. The inorganic sulfur, also called acid-labile sulfur, bridges the iron atoms. In a [2Fe – 2S] cluster, two iron atoms are bound to the protein by four sulfur residues and to each other by two inorganic sulfur atoms in a rhombic manner (fig. 1.7, panel B) (80). Previous studies showed also a coordination of the iron with three cysteines and one histidine, like the mitochondrial membrane protein mitoNEET (79). In general, FeS clusters are one-electron redox systems. For example, two redox states are observed in a [2Fe-2S] cluster: oxidized (both irons $Fe^{3+}$) and reduced (one iron $Fe^{3+}$ and one iron $Fe^{2+}$) (81). The midpoint redox potential for this type of FeS cluster usually ranges from -0.15 V to -0.45 V (77, 82). Rieske proteins are a special type of [2Fe-2S] ferredoxins, first characterized as subunits of the respiratory cytochrome $bc_1$ complex from mitochondria (83). Here, the FeS cluster is ligated to two cysteine and two histidine residues. The ligation to histidine residues is associated with rather positive midpoint redox potentials ranging from +0.1 V to +0.4 V (77) of Rieske proteins. The combination of three iron atoms coordinated by two inorganic

sulfur atoms and three organic sulfur residues results in a cuboidal [3Fe-2S] cluster (fig. 1.7, panel C). In its oxidized state, the cluster contains three $Fe^{3+}$ and by reduction, one iron atom is reduced to $Fe^{2+}$ (78). [4Fe-4S] clusters have a cubic arrangement, in which four iron atoms are coordinated by four inorganic sulfur atoms and four cysteine sulfur side chains (fig. 1.7, panel D).

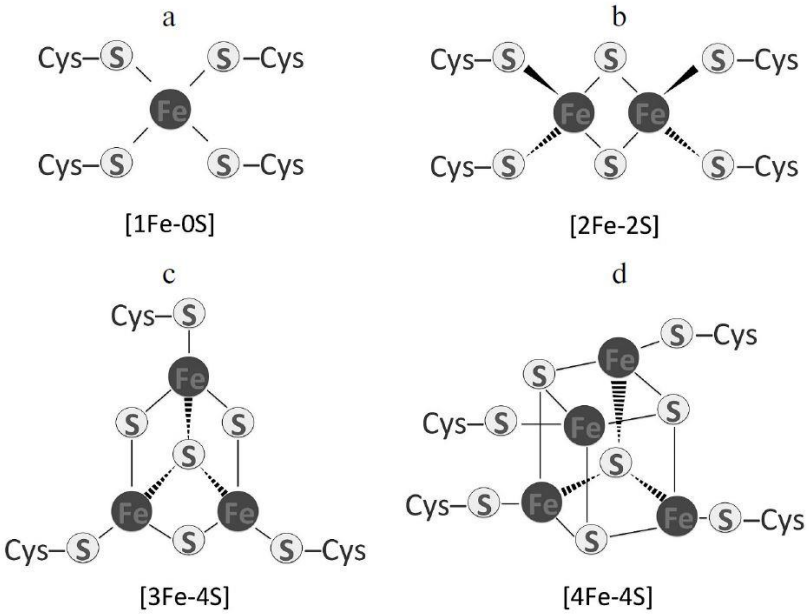


**Figure 1.7** The four main types of iron-sulfur clusters. Rubredoxins harbor [1Fe-0S] centers, characterized by one iron atom coordinated by four sulfur residues (a). Ferredoxins possess mainly [2Fe-2S] (b), [3Fe-4S] (c) or [4Fe-4S] (d) clusters. The [2Fe-2S] clusters have a rhombic arrangement with two iron atoms ligated to four organic sulfur residues and bridged to each other by two inorganic sulfur atoms. A cuboidal [3Fe-2S] cluster is formed by three iron atoms coordinated by three cysteine sulfur residues and four inorganic sulfur atoms. By the ligation of four irons atoms to four organic sulfur residues and four inorganic sulfur atoms, a cubic [4Fe-4S] cluster is formed (80).

## Isoprenoid quinones: redox cofactors of the membrane

Isoprenoid quinones are membrane bound compounds in all living organism, participating as electron and proton carriers in photosynthetic and respiratory transport chains (84). Due to their composition of a hydrophilic head group and a hydrophobic side chain, they are lipid soluble and anchored into the lipid bilayer of the membrane (84). Here, the hydrophobic part is located in the hydrophobic mid-plane region of the membrane, whereas the hydrophilic head group oscillates between the mid-plane region and the polar head group of the

phospholipids of the membrane (85). The basic structure of the isoprenoid quinones is a 1,4-benzoquinone, with the C5 conjugated to a hydrophobic isoprenoid chain (26) (fig. 1.8). Isoprenoid quinones can be divided into two main subclasses: benzoquinones and naphthoquinones. Naphthoquinones have a benzene ring conjugated to the 1,4-benzoquinone structure. All these quinones can participate in two-electron redox reactions, because the ring system accepts two electrons and two protons during reduction (fig. 1.8). Here, electrons and protons can be transferred at once, forming directly quinol, or the reduction takes place in two steps, with intermediate formation of a semiquinone radical. The radical can be stabilized by the protein environment, enabling two- and one-electron processes in respiratory chains (86).

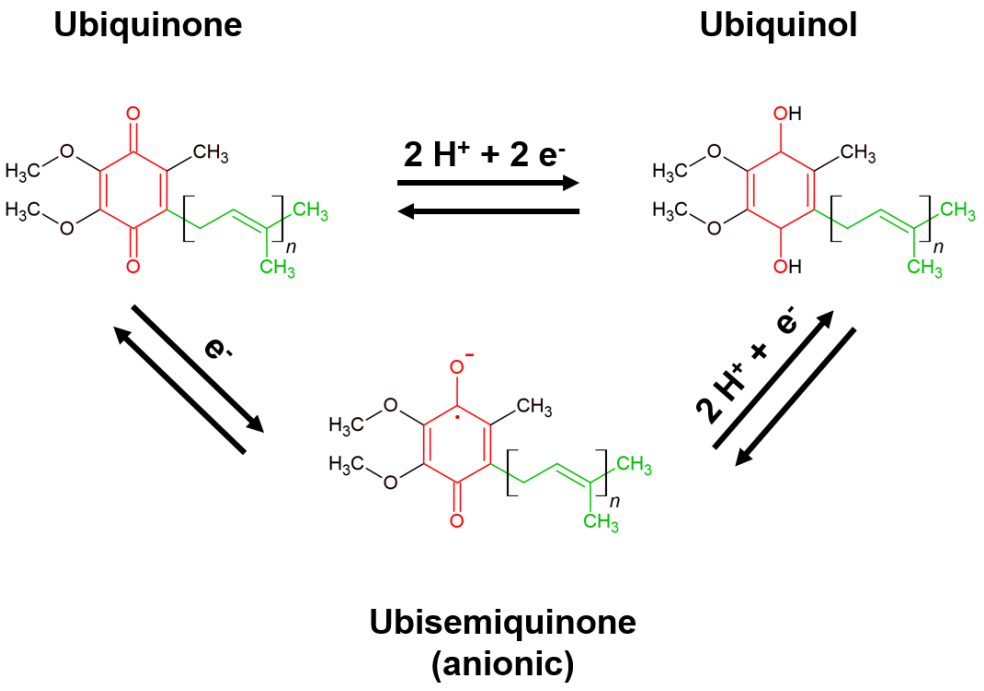


**Figure 1.8** Structure of ubiquinone. Ubiquinone belongs to the isoprenoid quinones (benzoquinones), with a 1,4-benzoquinone basic structure (red), conjugated to an isoprenoid chain (green) at C5, two methoxy groups at C2 and C3, and a methyl group at C6. Number of isoprenoid modules (indicated by brackets) varies among species. Ubiquinone can be reduced to ubiquinol in a single step, or two steps by forming the intermediate ubisemiquinone (84). Here, the anionic ubisemiquinone is depicted. Structures are from ChemSpider (4) (http://www.chemspider.com/; 23.09.2021) and were adapted with ChemSketch (5) (Version 2021.1.1).

Depending on the quinone type and the environment, the midpoint potential of the $Q/QH_2$ couple may vary between -0.07 V and +0.1 V (41). Thus, these compounds operate in a broad range of redox potentials, making them a perfect tool to mediate electron transfer between different redox complexes in the respiratory chain in various organisms. The selection of the quinone type for a specific reaction depends on the redox potential of the redox donor pair and redox acceptor pair. The redox potential of the quinone generally lies between the redox potentials of these two pairs to enable electron transfer (fig. 1.9) (41). In *E. coli*, UQ is utilized for aerobic respiration. With a redox potential of +0.1 V it is located perfectly between the $NADH/NAD^+$ (-0.32 V) and the $O_2/H_2O$ (+0.82) redox pairs. Under anaerobic conditions, *E. coli* uses, for example, formate as electron donor and fumarate as electron acceptor in a respiratory chain (21). Due to the low redox potential of the succinate/fumarate couple (+0.03 V), UQ would not be able to transfer the electrons from formate under standard conditions. Therefore, menaquinone (MK) is the preferred quinone utilized in the absence of oxygen, since it has a much lower redox potential (-0.07 V) compared to UQ.

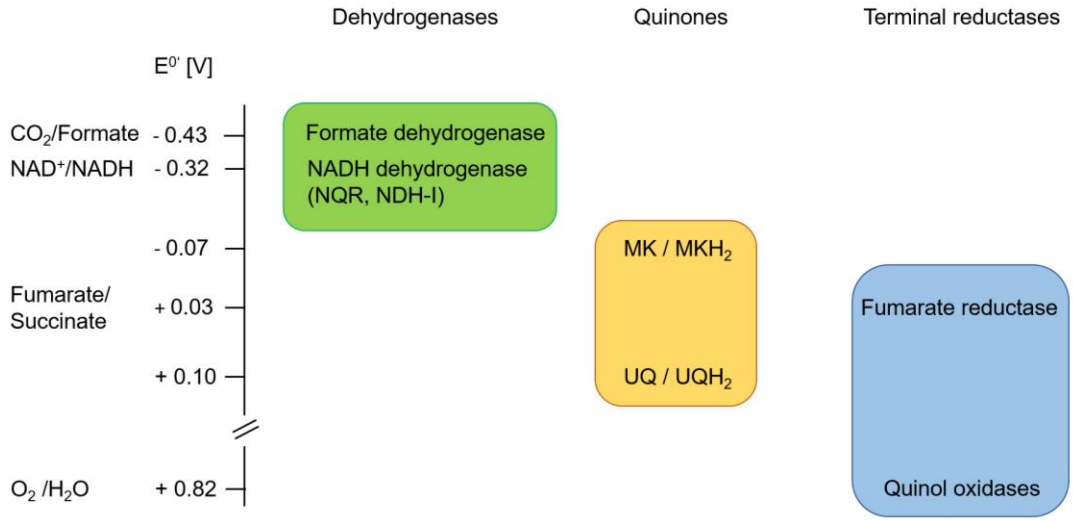


**Figure 1.9** Standard redox potentials ($E^{0'}$) of enzymes and electron donor and acceptor pairs operating in bacteria. Green: dehydrogenases. Yellow: quinones. Blue: terminal reductases. MK: menaquinone. $MKH_2$: menaquinol. UQ: ubiquinone. $UQH_2$: ubiquinol. Adapted from (41).

## 1.3 The anaerobic way of life

Many bacterial environments are anoxic or easily switch to anoxic conditions, due to the low availability of oxygen in water ($1.22 * 10^{-3}$ mol $dm^{-3}$ pure or fresh water in equilibrium with air at 25°C and 1.0 atm) (87). Thus, bacteria encountering this condition need to be prepared for energy conservation without oxygen. If a suitable electron acceptor is present, anaerobic respiration is conducted. Alternatively, fermentation can be performed to generate ATP.

### 1.3.1 Fermentation

Fermentation relies on the combination of internal redox reactions coupled to the synthesis of ATP by substrate-level phosphorylation (SLP). The degradation of glucose to different fermentative end products *via* glycolysis is one example of a fermentative pathway, where ATP is formed without a respiratory chain. In aerobic bacteria, the pyruvate generated by glycolysis and redox active substrates (e.g. NADH) are further converted by the oxidative TCA cycle and the respiratory chain (67). Under anoxic conditions the last two steps cannot be conducted, therefore reducing equivalents must be regenerated under formation of reduced end products such as lactate. The facultative anaerobic model organism *E. coli* converts sugars to acetate, ethanol, lactate, formate and succinate under anoxic conditions by mixed acid fermentation (88). These products are excreted into the environment to maintain intracellular redox balance. The ratio of the different fermentative end products depends on environmental conditions and the number of reducing equivalents, which have to be balanced. The ATP yield here is very low with 2 mol ATP per 1 mol glucose during SLP in glycolysis and 1 mol ATP per 1 mol glucose by the fermentation of pyruvate to acetate (88). Thus, the most important aim here is the regeneration of the electron acceptor $NAD^+$ from NADH, which is essential to keep glycolysis running (88). The conversion of pyruvate to lactate or succinate leads to the regeneration of 1 mol $NAD^+$, respectively, and

the conversion to ethanol results in the regeneration of 2 mol $NAD^+$ (88). In contrast, for the production of acetate from pyruvate no NADH is needed and thus, no $NAD^+$ is regenerated. Depending on the pH of the environment, the excretion of lactate may generate a $H^+$ gradient, which can also be used to form ATP (89). Note that besides balancing of the redox reactions, the uptake and excretion of carbon is also balanced in fermentation (90).

### 1.3.2 Anaerobic respiration: Menaquinone derivates as electron mediators

The respiratory systems of anaerobic bacteria are quite similar to the systems of aerobic bacteria, with the exception of the terminal electron acceptor and the enzyme, catalyzing the final redox reaction. As a rule, the reduction of an alternative organic or inorganic electron acceptor releases less energy compared to the reduction of oxygen, because the electron couple $O_2/H_2O$ is the most electropositive in nature (table 1.3). In many respiratory chains, electrons are transferred from one respiratory complex to the other with the help of quinones. Under anaerobic conditions, this is mediated by menaquinone (MK), thermoplasmaquinone (TPQ), methionaqionone (MTQ), demethylmenquinone (DMK) and methylmenaquinone (MMK) (84).

**Table 1.3** Respiratory energy conservation of typical microorganisms. Typical redox couples, participating in respiration, together with their midpoint potential are given. Redox couples are listed in order of their redox potential. Adapted from (67).

| Redox couple (ox./red.) | $\Delta E^{0'}$ [V] | Respiration type | Organism |
|---|---|---|---|
| $CO_2$/acetate | -0.3 | Carbonate respiration | *Acetobacterium woodii* (26) |
| $S^0/HS^-$ | -0.27 | Sulfur respiration | *Wolinella succinogenes* (91) |
| $CO_2/CH_4$ | -0.25 | Methanogenesis | *Methanosarcina thermophila* (92) |

| | | | |
|---|---|---|---|
| $SO_4^{2-}/HS^-$ | -0.22 | Sulfate respiration | *Desulfovibrio vulgaris* (93) |
| Fumarate/succinate | +0.03 | Fumarate respiration | *Wolinella succinogenes* (91) |
| $NO_3^-/NO_2^-$ | +0.4 | Nitrate respiration | *Paracoccus denitrificans* (94) |
| $Fe^{3+}/Fe^{2+}$ | +0.75 | Iron respiration | *Shewanella oneidensis* MR-1 (95) |
| $O_2/H_2O$ | +0.82 | Aerobic respiration | *Escherichia coli* (2) |

MK is an isoprenoid quinone belonging to the subclass of naphthoquinones, characterized by its benzene ring conjugated to the 1,4-benzoquinone structure (fig. 1.10). Because MKs are poorly soluble in aqueous solutions, 2,3-dimethyl-1,4-naphtoquinone (DMN) is often used for *in vitro* experiments. Structurally, DMN is an analogue to menaquinone but instead of the isoprenoid side chain it possesses a methyl group (fig. 1.10). Thus, DMN is much more soluble than MKs but the redox activity and the midpoint potential with -0.035 V (96) is quite similar. During *in vitro* enzyme assays, DMN reduction/oxidation is monitored spectrophotometrically. Here, the difference in absorbance of 270 nm – 290 nm is used with the extinction coefficient of $\varepsilon_{270\ nm-\ 290\ nm} = 15\ mM^{-1}\ cm^{-1}$ (97).

Considering the evolution of respiratory systems, MKs are the most ancient isoprenoid quinones, found in a broad range of archaea and bacteria (84). These quinones have a low redox potential (around -0.07 V) (41), probably because of their early appearance in evolution, when oxygen was still absent in the atmosphere and microorganisms thrived under anoxic conditions (84). Thus, MKs play an important role in obligate anaerobic organisms,

but also in facultative anaerobic species. The facultative anaerobic bacterium *E. coli* is able to synthesize naphthoquinones (menaquinone and demethylmenaquinone) and UQs. When cultivated under anoxic conditions the MK content in the membrane increases significantly, especially in the presence of electron acceptors such as fumarate or nitrate (98, 99). Thus, MK mediates electron transfer between protein complexes involved in anaerobic respiration in *E. coli*.

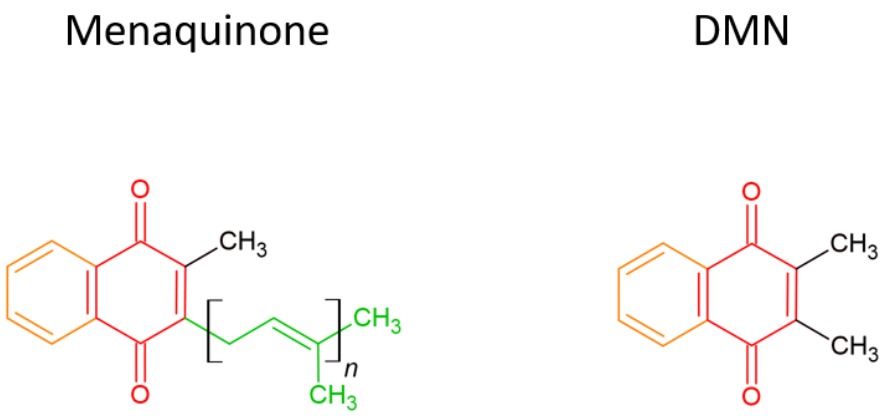


**Figure 1.10** Structure of menaquinone and 2,3-dimethyl-1,4-naphtoquinone (DMN). Both belong to the isoprenoid quinones (naphthoquinones), with a 1,4-benzoquinone basic structure (red), conjugated to a benzene ring (orange) at C2 and C3. Menaquinones possess a methyl group at C6 and an isoprenoid side chain at C5. Number of isoprenoid modules (indicated by brackets) varies among species. Instead of the isoprenoid side chain, DMN harbors a second methyl group at C5 (84). Structures are from ChemSpider (4) (http://www.chemspider.com/; 23.09.2021) and were adapted with ChemSketch (5) (Version 2021.1.1).

Redox reactions with MKs are known for e.g., hydrogenases, dehydrogenases (NQR, formate dehydrogenase), nitrate reductases, nitrite reductases and fumarate reductases. *Wolinella succinogenes* is a well characterized model organism for anaerobic respiration with MK, containing fumarate reductase, formate dehydrogenase, hydrogenase, nitrate reductase and nitrite reductase in its membrane (91). This set of respiratory enzymes enables *W. succinogenes* to adapt to different environmental conditions and to generate a PMF for ATP synthesis (91). Hydrogenase and formate dehydrogenase serve as electron input modules by oxidizing $H_2$ or formate and reducing MK (fig. 1.11). Each enzyme is composed of one hydrophobic (HydC; FdhC) and two hydrophilic subunits (HydAB; FdhAB). HydB

and FdhA are the catalytic subunits containing the oxidation sides for the substrates, HydA and FdhB harbor both iron-sulfur clusters for passing on the electrons. The two hydrophobic subunits each contain two hemes *b*, which are responsible for MK reduction. Furthermore, they anchor the protein complexes in the membrane. NADH dehydrogenases, such as the NQR of *Bacteroides fragilis* or *Prevotella bryantii*, are also known to reduce MK by the oxidation of NADH (100, 101). As mentioned previously, anaerobic respiration depends on enzymes, which are able to transfer electrons from $MKH_2$ to various electron acceptors. In *W. succinogenes*, the nitrate and nitrite reductases represent such enzymes (102). Among these, the periplasmic nitrate reductase system (NAP) is composed of NapGH and NapAB. NapG and NapH form a transmembrane protein complex, catalyzing $MKH_2$ oxidation and electron transport to the periplasmic NapAB complex with the help of iron-sulfur clusters in both subunits. NapB is a two-heme *c* protein accepting the electrons from NapGH and passing them on to NapA, which catalyzes the reduction of nitrate to nitrite (fig. 1.11) (102). Nitrite can be used as a further alternative electron acceptor with the help of the Nrf system. Here, the transmembrane four-heme *c* NrfH protein forms a complex with the five-heme *c* NrfA. NrfH oxidizes $MKH_2$ and NrfA reduces nitrite to ammonium (fig. 1.11). Furthermore, *W. succinogenes* possesses a quinol:fumarate oxidoreductase (QFR), catalyzing reduction of fumarate to succinate upon $MKH_2$ oxidation (91). Energy conservation by reduction of fumarate is called fumarate respiration, which represents an important mode of energy conservation in a variety of different microorganisms.

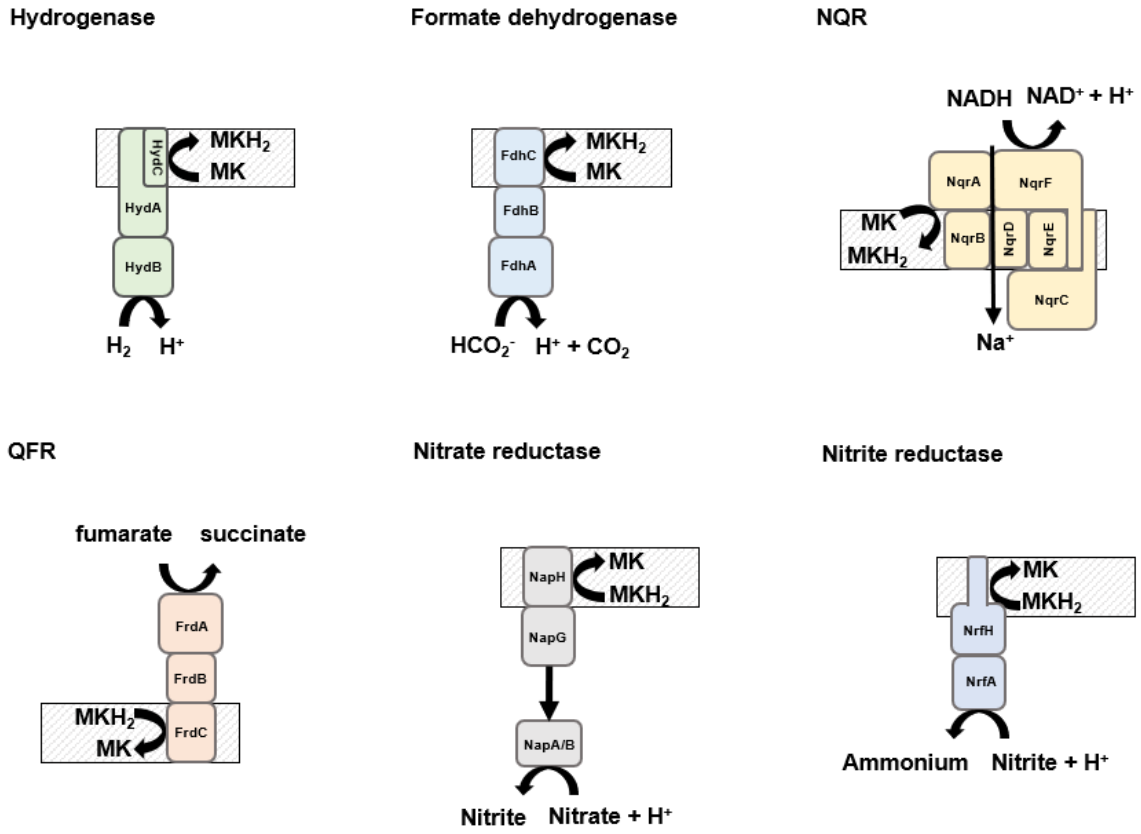


**Figure 1.11** Schematic overview of respiratory enzymes utilizing MK as electron mediator. Shown are the hydrogenase, formate dehydrogenase, quinol:fumarate reductase (QFR), nitrate reductase and nitrite reductase of *W. succinogenes* (adapted to (91, 102)), and the $Na^+$ -translocating NADH:quinone (NQR) oxidoreductase of *Bacteroides fragilis* (adapted to (100)) or *Prevotella bryantii*, which can oxidize also UQ *in vitro* (101). The inner bacterial membrane is indicated with grey stripes. Upper part represents the cytoplasm, lower part represents the periplasm.

### 1.3.3 Fumarate respiration: The quinol:fumarate oxidoreductase of *Wolinella succinogenes*

Succinate and fumarate are four-carbon dicarboxylates. They represent a redox couple utilized in aerobic or anaerobic respiration by succinate:quinone oxidoreductases (SQOR). Members of this superfamily catalyze the two-electron oxidation of succinate (or reduction of fumarate) and the two-electron reduction of quinone (or oxidation of quinol). Depending on the direction of the reaction, these enzymes can be classified as succinate:quinol reductases (SQR, equation 1.6) or quinol:fumarate reductases (QFR, equation 1.7) (103):

$$\text{succinate} + \text{quinone} \rightarrow \text{fumarate} + \text{quinol} \quad (1.6)$$

$$\text{fumarate} + \text{quinol} \rightarrow \text{succinate} + \text{quinone} \quad (1.7)$$

SQRs are found in aerobic organisms, catalyzing the oxidation of succinate in the TCA cycle. QFRs are present in the respiratory chain of anaerobes, generating energy by fumarate respiration. All known SQORs are composed of three to four subunits (Sdh/FrdABCD). Subunits A and B are hydrophilic and are located in the cytoplasm. These subunits are conserved among diverse species, including Gram-positive bacteria, Gram-negative bacteria, archaea and eukaryotes (103, 104). Notably, the binding sites for prosthetic groups and the dicarboxylate substrates are highly conserved. The subunits C and D are integral membrane proteins. SQR/QFR enzymes composed of three subunits have one large C subunit (~30 kDa) and enzymes with four subunits possess two small C and D subunits (both ~15 kDa). The membranous subunit(s) show large variations in their sequence, composition and cofactor content (105). Considering these hydrophobic subunits, succinate:quinone oxidoreductases are classified in four main types (A-D) (fig. 1.12). Type A harbors two hydrophobic subunits with two hemes *b* (105). It is present in thermo- and acidophilic archaea, such as *Thermoplasma acidophilum* (106) or *Thermus thermophilus* (107) (fig. 1.12, panel A). Here, succinate is oxidized and thermoplasma-quinone is reduced in the membrane. Type B of SQORs harbors one hydrophilic subunit, containing two hemes *b* (fig. 1.12, panel B). This type is known to work in both directions, with MK as electron acceptor/donor in the membrane (103). Examples of this type is the SQR of *Bacillus subtilis* (108), the QFR of *W. succinogenes* (109) and the QFR of *P. bryantii* (101). Type C SQR, with two membranous subunits and one heme *b*, is present in mitochondria and in *E. coli* (110) (fig. 1.12, panel C). This type was also shown to work in both directions, but exclusively with UQ (105). Type D, which is present in *E. coli* during anaerobic respiration, is a QFR with two hydrophilic subunits but does not contain heme (105, 111) (fig. 1.12, panel D). Here, fumarate is reduced to succinate upon $MKH_2$ reduction. In general, SQRs and QFRs may catalyze succinate oxidation or fumarate reduction *in vitro* using various quinones. However, the enzymes usually are optimized for one reaction *in vivo*. Thus,

several organism possess different types of succinate:quinone oxidoreductases. For example, *E. coli* expresses SQR during aerobic, but QFR during anaerobic growth. The SQR uses UQ and the QFR MK as electron acceptor/donor (112). *In vitro*, the reversed reactions are catalyzed providing the enzyme with excess of substrate, or with artificial quinones with a more favourable redox potential (103).

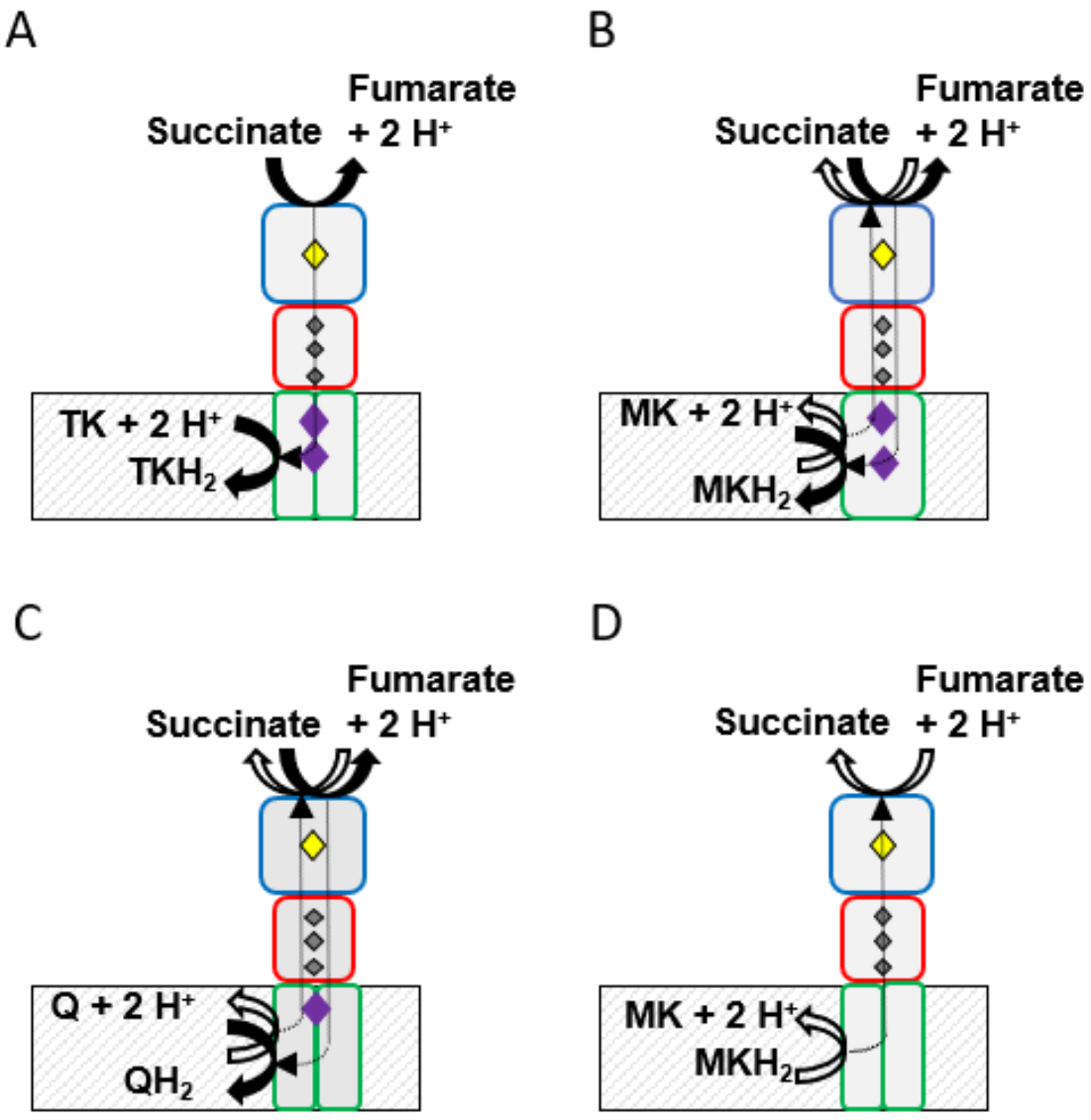


**Figure 1.12** Classification of succinate:quinone oxidoreductases, based on their composition and cofactor content. Type A harbors four subunits and two hemes *b*. Type B is composed of three subunits and two hemes *b*. Type C has four subunits and one heme *b*. Type D comprises four subunits, but no heme. Hydrophilic subunit A is drawn in blue, subunit B in red and subunits C/D in green. Hemes are symbolized as magenta diamonds, FeS clusters as grey diamonds and FADs as yellow diamonds. The direction of the reaction is indicated with filled arrows (SQR) and with open arrows (QFR). Upper part represents the cytoplasm, lower part represents the periplasm. TK, thermoplasma-quinone; $TKH_2$, thermoplasma-quinol. MK, menaquinone; $MKH_2$, menaquinol. Q, ubiquinone; $QH_2$, ubiquinol. Figure was modified from (113).

The enzyme of *W. succinogenes* is one of the best studied type B QFRs with three subunits (FrdABC) and two hemes *b* in FrdC (fig. 1.13). The subunits FrdA (~75 kDa) and FrdB (~27 kDa) depict the hydrophilic part of the enzyme with the catalytic fumarate reduction activity (114, 115). The FrdC subunit (~30 kDa) is hydrophobic and anchors the enzyme in the membrane (113, 115). Furthermore, several cofactors were identified in this enzyme: one covalently bound FAD in FrdA, three FeS clusters in FrdB and two hemes *b* in FrdC (114). In *W. succinogenes* it has been shown by crystallographic structure determination, that the QFR forms a homodimer, with a dimension of 75 Å x 120 Å x 50 Å (114). The catalytic site for $MKH_2$ oxidation, and therefore the entry site of the electrons into the protein, has to be located in FrdC. Due to missing electron densities of $MKH_2$ in QFR crystal structures, the exact location remains unclear (114). Only a cavity, near the distal heme and extending from the hydrophobic membrane phase to the periplasmic aqueous phase, was identified. In this cavity, a highly conserved glutamate residue (Glu66) is located, which could form a hydrogen bond to a hydroxyl group of $MKH_2$ (114, 116). This predicted interaction of Glu66 with $MKH_2$ was confirmed by mutant studies, where Glu66 was replaced by a glutamine residue. The mutated enzyme lacked the property to oxidize $MKH_2$ with fumarate as electron acceptor, whereas succinate oxidation with methylene blue was not affected (115). Structural analysis of the mutated QFR revealed no major structural alterations and also the midpoint potentials of the hemes *b* were not affected significantly, confirming the suggestion that Glu66 is an essential component of the $MKH_2$ oxidation site. After oxidation of $MKH_2$ by the hemes *b* in FrdC, the electrons are transferred *via* the FeS clusters to the covalently bound FAD and finally fumarate is reduced to succinate (fig. 1.13). Upon fumarate reduction, two $H^+$ from the cytoplasm are bound (117). Due to the additional transfer of two $H^+$ from the periplasm to the cytoplasm by the "E-pathway" during oxidation of the quinol, the electrogenic transport of $H^+$ of the QFR is counterbalanced (109). Thus, the QFR activity of *W. succinogenes* does not contribute to the formation of a PMF. The electron carriers of the

*W. succinogenes* QFR are presented in greater detail in Fig. 1.13 and in the following sections.

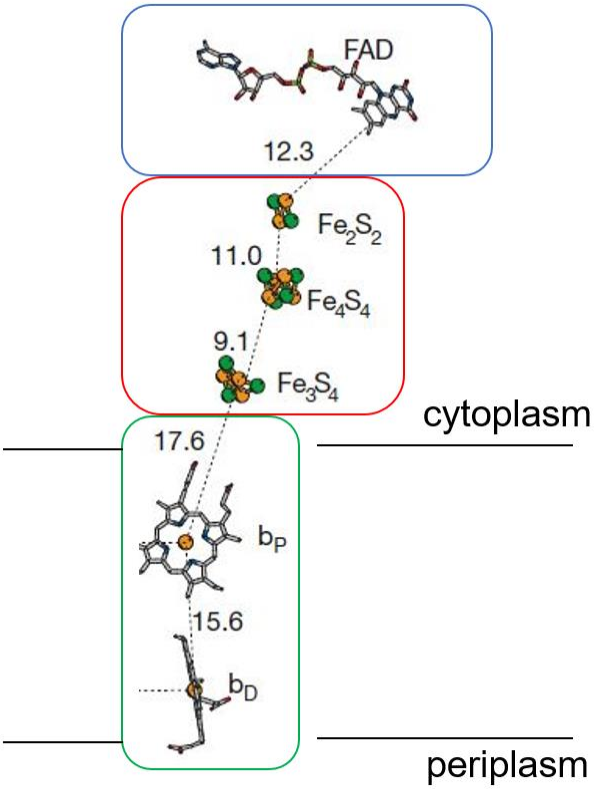


**Figure 1.13** Arrangement of cofactors in the QFR monomer of *W. succinogenes*. The QFR of *W. succinogenes* comprises three subunits: FrdA (blue), FrdB (red), FrdC (green). Edge to edge distances of the cofactors (in Ångstrom) are indicated by dotted lines. The distal heme *b* is represented by $b_D$ and the proximal heme *b* by $b_P$. The membrane plane is indicated by black lines, whereas the top represents the cytoplasm and the bottom the periplasm. Adapted from (114).

## Iron-porphyrin complexes (hemes *b*)

Heme proteins are a group of proteins, which harbor iron-porphyrin as cofactors. These redox proteins are ubiquitous in nature with diverse activities, like diatomic gas transportation/storage, electron transfer (118), transcriptional regulation (119), microRNA processing (120), circadian clock control (121) or ion channel regulation (122). Hemes are organic, heterocyclic compounds, with four pyrrole rings ligated to a porphyrin ring. Incorporation of an $Fe^{2+}$ (or $Fe^{3+}$) atom into the ring system is achieved by its ligation to four nitrogen atoms. Of these, two nitrogen atoms are imines, and two nitrogen atoms are amines

and deprotonated (67). In general, hemes undergo one-electron transfer, switching between the $Fe^{3+}$ and $Fe^{2+}$ state (123). Heme *b* (also known as protoheme IX) and heme *c* represent the most common heme types in biological systems, interacting as prosthetic groups with proteins (124). Structural differences between the heme types occur mainly in two side chains of the porphyrin ring. In hemes *b*, the side chain are two vinyl groups (fig. 1.14, panel A). Additional side chains are methyl groups (four) and propionic residues (two). Whereas heme *c* binds covalently to the protein by thioether bonds between two cysteine residues of the protein and the heme vinyl groups, heme *b* is non-covalently attached to proteins (125). In VIS absorbance spectra, the different heme types are identified by their typical absorbance maxima (126). Reduced hemes *b* exhibit a strong absorbance at 427 nm and a weak absorbance at 527 nm and 560 nm (fig. 1.14, panel B), whereas oxidized hemes *b* absorb intensively at 410 nm (127). Thus, by monitoring the change in absorbance at 427 nm and 410 nm, reduction and oxidation of hemes *b* can be followed.

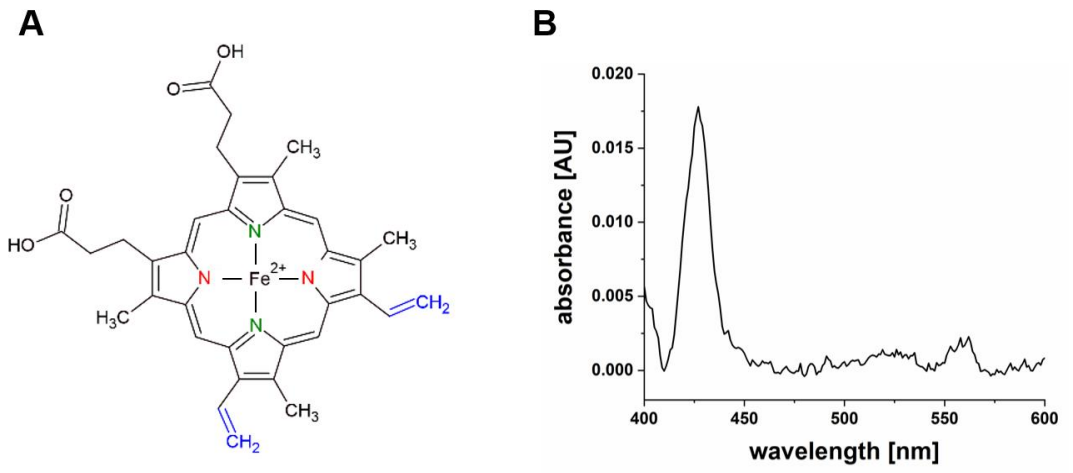


**Figure 1.14** Properties of hemes *b*. A: Structure of heme *b*. Hemes are organic, heterocyclic compounds, with four pyrrole rings ligated to a porphyrin ring. Incorporation of an $Fe^{2+}$ (or $Fe^{3+}$) atom into the ring system is achieved by ligation to four nitrogen atoms, with two imines (green) and two amines (red). Heme *b* differs from other heme types by two vinyl groups (blue) ligated to the porphyrin ring (41, 126). Structure is from ChemSpider (4) (http://www.chemspider.com/; 23.09.2021) and was adapted with ChemSketch (5) (Version 2021.1.1)**.** B: VIS difference spectrum of [dithionite reduced] minus [air oxidized] *P. bryantii* membranes. Reduced hemes *b* exhibit an intense maximum at 427 nm and two weak maxima (527 nm and 560 nm).

The FrdC subunit of the QFR of *W. succinogenes* is a di-heme protein, containing two hemes *b* as prosthetic groups and redox centers (114). The distal heme ($b_D$) has a low redox potential (-0.2 V); the proximal heme ($b_P$) has a high redox potential (-0.02 V) (115, 117, 128). It is suggested, that electrons from $MKH_2$ are transferred to the heme $b_D$ first and then to heme $b_P$, accompanied with a parallel, compensatory translocation of one proton per electron from the periplasm to the cytoplasm (109).

### 1.3.4 Generation of electrochemical gradients involving decarboxylation reactions

Besides fermentation and anaerobic respiration, bacteria have evolved several other strategies to gain energy without oxygen, e.g. by decarboxylation of dicarboxylic acids. One example is the decarboxylation reaction in *Propionigenium modestum,* which gains its total energy for growth by decarboxylation of succinate to propionate and $CO_2$ (47). Since the free energy change of a decarboxylation reaction is too small for SLP ($\Delta G^{0'}$ = -20.6 kJ/mol), the energy is used to generate an electrochemical sodium gradient across the membrane by membrane bound primary decarboxylase sodium ion pumps (47). Here, the methylmalonyl-CoA decarboxylase acts as a primary $Na^+$ pump (129), and with the help of a $Na^+$-translocating ATP synthase, the $Na^+$ gradient is used to drive ATP synthesis. Therefore, this mechanism of ATP synthesis is also called decarboxylation phosphorylation. This mode of ATP generation was also reported for other anaerobic bacteria, like *Veillonella alcalescens* (129). Besides methylmalonyl-CoA decarboxylases acting as primary sodium pumps, the oxaloacetate decarboxylase of *Klebsiella aerogenes* was also shown to be an electrogenic $Na^+$ transporter (130). Another interesting type of ATP generation by decarboxylation reactions is the malo-lactic fermentation performed by some lactic acid bacteria under alkaline conditions. In general, lactic acid bacteria are fermentative bacteria, gaining their energy mainly from SLP. With 2 to 3 ATP molecules generated per molecule of glucose, the

energy yield by fermentation is rather small (131). Here, additional energy is gained by a variety of secondary transport systems, generating a PMF. Thus, the energy is not conserved by a primary decarboxylation-dependent ion pump, but by the interplay between an electroneutral decarboxylase and a secondary transport system (132). Under alkaline conditions (above pH 6) malate is mainly present in its di-anionic state ($Mal^{2-}$), which is taken up into the cell and subsequently decarboxylated to lactate by the cytoplasmatic malolactic enzyme in a proton consuming reaction (131) (fig. 1.15). Due to a higher internal pH (above pH 7 during glycolysis) (133), lactate is present in its mono-anionic state ($Lac^-$), which is extruded by a $malate^{2-}$/$lactate^-$ antiporter. Thus this process is generating a PMF by translocating negative charge from the outside to the inside of the cell (outside positive, inside negative) and by consuming protons during malate decarboxylation (high pH inside, low pH outside) (131). This PMF drives the $F_1F_0$-ATPase to synthesize ATP (134).

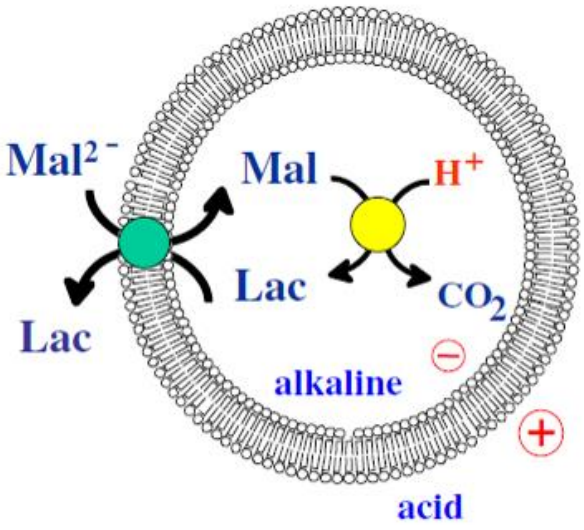


**Figure 1.15** Energy conservation in malolactic fermentation. Under alkaline conditions (above pH 6), malate is present in its di-anionic state ($Mal^{2-}$) and taken up into the cell. By the malolactic enzyme, $Mal^{2-}$ is decarboxylated to lactate in a proton consuming reaction. Lactate is present in the cell in its mono-anionic state ($Lac^-$, here Lac). Lactate is extruded by a $malate^{2-}$/$lactate^-$ antiporter. Thus, this process generates a PMF by translocating negative charge from the outside to the inside of the cell (outside positive, inside negative) and by consuming protons during malate decarboxylation (high pH inside, low pH outside) (131).

## 1.4 Association of *Prevotella* spp. with the microbiome of higher vertebrates

### 1.4.1 *Prevotella bryantii*: key player of the ruminal microbiome

The ruminal microbiome is one of the most diverse community of microorganisms, with $10^{10}$ – $10^{11}$ organism/mL bacteria, $10^{8}$ – $10^{9}$ organism/mL archaea, $10^{5}$ – $10^{6}$ organism/mL protozoa, $10^{3}$ – $10^{4}$ organism/mL fungi and a large, not fully characterized virome (135). However, only 5 to 15% of the ruminal bacterial species can be readily cultured (136). This diverse set of organisms enables the ruminant to utilize ligno-cellulose material and non-protein nitrogen as energy source (135). The anoxic environment of the rumen leads to a stepwise degradation of the substrates by various, specialized consortia of microorganisms. As a result, volatile fatty acids are formed, mainly acetate, propionate and butyrate (135), which serve as the major nutrient source for the animal. To regenerate $NAD^+$, which is reduced to NADH during fermentation, electron transfer proceeds in the absence of oxygen to other final electron acceptors. Here, the major electron sink is the reduction of $CO_2$ to $CH_4$ by the consumption of $H_2$, but also sulfate, nitrate and fumarate are used as terminal electron acceptors (137). In such an environment, the degradation of organic substrates under generation of energy for the microorganisms and the host requires a close interaction of the different species in the microbiome. The optimal interaction of the ruminal microbiome is not only important for the health of the animal, but also for millions of people, sustaining their livelihood by providing milk, meat and leather from ruminants in both, developed and developing countries. Yet, microbial fermentation in the rumen has also negative effects on the environment, such as emission of the greenhouse gas $CH_4$, or excessive nitrogen excretion by the ruminant (135). Due to the massive increase of livestock production over the last centuries, these problems become more and more challenging. Consequently, understanding the ruminal microbiome and the interactions with the host and external

influences like dietary factors is important to develop an efficient agricultural strategy for animal production while minimizing negative environmental side effects.

In 2015, Henderson and co-workers analyzed 742 ruminal samples from 32 animal species from 35 countries and found a "core microbiome" mainly composed of *Prevotella*, *Butyrivibrio* and *Ruminococcus* species (138). They demonstrated that *Prevotella* spp., especially *P. ruminicola, P. brevis* and *P. bryantii*, represents up to 70% of the rumen bacterial population (139, 140). With an extensive repertoire of glycoside hydrolases (> 100), these bacteria are able to utilize starches, other non-cellulosic polysaccharides and simple sugars as energy sources (140). In general, the *Prevotella* genus includes Gram-negative, non-spore-forming, obligate anaerobic bacteria, which are prevalent in the rumen and gastrointestinal tracts of herbivores and omnivores (141). They have also been isolated from other environments, such as the human oral cavity (142), human skin and soft-tissue infections (143), human female urogenital tract (144) and soil (145).

Due to its high abundance in the rumen, *P. bryantii* is often used as a model organism to investigate main metabolic routs of the ruminal microbiome. *P. bryantii* ferments sugars to acetate, formate and succinate (146, 147). Howlett and co-workers analyzed in 1976 the degradation of glucose by *P. bryantii*, grown in rich medium containing rumen fluid. Here, for every molecule of glucose, 1.1 mol succinate, 0.8 mol acetate and 0.35 mol formate were produced with a net uptake of 0.5 mol $CO_2$, leading to a theoretical generation of 2.7 ATP molecules per glucose by SLP during fermentation (146). However, this theoretical ATP yield was too low to account for the high molecular growth rate under the analyzed conditions, with a yield of 66 g dry weight per mol glucose, which is enormous considering the low ATP yield. In *E. coli*, the formation of ~6 mol ATP per mol glucose would be necessary to generate 66 g dry weight per mol glucose under anaerobic conditions (148). Due to the actual production of 2 mol ATP per mol glucose, this high growth rate is not realistic for fermentation in *E. coli*. Most likely, an anaerobic electron transport

phosphorylation reaction in *P. bryantii* increases the overall energetic yield. Indeed, *P. bryantii* operates a QFR in concert with a NQR, coupling the formation of succinate to the generation of a sodium gradient (101).

### 1.4.2 *Prevotella* species associated with diseases

*Prevotella* species are part of the human microbiome, where they are found in the nasopharynx, respiratory system (149), oral cavity (150) and gut system (151) without causing a disease. They are considered to be commensal bacteria of the healthy human microbiome, due to their high abundance, but rare involvement in infections. Yet, some *Prevotella* strains are clearly associated with diseases like inflammatory disorders, (periodontitis, rheumatoid arthritis), opportunistic infections, oral biofilm diseases or bacterial vaginosis (BV) (152, 153). Several studies indicate that a change of *Prevotella* abundance can trigger such diseases by modulating the immune system and its response (154–156). Accordingly, these strains are suggested to be important pathobionts in human diseases by promoting chronic inflammations. They are involved in complex ecological interactions and crosstalk with the host and other members of the microbiome, with indirect but potentially substantial effects on human health.

One example is *P. bivia*, which inhabits the vaginal milieu and is involved in BV. BV is the most commonly reported microbiological syndrome among women in reproductive age (157) and it is associated with a variety of health issues, such as preterm birth, pelvic inflammatory disease or increased susceptibility to sexual transmitted viruses or bacteria (e.g. HIV) (158). The factors triggering BV are unclear, but it is characterized by the loss of the healthy *Lactobacillus*-rich vaginal microbiome, replaced by strictly anaerobic microorganisms, such as *P. bivia* and *Gardnerella vaginalis*. Here, *P. bivia* is an important source of ammonia (159), lipopolysaccharides (160), and promotes degradation of the mucus with its sialidase activity (161). Furthermore, it is associated with a change in the vaginal

cytokine/chemokine profile, e.g. increased innate cytokine concentrations (IL-1α, IL-1β, IL-8, TNF-α). Although *P. bivia* is not considered to be the main pathogen, recent studies demonstrated a correlation between *P. bivia* abundance and severity of BV (162, 163). Typically, *P. bivia* co-occurs with *G. vaginalis* and it is suggested, that they interact synergistically. *G. vaginalis* is a marker strain for BV, and both *G. vaginalis* (161) and *P. bivia* (164) trigger BV phenotypes in mice models. It was proposed that amino acids released by *G. vaginalis* are metabolized by *P. bivia*, leading to a rise in ammonium concentration in a biofilm established by *G. vaginalis* and *P. bivia*. This increases the pH and might promote the formation of a microbial community characteristic for BV (165, 166). In support for this hypothesis, we showed that *P. bivia* exhibits high L-asparaginase and aspartate ammonia lyse activities, catalyzing the conversion of L-asparagine to the electron acceptor fumarate (159). However, the by-product ammonium is highly toxic. Thus, *P. bivia* depends on the ammonium-utilizing *G. vaginalis* and provides key nutrients to it. The production pattern of *P. bivia* growing on glucose in the presence of mixed amino acids substantiates this notion (159).

## 1.5 Aim and motivation for this thesis

*Prevotella bryantii* and *Prevotella bivia,* both members of the family *Prevotellaceae*, are important model organisms in the nutrition of ruminants (*P. bryantii*) and the development of bacterial vaginosis (*P. bivia*). By understanding energy conservation and anaerobic metabolism of these two related bacterial species, their contribution to the establishment of different ecosystems is deciphered.

Both the nutrition of the ruminant, and the production of methane, a greenhouse gas, depend on the composition and activity of the microbiota in the rumen. To optimize feeding strategies, and to minimize methane emission, detailed knowledge of microbial dynamics and interactions is required. The findings in this study give an insight into the metabolism and energy conservation of *P. bryantii*, one of the most abundant species in the rumen of ruminants. This is an important step to predict the catabolic functions of the rumen microbiota in the future.

*P. bivia* is an opportunistic pathogen associated with bacterial vaginosis (BV), but its role in the development of the disease is unclear. The aim of the study was to describe important catabolic reactions in *P. bivia*, which pave the way for the change in the vaginal microbiome, which is a hallmark of the disease.

## 1.6 References


1. Mitchell P. 1961. Coupling of phosphorylation to electron and hydrogen transfer by a chemi-osmotic type of mechanism. Nature 191:144–148. doi:10.1038/191144a0.
2. Voet D, Voet JG, Pratt CW. 2006. Biochemistry, 2. ed. Wiley, Hoboken, NJ.
3. Cooper GM. 2000. The cell. A molecular approach, 2. ed. ASM Press, Washington, DC. http://www.ncbi.nlm.nih.gov/bookshelf/br.fcgi?book=cooper.
4. Pence HE, Williams A. 2010. ChemSpider: An online chemical information resource. J Chem Educ 87:1123–1124. doi:10.1021/ed100697w.
5. Hunter AD. 1997. ACD/ChemSketch 1.0 (freeware); ACD/ChemSketch 2.0 and its tautomers, dictionary, and 3D plug-ins; ACD/HNMR 2.0; ACD/CNMR 2.0. J Chem Educ 74:905. doi:10.1021/ed074p905.
6. Meis L de. 2013. The concept of phosphate compounds of high and low energy, p. 85–103. *In* Sotelo JR, Benech JC (ed), Calcium and cellular metabolism. Transport and regulation, vol. 244. Springer.
7. Thauer RK, Jungermann K, Decker K. 1977. Energy conservation in chemotrophic anaerobic bacteria. Bacteriol Rev 41:100–180.
8. Satyanarayana U. 2017. Biochemistry - E-book. (with Biomedical Concepts, Clinical Correlates & Case Studies), 5th. Elsevier India, Gurgaon.
9. Borisov VB, Murali R, Verkhovskaya ML, Bloch DA, Han H, Gennis RB, Verkhovsky MI. 2011. Aerobic respiratory chain of *Escherichia coli* is not allowed to work in fully uncoupled mode. Proc Natl Acad Sci USA 108:17320–17324. doi:10.1073/pnas.1108217108.
10. Reddy GK, Wendisch VF. 2014. Characterization of 3-phosphoglycerate kinase from *Corynebacterium glutamicum* and its impact on amino acid production. BMC Microbiol. 14:54. doi:10.1186/1471-2180-14-54.
11. Smith CD, Chattopadhyay D, Pal B. 2011. Crystal structure of *Plasmodium falciparum* phosphoglycerate kinase: evidence for anion binding in the basic patch. Biochem Biophys Res Commun 412:203–206. doi:10.1016/j.bbrc.2011.07.045.
12. Mattevi A, Valentini G, Rizzi M, Speranza M, Bolognesi M, Coda A. 1995. Crystal structure of *Escherichia coli* pyruvate kinase type I: molecular basis of the allosteric transition. Structure 3:729–741. doi:10.1016/S0969-2126(01)00207-6.
13. Buss KA, Cooper DR, Ingram-Smith C, Ferry JG, Sanders DA, Hasson MS. 2001. Urkinase: structure of acetate kinase, a member of the ASKHA superfamily of phosphotransferases. J Bacteriol 183:680–686. doi:10.1128/JB.183.2.680-686.2001.
14. Fraser ME, James MN, Bridger WA, Wolodko WT. 1999. A detailed structural description of *Escherichia coli* succinyl-CoA synthetase. J Mol Biol. 285:1633–1653. doi:10.1006/jmbi.1998.2324.
15. Kaleta C, Schäuble S, Rinas U, Schuster S. 2013. Metabolic costs of amino acid and protein production in *Escherichia coli*. Biotechnol J. 8:1105–1114. doi:10.1002/biot.201200267.
16. Schmauder H-P. 1992. Allgemeine Mikrobiologie. J Basic Microbiol 32:429–430. doi:10.1002/jobm.3620320623.
17. Nicholls DG, Ferguson S. 2013. Bioenergetics, 4th ed. Elsevier Science, Burlington. http://gbv.eblib.com/patron/FullRecord.aspx?p=1195616.
18. Müller F. 2018. Chemistry and biochemistry of flavoenzymes. CRC revivals. CRC Press, Boca Raton, FL.
19. Bragg PD, Hou C. 1967. Reduced nicotinamide adenine dinucleotide oxidation in *Escherichia coli* particles. Arch biochem Biophys 119:202–208. doi:10.1016/0003-9861(67)90447-X.
20. Melo AMP, Bandeiras TM, Teixeira M. 2004. New insights into type II NAD(P)H:quinone oxidoreductases. Microbiol Mol Biol Rev 68:603–616. doi:10.1128/MMBR.68.4.603-616.2004.
21. Unden G, Bongaerts J. 1997. Alternative respiratory pathways of *Escherichia coli*: energetics and transcriptional regulation in response to electron acceptors. Biochim Biophys Acta 1320:217–234. doi:10.1016/S0005-2728(97)00034-0.
22. Sturr MG, Krulwich TA, Hicks DB. 1996. Purification of a cytochrome *bd* terminal oxidase encoded by the *Escherichia coli app* locus from a d*cyo* d*cyd* strain complemented by genes from *Bacillus firmus* OF4. J Bacteriol 178:1742–1749. doi:10.1128/jb.178.6.1742-1749.1996.
23. Minagawa J, Mogi T, Gennis RB, Anraku Y. 1992. Identification of heme and copper ligands in subunit I of the cytochrome *bo* complex in *Escherichia coli*. J Biol Chem 267:2096–2104.
24. Anraku Y, Gennis RB. 1987. The aerobic respiratory chain of *Escherichia coli*. Trends Biochem Sci 12:262–266. doi:10.1016/0968-0004(87)90131-9.
25. Mitchell P, Moyle J. 1969. Estimation of membrane potential and pH difference across the cristae membrane of rat liver mitochondria. Eur J Biochem 7:471–484. doi:10.1111/j.1432-1033.1969.tb19633.x.
26. Muras V, Toulouse C, Fritz G, Steuber J. 2019. Respiratory membrane protein complexes convert

chemical energy. Subcell Biochem 92:301–335. doi:10.1007/978-3-030-18768-2_10.

27. Wikström M. 1984. Two protons are pumped from the mitochondrial matrix per electron transferred between NADH and ubiquinone. FEBS Lett 169:300–304. doi:10.1016/0014-5793(84)80338-5.
28. Galkin A, Dröse S, Brandt U. 2006. The proton pumping stoichiometry of purified mitochondrial complex I reconstituted into proteoliposomes. Biochim Biophys Acta 1757:1575–1581. doi:10.1016/j.bbabio.2006.10.001.
29. Matsushita K, Ohnishi T, Kaback HR. 1987. NADH-ubiquinone oxidoreductases of the *Escherichia coli* aerobic respiratory chain. Biochemistry 26:7732–7737. doi:10.1021/bi00398a029.
30. Jasaitis A, Borisov VB, Belevich NP, Morgan JE, Konstantinov AA, Verkhovsky MI. 2000. Electrogenic reactions of cytochrome *bd*. Biochemistry 39:13800–13809. doi:10.1021/bi001165n.
31. Rühle T, Leister D. 2015. Assembly of $F_1F_0$-ATP synthases. Biochim Biophys Acta 1847:849–860. doi:10.1016/j.bbabio.2015.02.005.
32. Jiang W, Hermolin J, Fillingame RH. 2001. The preferred stoichiometry of c subunits in the rotary motor sector of *Escherichia coli* ATP synthase is 10. Proc Natl Acad Sci USA 98:4966–4971. doi:10.1073/pnas.081424898.
33. Hackenbrock CR, Chazotte B, Gupte SS. 1986. The random collision model and a critical assessment of diffusion and collision in mitochondrial electron transport. J Bioenerg Biomembr 18:331–368. doi:10.1007/BF00743010.
34. Vonck J, Schäfer E. 2009. Supramolecular organization of protein complexes in the mitochondrial inner membrane. Biochim Biophys Acta. 1793:117–124. doi:10.1016/j.bbamcr.2008.05.019.
35. Acin-Perez R, Enriquez JA. 2014. The function of the respiratory supercomplexes: the plasticity model. Biochim Biophys Acta 1837:444–450. doi:10.1016/j.bbabio.2013.12.009.
36. Davies KM, Strauss M, Daum B, Kief JH, Osiewacz HD, Rycovska A, Zickermann V, Kühlbrandt W. 2011. Macromolecular organization of ATP synthase and complex I in whole mitochondria. Proc Natl Acad Sci USA 108:14121–14126. doi:10.1073/pnas.1103621108.
37. Davies KM, Blum TB, Kühlbrandt W. 2018. Conserved in situ arrangement of complex I and $III_2$ in mitochondrial respiratory chain supercomplexes of mammals, yeast, and plants. Proc Natl Acad Sci USA 115:3024–3029. doi:10.1073/pnas.1720702115.
38. Reyes-Galindo M, Suarez R, Esparza-Perusquía M, Lira-Sánchez J de, Pardo JP, Martínez F, Flores-Herrera O. 2019. Mitochondrial respirasome works as a single unit and the cross-talk between complexes I, $III_2$ and IV stimulates NADH dehydrogenase activity. Biochim Biophys Acta 1860:618–627. doi:10.1016/j.bbabio.2019.06.017.
39. Milenkovic D, Blaza JN, Larsson N-G, Hirst J. 2017. The enigma of the respiratory chain supercomplex. Cell Metab. 25:765–776. doi:10.1016/j.cmet.2017.03.009.
40. Fedor JG, Hirst J. 2018. Mitochondrial supercomplexes do not enhance catalysis by quinone channeling. Cell Metab. 28:525-531.e4. doi:10.1016/j.cmet.2018.05.024.
41. Magalon A, Alberge F. 2016. Distribution and dynamics of OXPHOS complexes in the bacterial cytoplasmic membrane. Biochim Biophys Acta 1857:198–213. doi:10.1016/j.bbabio.2015.10.015.
42. Melo AMP, Teixeira M. 2016. Supramolecular organization of bacterial aerobic respiratory chains: From cells and back. Biochim Biophys Acta 1857:190–197. doi:10.1016/j.bbabio.2015.11.001.
43. Brzezinski P. 2020. New structures reveal interaction dynamics in respiratory supercomplexes. Trends Biochem Sci 45:3–5. doi:10.1016/j.tibs.2019.10.011.
44. Hirst J. 2018. Open questions: respiratory chain supercomplexes-why are they there and what do they do? BMC Biol 16:111. doi:10.1186/s12915-018-0577-5.
45. Steuber J, Schmid C, Rufibach M, Dimroth P. 2000. $Na^+$ translocation by complex I (NADH:quinone oxidoreductase) of *Escherichia coli*. Mol microbiol. 35:428–434. doi:10.1046/j.1365-2958.2000.01712.x.
46. Gemperli AC, Dimroth P, Steuber J. 2003. Sodium ion cycling mediates energy coupling between complex I and ATP synthase. Proc Natl Acad Sci USA 100:839–844. doi:10.1073/pnas.0237328100.
47. Hilpert W, Schink B, Dimroth P. 1984. Life by a new decarboxylation-dependent energy conservation mechanism with $Na^+$ as coupling ion. EMBO J. 3:1665–1670.
48. Mulkidjanian AY, Dibrov P, Galperin MY. 2008. The past and present of sodium energetics: may the sodium-motive force be with you. Biochim Biophys Acta 1777:985–992. doi:10.1016/j.bbabio.2008.04.028.
49. Padan E, Venturi M, Gerchman Y, Dover N. 2001. $Na^+/H^+$ antiporters. Biochim Biophys Acta 1505:144–157. doi:10.1016/S0005-2728(00)00284-X.
50. Steuber J, Vohl G, Muras V, Toulouse C, Claußen B, Vorburger T, Fritz G. 2015. The structure of $Na^+$-translocating of NADH:ubiquinone oxidoreductase of *Vibrio cholerae*: implications on coupling between electron transfer and $Na^+$

transport. Biol Chem 396:1015–1030. doi:10.1515/hsz-2015-0128.

51. van de Vossenberg JL, Ubbink-Kok T, Elferink MG, Driessen AJ, Konings WN. 1995. Ion permeability of the cytoplasmic membrane limits the maximum growth temperature of bacteria and archaea. Mol Microbiol 18:925–932. doi:10.1111/j.1365-2958.1995.18050925.x.
52. Vorburger T, Nedielkov R, Brosig A, Bok E, Schunke E, Steffen W, Mayer S, Götz F, Möller HM, Steuber J. 2016. Role of the $Na^+$-translocating NADH:quinone oxidoreductase in voltage generation and $Na^+$ extrusion in *Vibrio cholerae*. Biochim Biophys Acta 1857:473–482. doi:10.1016/j.bbabio.2015.12.010.
53. Steuber J, Vohl G, Casutt MS, Vorburger T, Diederichs K, Fritz G. 2014. Structure of the *V. cholerae* $Na^+$-pumping NADH:quinone oxidoreductase. Nature 516:62–67. doi:10.1038/nature14003.
54. Türk K, Puhar A, Neese F, Bill E, Fritz G, Steuber J. 2004. NADH oxidation by the $Na^+$-translocating NADH:quinone oxidoreductase from *Vibrio cholerae*: functional role of the NqrF subunit. J Biol Chem 279:21349–21355. doi:10.1074/jbc.M311692200.
55. Juárez O, Morgan JE, Nilges MJ, Barquera B. 2010. Energy transducing redox steps of the $Na^+$-pumping NADH:quinone oxidoreductase from *Vibrio cholerae*. Proc Natl Acad Sci USA 107:12505–12510. doi:10.1073/pnas.1002866107.
56. Casutt MS, Huber T, Brunisholz R, Tao M, Fritz G, Steuber J. 2010. Localization and function of the membrane-bound riboflavin in the $Na^+$-translocating NADH:quinone oxidoreductase ($Na^+$-NQR) from *Vibrio cholerae*. J Biol Chem 285:27088–27099. doi:10.1074/jbc.M109.071126.
57. Tao M, Casutt MS, Fritz G, Steuber J. 2008. Oxidant-induced formation of a neutral flavosemiquinone in the $Na^+$-translocating NADH:Quinone oxidoreductase ($Na^+$-NQR) from *Vibrio cholerae*. Biochim Biophys Acta 1777:696–702. doi:10.1016/j.bbabio.2008.04.006.
58. Page CC, Moser CC, Chen X, Dutton PL. 1999. Natural engineering principles of electron tunnelling in biological oxidation-reduction. Nature 402:47–52. doi:10.1038/46972.
59. Renault G, Raynal E, Sinet M, Berthier JP, Godard B, Cornillault J. 1982. A laser fluorimeter for direct cardiac metabolism investigation. Opt Laser Technol. 14:143–148. doi:10.1016/0030-3992(82)90110-4.
60. Miura R. 2001. Versatility and specificity in flavoenzymes: control mechanisms of flavin reactivity. Chem Rec 1:183–194. doi:10.1002/tcr.1007.
61. Edwards AM. 2014. Structure and general properties of flavins. Methods Mol Biol 1146:3–13. doi:10.1007/978-1-4939-0452-5_1.
62. Macheroux P. 1999. UV-visible spectroscopy as a tool to study flavoproteins. Methods Mol Biol 131:1–7. doi:10.1385/1-59259-266-X:1.
63. Massey V. 2000. The chemical and biological versatility of riboflavin. Biochem Soc Trans 28:283–296.
64. Massey V, Palmer G. 1966. On the existence of spectrally distinct classes of flavoprotein semiquinones. A new method for the quantitative production of flavoprotein semiquinones. Biochemistry 5:3181–3189. doi:10.1021/bi00874a016.
65. Weimar WR, Neims AH. 1975. Physical and Chemical Properties of Flavins; Binding of Flavins to Protein and Conformational Effects; Biosynthesis of Riboflavin, p. 1–47. *In* Rivlin RS (ed), Riboflavin. Springer US, Boston, MA.
66. Ghisla S, Massey V. 1989. Mechanisms of flavoprotein-catalyzed reactions. Eur J Biochem 181:1–17. doi:10.1111/j.1432-1033.1989.tb14688.x.
67. Madigan MT, Martinko JM, Brock TD. 2006. Brock biology of microorganisms, 11. ed., internat. ed. Pearson Prentice Hall, Upper Saddle River, NJ.
68. Casutt MS, Schlosser A, Buckel W, Steuber J. 2012. The single NqrB and NqrC subunits in the $Na^+$-translocating NADH: quinone oxidoreductase ($Na^+$-NQR) from *Vibrio cholerae* each carry one covalently attached FMN. Biochim Biophys Acta. 1817:1817–1822. doi:10.1016/j.bbabio.2012.02.012.
69. Heuts DPHM, Scrutton NS, McIntire WS, Fraaije MW. 2009. What's in a covalent bond? On the role and formation of covalently bound flavin cofactors. FEBS J. 276:3405–3427. doi:10.1111/j.1742-4658.2009.07053.x.
70. Dym O, Eisenberg D. 2001. Sequence-structure analysis of FAD-containing proteins. Protein Sci 10:1712–1728. doi:10.1110/ps.12801.
71. Liu Y, Fiskum G, Schubert D. 2002. Generation of reactive oxygen species by the mitochondrial electron transport chain. J Neurochem 80:780–787. doi:10.1046/j.0022-3042.2002.00744.x.
72. Muras V, Dogaru-Kinn P, Minato Y, Häse CC, Steuber J. 2016. The $Na^+$-translocating NADH:quinone oxidoreductase enhances oxidative stress in the cytoplasm of *Vibrio cholerae*. J Bacteriol 198:2307–2317. doi:10.1128/JB.00342-16.
73. Brawn K, Fridovich I. 1981. DNA strand scission by enzymically generated oxygen radicals. Arch biochem Biophys 206:414–419. doi:10.1016/0003-9861(81)90108-9.
74. Keyer K, Imlay JA. 1997. Inactivation of dehydratase 4Fe-4S clusters and disruption of iron homeostasis upon cell exposure to peroxynitrite. J Biol Chem 272:27652–27659.

doi:10.1074/jbc.272.44.27652.
75. Gregory EM, Yost FJ, Fridovich I. 1973. Superoxide dismutases of *Escherichia coli*: intracellular localization and functions. J Bacteriol 115:987–991.
76. Sooch BS, Kauldhar BS, Puri M. 2014. Recent insights into microbial catalases: isolation, production and purification. Biotechnol Adv. 32:1429–1447. doi:10.1016/j.biotechadv.2014.09.003.
77. Meyer J. 2008. Iron-sulfur protein folds, iron-sulfur chemistry, and evolution. J Biol Inorg Chem. 13:157–170. doi:10.1007/s00775-007-0318-7.
78. Sticht H, Rösch P. 1998. The structure of iron–sulfur proteins. Prog Biophys Mol Biol 70:95–136. doi:10.1016/S0079-6107(98)00027-3.
79. Wiley SE, Paddock ML, Abresch EC, Gross L, van der Geer P, Nechushtai R, Murphy AN, Jennings PA, Dixon JE. 2007. The outer mitochondrial membrane protein mitoNEET contains a novel redox-active 2Fe-2S cluster. J Biol Chem 282:23745–23749. doi:10.1074/jbc.C700107200.
80. Stiban J, So M, Kaguni LS. 2016. Iron-sulfur clusters in mitochondrial metabolism: multifaceted roles of a simple cofactor. Biochemistry (Mosc) 81:1066–1080. doi:10.1134/S0006297916100059.
81. Leggate EJ, Bill E, Essigke T, Ullmann GM, Hirst J. 2004. Formation and characterization of an all-ferrous Rieske cluster and stabilization of the $[2Fe\text{-}2S]^0$ core by protonation. Proc Natl Acad Sci USA 101:10913–10918. doi:10.1073/pnas.0402711101.
82. Cammack R, Rao KK, Bargeron CP, Hutson KG, Andrew PW, Rogers LJ. 1977. Midpoint redox potentials of plant and algal ferredoxins. Biochem J 168:205–209. doi:10.1042/bj1680205.
83. Rieske JS, MacLennan DH, Coleman R. 1964. Isolation and properties of an iron-protein from the (reduced coenzyme Q)-cytochrome *c* reductase complex of the respiratory chain. Biochem Biophys Res Commun 15:338–344. doi:10.1016/0006-291X(64)90171-8.
84. Nowicka B, Kruk J. 2010. Occurrence, biosynthesis and function of isoprenoid quinones. Biochim Biophys Acta 1797:1587–1605. doi:10.1016/j.bbabio.2010.06.007.
85. Fiorini R, Ragni L, Ambrosi S, Littarru GP, Gratton E, Hazlett T. 2008. Fluorescence studies of the interactions of ubiquinol-10 with liposomes. J Photochem Photobiol 84:209–214. doi:10.1111/j.1751-1097.2007.00221.x.
86. Søballe B, Poole RK. 1999. Microbial ubiquinones: multiple roles in respiration, gene regulation and oxidative stress management. Microbiology 145 (Pt 8):1817–1830. doi:10.1099/13500872-145-8-1817.
87. Xing W, Yin M, Lv Q, Hu Y, Liu C, Zhang J. 2014. Oxygen solubility, diffusion coefficient, and solution viscosity, p. 1–31. *In* Xing W, Yin G, Zhang J (ed), Rotating electrode methods and oxygen reduction electrocatalysts. Elsevier, Amsterdam.
88. Clark DP. 1989. The fermentation pathways of *Escherichia coli*. FEMS Microbiol. Rev.:223–234. doi:10.1111/j.1574-6968.1989.tb03398.x.
89. Konings WN. 1985. Generation of metabolic energy by end-product efflux. Trends Biochem Sci 10:317–319. doi:10.1016/0968-0004(85)90172-0.
90. Buckel W. 2021. Energy conservation in fermentations of anaerobic bacteria. Front Microbiol 12. doi:10.3389/fmicb.2021.703525.
91. Kröger A, Biel S, Simon J, Gross R, Unden G, Lancaster CD. 2002. Fumarate respiration of *Wolinella succinogenes*: enzymology, energetics and coupling mechanism. Biochim Biophys Acta 1553:23–38. doi:10.1016/S0005-2728(01)00234-1.
92. Lackner N, Hintersonnleitner A, Wagner AO, Illmer P. 2018. Hydrogenotrophic methanogenesis and autotrophic growth of *Methanosarcina thermophila*. Archaea 2018:4712608. doi:10.1155/2018/4712608.
93. Keller KL, Wall JD. 2011. Genetics and molecular biology of the electron flow for sulfate respiration in *Desulfovibrio*. Front Microbiol 2:135. doi:10.3389/fmicb.2011.00135.
94. Boogerd FC, van Verseveld HW, Stouthamer AH. 1981. Respiration-driven proton translocation with nitrite and nitrous oxide in *Paracoccus denitrificans*. Biochim Biophys Acta 638:181–191. doi:10.1016/0005-2728(81)90226-7.
95. Shi L, Squier TC, Zachara JM, Fredrickson JK. 2007. Respiration of metal (hydr)oxides by *Shewanella* and *Geobacter*: a key role for multihaem *c*-type cytochromes. Mol microbiol. 65:12–20. doi:10.1111/j.1365-2958.2007.05783.x.
96. Madej MG, Nasiri HR, Hilgendorff NS, Schwalbe H, Lancaster CRD. 2006. Evidence for transmembrane proton transfer in a dihaem-containing membrane protein complex. EMBO J 25:4963–4970. doi:10.1038/sj.emboj.7601361.
97. Lemma E, Unden G, Kröger A. 1990. Menaquinone is an obligatory component of the chain catalyzing succinate respiration in *Bacillus subtilis*. Arch Microbiol 155:62–67. doi:10.1007/BF00291276.
98. Unden G. 1988. Differential roles for menaquinone and demethylmenaquinone in anaerobic electron transport of *E. coli* and their *fnr*-independent expression. Arch Microbiol 150:499–503. doi:10.1007/BF00422294.
99. Wissenbach U, Kröger A, Unden G. 1990. The specific functions of menaquinone and demethylmenaquinone in anaerobic respiration with fumarate, dimethylsulfoxide, trimethylamine

N-oxide and nitrate by *Escherichia coli*. Arch Microbiol 154:60–66. doi:10.1007/BF00249179.

100. Ito T, Gallegos R, Matano LM, Butler NL, Hantman N, Kaili M, Coyne MJ, Comstock LE, Malamy MH, Barquera B. 2020. Genetic and biochemical analysis of anaerobic respiration in *Bacteroides fragilis* and its importance *in vivo*. mBio 11. doi:10.1128/mBio.03238-19.
101. Schleicher L, Trautmann A, Stegmann D, Fritz G, Gätgens J, Bott M, Hein S, Simon J, Seifert J, Steuber J. 2021. A sodium-translocating module linking succinate production to formation of a membrane potential in *Prevotella bryantii*. Appl Environ Microbiol: AEM0121121. doi:10.1128/AEM.01211-21.
102. Kern M, Simon J. 2009. Electron transport chains and bioenergetics of respiratory nitrogen metabolism in *Wolinella succinogenes* and other Epsilonproteobacteria. Biochim Biophys Acta 1787:646–656. doi:10.1016/j.bbabio.2008.12.010.
103. Hägerhäll C. 1997. Succinate: quinone oxidoreductases. variations on a conserved theme. Biochim Biophys Acta 1320:107–141. doi:10.1016/s0005-2728(97)00019-4.
104. Lancaster CD, Kröger A. 2000. Succinate: quinone oxidoreductases: new insights from X-ray crystal structures. Biochim Biophys Acta 1459:422–431. doi:10.1016/S0005-2728(00)00180-8.
105. Hägerhäll C, Hederstedt L. 1996. A structural model for the membrane-integral domain of succinate:quinone oxidoreductases. FEBS Lett 389:25–31. doi:10.1016/0014-5793(96)00529-7.
106. Schäfer G, Anemüller S, Moll R. 2002. Archaeal complex II: ‘classical‘ and ‘non-classical’ succinate:quinone reductases with unusual features. Biochim Biophys Acta 1553:57–73. doi:10.1016/s0005-2728(01)00232-8.
107. Kolaj-Robin O, O'Kane SR, Nitschke W, Léger C, Baymann F, Soulimane T. 2011. Biochemical and biophysical characterization of succinate: quinone reductase from *Thermus thermophilus*. Biochim Biophys Acta 1807:68–79. doi:10.1016/j.bbabio.2010.10.009.
108. Matsson M, Tolstoy D, Aasa R, Hederstedt L. 2000. The distal heme center in *Bacillus subtilis* succinate:quinone reductase is crucial for electron transfer to menaquinone. Biochemistry 39:8617–8624. doi:10.1021/bi000271m.
109. Lancaster CD. 2002. *Wolinella succinogenes* quinol:fumarate reductase—2.2-Å resolution crystal structure and the E-pathway hypothesis of coupled transmembrane proton and electron transfer. Biochim Biophys Acta 1565:215–231. doi:10.1016/S0005-2736(02)00571-0.
110. Yankovskaya V, Horsefield R, Törnroth S, Luna-Chavez C, Miyoshi H, Léger C, Byrne B, Cecchini G, Iwata S. 2003. Architecture of succinate dehydrogenase and reactive oxygen species generation. Science 299:700–704. doi:10.1126/science.1079605.
111. Iverson TM, Luna-Chavez C, Cecchini G, Rees DC. 1999. Structure of the *Escherichia coli* fumarate reductase respiratory complex. Science 284:1961–1966. doi:10.1126/science.284.5422.1961.
112. Cecchini G, Schröder I, Gunsalus RP, Maklashina E. 2002. Succinate dehydrogenase and fumarate reductase from *Escherichia coli*. Biochim Biophys Acta 1553:140–157. doi:10.1016/s0005-2728(01)00238-9.
113. Lancaster CRD. 2013. The di-heme family of respiratory complex II enzymes. Biochim Biophys Acta 1827:679–687. doi:10.1016/j.bbabio.2013.02.012.
114. Lancaster CR, Kröger A, Auer M, Michel H. 1999. Structure of fumarate reductase from *Wolinella succinogenes* at 2.2 A resolution. Nature 402:377–385. doi:10.1038/46483.
115. Lancaster CR, Gross R, Haas A, Ritter M, Mäntele W, Simon J, Kröger A. 2000. Essential role of Glu-C66 for menaquinol oxidation indicates transmembrane electrochemical potential generation by *Wolinella succinogenes* fumarate reductase. Proc Natl Acad Sci USA 97:13051–13056. doi:10.1073/pnas.220425797.
116. Lancaster CRD, Sauer US, Gross R, Haas AH, Graf J, Schwalbe H, Mäntele W, Simon J, Madej MG. 2005. Experimental support for the "E pathway hypothesis" of coupled transmembrane $e^-$ and $H^+$ transfer in dihemic quinol:fumarate reductase. Proc Natl Acad Sci USA 102:18860–18865. doi:10.1073/pnas.0509711102.
117. Haas AH, Lancaster CRD. 2004. Calculated coupling of transmembrane electron and proton transfer in dihemic quinol:fumarate reductase. Biophys J. 87:4298–4315. doi:10.1529/biophysj.104.042945.
118. Paoli M, Marles-Wright J, Smith A. 2002. Structure-function relationships in heme-proteins. DNA Cell Biol 21:271–280. doi:10.1089/104454902753759690.
119. Zhang L, Hach A, Wang C. 1998. Molecular mechanism governing heme signaling in yeast: a higher-order complex mediates heme regulation of the transcriptional activator HAP1. Mol Cell Biol. 18:3819–3828. doi:10.1128/mcb.18.7.3819.
120. Faller M, Matsunaga M, Yin S, Loo JA, Guo F. 2007. Heme is involved in microRNA processing. Nat Struct Mol Biol 14:23–29. doi:10.1038/nsmb1182.
121. Kaasik K, Lee CC. 2004. Reciprocal regulation of haem biosynthesis and the circadian clock in mammals. Nature 430:467–471. doi:10.1038/nature02724.
122. Tang XD, Xu R, Reynolds MF, Garcia ML, Heinemann SH, Hoshi T. 2003. Haem can bind to and inhibit mammalian calcium-dependent Slo1 BK channels. Nature 425:531–535.

doi:10.1038/nature02003.

123. Kim HJ, Khalimonchuk O, Smith PM, Winge DR. 2012. Structure, function, and assembly of heme centers in mitochondrial respiratory complexes. Biochim Biophys Acta 1823:1604–1616. doi:10.1016/j.bbamcr.2012.04.008.
124. Reedy CJ, Elvekrog MM, Gibney BR. 2008. Development of a heme protein structure-electrochemical function database. Nucleic Acids Res. 36:D307-13. doi:10.1093/nar/gkm814.
125. Li T, Bonkovsky HL, Guo J. 2011. Structural analysis of heme proteins: implications for design and prediction. BMC Struct Biol. 11:13. doi:10.1186/1472-6807-11-13.
126. Yamanaka T, Okunuki K. 1974. Cytochromes, p. 349–400. *In* Neilands JB (ed), Microbial Iron Metabolism. A Comprehensive Treatise, 1st ed. Elsevier Reference Monographs, s.l.
127. Preger V, Tango N, Marchand C, Lemaire SD, Carbonera D, Di Valentin M, Costa A, Pupillo P, Trost P. 2009. Auxin-responsive genes *AIR12* code for a new family of plasma membrane b-type cytochromes specific to flowering plants. Plant Physiol 150:606–620. doi:10.1104/pp.109.139170.
128. Kröger A, Innerhofer A. 1976. The function of the *b* cytochromes in the electron transport from formate to fumarate of *Vibrio succinogenes*. Eur J Biochem 69:497–506. doi:10.1111/j.1432-1033.1976.tb10934.x.
129. Hilpert W, Dimroth P. 1982. Conversion of the chemical energy of methylmalonyl-CoA decarboxylation into a $Na^+$ gradient. Nature 296:584–585. doi:10.1038/296584a0.
130. Dimroth P. 1982. The generation of an electrochemical gradient of sodium ions upon decarboxylation of oxaloacetate by the membrane-bound and $Na^+$-activated oxaloacetate decarboxylase from *Klebsiella aerogenes*. Eur J Biochem 121:443–449. doi:10.1111/j.1432-1033.1982.tb05807.x.
131. Konings WN. 2006. Microbial transport: adaptations to natural environments. Antonie Van Leeuwenhoek 90:325–342. doi:10.1007/s10482-006-9089-3.
132. Dimroth P, Schink B. 1998. Energy conservation in the decarboxylation of dicarboxylic acids by fermenting bacteria. Arch Microbiol 170:69–77. doi:10.1007/s002030050616.
133. Poolman B, Driessen AJ, Konings WN. 1987. Regulation of solute transport in streptococci by external and internal pH values. Microbiol Rev 51:498–508.
134. Poolman B, Molenaar D, Smid EJ, Ubbink T, Abee T, Renault PP, Konings WN. 1991. Malolactic fermentation: electrogenic malate uptake and malate/lactate antiport generate metabolic energy. J Bacteriol 173:6030–6037. doi:10.1128/jb.173.19.6030-6037.1991.
135. Newbold CJ, Ramos-Morales E. 2020. Review: Ruminal microbiome and microbial metabolome: effects of diet and ruminant host. Animal 14:s78-s86. doi:10.1017/S1751731119003252.
136. Stevenson DM, Weimer PJ. 2007. Dominance of *Prevotella* and low abundance of classical ruminal bacterial species in the bovine rumen revealed by relative quantification real-time PCR. Appl Microbiol Biotechnol 75:165–174. doi:10.1007/s00253-006-0802-y.
137. Morgavi DP, Forano E, Martin C, Newbold CJ. 2010. Microbial ecosystem and methanogenesis in ruminants. Animal 4:1024–1036. doi:10.1017/S1751731110000546.
138. Henderson G, Cox F, Ganesh S, Jonker A, Young W, Janssen PH. 2015. Rumen microbial community composition varies with diet and host, but a core microbiome is found across a wide geographical range. Sci rep 5:14567. doi:10.1038/srep14567.
139. Gylswyk NO. 1990. Enumeration and presumptive identification of some functional groups of bacteria in the rumen of dairy cows fed grass silage-based diets. FEMS Microbiol Lett 73:243–261. doi:10.1111/j.1574-6968.1990.tb03948.x.
140. White BA, Lamed R, Bayer EA, Flint HJ. 2014. Biomass utilization by gut microbiomes. Annu Rev Microbiol 68:279–296. doi:10.1146/annurev-micro-092412-155618.
141. Purushe J, Fouts DE, Morrison M, White BA, Mackie RI, Coutinho PM, Henrissat B, Nelson KE. 2010. Comparative genome analysis of *Prevotella ruminicola* and *Prevotella bryantii:* insights into their environmental niche. Microb Ecol 60:721–729. doi:10.1007/s00248-010-9692-8.
142. Downes J, Liu M, Kononen E, Wade WG. 2009. *Prevotella micans* sp. nov., isolated from the human oral cavity. Int J Sys Evol Microbiol 59:771–774. doi:10.1099/ijs.0.002337-0.
143. Downes J, Sutcliffe IC, Hofstad T, Wade WG. 2006. *Prevotella bergensis* sp. nov., isolated from human infections. Int J Sys Evol Microbiol 56:609–612. doi:10.1099/ijs.0.63888-0.
144. Hillier SL, Krohn MA, Rabe LK, Klebanoff SJ, Eschenbach DA. 1993. The normal vaginal flora, $H_2O_2$-producing *lactobacilli*, and bacterial vaginosis in pregnant women. Clin Infect Dis 16 Suppl 4:S273-81. doi:10.1093/clinids/16.supplement_4.s273.
145. Ueki A, Akasaka H, Satoh A, Suzuki D, Ueki K. 2007. *Prevotella paludivivens* sp. nov., a novel strictly anaerobic, Gram-negative, hemicellulose-decomposing bacterium isolated from plant residue and rice roots in irrigated rice-field soil. Int J Sys Evol Microbiol 57:1803–1809. doi:10.1099/ijs.0.64914-0.
146. Howlett MR, Mountfort DO, Turner KW, Roberton AM. 1976. Metabolism and growth yields in *Bacteroides ruminicola* strain $B_14$. Appl

Environ Microbiol 32:274–283.
147. Hackmann TJ, Ngugi DK, Firkins JL, Tao J. 2017. Genomes of rumen bacteria encode atypical pathways for fermenting hexoses to short-chain fatty acids. Environ Microbiol. 19:4670–4683. doi:10.1111/1462-2920.13929.
148. Hempfling WP, Mainzer SE. 1975. Effects of varying the carbon source limiting growth on yield and maintenance characteristics of *Escherichia coli* in continuous culture. J Bacteriol 123:1076–1087. doi:10.1128/jb.123.3.1076-1087.1975.
149. Charlson ES, Bittinger K, Haas AR, Fitzgerald AS, Frank I, Yadav A, Bushman FD, Collman RG. 2011. Topographical continuity of bacterial populations in the healthy human respiratory tract. Am J Respir Crit Care Med 184:957–963. doi:10.1164/rccm.201104-0655OC.
150. Könönen E. 1993. Pigmented *Prevotella* species in the periodontally healthy oral cavity. FEMS Immunol Med Microbiol 6:201–205. doi:10.1111/j.1574-695X.1993.tb00327.x.
151. Arumugam M, Raes J, Pelletier E, Le Paslier D, Yamada T, Mende DR, Fernandes GR, Tap J, Bruls T, Batto J-M, Bertalan M, Borruel N, Casellas F, Fernandez L, Gautier L, Hansen T, Hattori M, Hayashi T, Kleerebezem M, Kurokawa K, Leclerc M, Levenez F, Manichanh C, Nielsen HB, Nielsen T, Pons N, Poulain J, Qin J, Sicheritz-Ponten T, Tims S, Torrents D, Ugarte E, Zoetendal EG, Wang J, Guarner F, Pedersen O, Vos WM de, Brunak S, Doré J, Antolín M, Artiguenave F, Blottiere HM, Almeida M, Brechot C, Cara C, Chervaux C, Cultrone A, Delorme C, Denariaz G, Dervyn R, Foerstner KU, Friss C, van de Guchte M, Guedon E, Haimet F, Huber W, van Hylckama-Vlieg J, Jamet A, Juste C, Kaci G, Knol J, Lakhdari O, Layec S, Le Roux K, Maguin E, Mérieux A, Melo Minardi R, M'rini C, Muller J, Oozeer R, Parkhill J, Renault P, Rescigno M, Sanchez N, Sunagawa S, Torrejon A, Turner K, Vandemeulebrouck G, Varela E, Winogradsky Y, Zeller G, Weissenbach J, Ehrlich SD, Bork P. 2011. Enterotypes of the human gut microbiome. Nature 473:174–180. doi:10.1038/nature09944.
152. Larsen JM. 2017. The immune response to *Prevotella* bacteria in chronic inflammatory disease. Immunology 151:363–374. doi:10.1111/imm.12760.
153. Tett A, Pasolli E, Masetti G, Ercolini D, Segata N. 2021. *Prevotella* diversity, niches and interactions with the human host. Nat Rev Microbiol 19:585–599. doi:10.1038/s41579-021-00559-y.
154. Aquino SG de, Abdollahi-Roodsaz S, Koenders MI, van de Loo FAJ, Pruijn GJM, Marijnissen RJ, Walgreen B, Helsen MM, van den Bersselaar LA, Molon RS de, Avila Campos MJ, Cunha FQ, Cirelli JA, van den Berg WB. 2014. Periodontal pathogens directly promote autoimmune experimental arthritis by inducing a TLR2- and IL-1-driven Th17 response. J Immunol 192:4103–4111. doi:10.4049/jimmunol.1301970.
155. Schincaglia GP, Hong BY, Rosania A, Barasz J, Thompson A, Sobue T, Panagakos F, Burleson JA, Dongari-Bagtzoglou A, Diaz PI. 2017. Clinical, immune, and microbiome traits of gingivitis and peri-implant mucositis. J Dent Res 96:47–55. doi:10.1177/0022034516668847.
156. Maeda Y, Kurakawa T, Umemoto E, Motooka D, Ito Y, Gotoh K, Hirota K, Matsushita M, Furuta Y, Narazaki M, Sakaguchi N, Kayama H, Nakamura S, Iida T, Saeki Y, Kumanogoh A, Sakaguchi S, Takeda K. 2016. Dysbiosis contributes to arthritis development via activation of autoreactive T Cells in the intestine. Arthritis Rheumatol 68:2646–2661. doi:10.1002/art.39783.
157. Gottschick C, Deng Z-L, Vital M, Masur C, Abels C, Pieper DH, Rohde M, Mendling W, Wagner-Döbler I. 2017. Treatment of biofilms in bacterial vaginosis by an amphoteric tenside pessary-clinical study and microbiota analysis. Microbiome 5:119. doi:10.1186/s40168-017-0326-y.
158. Onderdonk AB, Delaney ML, Fichorova RN. 2016. The human microbiome during bacterial vaginosis. Clin Microbiol Rev 29:223–238. doi:10.1128/CMR.00075-15.
159. Schleicher L, Herdan S, Fritz G, Trautmann A, Seifert J, Steuber J. 2021. Central carbon metabolism, sodium-motive electron transfer, and ammonium formation by the vaginal pathogen *Prevotella bivia*. Int J Mol Sci 22:11925. doi:10.3390/ijms222111925.
160. Aroutcheva A, Ling Z, Faro S. 2008. *Prevotella bivia* as a source of lipopolysaccharide in the vagina. Anaerobe 14:256–260. doi:10.1016/j.anaerobe.2008.08.002.
161. Gilbert NM, Lewis WG, Lewis AL. 2013. Clinical features of bacterial vaginosis in a murine model of vaginal infection with *Gardnerella vaginalis*. PLoS One 8:e59539. doi:10.1371/journal.pone.0059539.
162. Anahtar MN, Byrne EH, Doherty KE, Bowman BA, Yamamoto HS, Soumillon M, Padavattan N, Ismail N, Moodley A, Sabatini ME, Ghebremichael MS, Nusbaum C, Huttenhower C, Virgin HW, Ndung'u T, Dong KL, Walker BD, Fichorova RN, Kwon DS. 2015. Cervicovaginal bacteria are a major modulator of host inflammatory responses in the female genital tract. Immunity 42:965–976. doi:10.1016/j.immuni.2015.04.019.
163. Gosmann C, Anahtar MN, Handley SA, Farcasanu M, Abu-Ali G, Bowman BA, Padavattan N, Desai C, Droit L, Moodley A, Dong M, Chen Y, Ismail N, Ndung'u T, Ghebremichael MS, Wesemann DR, Mitchell C, Dong KL, Huttenhower C, Walker BD, Virgin HW, Kwon

DS. 2017. *Lactobacillus*-deficient cervicovaginal bacterial communities are associated with increased HIV acquisition in young south african women. Immunity 46:29–37. doi:10.1016/j.immuni.2016.12.013.

164. Gilbert NM, Lewis WG, Li G, Sojka DK, Lubin JB, Lewis AL. 2019. *Gardnerella vaginalis* and *Prevotella bivia t*rigger distinct and overlapping phenotypes in a mouse model of bacterial vaginosis. J Infect Dis 220:1099–1108. doi:10.1093/infdis/jiy704.
165. Muzny CA, Taylor CM, Swords WE, Tamhane A, Chattopadhyay D, Cerca N, Schwebke JR. 2019. An updated conceptual model on the pathogenesis of bacterial vaginosis. J Infect Dis 220:1399–1405. doi:10.1093/infdis/jiz342.
166. Pybus V, Onderdonk AB. 1997. Evidence for a commensal, symbiotic relationship between *Gardnerella vaginalis* and *Prevotella bivia* involving ammonia: potential significance for bacterial vaginosis. J Infect Dis 175:406–413. doi:10.1093/infdis/175.2.406.

# Chapter 2 - Anoxic cell rupture of *Prevotella bryantii* by high-pressure homogenization protects the $Na^+$-translocating NADH:quinone oxidoreductase from oxidative damage

**Lena Schleicher[1], Günter Fritz[1], Jana Seifert[2], Julia Steuber[1*]**

[1]Institute of Microbiology, University of Hohenheim, Stuttgart, Germany

[2]Institute of Animal Science, University of Hohenheim, Stuttgart, Germany

* Correspondence: Julia Steuber, julia.steuber@uni-hohenheim.de, +49 711 459 22228

Archives of Microbiology
https://doi.org/10.1007/s00203-019-01805-x

SHORT COMMUNICATION

# Anoxic cell rupture of *Prevotella bryantii* by high-pressure homogenization protects the $Na^+$-translocating NADH:quinone oxidoreductase from oxidative damage

**Lena Schleicher[1] · Günter Fritz[1] · Jana Seifert[2] · Julia Steuber[1]**

Received: 3 September 2019 / Revised: 20 December 2019 / Accepted: 31 December 2019


**Abstract** Respiratory NADH oxidation in the rumen bacterium *Prevotella bryantii* is catalyzed by the $Na^+$-translocating NADH:quinone oxidoreductase (NQR). A method for cell disruption and membrane isolation of *P. bryantii* under anoxic conditions using the EmulisFlex-C3 homogenizer is described. We compared NQR activity and protein yield after oxic and anoxic cell disruption by the EmulsiFlex, by ultrasonication, and by glass beads treatment. With an overall membrane protein yield of 50 mg $L^{-1}$ culture and a NADH oxidation activity of 0.8 µmol $min^{-1}$ $mg^{-1}$, the EmulsiFlex was the most efficient method. Anoxic preparation yielded fourfold higher NQR activity compared to oxic preparation. *P. bryantii* lacks genes coding for superoxide dismutases and cell extracts do not exhibit superoxide dismutase activity. We propose that inactivation of NQR during oxic cell rupture is caused by superoxide, which accumulates in *P. bryantii* extracts exposed to air. Anoxic cell rupture is indispensable for the preparation of redox-active proteins and enzymes such as NQR from *P. bryantii*.

**Keywords** EmulsiFlex-C3 homogenizer · *Prevotella bryantii* · Cell rupture · $Na^+$-translocating NADH:quinone oxidoreductase (NQR) · Superoxide

## Short Communication

*Prevotella bryantii* is a Gram-negative obligate anaerobe, which is found in anoxic zones of the intestine, such as the rumen of cows (Deusch and Seifert 2015). During the fermentation of sugar (Hackmann et al. 2017), NADH oxidation is catalyzed by a single enzyme, the $Na^+$-NADH:quinone oxidoreductase (NQR) (Deusch et al. 2019). The NQR sodium pump has been mainly studied in facultative anaerobes, such as *Vibrio cholerae* (Steuber et al. 2015). In *V. cholerae*, respiration in the presence of $O_2$ led to the formation of superoxide (Muras et al. 2016), which inactivates the NQR (Pfenninger-Li et al. 1996; Steuber et al. 1997), due to modifications of its redox cofactors (flavins and iron-sulphur centers) (Macomber and Imlay 2009). In aerobes, this is prevented by protective enzymes such as superoxide dismutase (SOD). Here, we addressed the putative inactivation of *P. bryantii* NQR by oxidative damage by comparing its activity in oxically and anoxically prepared membranes. We also compared overall yield of membrane proteins after cell rupture by the EmulsiFlex, by ultrasonication, or by treatment with glass beads. *P. bryantii* NQR is prone to oxidative damage during preparation of cellular extracts since *P. bryantii* lacks SOD, as confirmed by enzymatic tests.

The very first and most critical step in the purification of proteins is the breakage of cells. Different methods can be used to disrupt microorganisms, like enzymatic lysis by destabilizing the cell wall. Alternatively, ultrasonication or compulsion followed by rapid relieve of pressure can be performed. The latter is achieved with the help of the EmulsiFlex-C3 homogenizer (Avestin Inc., Ottawa, Canada) (Tong 2011). Unlike lysis by enzymes or by ultrasonication, which can be performed in an anaerobic chamber under exclusion of $O_2$, high-pressure cell rupture under anoxic conditions, required for preparation of oxygen-labile components of cells, is

Communicated by Erko Stackebrandt.

**Electronic supplementary material** The online version of this article (https ://doi.org/10.1007/s0020 3-019-01805 -x) contains supplementary material, which is available to authorized users.

* Julia Steuber

julia.steuber@uni-hohenheim.de

[1] Institute of Microbiology, University of Hohenheim, Stuttgart, Germany

[2] Institute of Animal Science, University of Hohenheim, Stuttgart, Germany

difficult to achieve. We established a method for anoxic rupture of *Prevotella bryantii* $B_14$ using the EmulsiFlex-C3 homogenizer. The protocol for anoxic cell disruption involves the use of an anaerobic chamber (COY laboratory products) and special equipment (supplementary data, supplementary Fig. S1). Buffers were made anoxic by flushing with $N_2$ before entering the chamber. Outside of the chamber, the anoxic suspension was handled in gas-tight vials or syringes. Cells were cultivated in anoxic medium supplemented with the reducing agent L-cystein HCl (1 g $L^{-1}$) and resazurin (0.5 µM, added from a 0.5 mM stock solution in $H_2O$). Resazurin is a redox indicator, which turns pink if $O_2$ is present, but remains colorless if anoxic and reducing conditions are maintained during handling of cell suspensions (Uchino 2013). The continuous, optical inspection of media and cellular extracts is important. If cell suspensions and cellular extracts turn pink, the overall procedure is not anoxic any longer, and samples must be discarded. It is not recommended to re-reduce the solutions by adding L-cystein HCl. For harvesting the cells, the culture (OD at 600 nm, 2.5–3.0) grown in gas-tight serum bottles (1 L) was transferred into the anaerobic chamber and filled into gas-tight beakers for subsequent centrifugation outside of the anaerobic chamber (9000 g, 30 min, 4 °C). Afterwards, beakers were placed into the anaerobic chamber, and cells were resuspended twice in anoxic cell lysis buffer (20 mM Tris-$H_2SO_4$ pH 7.5 with 50 mM $K_2SO_4$). 10 g of cells (wet weight) was resuspended in 30 mL 20 mM Tris–$H_2SO_4$ pH 7.5, containing 50 mM K $_2SO_4$, 5 mM M $gSO_4$, 1 mM dithiothreitol, 1 mM phenylmethylsulfonylfluorid, 0.1 mM diisopropyl fluorophosphate and traces of DNase I (Roche) (Deusch et al. 2019). A detailed, step-by-step protocol, which is a modification of the protocol described by the manufacturer (https ://www.avesti n.com/emuls iflex -c3.htm) and by (Tong 2011), is given in the electronic supplementary material (Fig. S1). Importantly, the EmulsiFlex must be modified with a plug, which replaces the screw cap of the funnel (Fig. 1). In this plug three plastic disposable syringes are inserted (without stamp) and closed with rubber plugs. A nitrogen gas bottle is connected to one syringe with a cannula to flush the funnel continuously with $N_2$. Continuous flow of $N_2$ bubbles is monitored with the help of a tubing ending in a beaker filled with water. One syringe is used to inject anoxic buffer and cell suspensions into the funnel. To disrupt the cells, the outlet tubing is connected to a cannula, which in turn is connected to a syringe in the plug on top of the funnel. In this way, the cells run in cycles through the device and the pressure can be increased to 20.000 psi for 10 min. Afterwards, the outlet tubing is connected with a cannula to a gas-tight serum bottle (Fig. S1). To operate the device oxically again, one simply has to remove the plug.

The method described above was compared to methods based on glass beads (Taskova et al. 2006) or ultrasonication with a sonotrode (Sonopuls 3100 MS 73 Bandelin; 4 min ultrasonication with 10.5 s pulse and 20 s resting time alternately; 75% amplitude; 2.9 kJ). For oxic or anoxic cell rupture by ultrasonication, the sonotrode was inserted into resuspended cells exposed to air, or flushed with N2, respectively. For glass bead cell disruption, the cells were resuspended in a 50 mL falcon tube and glass beads (Ø 5 mm) were added. Cells were disrupted by vortexing for 10 min. For anoxic cell disruption with glass beads, this procedure was done in the anaerobic chamber. Membranes were obtained from cell extracts by ultracentrifugation as described previously (Deusch et al. 2019). In subsequent steps, anoxically prepared cell fractions and membranes were never exposed to air, but always manipulated in the anaerobic chamber.

NQR activity with oxically or anoxically prepared membranes of *P. bryantii* (80–100 µg protein) was tested by monitoring the NADH oxidation at 340 nm photometrically, with 100 µM NADH and 100 µM ubiquinone-1 in 20 mM potassium phosphate buffer with

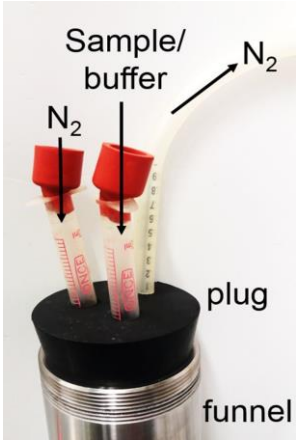


**Figure 1** EmulsiFlex-C3 funnel for anoxic cell disruption. The screw cap is removed and replaced by a plug, which containes three plastic disposable syringes. The stamps of the syringes are removed and rubber plugs are inserted on top instead. One syringe is connected to a nitrogen bottle, the other syringe is required for the outlet of N $_2$. The third syringe is used to inject anoxic buffer or sample into the system

200 mM NaCl at pH 7.5 (Juárez et al. 2009). This experiment was repeated three times for oxically and anoxically prepared membranes (Table 1). Table 1 shows the overall membrane protein yield [determined by the BCA method (Smith et al. 1985)] and the specific NADH oxidation activity of membranes from oxic or anoxic crude extracts from 5 g (wet weight) *P. bryantii* cells. The EmulsiFlex is the most efficient method to

**Table 1** Comparison of protein yield and specific NADH oxidation activity of *P. bryantii* membranes. Cells were disrupted with the EmulsiFlex- C3 homogenizer, ultrasonication or glass beads, and under oxic or anoxic conditions, respectively.

| | Cell rupture method | | | | | |
|---|---|---|---|---|---|---|
| | EmulsiFlex-C3 homogenizer | | Ultrasonication | | Glass beads | |
| | + $O_2$ | −$O_2$ | + $O_2$ | −$O_2$ | +$O_2$ | −$O_2$ |
| Protein yield membrane [mg] from 5 g cells (wet weight) | 50 | 40 | 3 | 3 | 2 | 3 |
| Specific activity of NADH oxidation [µmol $min^{-1}$ $mg^{-1}$] of membranes | 0.20 ± 0.02 | 0.80 ± 0.03 | 0.22 ± 0.01 | 0.46 ± 0.02 | 0.15 ± 0.01 | 0.21 ± 0.02 |

break up *P. bryantii* cells. The protein yield is 40–50 mg, which is more than 10 times higher than the protein yield with ultrasonication or glass beads (2–3 mg). In oxic crude extracts, the specific NADH oxidation activity is always similar (0.15–0.22 µmol $min^{-1}$ $mg^{-1}$), independent of the disruption method. In contrast, anoxic cell disruption with the EmulsiFlex yields a fourfold higher activity (0.8 µmol $min^{-1}$ $mg^{-1}$) compared to oxic cell rupture. Anoxic cell disruption with ultrasonication results in a twofold higher activity of extracts (0.46 µmol $min^{-1}$ $mg^{-1}$), compared to the oxically prepared extracts. Anoxic preparation does not result in increased activities if cells are broken with glass beads. These results demonstrate that cell disruption with the EmulsiFlex-C3 homogenizator is the most efficient method for *P. bryantii* cell rupture with respect to NQR activity and overall membrane protein yield. Moreover, up-scaling of the process is easy, since the EmulsiFlex is a continuously operated disruption system where cell suspensions can be loaded repeatedly into the sample cylinder. Up-scaling is easy both under oxic or anoxic conditions, where constant flushing with $N_2$ is possible. In contrast, cell rupture by e.g. French Press has a fixed maximum volume of cell suspension. For anoxic rupture with the French Press all suspensions must be transferred into the pressure cell in the anaerobic chamber, preventing the continuous up-scaling of the process. We considered that diminished NQR activity in oxically prepared membranes is caused by the inactivation of the enzyme by superoxide. In many organisms, superoxide is removed with the help of superoxide dismutases. For example, *V. cholerae* possesses three SODs (accession numbers UNIPROT: A0A0H3AKF7, A0A0H3AJ73, A0A0H3AIV1) protecting the organism from superoxide. A search for SOD homologs using the UNIPROT and KEGG databases in the *P. bryantii* genome (https://www.ncbi.nlm.nih.gov/Taxonomy/Browser/wwwtax.cgi?lvl=0&id=752555) was not successful. To confirm the absence of SOD in *P. bryantii*, we conducted SOD enzyme activity measurements with a superoxide dismutase activity assay kit (BioVision). Here, xanthine oxidase is used to produce superoxide anions. With these superoxide anions a water-soluble formazan dye is formed, which absorbs at 450 nm. This reaction is prevented by SODs. The kit is designed for an endpoint measurement with a microplate reader. We used a 0.5 cm quartz cuvette and a UV/VIS spectrophotometer (SPECORD® S600 AnalytikJena) to follow the absorbance at 450 nm over time. Reaction is started by adding 50 µl of the enzyme working solution, containing the xanthine oxidase (Fig. 2a). By adding 100 U SOD (from bovine, Sigma) the formation of formazan is prevented completely (Fig. 2b). If *P. bryantii* crude extract (0.13 mg protein) is added, no inhibition of formazan production is observed (Fig. 2c). We also tested *P. bivia* crude extracts for SOD activity. Unlike *P. bryantii*, *P. bivia* is expected to show SOD activity since a UNIPROT search revealed the presence of a SOD homolog (accession numbers: I4Z9K0_9BACT). Indeed, *P. bivia* crude extract (0.13 mg protein) exhibits SOD activity (Fig. 2d).

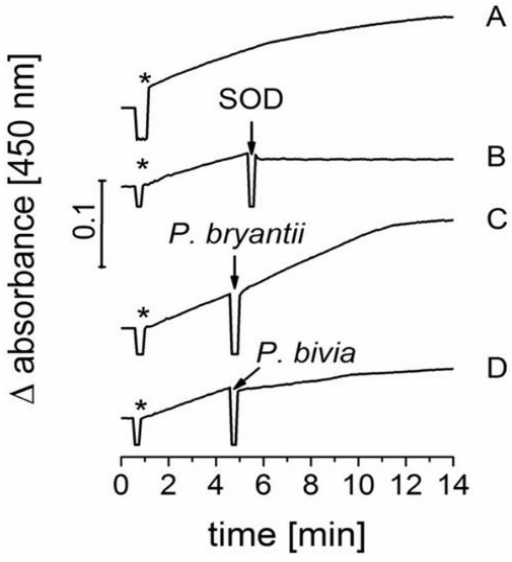

**Figure 2** *P. bryantii* cell extracts do not exhibit superoxide dismutase activity. Superoxide dismutase activity was analyzed by monitoring the formation of formazan (450 nm) by superoxide anions produced by xanthine oxidase added at the start of the reaction, indicated by asterisks (*). After ~ 4 min crude extracts (0.13 mg) were added to analyze the SOD activity. **A** no addition. **B** Addition of 100 U bovine SOD. **C** with *P. bryantii* crude extract. **D** with *P. bivia* crude extract.

## Acknowledgements

Open Access funding provided by Projekt DEAL. This work was supported by grants from the Deutsche Forschungsgemeinschaft to Günter Fritz (FR1488/8-1), Julia Steuber (FR1321/7-1) and Jana Seifert (SE2059/3-1).

## Compliance with Ethical Standards

**Conflict of Interest** The authors declare that they have no conflict of interest.



## References

Deusch S, Seifert J (2015) Catching the tip of the iceberg - evaluation of sample preparation protocols for metaproteomic studies of the rumen microbiota. Proteomics 15:3590–3595. https ://doi. org/10.1002/pmic.20140 0556

Deusch S, Bok E, Schleicher L, Seifert J, Steuber J (2019) Occurrence and function of the $Na^+$-translocating NADH: quinone oxidoreductase in *Prevotella spp*. Microorganisms. https ://doi. org/10.3390/micro organ isms7 05011 7

Hackmann TJ, Ngugi DK, Firkins JL, Tao J (2017) Genomes of rumen bacteria encode atypical pathways for fermenting hexoses to short chain fatty acids. Environ Microbiol 19:4670–4683. https ://doi. org/10.1111/1462-2920.13929

Juárez O, Athearn K, Gillespie P, Barquera B (2009) Acid residues in the transmembrane helices of the N $a^+$-pumping NADH:quinone oxidoreductase from *Vibrio cholerae* involved in sodium translocation. Biochemistry 48:9516–9524. https ://doi. org/10.1021/bi900 845y

Macomber L, Imlay JA (2009) The iron-sulfur clusters of dehydratases are primary intracellular targets of copper toxicity. Proc Natl Acad Sci USA 106:8344–8349. https ://doi.org/10.1073/pnas.08128 08106

Muras V, Dogaru-Kinn P, Minato Y, Häse CC, Steuber J (2016) The $Na^+$-translocating NADH:quinone oxidoreductase enhances oxidative stress in the cytoplasm of *Vibrio cholerae*. J Bacteriol 198:2307–2317. https ://doi.org/10.1128/JB.00342 -16

Pfenninger-Li XD, Albracht SP, van Belzen R, Dimroth P (1996) NADH:ubiquinone oxidoreductase of *Vibrio alginolyticus*: purification, properties, and reconstitution of the $Na^+$ pump. Biochemistry 35:6233–6242. https ://doi.org/10.1021/bi953 032l

Smith PK, Krohn RI, Hermanson GT, Mallia AK, Gartner FH, Provenzano MD, Fujimoto EK, Goeke NM, Olson BJ, Klenk DC (1985) Measurement of protein using bicinchoninic acid. Anal Biochem 150:76–85. https ://doi.org/10.1016/0003-2697(85)90442 -7

Steuber J, Krebs W, Dimroth P (1997) The $Na^+$-translocating NADH:ubiquinone oxidoreductase from *Vibrio alginolyticus*–redox states of the FAD prosthetic group and mechanism of $Ag^+$ inhibition. Eur J Biochem 249:770–776. https ://doi. org/10.1111/j.1432-1033.1997.t01-2-00770 .x

Steuber J, Vohl G, Muras V, Toulouse C, Claußen B, Vorburger T, Fritz G (2015) The structure of N $a^+$-translocating of NADH:ubiquinone oxidoreductase of *Vibrio cholerae*: implications on coupling between electron transfer and $Na^+$ transport. Biol Chem 396:1015–1030. https ://doi.org/10.1515/hsz-2015-0128

Taskova RM, Zorn H, Krings U, Bouws H, Berger RG (2006) A comparison of cell wall disruption techniques for the isolation of intracellular metabolites from *Pleurotus* and *Lepista sp*. Z Naturforsch C J Biosci 61:347–350. https ://doi.org/10.1515/znc-2006-5-608

Tong Z (2011) How to use an Avestin Emulsiflex C3 homogenizer to disrupt cells. Bio-Protocol. https: //doi.org/10.21769/BioPro toc.1 1

Uchino Y (2013) A simple preparation of liquid media for the cultivation of strict anaerobes. J Pet Environ Biotechnol. https ://doi. org/10.4172/2157-7463.S3-001

## Supplementary Material

Archives of Microbiology
Supplementary Data

# Anoxic cell rupture of *Prevotella bryantii* by high-pressure homogenization protects the $Na^+$- translocating NADH:quinone oxidoreductase from oxidative damage

**Lena Schleicher[1], Günter Fritz[1], Jana Seifert[2], Julia Steuber[1]***

[1]Institute of Microbiology, University of Hohenheim, Stuttgart, Germany
[2]Institute of Animal Science, University of Hohenheim, Stuttgart, Germany

In the following, a step-by-step description for anoxic operation of the EmulsiFlex-C3 homogenizer is given. This process is illustrated in fig. S2.1.

How to prepare the Emulsiflex for anoxic cell rupture (Fig. S2.1A)

1. Drill three holes (Ø 0.9 cm) into the black plug (Ø 6.4 cm at the top, Ø 5.4 cm at the bottom) which replaces the screw cap of the funnel
2. Insert three 2 mL plastic disposable syringes into the black plug
3. Remove stamps of plastic syringes and close two of the cylinders with red rubber plugs
4. Seal the black plug tight to the funnel with cable ties
5. Connect the nitrogen gas bottle to the first syringe cylinder with the help of a cannula inserted into the red rubber plug
6. Connect the open syringe cylinder with a tubing, ending up in a beaker with water
7. Turn on nitrogen
8. Check for nitrogen bubbles in the beaker and adjust pressure if necessary
9. Flush the funnel (10-15 min) with nitrogen
10. Connect the outlet tubing with a steel cannula (Ø 2 mm, length 6 cm)
11. Switch on the Emulsiflex
12. Switch on the cooling system

Emulsiflex is ready for anoxic cell disruption

How to handle anoxic buffers and suspensions for subsequent cell rupture

1. In the anaerobic chamber, anoxic buffers and cell suspension are ready for cell rupture
2. 2x 50 mL cell lysis buffer is filled into glass syringes and the cannula is sealed with a rubber stopper
3. Cell suspension is filled into a glass syringe and the cannula is also sealed with a rubber stopper
4. Filled syringes are taken out of the anaerobic chamber and placed on ice to cool

Buffers and cells are now ready for the next steps

How to disrupt cells (Fig. S2.1A, B)

1. Please note that the funnel is flushed with $N_2$ continuously
2. Inject 50 mL of anoxic cell lysis buffer into the funnel by sticking with the cannula through the red rubber plug on top of the free (third) syringe cylinder.
3. Turn red stop knob of device clockwise and push green knob to start pump
4. Pump anoxic cell lysis buffer through the system for equilibration
5. Press red stop knob to stop the device
6. Inject anoxic cell suspension into the funnel through the red rubber plug of the free (third) syringe cylinder
7. Connect cannula from outlet tubing with the free (third) syringe cylinder
8. Start pump
9. Let the cell suspension run through the tubing back to the funnel (see Fig. 2.1B)
10. Turn on air pressure. Air pressure at 40 psi, gauge pressure at ≤ 20.000 psi depending on organism

11. To disrupt *P. bryantii* cells maximum pressure (20.000 psi) is applied for 10 min

How to collect broken cells (Fig. S2.1C)

1. Press red stop knob to stop the device
2. Turn off air pressure
3. Remove the outlet tubing from the funnel and connect it by a cannula to a gas-tight serum bottle. This serum bottle was sealed with a rubber cap fastened with an aluminium ring, and was flushed with $N_2$. Insert an open cannula into the plug while filling the bottle with crude extract to avoid overpressure.
4. Start pump
5. Pump the disrupted cells out of the device into the gas tight serum bottle
6. Remove open cannula
7. The crude cell extract in the gas-tight serum bottle is placed into the anaerobic chamber for subsequent fractionation and characterization

Cleaning of Emulsiflex

1. Black plug with syringe cylinders is dismantled and cleaned first with 80 % ethanol, then with deionized water
2. All cannulas and tubings are removed and cleaned first with 80 % ethanol, then with deionized water
3. EmulsiFlex is flushed with deionized water, 500 mM NaOH, deionized water and finally with 80 % ethanol
4. Leave 1/3 of a funnel volume of 80 % ethanol in the funnel for storage

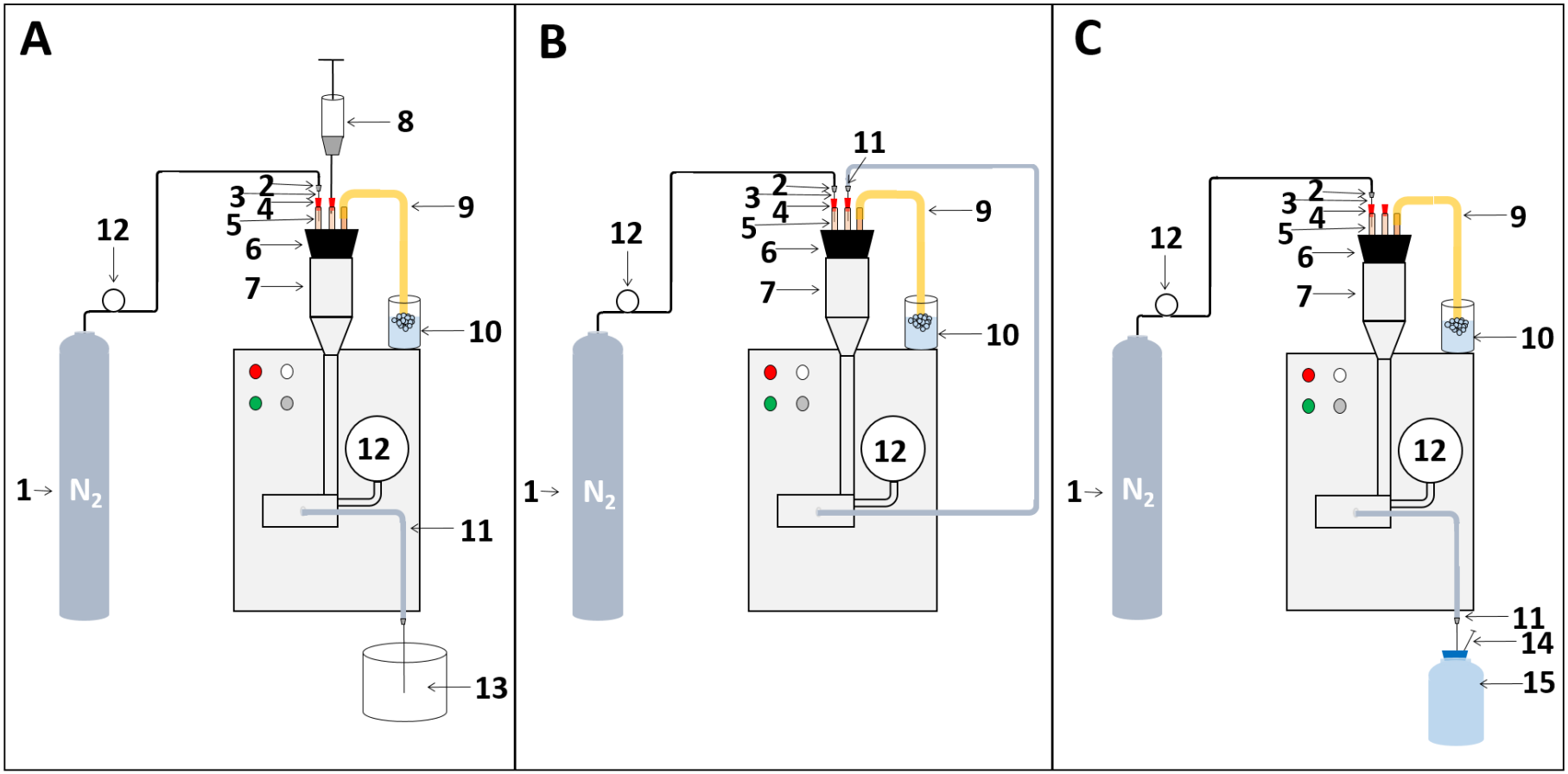


**Supplementary figure S1** Anoxic cell disruption with the Emulsiflex. Throughout the process, the N 2 gas bottle (1) is connected to the funnel, which is continuously flushed with N 2. A) Assembly for equilibration of the device with anoxic cell lysis buffer. The sample outlet tubing (11) is connected to the waste (13). B) Assembly for cell disruption. The sample outlet tubing (11) is connected to a syringe cylinder (5) to run the sample through the device and back to the funnel. C) Collection of the disrupted cells. The sample outlet tubing (11) is connected to an anoxic gas-tight serum bottle (15). 1: nitrogen gas bottle, 2: adapter for tubing and cannula, 3: steel cannula, 4: red rubber plug, 5: syringe cylinder (outer part of syringe, without stamp), 6: black plug, 7: funnel (sample container), 8: syringe with buffer or cell suspension, 9: outlet tubing for nitrogen, 10: beaker with water, 11: outlet tubing for broken cells, 12: pressure gauge, 13: waste, 14: open cannula, 15: serum bottle filled with $N_2$.

# Chapter 3 - A sodium-translocating module linking succinate production to formation of a membrane potential in *Prevotella bryantii*

**Lena Schleicher*†, Andrej Trautmann*‡, Dennis P. Stegmann*†, Günter Fritz*†, Jochem Gätgens¶, Michael Bott¶, Sascha Hein§, Jörg Simon§, Jana Seifert*‡, Julia Steuber*†#**

* HoLMiR- Hohenheim Center for Livestock Microbiome Research, University of Hohenheim, Leonore-Blosser-Reisen-Weg 3, 70599 Stuttgart, Germany

† Institute of Biology, University of Hohenheim, Garbenstraße 30, 70599 Stuttgart, Germany

‡ Institute of Animal Science, University of Hohenheim, Emil-Wolff-Straße 8, 70599 Stuttgart, Germany

§ Microbial Energy Conversion and Biotechnology, Department of Biology, Technical University of Darmstadt, Schnittspahnstraße 10, 64287 Darmstadt, Germany

¶ Institute of Bio- and Geosciences, IBG-1: Biotechnology, Forschungszentrum Jülich, 52425 Jülich, Germany

# Correspondence: Julia Steuber, julia.steuber@uni-hohenheim.de, +49 711 459 22228

AMERICAN SOCIETY FOR MICROBIOLOGY | Applied and Environmental Microbiology®

ENVIRONMENTAL MICROBIOLOGY

# A Sodium-Translocating Module Linking Succinate Production to Formation of Membrane Potential in *Prevotella bryantii*

**Lena Schleicher,[a,b] Andrej Trautmann,[a,c] Dennis P. Stegmann,[a,b] Günter Fritz,[a,b] Jochem Gätgens,[e] Michael Bott,[e] Sascha Hein,[d] Jörg Simon,[d] Jana Seifert,[a,c] Julia Steuber[a,b]**

[a] Hohenheim Center for Livestock Microbiome Research, University of Hohenheim, Stuttgart, Germany
[b] Institute of Biology, University of Hohenheim, Stuttgart, Germany
[c] Institute of Animal Science, Unviersity of Hohenheim, Stuttgart, Germany
[d] Microbial Energy Conservation and Biotechnology, Technical University of Darmstadt, Darmstadt, Germany
[e] Institute of Bio- and Geoscience, IBG-1: Biotechnology, Forschungszentrum Jülich, Jülich, Germany

**Abstract** Ruminants such as cattle and sheep depend on the breakdown of carbohydrates from plant-based feedstuff, which is accomplished by the microbial community in the rumen. Roughly 40% of the members of the rumen microbiota belong to the family *Prevotellaceae*, which ferments sugars to organic acids such as acetate, propionate, and succinate. These substrates are important nutrients for the ruminant. In a metaproteome analysis of the rumen of cattle, proteins that are homologous to the $Na^+$-translocating NADH:quinone oxidoreductase (NQR) and the quinone:fumarate reductase (QFR) were identified in different *Prevotella* species. Here, we show that fumarate reduction to succinate in anaerobically growing *Prevotella bryantii* is coupled to chemiosmotic energy conservation by a supercomplex composed of NQR and QFR. This sodium-translocating NADH:fumarate oxidoreductase (SNFR) supercomplex was enriched by blue native PAGE (BN-PAGE) and characterized by in-gel enzyme activity staining and mass spectrometry. High NADH oxidation (850 nmol $min^{-1}$ $mg^{-1}$), quinone reduction (490 nmol $min^{-1}$ $mg^{-1}$), and fumarate reduction (1,200 nmol $min^{-1}$ $mg^{-1}$) activities, together with high expression levels, demonstrate that SNFR represents a charge-separating unit in *P. bryantii*. Absorption spectroscopy of SNFR exposed to different substrates revealed intramolecular electron transfer from the flavin adenine dinucleotide (FAD) cofactor in NQR to heme *b* cofactors in QFR. SNFR catalyzed the stoichiometric conversion of NADH and fumarate to $NAD^+$ and succinate. We propose that the regeneration of $NAD^+$ in *P. bryantii* is intimately linked to the buildup of an electrochemical gradient which powers ATP synthesis by electron transport phosphorylation.

**Importance** Feeding strategies for ruminants are designed to optimize nutrient efficiency for animals and to prevent energy losses like enhanced methane production. Key to this are the fermentative reactions of the rumen microbiota, dominated by *Prevotella* spp. We show that succinate formation by *P. bryantii* is coupled to NADH oxidation and sodium gradient formation by a newly described supercomplex consisting of $Na^+$-translocating NADH:quinone oxidoreductase (NQR) and fumarate reductase (QFR), representing the sodium-translocating NADH:fumarate oxidoreductase (SNFR) supercomplex. SNFR is the major charge-separating module, generating an electrochemical sodium gradient in *P. bryantii*. Our findings offer clues to the observation that use of fumarate as feed additive does not significantly increase succinate production, or decrease methanogenesis, by the microbial community in the rumen.

**Citation** Schleicher L, Trautmann A, Stegmann DP, Fritz G, Gätgens J, Bott M, Hein S, Simon J, Seifert J, Steuber J. 2021. A sodium-translocating module linking succinate production to formation of membrane potential in *Prevotella bryantii*. Appl Environ Microbiol 87:e01211-21. https://doi.org/10.1128/AEM.01211-21.

**Editor** Alfons J. M. Stams, Wageningen University



Address correspondence to Julia Steuber, julia.steuber@uni-hohenheim.de.

**Received** 25 June 2021
**Accepted** 16 August 2021
**Accepted manuscript posted online** 1 September 2021
**Published** 14 October 2021

**Keywords** $Na^+$-translocating NADH:quinone oxidoreductase, fumarate reductase, supercomplex, *Prevotella bryantii*, rumen, anaerobic respiration

Human nutrition heavily depends on ruminants such as cattle and sheep, which require nutrients provided by their rumen microbiota in the course of anoxic degradation of feed (1). In the rumen, a consortium of anaerobic microorganisms provides enzymes and metabolic pathways for the degradation of plant-based feed. The rumen microbiome is highly similar across the globe (2) and offers energy-rich substrates such as acetate, succinate, and propionate to the ruminant. These carboxylic acids are typical electron sinks released by fermenting bacteria to maintain their internal redox balance. The complete breakdown of complex organic matter such as cellulose under anoxic conditions in the rumen requires primary and secondary fermenting bacteria, as well as methanogenic archaea (3). In fact, the formation of methane is the main electron sink in the ruminal degradation of carbohydrates. Its release to the atmosphere diminishes the energy available to the ruminant (4) and has a negative impact on global climate (5). Members of the family *Prevotellaceae* represent the most abundant organisms in the rumen (1, 4). The metabolism of *Prevotella* spp. is expected to have a strong impact on overall carbon flux in the rumen ecosystem and on the nutrition of the host, the ruminant.

In the past, *Prevotella* spp. were thought to depend exclusively on ATP generation by substrate-level phosphorylation (6). Proteome analysis of the rumen microbiota from dairy cows (7) and studies with *Prevotella bryantii* (7), *Prevotella copri* (8) and *Bacteroides fragilis* (9) suggested an important catabolic role of two enzymes, the $Na^+$-translocating NADH:quinone oxidoreductase (NQR) and the fumarate:menaquinol oxidoreductase (QFR) producing succinate, which is excreted from the cells. NQR is a respiratory enzyme composed of six subunits (NqrABCDEF) embedded in the inner membrane of several Gram-negative bacteria, including human pathogens such as *Vibrio cholerae* (10). NQR from *P. bryantii* exhibits high sequence similarity to the *V. cholerae* NQR (7), including the conserved domains for the binding of six cofactors: one flavin adenine dinucleotide (FAD), two iron-sulfur centers, one riboflavin, and two covalently bound flavin mononucleotides (FMNs) (10, 11). The NqrF subunit harbors the FAD and is the entry point for the electrons into the protein complex, oxidizing NADH to $NAD^+$. NqrA was shown to interact with ubiquinone-8 (12) and is therefore most likely responsible for the reduction of quinone to quinol as a final step of the electron transfer within NQR. Exergonic NADH: quinone oxidoreduction drives endergonic transport of sodium ions from the cytoplasm to the periplasm through NqrB (11), resulting in an electrochemical $Na^+$ gradient. The *P. bryantii* QFR is highly similar to the type B class of QFRs (7, 13), exemplified by the enzyme from *Wolinella succinogenes*. Sequence comparisons suggest that the subunit FrdA contains one covalently bound flavin close to the fumarate binding site and that FrdB has three iron-sulfur clusters. FrdA and FrdB presumably interact with membranebound FrdC, which contains two hemes *b* and offers a binding site for menaquinol (14). QFR operates in fumarate respiration with NADH as an electron donor under generation of a transmembrane voltage (15). QFR also participates in the reductive branch of mixedacid fermentation leading to succinate (16).

Here, we demonstrate the existence of a sodium-translocating supercomplex consisting of NQR and QFR in the membrane of *P. bryantii* which we term SNFR (sodium-translocating NADH:fumarate oxidoreductase). Respiratory supercomplexes in prokaryotes (17, 18) and in the inner membrane of mitochondria (19) have been known for many years. In *P. bryantii*, the SNFR couples NADH oxidation with reduction of fumarate to succinate to generate a membrane potential. The implications of our findings for the metabolism of *P. bryantii* and for carbon flux in the rumen ecosystem are discussed.

## Results

**Reduction of fumarate during glucose fermentation by *P. bryantii*.** The presence of gene clusters coding for membrane-bound redox enzymes (see Fig. S1 in the supplemental material) raised the question of the composition and metabolic function of an electron transport chain in *P. bryantii*. In proteomic studies with *P. bryantii* (7), NQR and QFR subunits were identified which exhibit sequence similarity to *V. cholerae* NQR and *W. succinogenes* QFR, respectively (Fig. S2 and S3). *P. bryantii* lacks genes coding for hydrogenases and formate dehydrogenases. Further electron acceptors to be considered are nitrate, sulfate, and elemental sulfur. The genome of *P. bryantii* (Joint Genome Institute Integrated Microbial Genomes [JGI IMG]) lacks genes coding for enzymes involved in dissimilatory nitrate reduction (nitrate reductase, nitrite reductase, $N_2O$ reductase, and NO reductase), sulfate reduction (ATP sulfurylase, phosphoadenosine phosphosulfate reductase, and sulfite reductase), or sulfur reduction (polysulfide reductase). Genes conferring the ability to utilize acceptors such as manganese, iron, and cobalt are also absent in *P. bryantii*. These findings are in accordance with our previous proteomic study (7). Thus, only fumarate is predicted based on annotation to serve as a terminal electron acceptor in *P. bryantii*, which is reduced by quinol:fumarate oxidoreductase (QFR).

QFR is encoded by the *frdCAB* operon (Fig. S1). The complex is composed of FrdA and FrdB, oriented toward the cytoplasm, and the membrane-bound FrdC subunit. This QFR belongs to the type B class of quinol:fumarate oxidoreductases (13). During growth of *P. bryantii* with

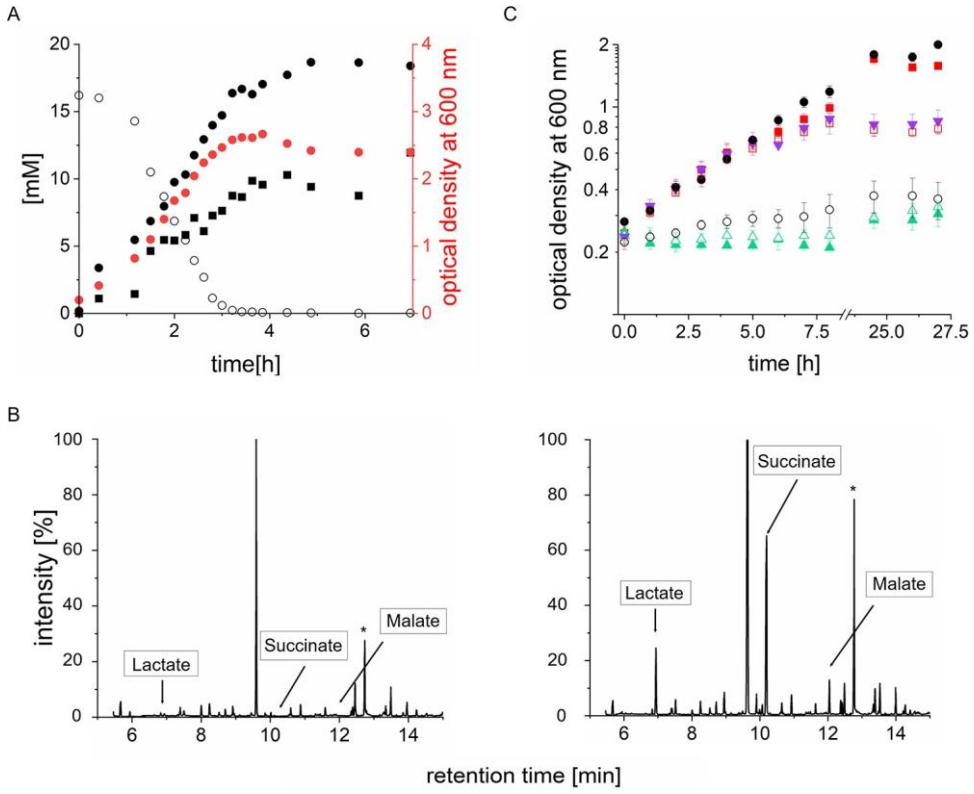


**Figure 1** Growth of *P. bryantii.* (A) Concentrations of glucose (open circles), succinate (black circles), and acetate (black squares) and optical density at 600 nm (red circles) were monitored during growth in tryptone- and glucose-containing medium (2 liters). (B) GC-TOF mass spectrometry of metabolites in *P. bryantii* growth medium containing tryptone (1 g liter$^{-1}$) and 16 mM glucose. (Left) Before inoculation (t = 0); (right) after 16 h. Cysteine, a component of the medium, is indicated by an asterisk. (C) Growth of *P. bryantii* in Hungate tubes with medium containing 16 mM glucose and tryptone (1 g liter$^{-1}$) (black circles), 16 mM glucose (solid red squares), 4 mM glucose (open red squares), 4 mM glucose and 5 mM fumarate (magenta triangles), tryptone (1 g liter$^{-1}$) (open circles), 20 mM fumarate (open green triangles), and 5 mM fumarate (solid green triangles). Averages and standard deviations for three biological replicates are shown.

16 mM glucose and 1 g/liter tryptone, glucose was completely consumed within 3 h and succinate was formed in parallel, reaching 18 mM in the stationary phase (Fig. 1A). This result clearly suggests that QFR is active and generates succinate from fumarate.

Besides succinate, lactate and malate were identified in the medium after 16 h of growth (Fig. 1B, right). *P. bryantii* produced acetate from glucose (20) as confirmed here (Fig. 1A). This indicated formation of ATP from pyruvate via acetyl coenzyme A (acetyl-CoA) and acetyl phosphate. Peptides and amino acids (from tryptone) were poor growth substrates for *P. bryantii* (Fig. 1C), though tryptone improved growth on glucose slightly (Fig. 1C). With 4 mM glucose, the final optical density at 600 nm ($OD_{600}$) decreased to 0.78 (compared to an $OD_{600}$ of ~2 with 16 mM glucose). Comparing growth with 4 mM glucose in the absence or presence of 5 mM fumarate revealed no difference in growth rate or yield of *P. bryantii*. When fumarate was the sole carbon source (5 mM or 20 mM), only a slight increase in $OD_{600}$ of 0.05 after 27 h was observed (Fig. 1C). The breakdown of glucose is linked to the production of succinate from endogenously formed fumarate, and this reaction is likely to be catalyzed by QFR. This reaction requires quinol as an electron donor provided by NQR, as described below.

***P. bryantii* membranes exhibit NADH oxidation and fumarate reduction activities with menaquinone as the electron carrier**. The NQR from facultative anaerobes such as *Vibrio* spp. was shown to operate with ubiquinone, not menaquinone (12). On the other hand, QFR of *W. succinogenes* reacts with menaquinone (14). The genome of *P. bryantii* harbors genes for menaquinone synthesis (21) but not for ubiquinone synthesis. Quinone extraction followed by high-performance liquid chromatography (HPLC) coupled to mass spectrometry confirmed that *P. bryantii* contains only menaquinones. A typical HPLC profile revealed quinones eluting at 15.2 min, 23.7 min, 32.8 min, and 45.7 min (Fig. 2A) assigned to menaquinones with 9 ($MK_9$), 10 ($MK_{10}$), 11 ($MK_{11}$), and 12 ($MK_{12}$) isoprenoid units by mass spectrometry and UV/visible-spectrum (Vis) spectroscopy (Fig. S4). Some extracts also contained traces of $MK_{13}$. $MK_{12}$ is the most abundant

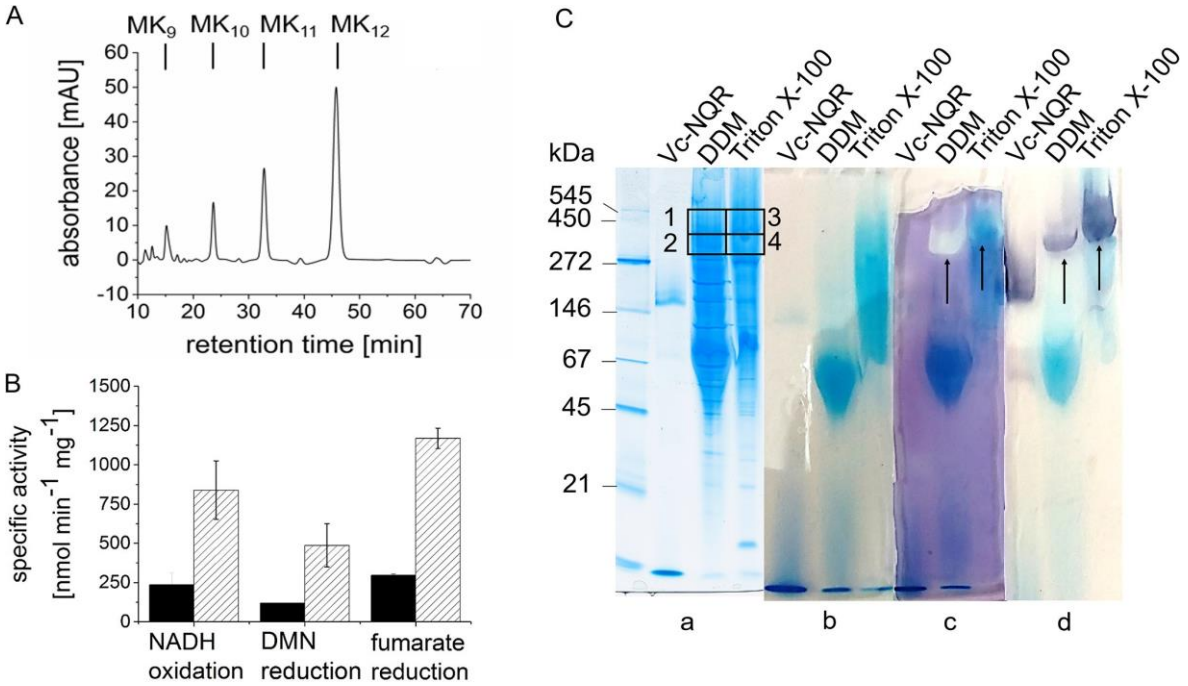


**Figure 2** NADH oxidation and fumarate reduction by solubilized membranes from *P. bryantii* with menaquinone as the electron carrier. (A) Quinone composition of membranes from *P. bryantii* analyzed by HPLC. (B) Specific enzyme activities of NADH oxidation, DMN reduction, and fumarate reduction in DDM-solubilized membranes of *P. bryantii*. Solubilized membranes from *P. bryantii* were prepared under oxic (solid bars) or anoxic (hatched bars) conditions. NADH oxidation and DMN reduction were followed simultaneously. Reduction of fumarate was monitored from the oxidation of benzyl viologen at 546 nm in a separate assay. Mean values and standard deviations from three technical replicates are shown. (C) Blue native PAGE of solubilized *P. bryantii* membranes and detection of proteins with NADH dehydrogenase or fumarate reductase activity. Membranes solubilized with 5% Triton X-100 or 2.5% DDM (approximately 70 µg protein per lane) were separated by BN-PAGE with a gradient from 4% to 16% acrylamide. NQR from *V. cholerae* (4 µg) was used as a control. Each sample was loaded in triplicate, and the BN-PAGE gel was cut into three parts. (a) Coomassie-stained BN gel. Boxes 1 to 4 indicate proteins subjected to tryptic digestion and mass spectrometry analysis. (b) BN gel after run, unstained. (c) BN-PAGE treated to reveal fumarate reductase activity. (d) BN gel treated to reveal NADH dehydrogenase activity. Arrows highlight high-molecular-mass complexes exhibiting both activities.

quinone in the membrane of *P. bryantii.* Thus, NQR from *P. bryantii* is highly likely to interact with menaquinone. In accord with that notion, 2,3-dimethyl 1,4-naphthoquinone (DMN), a menaquinone derivative with a methyl group replacing the hydrophobic isoprenoid side chain, acted as an in vitro electron acceptor for NQR. *P. bryantii* membranes which were prepared under aerobic conditions exhibited NADH oxidation and DMN reduction activities of 150 nmol $min^{-1}$ $mg^{-1}$ and 70 nmol $min^{-1}$ $mg^{-1}$, respectively.

Membranes of *P. bryantii* were solubilized with different detergents, such as digitonin, Triton X-100, and n-dodecyl b-D-maltoside (DDM), and the activities of solubilized NQR with DMN as the electron acceptor were determined. Digitonin (4%, wt/vol) was not suited for solubilization, since the supernatant after ultracentrifugation contained nearly no protein. With 2% (wt/vol) Triton X-100, nearly half of the total protein of membranes was retrieved in the solubilized supernatant, which exhibited 250 nmol $min^{-1}$ $mg^{-1}$ NADH oxidation and 80 nmol $min^{-1}$ $mg^{-1}$ DMN reduction activities. The best results were achieved with DDM (2.5%, wt/vol), solubilizing approximately 75% of the membrane proteins, with 300 nmol $min^{-1}$ $mg^{-1}$ NADH oxidation and 100 nmol $min^{-1}$ $mg^{-1}$ DMN reduction activities. In general, preparation of membranes and solubilized membrane proteins from *P. bryantii* under anoxic conditions resulted in increased NQR and QFR activities (Fig. 2B). Specific activities of 300 nmol $min^{-1}$ $mg^{-1}$ NADH oxidized, 100 nmol $min^{-1}$ $mg^{-1}$ DMN reduced, and 300 nmol $min^{-1}$ $mg^{-1}$ fumarate reduced were measured with solubilizates prepared under oxic conditions. Solubilizates prepared under anoxic conditions had specific activities of 850 nmol $min^{-1}$ $mg^{-1}$ NADH oxidized, 490 nmol $min^{-1}$ $mg^{-1}$ DMN reduced, and 1,200 nmol $min^{-1}$ $mg^{-1}$ fumarate reduced (Fig. 2B). The substoichiometric formation of $DMNH_2$ from NADH by NQR is likely due to incomplete reduction of quinones by NQR under formation of semiquinones (22), or by electron transfer to $O_2$ (23). We previously observed a stimulation of NADH oxidation and quinone reduction activities of *P. bryantii* membranes by $Na^+$ (7).

In accordance with these findings, specific NADH oxidation and quinone reduction activities of membranes solubilized with DDM decreased by ca. 70% when the $Na^+$ concentration in the assays was lowered from 1 mM to 10 µM $Na^+$.

**A supercomplex consisting of NQR and QFR in *P. bryantii* membranes**. Aggregation state and protein composition of NQR and QFR in DDM and Triton X-100 solubilizates were studied by blue native PAGE (BN-PAGE) followed by in-gel activity staining and mass spectrometry. The apparent masses of protein complexes were estimated from a comparison with standards covering the range from 545 to 21 kDa and with purified NQR from *Vibrio cholerae* with an apparent mass of 220 kDa (11). Purified NQR from *V. cholerae* and DDM and Triton X-100 solubilizates were separated by BN-PAGE in triplicate, and separate staining was performed with Coomassie blue to stain all proteins (Fig. 2C, panel a), with NADH plus nitroblue tetrazolium chloride (NBT) to stain proteins exhibiting NADH dehydrogenase activity (Fig. 2C, panel d), and with reduced benzyl viologen ($BV_{red}$) plus fumarate to stain proteins exhibiting fumarate reductase activity (Fig. 2C, panel c). A control shows NQR, DDM, and Triton X-100 solubilizates before staining (Fig. 2C, panel b). Purified NQR complex from *V. cholerae* comprising six subunits (NqrABCDEF) migrated as single band at an apparent mass slightly above 146 kDa, as detected by Coomassie staining (Fig. 2C, panel a) and by NADH oxidation activity of subunit NqrF (Fig. 2C, panel d). Much larger protein complexes exhibiting NADH dehydrogenase activity were detected in membranes solubilized with DDM or Triton X-100, with one prominent complex migrating slightly above the 272-kDa marker (DDM) and at least two complexes slightly above 272 kDa and around 500 kDa (Triton X-100). This suggested that NqrF was part of a supercomplex. The prominent protein bands above 272 kDa exhibited both NADH oxidation and fumarate reductase activities (Fig. 2C, panels c and d), indicating a supercomplex composed of NQR and QFR. This supercomplex was observed in 5 biological replicates. To study the protein composition of supercomplexes, Coomassie-stained protein bands migrating at molecular masses similar to those of the bands detected by enzyme activity staining were excised from the gel (Fig. 2C, panel a, boxes 1 to 4) and subjected to tryptic digestion and mass spectrometry. Besides NQR and QFR, *P. bryantii* contains genes coding for the Rhodobacter nitrogen fixation (RNF) complex, the electrogenic ferredoxin:$NAD^+$ oxidoreductase (24), and an 11-subunit complex with putative electron transfer and cation transport activity (8, 25) (Fig. S1). Mass-spectrometric data from samples 1 to 4 (Fig. 2C) were analyzed with respect to the presence of the subunits of membrane-bound complexes. Large amounts of unique peptides were found for subunits NqrA from NQR and FrdA from QFR (Fig. 3). We also detected smaller amounts of peptides indicating the presence of subunits from RNF and the 11-subunit complex. Subunits NqrA, FrdA, and RnfC are large hydrophilic subunits (Table S1) which are readily detected. Results of an *in silico* tryptic digestion of NQR, QFR, and RNF are presented in Table S2. Peptides from NQR, QFR, and RNF subunits identified by mass spectrometry (Table S3), and the complete set of mass-spectroscopic data (Table S4) are also reported. The comigration on BN-PAGE at an apparent molecular mass higher than that of the NQR complex isolated from *V. cholerae* (Fig. 2C) suggested tight interaction of NQR and QFR in a sodium-NQR fumarate reductase (SNFR) supercomplex. These high-molecular-mass protein bands exhibited both NADH oxidation and fumarate reduction activities. Samples 2 and 4 (Fig. 2C) migrating at an apparent mass above 272 kDa could represent a supercomplex comprising one NQR complex and one QFR complex (calculated mass, 330 kDa). Protein bands exhibiting NADH oxidation and fumarate reduction activities migrating at 450 kDa (Fig. 2C, samples 1 and 3) could represent aggregates of NQR and QFR at different ratios or bound to other proteins. Note that QFRs may form dimers as observed in three-dimensional (3D) structures of QFRs from *Wolinella succinogenes* and *Escherichia coli* (26, 27). Furthermore, gene expression of the *rnfG, nqrF* and *frdA* genes of *P. bryantii* was analyzed by reverse transcription-quantitative PCR (RT-qPCR) (Fig. 3) in two biological replicates.

**Properties of the SNFR supercomplex**. NQR and QFR subunits of the SNFR supercomplex in solubilizates were identified by in-gel fluorography and immune staining. Subunits NqrB (41.7 kDa), NqrC (23.2 kDa) and FrdA (73.6 kDa) exhibit fluorescence in the denatured state, due to covalently bound flavins (29, 30). Prominent fluorescent bands slightly below 25 kDa were observed both in native and in DDM-solubilized membranes from *P. bryantii* after separation by SDS-PAGE (Fig. 4A, left). These bands corresponded to subunits NqrB and NqrC, which comigrated under these conditions (7, 31). Due to their hydrophobicity, they migrate below NqrC', a truncated version of NqrC from *V. cholerae* (32). NqrC' lacks the hydrophobic transmembrane helix but retains the covalently attached FMN, giving rise to a fluorescent band with a molecular mass of 25 kDa (Fig. 4A, left). A protein band with weak fluorescence intensity at about 75 kDa in native and solubilized membranes was assigned to FrdA with its covalently attached FAD (Fig. 4A, left). A complete list of identified peptides (Table S5). In order to identify the NqrF subunit in solubilized *P. bryantii* membranes.

| | sample | 1 | 2 | 3 | 4 |
|---|---|---|---|---|---|
| Number of peptides | NqrA | 19 | 28 | 23 | 25 |
| | FrdA | 29 | 18 | 26 | 18 |
| | RnfC | 10 | 14 | 7 | 7 |

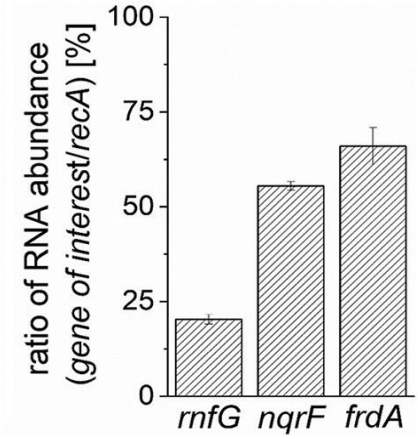


**Figure 3** Relative abundance of NQR, QFR, and RNF in *P. bryantii*. (Left) Number of unique peptides from NqrA, FrdA, and RnfC subunits identified by mass-spectrometric analyses of samples 1 to 4, obtained from Coomassie-stained BN-PAGE gels (Fig. 2C, panel a). (Right) Abundance of *rnfG*, *nqrF*, and *frdA* transcripts in relation to abundance of recA (100%). Samples from two biological replicates were measured in three technical replicates each.

antibodies were raised against the purified FAD domain of *P. bryantii* NqrF. An immune-reactive band around 35 kDa was observed with the purified FAD domain of NqrF, in accordance with its calculated molecular mass (33.5 kDa) (Fig. 4A, right). As expected, solubilized membranes exhibited an immune-reactive band at about 45 kDa, which was assigned to full-length NqrF with a calculated molecular mass of 47.1 kDa (Fig. 4A, right).

To study the stability of the SNFR supercomplex solubilized from *P. bryantii* membranes with DDM, second-dimension SDS-PAGE was performed after first-dimension BN-PAGE. The SNFR with an apparent mass of 330 kDa identified by NADH dehydrogenase activity stain in BN-PAGE dissociated into three prominent complexes (bands 6, 7, and 8 in Fig. 4B). Band 6 exhibited cross-reactivity with anti-NqrF-FAD domain antibodies. Bands 5, 6, 7, and 8 contained covalently attached flavins, indicating the presence of FrdA, NqrB, and NqrC subunits. Their prevalence was confirmed by mass-spectrometric analyses of peptides derived from band 6 (Table S6), with FrdA (22 peptides), FrdB (4 peptides), NqrA (22 peptides), NqrF (7 peptides), NqrC (6 peptides), and NqrB (3 peptides). FrdC, NqrD, and NqrE were not detected, but note that these small, hydrophobic proteins (Table S1) are difficult to detect by the mass spectrometry method used here. Bands 7 and 8 migrated at lower apparent masses in the second dimension SDS-PAGE, most likely due to the lack of NqrF and NqrB, which were not detected by mass spectrometry. Bands 7 and 8 exhibited very similar compositions (Table S6), with FrdA (8 peptides), FrdB (1 to 5 peptides), NqrA (3 peptides), and NqrC (3 peptides). In the DDM solubilizates, the minor fraction of 500 kDa SNFR observed on BN-PAGE (Fig. 2C) was also detected by second-dimension SDS-PAGE (band 5 in Fig. 4B), containing peptides from FrdA (27 peptides), FrdB (10 peptides), NqrA (5 peptides), NqrF (4 peptides), NqrC (1 peptide), and NqrB (1 peptide). Peptides derived from other membrane-bound and soluble proteins were also detected (Table S7).

We conclude that the SNFR supercomplex does not readily dissociate despite the presence of SDS, indicating tight interactions between NQR and QFR. Size exclusion chromatography of the DDM solubilizate confirmed this notion (Fig. 4C). A large complex containing subunits NqrF, NqrB/C, and FrdA and heme b (Fig. S5) eluting at 55 ml represented SNFR with an apparent molecular weight of 480 kDa (Fig. 4D).

**Intramolecular electron transfer in the SNFR supercomplex.** Electron transfer between substrates and redox centers of SNFR was followed by recording UV/Vis difference spectra. The redox state of FrdC hemes b indicated the degree of reduction of QFR. Reduced hemes b have absorption maxima at 560 nm, 527 nm, and 427 nm. In their oxidized state, they exhibit a characteristic absorption maximum at 410 nm. QFR and NQR contain flavins, which can be detected by a decrease of absorbance at 448 nm upon reduction. First, these redox cofactors of SNFR in *P. bryantii* membranes were identified after reduction with a large excess of dithionite. A cuvette containing air-oxidized membranes in 20 mM potassium phosphate buffer pH 7.5 was placed in beam 1 of the double-beam photometer. A second cuvette containing dithionitereduced membranes was analyzed in beam 2.

Figure 5A (top) shows the difference spectrum of the dithionite-reduced minus the air-oxidized membranes. Three maxima at 560 nm, 527 nm, and 427 nm were observed, with a minimum at 448 nm. These were assigned to fully reduced hemes *b* and flavins, respectively. We asked if NADH reduces the hemes *b* of

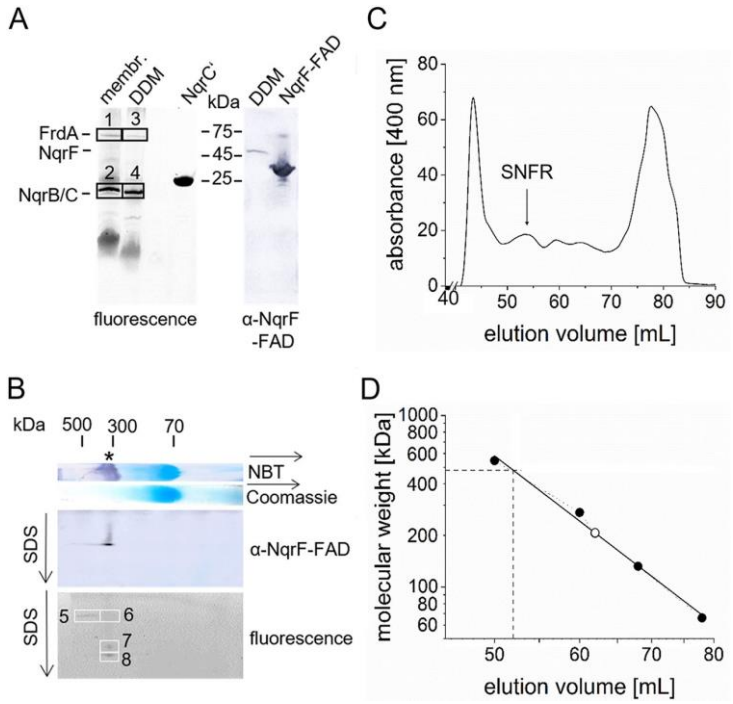


**Figure 4** Characterization of the SNFR supercomplex from *P. bryantii*. (A) Membranes (100 µg) and membranes solubilized with DDM (100 µg) were separated by SDS-PAGE to detect flavinylated proteins (left, with 2 µg of truncated NqrC' protein as the positive control). (Right) Western blot of DDM solubilizates (100 µg) and the FAD-binding domain of subunit NqrF (NqrF-FAD; 10 µg) using anti-NqrF-FAD domain antibodies. (B) 2D BN/SDS-PAGE of DDM solubilizates (70 µg). The lane from a BN-PAGE gel stained with Coomassie was placed on top of the SDS-PAGE gel. NADH dehydrogenase activity stain (NBT) indicated the position of the SNFR supercomplex (*). Flavinylated proteins in the SDS-PAGE were detected by in-gel fluorography. Afterward, immunostaining with anti-NqrF-FAD domain antibodies was performed. Boxes 1 to 8 indicate the positions of fluorescent protein bands subjected to proteolysis and mass spectrometry for identification of subunits. (C) SNFR in DDM solubilizates separated by size exclusion chromatography. (D) The molecular weight of SNFR was estimated from a calibration with protein standards (66 kDa, 132 kDa, 220 kDa, 272 kDa, and 545 kDa).

the QFR in *P. bryantii* membranes under participation of NQR as the electron entry site. Two quartz cuvettes were filled with aliquots of air-oxidized membranes of *P. bryantii*. To the aliquot in beam 2, 125 µM NADH were added, and the difference spectrum of NADH-reduced minus air-oxidized membranes was recorded. Peaks at 427 and 560 nm revealed partial reduction of hemes *b* of QFR, indicating electron transfer from NADH via NQR and quinol to QFR (Fig. 5A, middle). If these hemes *b* are redox centers of QFR, their reoxidation with fumarate should be possible. To test this assumption, membranes were allowed to react with 125 µM NADH, one aliquot was mixed with 12.5 mM fumarate, and the difference spectrum was recorded (Fig. 5A, bottom). The shift in maximum peak to 410 nm indicated the presence of oxidized hemes *b*, demonstrating reoxidation of QFR by fumarate. These results demonstrated electron transfer from NADH to fumarate by NQR and QFR in *P. bryantii* membranes.

Electron transfer was also tested after solubilization of membranes with Triton X-100. Figure 5B (top) shows the difference spectrum of the NADH-reduced minus the air-oxidized solubilized membranes. Here, the prominent maximum of reduced heme *b* at 427 nm was detected. Figure 5B (middle) depicts the difference spectrum of the NADH reduced solubilizates mixed with fumarate, minus the NADH-reduced solubilizate. Three minima at 428 nm, 527 nm, and 560 nm were detected, indicating reoxidation of the hemes *b* of QFR by fumarate. Furthermore, a maximum at 410 nm appeared which is characteristic for oxidized hemes *b*. These findings are in accord with NADH:fumarate oxidoreduction by the combined action of NQR and QFR in the SNFR supercomplex. QFR catalyzes succinate:quinone oxidoreduction under participation of hemes *b* (33). Air-oxidized Triton X-100-solubilized membranes (beam 1) were compared with an aliquot treated with 12.5 mM succinate (beam 2). In the difference spectrum of succinate-reduced minus airoxidized solubilized membranes (Fig. 5B, bottom), a typical maximum of reduced heme *b* at 427 nm was identified. Comparing the change in absorbance units (ΔAU) of NADH- or succinate-reduced solubilized

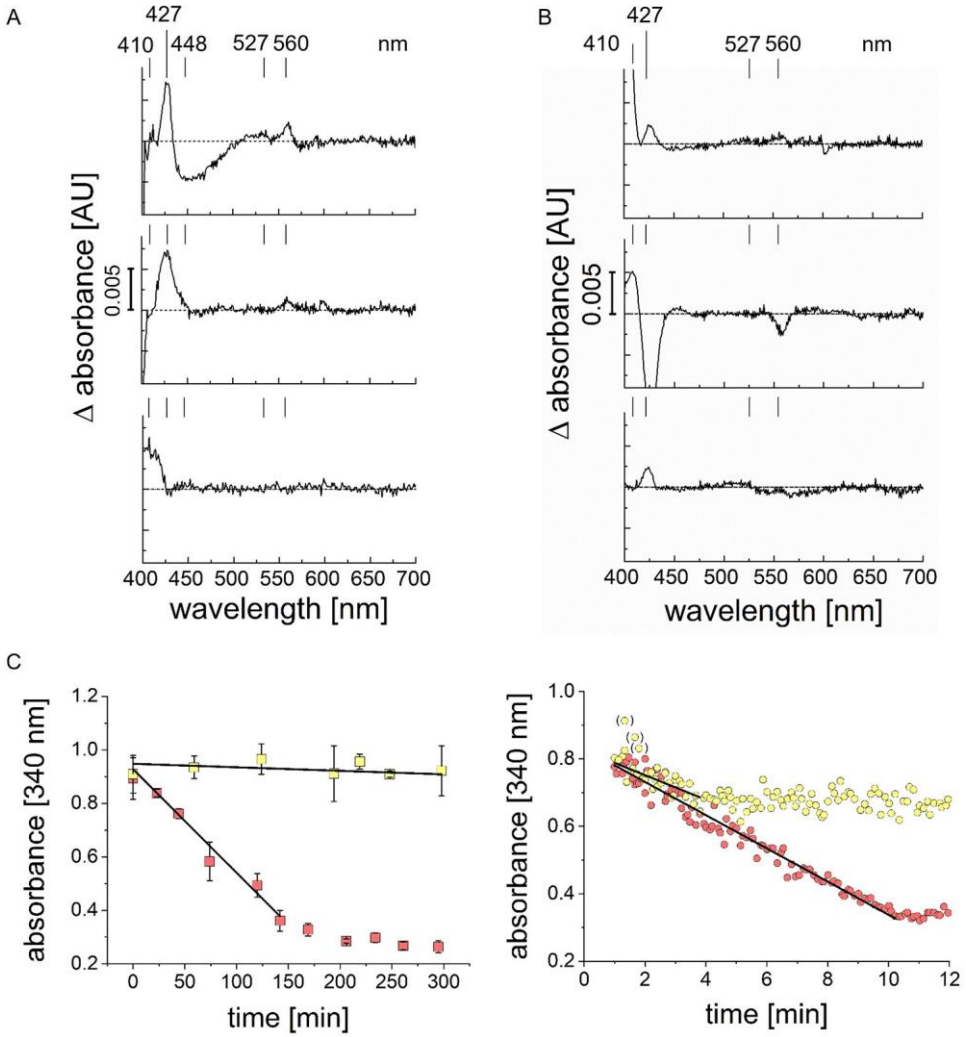


**Figure 5** Membrane-bound redox centers and NADH:fumarate oxidoreduction activity of *P. bryantii*. Vis difference spectra of membranes (0.5 mg protein/ml) (A) and Triton X-100-solubilized membranes (0.5 mg protein/ml) (B) with signatures of reduced heme b (427, 527, and 560 nm), oxidized heme *b* (410 nm), and reduced flavin (448 nm). (A) Traces, from top to bottom: [dithionite reduced] minus [air oxidized], [NADH reduced] minus [air oxidized], [NADH reduced] minus [NADH reduced with added fumarate]. (B) Traces, from top to bottom: [NADH reduced] minus [air oxidized], [NADH reduced] minus [NADH reduced with added fumarate], [succinate reduced] minus [air oxidized]. (C) Oxidation of NADH (initial concentration, 200 µM) by membranes (0.1 mg protein). (Left) No electron acceptor added (yellow squares) or 10 mM fumarate added (red squares). (Right) DMN (65 µM) (yellow circles) or with 65 µM DMN and 10 mM fumarate (red circles) added. Typical traces from at least 3 replicates are presented. In panel C (left), means and standard deviations (n = 3) are shown.

membranes revealed similar intensities (~0.0025 AU), suggesting that a similar proportion of hemes *b* in QFR underwent reduction. Rate measurements of NADH oxidation by *P. bryantii* membranes with DMN and/or fumarate as electron acceptors showed only residual activity in the absence of both DMN and fumarate (0.2 nmol $min^{-1}$ $mg^{-1}$) (Fig. 5C, left). Adding fumarate increased the rates to ~10 nmol $min^{-1}$ $mg^{-1}$ and after approximately 150 min nearly all NADH was consumed (150 nmol from an initial 200 nmol) (Fig. 5C, left). With DMN as the electron acceptor, NADH oxidation activity increased to 150 nmol $min^{-1}$ $mg^{-1}$ (Fig. 5C, right), indicating that the amount of endogenous menaquinone limits electron transfer in vitro. Interestingly, after ~5 min and a consumption of 75 nmol NADH, the NADH concentration did not further decrease, reflecting an equilibrium of $DMN/DMNH_2$ and $NAD^+/NADH$. Highest NADH oxidation activity was observed in the presence of both DMN and fumarate (200 nmol $min^{-1}$ $mg^{-1}$) (Fig. 5C, right). After 10 min, NADH was completely oxidized. We conclude that fumarate acts as an electron acceptor for the SNFR supercomplex in its native membrane environment. Menaquinone acts as the electron carrier between NQR and QFR. Short-chain

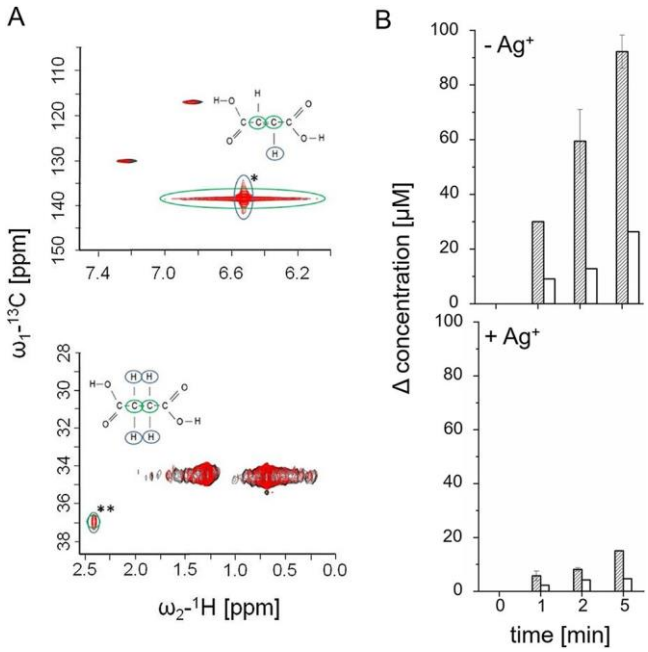


**Figure 6** Succinate formation by the SNFR supercomplex from *P. bryantii*. (A) Membranes (100 µg) were allowed to react with NADH, DMN, and fumarate for 12 min, and 2D $^1$H and $^{13}$C NMR spectra were recorded (red traces). In the control reaction (black traces), fumarate was omitted. (Top) Fumarate peak in 2D $^1$H and $^{13}$C NMR spectrum; (bottom) succinate peak in 2D $^1$H and $^{13}$C NMR spectrum. Typical resonances for fumaric acid (*) and succinic acid (**) are indicated. Resonance assigned to carbon atoms (green) and hydrogen atoms (blue) are highlighted. (B) NADH oxidation by DDM solubilizate (100 µg) in the presence of DMN and fumarate was followed at 340 nm. At indicated times, aliquots were subjected to 1D $^1$H NMR to determine succinate concentrations. NADH consumed (hatched bars) and succinate formed (open bars) are presented as the concentration difference at indicated time and at the start of the reaction. The reaction was performed in the absence (top) or presence (bottom) of 3 µM $AgNO_3$. Averages and standard deviations for two technical replicates are shown.

menaquinones such as DMN stimulated overall SNFR activity 20-fold, suggesting exchange of SNFR-bound and free menaquinone, as previously reported for other supercomplexes (34).

**Succinate formation by the SNFR supercomplex**. *P. bryantii* membranes catalyzed the complete oxidation of NADH (200 µM) with an excess of fumarate (10 mM) in the presence of only 65 µM DMN (Fig. 5C), indicating electron transfer to fumarate. Using nuclear magnetic resonance (NMR) spectroscopy, we demonstrated stoichiometric formation of succinate in the reaction assay containing membranes, NADH, DMN, and fumarate. After completion of the reaction (12 min), aliquots were retrieved for 1D $^1$H, 2D $^1$H, and $^{13}$C NMR measurements. The assay mixture devoid of fumarate (but with NADH and DMN) served as a control. Figure 6A depicts the 2D $^1$H and $^{13}$C NMR spectra, highlighting the typical ranges of fumarate (top) and succinate (bottom). The dicarboxylic acids are distinguished by the chemical shift of C-3 and C-4 carbon atoms and their bound H atoms. The complete reaction mix revealed resonances assigned to succinic acid, which were not detected in the control reaction devoid of fumarate. Quantification of the $^1$H NMR signal showed that the oxidation of 200 µM NADH led to the formation of 170 ± 0.02 µM succinic acid (n = 3), indicating transfer of electrons from NADH to fumarate. We followed time-dependent formation of succinate with NADH as the electron donor using DDM-solubilized membranes and studied the effect of $Ag^+$, a specific inhibitor of NQR (35, 36) (Fig. 6B). At each time point (1, 2, and 5 min after start of the reaction), the concentrations of NADH and succinate were determined. Per mole of succinate, approximately 3 mol NADH was consumed, in accord with ratios of NADH oxidation and quinone reduction activities observed with DDM solubilizates (Fig. 6B, top). In the presence of $Ag^+$, succinate formation was inhibited by at least 80%, demonstrating that fumarate reduction in P. *bryantii* membranes required active NQR (Fig. 6B, bottom).

**An electrochemical sodium gradient in *P. bryantii***. We studied the formation of a membrane potential (DW) by *P. bryantii* using the dye $DiOC_2$ (3,39-diethyloxacarbocyanine iodide). The uptake of $DiOC_2$ by cells is promoted by ΔΨ (inside negative), and cells with a higher ΔΨ exhibit increased red fluorescence. The highest ΔΨ was observed in the presence of 155 mM $Na^+$. Fluorescence emission decreased by ca. 80% when $Na^+$ was replaced by $K^+$ (Fig. 7). Incubation of $Na^+$-treated cells with the $Na^+$specific ionophore monensin

resulted in a drastic decrease in transmembrane voltage by ca. 90%. With the protonophore carbonyl cyanide 3-chlorophenylhydrazone (CCCP), ΔΨ was decreased by ca. 70%. These results demonstrate that *P. bryantii* established an electrochemical $Na^+$ gradient, suggesting redox-driven $Na^+$ transport by the NQR in *P. bryantii*. Besides the $Na^+$ gradient, *P. bryantii* maintained an electrochemical $H^+$ gradient, as shown by partial dissipation of ΔΨ in the presence of a protonophore.

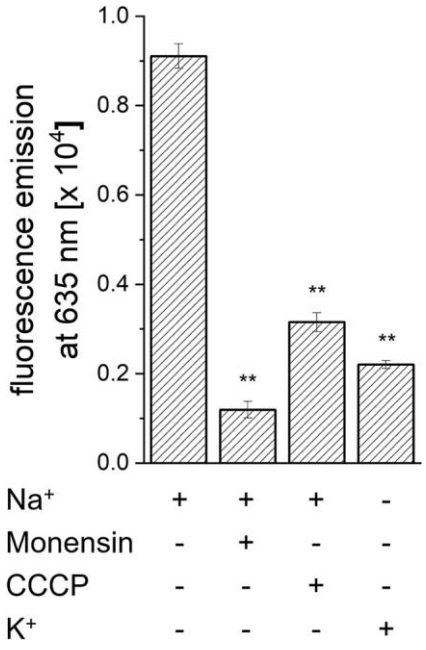


**Figure 7** Electrochemical $Na^+$ gradient in *P. bryantii*. The intensity of fluorescence emission is a measure for the membrane potential established by cells. The fluorescence emission of the fluorophore without added cells (control) was subtracted. The ionophores monensin and carbonyl cyanide-m-chlorophenylhydrazone (CCCP) (each at 2.5 µM) were added as indicated. Mean values and averages from three technical replicates are shown. Asterisks indicate significant differences from cells incubated with $Na^+$ in the absence of ionophore ($P < 0.05$).

## Discussion

In this study, evidence for a sodium-translocating NADH:fumarate oxidoreductase complex (SNFR) in *P. bryantii* is presented. SNFR is a membrane-bound supercomplex composed of the $Na^+$-translocating oxidoreductase (NQR); and the fumarate reductase (QFR). SNFR represents an important functional module, which most likely generates a sodium-motive force in *P. bryantii*. This supercomplex intimately connects NADH-driven sodium ion translocation to an important step in sugar degradation by *P. bryantii*, namely, the formation of succinate, which is excreted as an end product (8, 37) (Fig. 8). Menaquinone acts as an electron carrier between NQR and QFR within the SNFR supercomplex. QFR of *P. bryantii* is closely related to the *W. succinogenes* enzyme and is therefore thought not to contribute to the generation of an electrochemical potential. It has been shown for the QFR of *W. succinogenes* that the transmembrane electron transfer from quinol, located on the periplasmic side, via the heme groups to the fumarate reduction site, located on the cytoplasmic side, is coupled to compensatory proton flux from the periplasm into the cytoplasm (38). Thus, the overall reaction of *W. succinogenes* QFR is electroneutral. If *P. bryantii* and *W. succinogenes* QFR share the same architecture, only NQR contributes to membrane potential formation in the SNFR complex. In SNFR, a donor:quinone dehydrogenase (NQR) is coupled to a quinol:acceptor reductase (QFR) in a simple electron transfer chain that produces a sodium-motive force. This module is reminiscent of the formate (or $H_2$):fumarate oxidoreductase system in *W. succinogenes*, where the electrogenic formate ($H_2$):quinone oxidoreductase provides quinol to the non electrogenic quinol:fumarate oxidoreductase (QFR) (39). With the help of SNFR, the disposal of redox equivalents by succinate formation, as well as the regeneration of $NAD^+$ required for the initial breakdown of glucose, is coupled to the buildup of a sodium-motive force. Thus, SNFR increases the energy yield during growth of *P. bryantii* on glucose. Addition of fumarate did not improve growth of *P. bryantii* with glucose as the carbon source, indicating that *P. bryantii* did not benefit from surplus electron acceptor under the given growth conditions. Possible explanations are (i) the lack of fumarate uptake systems and (ii) the endogenous supply of fumarate produced during the degradation of glucose. *P. bryantii* harbors a gene related to *dcuB* (UniProt accession number D8DV98), coding for a putative succinate:fumarate antiporter (40). Also, two genes coding for putative $Na^+$-coupled dicarboxylate transporters are found (UniProt accession numbers A0A1H9DU78 and D8DTN2) (41). This suggests that the utilization of exogenous fumarate by *P. bryantii* is not limited by transport. Rather, one would suspect that the rate of fumarate formation from glucose is high, resulting in cytoplasmic fumarate concentrations that are saturating for the SNFR supercomplex. Notably, we observed roughly equimolar conversion of glucose (16 mM) to succinate (18 mM). This is in marked contrast to mixed-acid fermentation in *E. coli*, where ca. 0.2 mol succinate is formed from 1 mol glucose (40). In *P. bryantii*, phosphoenolpyruvate (PEP) is carboxylated by PEP-carboxykinase, yielding nucleotide (ATP or GTP) and oxaloacetate. Oxaloacetate is reduced to malate, and the conversion of malate by fumarase yields fumarate. This pathway to fumarate, and the subsequent reduction to succinate by the SNFR, is an important metabolic route leading to the generation of an electrochemical

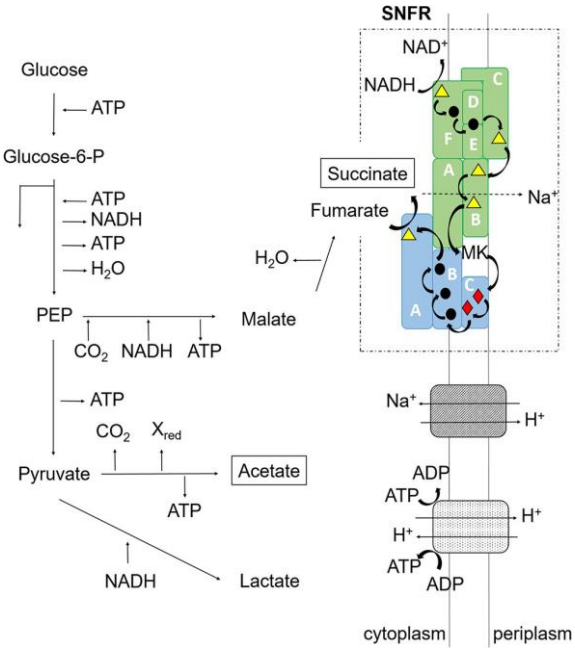


**Figrue 8** The SNFR supercomplex represents the major charge-separating module in *P. bryantii*. Major end products are shown in black boxes. Blue, fumarate reductase (QFR); green, $Na^+$-translocating NADH:quinone (NQR); hatching, $Na^+/H^+$ antiporter; stippling, $F_1F_o$ ATPase/ATP synthase. Subunits of NQR (lettered A to F) and QFR (lettered A to C) are indicated. Colored symbols in the protein complexes represent cofactors. Yellow triangle, flavin; black circle, iron-sulfur center; red diamond, heme *b*. NQR and QFR form a sodium-translocating NADH:fumarate oxidoreductase (SNFR) supercomplex (dashed box).

sodium gradient in *P. bryantii* (Fig. 8). Considering critical, conserved residues in the cation binding site (42), the $F_1F_o$ synthase of *P. bryantii* is a proton- rather than a sodium-dependent enzyme, but the bioenergetic sodium and proton cycles are connected by the putative $Na^+/H^+$ antiporters NhaC and NhaD (UniProt accession numbers D8DUX6 and D8DYG5) of *P. bryantii*. Hence, the sodium-motive force established by SNFR will promote ATP synthesis (Fig. 8).

In the past, feeding experiments with cattle were conducted to test if fumarate addition to the diet reduces methane production. Several bacterial species in the rumen are considered to reduce fumarate under oxidation of hydrogen, which also acts as an electron donor for methanogens. Providing fumarate was expected to diminish hydrogen levels, resulting in overall lower methane production. This hypothesis has not yet been unequivocally confirmed *in vivo* (43) or in vitro with batch cultures (4). A metaproteomic survey of the rumen revealed up to 12 other *Prevotella* species utilizing NQR and QFR (7). The rumen microbial community is dominated by *Prevotella* spp. Our finding that *P. bryantii* does not benefit from exogenous fumarate at high glucose concentrations offers a rationale for previous feeding experiments.

## Materials and Methods

**Bacterial strains and growth conditions**. *P. bryantii* $B_14$ was grown at 39°C in a synthetic medium composed of 1% tryptone (wt/vol), D-glucose (as indicated), 50 mM $NaHCO_3$, 15% (vol/vol) mineral solution 1 (17 mM $K_2HPO_4$), 15% (vol/vol) mineral solution 2 [17 mM $KH_2PO_4$, 45 mM $(NH_4)_2SO_4$, 100 mM NaCl, 5 mM $MgSO_4$, 5.4 mM $CaCl_2$], 0.44 µM resazurin sodium salt, and short-chain fatty acids (vol/vol): 0.17% acetic acid, 0.01% n-valeric acid, 0.01% isovaleric acid, 0.03% n-butyric acid, 0.01% isobutyric acid, and 0.06% propionic acid. Medium was prepared and boiled. Immediately after boiling, 8 mM L-cysteine HCl was added. While cooling on ice, the medium was gassed with $CO_2$ continuously. The pH of the medium was adjusted to 7.5 using NaOH. The medium was used to fill Hungate tubes (7 ml) or serum bottles (100 ml or 1 liter) which were flushed with $CO_2$. Tubes and bottles were sealed gas tight with rubber stoppers and were autoclaved. After autoclaving, 1.5% (vol/vol) of a sterile vitamin solution was added to each tube. The vitamin solution contained 105 µM hemin, 250 µM menadione, 8.5 µM folic acid, 420 µM thiamine hydrochloride, 372 µM riboflavin, 1.2 µM nicotinamide, 580 µM pyridoxamine dihydrochloride, 296 µM calcium pantothenate, 51 µM aminobenzoic acid, 14 µM biotin, and 0.3 µM cyanocobalamin. Medium was inoculated with 5% (vol/vol) of an active culture or glycerol stock. To follow glucose consumption and succinate production during growth of *P. bryantii*, cells were cultivated in 1 liter medium at 39°C with stirring. Samples for determination of optical density, glucose

and succinate were taken with a syringe. Growth experiments with glucose, tryptone, or fumarate (added separately or in combination, as indicated) were performed in triplicate using Hungate tubes. The optical density of the cultures at 600 nm was determined with a cell density meter (WPA Biowave CO8000) allowing measurements up to an $OD_{600}$ of 2. If tryptone was omitted, 10 mM $NH_4Cl$ and 0.36 µM methionine were added to the medium.

**Membrane potential**. ΔΨ established by *P. bryantii* cells was estimated using the BacLight bacterial membrane potential kit (Invitrogen) and a Tecan Infinite F200 Pro plate reader (44). *P. bryantii* cells were cultivated in Hungate tubes until an $OD_{600}$ of 0.8 was reached. The following steps were performed in the anaerobic chamber. Cells were harvested, diluted in sodium buffer (10 mM sodium phosphate [pH 7.4], 145 mM NaCl) or potassium buffer (10 mM potassium phosphate [pH 7.4], 145 mM KCl) and resuspended in the corresponding buffer to yield a cell suspension with an $OD_{600}$ of 0.25. The residual $Na^+$ concentration of the potassium buffer was ~320 µM. Aliquots (800 ml) were centrifuged (16,000x *g*, 5 min), and cells were washed twice in the corresponding buffer. Cell suspensions were mixed with CCCP or monensin (final concentration, 2.5 µM) as indicated. After incubation for 10 min (20°C), the fluorescent dye 3,39-diethyloxacarbocyanine iodide ($DiOC_2$; 15 µM) was added, and incubation was continued for 60 min in the dark. Outside the glove box, three aliquots (200 ml) of each sample were applied to a black, flat-bottom 96-well plate (polystyrene; 4titude). To determine red fluorescence intensities, excitation was set to 480 nm (bandwidth, 20 nm) and emission to 635 nm (bandwidth, 35 nm; gain, 117). Fluorescence emission intensities were in the linear range of the fluorescence detector. Fluorescence intensities of buffer with dye and of cell suspensions were determined for background corrections. As expected, an increase in red fluorescence intensity indicating a transmembrane potential was accompanied with a decrease in green fluorescence intensity monitored in parallel (emission, 535 nm; bandwidth, 25 nm; gain, 107).

**Expression and purification of the NqrF-FAD domain of *P. bryantii* NQR**. The FAD domain of subunit NqrF of *P. bryantii* NQR was purified as described for the FAD domain of *V. cholerae* NqrF (45), modified as follows. The coding fragment of the NqrF-FAD domain (amino acids 129 to 422), comprising an N-terminal $His_6$ tag followed by a human rhinovirus (HRV)-3C protease cleavage site, was cloned into pET15b (Fig. S7), yielding plasmid pPbyF1. Gene synthesis, cloning, and transformation of *E. coli* Tuner (DE3) were performed by GenScript (USA). *E. coli* pPbyF1 was grown in medium (1.6% [wt/vol] tryptone, 1% [wt/vol] yeast extract, 0.5% [wt/vol] NaCl, 10 mM glucose, 200 µg/ml ampicillin) at 37°C to the exponential phase, and gene expression was induced by addition of 0.5 mM isopropyl-1-thio-b-D-galactopyranoside (IPTG). After 16 h of induction at 20°C, cells were harvested by centrifugation and washed once with 10 mM Tris-HCl (pH 7.5), 300 mM NaCl. The cells were disrupted in a continuous cell lysis system at 20,000 $lb/in^2$ (Emulsiflex C3; Avestin). The FAD domain was purified by nickel affinity chromatography (46), using buffer A (50 mM sodium phosphate [pH 8.0], 300 mM NaCl) for loading, buffer A with 5 mM imidazole for washing, and buffer A with 400 mM imidazole for elution. Thirty-seven units of HRV-3C protease comprising a $His_6$ tag (47) per mg FAD domain was added, and the combined proteins were dialyzed against buffer A overnight at 4°C. After dialysis, noncleaved FAD domain and protease were separated from the FAD domain without a $His_6$ tag by nickel affinity chromatography. The flowthrough, containing processed NqrF-FAD domain, was dialyzed overnight against 50 mM HEPES-NaOH (pH 7.0), 5% glycerol (vol/vol), and 0.1 mM EDTA, concentrated to 15 mg/ml, and stored in liquid nitrogen.

**Isolation and solubilization of *P. bryantii* membranes under oxic conditions**. Cells were harvested at an $OD_{600}$ of 2.0 by centrifugation at 9,000x *g* for 30 min (4°C). The cells were washed twice in 20 mM Tris-$H_2SO_4$ (pH 7.5), 50 mM $K_2SO_4$. Cell disruption was performed as described earlier (48), with some modifications. Cells (10 g wet weight) were resuspended in 30 ml 20 mM Tris-$H_2SO_4$ (pH 7.5) containing 50 mM $K_2SO_4$, 5 mM $MgSO_4$, 1 mM dithiothreitol, 1 mM phenylmethylsulfonyl fluoride, 0.1 mM diisopropyl fluorophosphate, and traces of DNase I (Roche). The suspension was passed three times through an Emulsiflex C3 high-pressure homogenizer (Avestin) at 20,000 $lb/in^2$. Cell debris and unbroken cells were removed by centrifugation at 27,000x *g* for 30 min at 4°C. Membranes were collected by ultracentrifugation at 50,000 rpm (Beckman Ti70 rotor) for 1 h at 4°C, washed once in 20 mM Tris-$H_2SO_4$ (pH 7.5) containing 50 mM $K_2SO_4$ and 5% (vol/vol) glycerol, and resuspended in the same buffer. The membrane suspension (10 mg protein/ml) was frozen by pipetting aliquots of 30 ml into a reservoir of liquid $N_2$. The frozen droplets were collected and stored in liquid $N_2$ until further use.

For the solubilization of the membranes, different detergents were tested. 1 ml of membranes (10 mg) was incubated with 4% digitonin (wt/vol), 5% Triton X-100 (vol/vol), or 2.5% DDM (wt/vol) in a total volume of 1.5 ml. Protein/detergent ratios were 1:6 for digitonin, 1:7.5 for Triton X-100, and 1:3.75 for DDM. After incubation of membranes with the detergent solutions for 2 h at 6°C, the membrane suspensions were ultracentrifuged at 50,000 rpm (Beckman Ti70 rotor) for 30 min at 4°C. Supernatants containing solubilized membrane proteins were frozen and stored in liquid $N_2$ as described above for membrane suspensions.

**Isolation and solubilization of *P. bryantii* membranes under anoxic conditions.** Anoxic cells of *P. bryantii* (10 g wet weight in 30 ml cell lysis buffer)

were broken by the Emulsiflex C3 high-pressure homogenizer, which was operated under exclusion of $O_2$ (49). For anoxic membrane isolation and solubilization, all steps described for oxic preparation were performed in an anaerobic chamber (Coy Laboratory Products) under an atmosphere of 5% $H_2$ and 95% $N_2$. $O_2$ levels were monitored continuously (CAM-12; Coy Laboratory Products). All plastic materials were placed in the glove box several weeks before use. Buffers and other substances were made anoxic by flushing with $N_2$ before entering the chamber. Outside the anaerobic chamber, samples were handled in gas-tight vials.

**Size exclusion chromatography.** DDM solubilizate (2 ml, 20 mg) was loaded on a Cytiva HiLoad 16/ 600 Superdex 200-pg column connected to a chromatographic system (Äkta Explorer). The absorbance at 400 nm was recorded. Elution was performed with 20 mM Tris-$H_2SO_4$ (pH 8.0), 50 mM $K_2SO_4$, 5% glycerol, and 0.03% (by weight) DDM. Fractions of 1 ml were collected, concentrated by ultrafiltration (membrane cutoff, 100 kDa) and analyzed by SDS-PAGE, immunostaining, and Vis spectroscopy.

**Quinone isolation and identification.** Quinone extraction from *P. bryantii* cells was performed as described in reference 50. The extracted quinones were separated by using reverse-phase HPLC (RPHPLC) and an OmniSpher 5 $C_{18}$ 150- by 4.6-mm column from Agilent. The Hitachi LaChrom Elite HPLC system was equilibrated with a 7:3 mixture of methanol-isopropanol with a flow rate of 1 ml $min^{-1}$. After equilibration, 100 µl of the quinone extract was injected into the HPLC, and elution was followed for 80 min. The fractions absorbing at 260 nm were collected, and the solvent was evaporated. The precipitated quinones were dissolved in 50 µl chloroform, and high-resolution mass spectrometry (HR-MS) was performed on a Finnigan LCQ Deca LC/MS system (Thermo Scientific).

**Enzyme kinetics.** If not indicated otherwise, enzyme kinetics were carried out in a 1-cm quartz cuvette at 20°C using a diode array spectrophotometer (Black-comet; StellarNet Inc.). The detector and the light source (SL5 UV-Vis lamp; StellarNet Inc.) were placed outside the anaerobic chamber, whereas the cuvette holder was placed inside. These three components were connected with fiber optic cables. NADH oxidation was followed at 340 nm ($\varepsilon_{NADH}$ = 6.22 $mM^{-1}$ $cm^{-1}$) (51) in buffer (20 mM potassium phosphate [pH 7.5], 200 mM NaCl) containing 100 mM DMN ($\varepsilon_{DMN}$ = 15.2 $mM^{-1}$ $cm^{-1}$). DMN reduction was monitored simultaneously at 270 to 290 nm (52). The stimulation of NADH oxidation and quinone reduction activities of DDM solubilizates by $Na^+$ was determined as described previously for *P. bryantii* membranes (7). The residual $Na^+$ concentration of the reaction buffer (20 mM Tris $H_2SO_4$ [pH 7.5]) was 10 µM. Fumarate reduction assays were performed in buffer (20 mM potassium phosphate [pH 7.5]) containing benzyl viologen (~0.5 mM), which was reduced by adding sodium dithionite crystals to achieve an absorbance of 1 at 564 nm (53). Then, 50 to 100 µg of protein was added, followed by the addition of 10 mM fumarate. Decrease in absorbance of benzyl viologen was monitored at 564 nm ($\varepsilon_{BV}$ = 19.5 $mM^{-1}$ $cm^{-1}$). The fumarate reduction assay was performed in the anaerobic chamber using anoxic materials and buffers. Linear regression analysis of initial data points was performed to calculate the initial rates (n = 3).

**UV/Vis difference spectra.** The method described in reference 54 was modified as follows. The absorption spectrum of reduced cofactors in membranes and solubilized membranes was compared with an aliquot of the same sample with cofactors in their oxidized state using a double beam UV/Vis spectrophotometer (Perkin Elmer; Lambda 16) at 20°C. Light was split by a half mirror, passing separately through the reference sample (beam 1) and through the test sample (beam 2). The light intensities passing through the sample and through the reference were compared. The range of 300 to 800 nm was monitored with an interval of 1 nm and a scan speed of 480 nm/min. The software Lambda-SPX calculated the difference in absorbance of beam 2 and that of beam 1 at a given wavelength. Cellular fractions, buffers, and reactants were anoxic or were made anoxic by flushing with $N_2$ and were added to the cuvettes in the anaerobic chamber. The filled cuvettes were sealed gas tight with rubber stoppers to be placed into the photometer outside, where the recordings were started immediately (4 min after addition of reactants to the anaerobic chamber). Membranes and solubilized membranes (with 5% Triton X-100) were analyzed at a concentration of ~500 µg of protein per ml in 20 mM potassium phosphate buffer, pH 7.5. To the cuvette placed in beam 2, reactants were added, as specified below. To obtain baseline spectra, which reflected the turbidity of the sample for subsequent correction, aliquots of air-oxidized membranes, or air-oxidized solubilized membranes, were placed in beam 1 and beam 2.

The first set of experiments aimed the identification of all redox cofactors with putative Vis absorbances in membranes of *P. bryantii*. To this end, air-oxidized membranes were analyzed in beam 1. In beam 2, an aliquot of this membrane suspension mixed with crystals of solid sodium dithionite, to fully reduce the cofactors, was analyzed. The difference spectrum of dithionite-reduced minus air-oxidized membranes was recorded.

In the second set of experiments, we addressed the putative electron transfer between the NQR and the QFR in membranes and solubilized membranes of *P. bryantii*. As a reference, air-oxidized membranes or solubilized membranes in 20 mM potassium phosphate buffer (pH 7.5) supplemented with 200 mM $Na_2SO_4$ and 175 µM DMN were placed in beam 1. In beam 2, an anoxic aliquot treated with 125 µM NADH was analyzed. The difference spectrum of NADH-reduced minus air-oxidized membranes or solubilized membranes was recorded.

In the third set of experiments, the reoxidation of NADH-reduced solubilized membranes with fumarate was investigated. Here, we used two aliquots containing anoxic NADH-reduced membranes or solubilized membranes. To one aliquot, 12.5 mM fumarate was added in the anaerobic chamber, and the cuvette was placed in beam 2. The difference spectrum of fumarate-reoxidized (beam 2) minus NADHreduced membranes, or solubilized membranes (beam 1), was recorded.

In the fourth set of experiments, succinate was used as the reducing agent. In beam 1, we placed a cuvette with an aliquot of air-oxidized, solubilized membranes. In beam 2, an aliquot of anoxic, solubilized membranes was allowed to react with 12.5 mM succinate disodium salt. The difference spectrum of succinate-reduced minus air-oxidized solubilized membranes was recorded.

All experiments were repeated at least three times. Representative difference spectra are presented.

**Analytical methods.** Protein concentration was determined spectrophotometrically with the bicinchoninic acid (BCA) method (55) using the reagent from Pierce. Bovine serum albumin served as the standard. Sodium was determined by flame atomic absorption spectroscopy (AA240 instrument; Agilent Technologies). D-Glucose and acetate concentrations were determined as described previously (20). Gas chromatography–time-of-flight (GC-TOF) mass spectrometry was used to identify metabolites in the supernatant of a 1-liter *P. bryantii* overnight culture ($OD_{600}$, ~2) (56). Succinate was measured with an ion chromatograph (761 Compact IC; Metrohm) equipped with a Metrosep organic acid column (particle size, 9 mm; 250 by 7.8 mm; Metrohm) and an electron conductivity detector. To 9 ml 0.5 mM $H_2SO_4$, 1 ml of culture supernatant was added, and an aliquot of 20 µl was analyzed under isocratic conditions in 0.5 mM $H_2SO_4$ at a flow rate of 0.5 ml $min^{-1}$.

**Mass spectrometry**. For the identification of proteins separated on BN or SDS gels, protein bands of interest were cut out and subjected to tryptic digestion (57). Nano-LC electrospray ionization (ESI) MS/MS experiments were performed on an Ultimate 3000 RSLCnano system (Dionex, Thermo Fisher Scientific, Germany) coupled to a Q-Exactive HF-X mass spectrometer (Thermo Fisher Scientific, Germany) using a NanosprayFlex source (Thermo Fisher Scientific, Germany). Tryptic peptides were directly injected onto a precolumn (m-precolumn $C_{18}$ PepMap100; 300µm, 100 Å, 5µm by 5 mm; Thermo Fisher Scientific) and an analytical column (NanoEase M/Z HSS $C_{18}$ T3; 1.8 mm, 100 Å, 75 mm by 250 mm; Waters GmbH, Germany) operated at constant temperature of 35°C.

Gradient elution was performed at a flow rate of 300 nl/min using a 30-min gradient from 2% to 55% solvent B (0.1% formic acid, 80% acetonitrile) in solvent A (0.1% formic acid). The Q-Exactive HF-X instrument was operated under the control of Xcalibur software (version 4.3; Thermo Fisher Scientific, Inc., USA). Internal calibration was performed using lock-mass ions from ambient air (58). Survey spectra (m/z = 300 to 1,800) were detected in the Orbitrap instrument at a resolution of 60,000 at m/z 200. Datadependent MS/MS mass spectra were generated for the 20 most abundant peptide precursors in the Orbitrap using high-energy collision dissociation (HCD) fragmentation at a resolution of 15,000 with normalized collision energy of 27.

Mascot 2.6 (Matrix Science, UK) was used as the search engine for protein identification. Spectra were searched against the protein databases of *Prevotellaceae* using FASTA-formatted protein sequences retrieved from NCBI (https://www.ncbi.nlm.nih.gov/protein/?term=Prevotellaceae) (June 2018). Search parameters specified trypsin, allowing three missed cleavages, a 5-ppm mass tolerance for peptide precursors and 0.02-Da tolerance for fragment ions. Methionine oxidation was allowed as a variable modification, and carbamidomethylation of cysteine residues was set as a fixed modification. The Mascot results were transferred to Scaffold software 4.8.6 (Proteome Software, USA). Peptide identifications were accepted with a peptide probability greater than 80.0% as specified by the Peptide Prophet algorithm (59). Proteins had to be identified by at least two peptides and a protein probability of at least 99% to be accepted. Protein probabilities were assigned by the Protein Prophet algorithm (60).

**NMR spectroscopy**. To detect succinate and fumarate in enzymatic assays by 1D $^1H$, 2D $^1H$, and $^{13}C$ NMR, NADH oxidation by *P. bryantii* membranes was monitored spectroscopically under anoxic conditions as described above. Enzymatic activity was completed when no decrease of absorbance was observed, and subsequently, the sample was dried at room temperature with a vacuum concentrator (Eppendorf concentrator; program V-AQ). Afterward, the pellet was resuspended in 50 mM $Na_2HPO_4$ (pH 7) and 5 mM 3-trimethylsilyl propionic-2,2,3,3 acid sodium salt (TSP; Sigma-Aldrich) as an internal reference for $^1H$ and $^{13}C$ chemical shift calibration. Note that the phosphate buffer contained $D_2O$ instead of $H_2O$. The resuspended sample was used to fill NMR tubes for 1D $^1H$, 2D $^1H$, and $^{13}C$ measurements. NMR spectra were recorded using a Bruker Avance III HD NMR 600 MHz spectrometer equipped with a 5-mm BBO Prodigy cryoprobe. For structural identification of fumaric and succinic acid, 1D $^1H$ as well as 2D heteronuclear NMR experiments (gradient-selected heteronuclear single quantum coherence [*g*HSQC] and gradient-selected heteronuclear multiple-bond correlation [*g*HMBC]) (61) were recorded at 298 K. For acquisition, processing and evaluation of NMR spectra, the software TopSpin 3.5pl7 (Bruker) was used. To monitor NADH oxidation and succinate formation by DDM solubilizates over time, NADH oxidation was followed anoxically at 340 nm in

20 mM potassium phosphate (pH 7.5), 100 mM $Na_2SO_4$, containing 10 mM NADH, 20 mM DMN, 10 mM fumarate, and 80 µg DDM-solubilized membranes of *P. bryantii.* Three assay mixtures were prepared, and the reactions were stopped after 1, 2, and 5 min by rapid freezing of the mixture in liquid $N_2$. Note that NADH oxidation was completed after 5 min. The same experiment was conducted with 3 µM $AgNO_3$ added to the assay. A 4-fold volume of acetone was added to the reaction mixtures. After storage overnight at 220°C, precipitated proteins were sedimented by centrifugation (5 min at 14,500x *g*), and supernatants were analyzed by NMR spectroscopy.

**1D PAGE and activity staining.** Denaturing polyacrylamide gel electrophoresis (SDS-PAGE) was performed with a 12% polyacrylamide gel. Protein and membrane suspensions were diluted in 5x SDS sample buffer (500 mM dithiothreitol [DTT], 1 M Tris-HCl [pH 6.8], 5% SDS, 28.8% glycerol [wt/vol], bromophenol blue) and boiled for 5 min before loading on SDS gel. For the blue native (BN) PAGE, ServaGel native gels (Serva) with a gradient from 4% to 16% acrylamide were used. The electrophoresis was performed following the instructions of the manufacturer, modified as follows. First, the gel was run at 90 V for 30 min. Then the voltage was increased to 100 V for ~1 h. When 1/3 to 1/2 of the electrophoresis was completed, 1x anode buffer (50 mM bis-Tris [pH 7.0]) with 0.002% (wt/vol) Coomassie blue was changed to 1x anode buffer. The cathode buffer was always 50 mM Tricine, 15 mM bis-Tris (pH 7.0). The voltage was further increased to 200 V until the blue front reached the bottom of the gel. Note that the Coomassie dye was added to the anode buffer and not to the cathode buffer to improve detection of bands after activity staining.

To detect NADH-oxidizing proteins in gels, nitroblue tetrazolium (NBT) staining was performed as described in reference 62. The purified His-tagged NQR complex (48) served as the positive control. To detect fumarate reductase, the gel was placed in the anaerobic chamber and incubated with 10 ml 50 mM potassium phosphate (pH 7.5), 10 mM benzyl viologen, and 2 mg of solid sodium dithionite. The gel was shaken gently for 10 min. Sodium fumarate (2 mM) was added, and the gel was incubated for another 5 min. Fumarate reductase activity resulted in a clear band, due to oxidation of benzyl viologen with fumarate as the electron acceptor. For documentation, the gel was transferred to another tray filled with 50 mM potassium phosphate (pH 7.5) and photographed.

**2D PAGE**. The stability of the NQR/QFR supercomplex was studied with the help of 2D BN/SDS. For 2D SDS/BN-PAGE, 1D BN-PAGE was performed as described above. Afterward, the lane of interest was excised and incubated with 1% SDS and 1% b-mercaptoethanol for 2 h. Meanwhile, a 12% SDS separating gel was poured between two glass plates (approximately two-thirds high) with a 1.5-mm spacer. After polymerization, the 1D lane was excised and placed on top of the separating gel. To melt the lane to the 2D SDS gel, an SDS stacking gel was added. SDS-PAGE was performed as described above.

**In-gel fluorography.** Fluorescence of covalently bound flavins in NqrB, NqrC, and FrdA was detected using the ImageQuant LAS 4000 imager ($\lambda_{excitation}$ = 460 nm; emission filter, Y515 CyTM2). As a positive control, the purified NqrC' subunit was used. This protein is a truncated variant of the NqrC subunit of the *V. cholerae* NQR comprising the covalently attached FMN but lacking the N-terminal transmembrane helix (32). The molecular mass of NqrC' is 25.38 kDa.

**Western blotting and immune detection of proteins separated by SDS-PAGE.** SDS-PAGE and Western blot analysis were performed as described previously (63). The nitrocellulose membrane was incubated for 1 h with polyclonal rabbit antiserum (1:20,000 dilution; BioGenes GmbH) containing antibodies against the NqrF-FAD domain of *P. bryantii*. The antiserum exhibited no cross-reactivity with purified NqrF-FAD domain of *V. cholerae*. After two washing steps with phosphate-buffered saline-Tween (PBST; 137 mM NaCl, 2.7 mM KCl, 1.8 mM $KH_2PO_4$, 10 mM $Na_2HPO_4$, and 0.05% Tween-20 [wt/vol]), the membrane was incubated for 1 h with horseradish peroxidase (HRP)-conjugated secondary anti-rabbit immunoglobulin antibodies (1:3,000 dilution). Immune detection was performed using the chemiluminescence Clarity Western enhanced chemiluminescence (ECL) blotting substrates (Bio-Rad). Exposure (~1 min) and detection were performed with Image Quant LAS 400 (GE Healthcare). The purified NqrFFAD domain of *P. bryantii* was used as a positive control.

**Quantitative real-time PCR analysis.** Total RNA from *P. bryantii* was isolated from 2 ml of cultures in mid-exponential phase. Cells were harvested by centrifugation at 15,000 rpm for 1 min. Cells were resuspended in 600 ml RLT Plus buffer provided with the RNeasy Plus minikit (Qiagen). Cell lysis and RNA isolation were performed with the RNeasy PowerMicrobiome kit (Qiagen). Since the RNA preparation was still contaminated with genomic DNA, a second DNase I degradation step was performed using the RNA Clean & Concentrator kit from Zymo Research. RNA was quantified with the help of the NanoDrop 2000c spectrophotometer (Thermo Scientific). The quality of the RNA was confirmed by gel electrophoresis (Fig. S6) and PCR.

cDNA synthesis was performed as recommended by the standard protocol of the First Strand cDNA synthesis kit (Thermo Scientific), using random hexamer primers. The amount of total RNA used to synthesize cDNA was 1 mg. The thermal cycling parameters for the RT reactions were 25°C for 5 min, 37°C for 60 min, and finally 70°C for 5 min to inactivate the reverse transcriptase. Afterward, a PCR was done with cDNA as the template and gene-specific primers. Primers were

designed using NCBI sequence sources and the Primer3 online primer designing tool (64). The corresponding PCR products were confirmed by sequencing (Eurofins). Primers were designed for nqrF D8DWB6_PREBR (*nqrF* forward primer, 59CTCAGGTCGGTTTCCAGGAT39, and *nqrF* reverse primer, 59ATTTGGATTGGTGGTGGTGC39), frdA D8DXM6_PREBR (*frdA* forward primer, 59CAGGGTG GTATCAATGCTGC39, and *frdA* reverse primer, 59GTTCATTCGGTGGTGCTCAG39), *rnfG* A0A1H9FEX3_PREBR (*rnfG* forward primer, 59CAGAAAAGACCCTTGCTGCA39, and *rnfG* reverse primer, 59CGGTGCAGCAGTAGAAAG TG39) and for the reference gene *recA* D8DYF7_PREBR (*recA* forward primer, 59CTTTCGACCGCTTCTATGCC39, and reverse primer, 59AGGCGATATGGGTGACAACA39). In this PCR, reverse transcriptase minus controls were conducted for each biological replicate to assess for genomic DNA contamination of the RNA sample and a no-template negative control (NTC) was performed to guarantee the purity of the reagents.

RT-qPCRs were performed with the Platinum SYBR green qPCR SuperMix-UDG kit from Invitrogen. For temperature cycling and fluorescence measurements a Bio-Rad CFX 96 cycler and the appropriate CFX Manager software (Bio-Rad) were used. Samples from two biological replicates were measured in three technical replicates each. Mean values and standard deviations of these data were used to compare expression by the $2^{-\Delta\Delta CT}$ method (where $C_T$ is the threshold cycle) (65).

## Acknowledgements

Funding by the Deutsche Forschungsgemeinschaft to Julia Steuber and Jana Seifert (project number 327953272) is gratefully acknowledged.

We thank Johannes Günther, Jens Pfannstiel, and Berit Würtz for their support in the analyses of NMR and mass-spectroscopic data obtained at the Core Facility, University of Hohenheim.

## References

1. Deusch S, Camarinha-Silva A, Conrad J, Beifuss U, Rodehutscord M, Seifert J. 2017. A structural and functional elucidation of the rumen microbiome influenced by various diets and microenvironments. Front Microbiol. 8:1605. doi:10.3389/fmicb.2017.01605.
2. Henderson G, Cox F, Ganesh S, Jonker A, Young W, Janssen PH. 2015. Rumen microbial community composition varies with diet and host, but a core microbiome is found across a wide geographical range. Sci Rep. 5:14567. doi:10.1038/srep14567.
3. Schink B. 1997. Energetics of syntrophic cooperation in methanogenic degradation. Microbiol Mol Biol Rev. 61:262–280.
4. Ungerfeld EM, Kohn RA, Wallace RJ, Newbold CJ. 2007. A meta-analysis of fumarate effects on methane production in ruminal batch cultures. J Anim Sci. 85:2556–2563. doi:10.2527/jas.2006-674.
5. Conrad R. 2009. The global methane cycle: recent advances in understanding the microbial processes involved. Environ Microbiol Rep 1:285–292. doi:10.1111/j.1758-2229.2009.00038.x.
6. Takahashi N, Yamada T. 2000. Glucose metabolism by *Prevotella intermedia* and *Prevotella nigrescens*. Oral Microbiol Immunol. 15:188–195. doi:10.1034/j.1399-302x.2000.150307.x.
7. Deusch S, Bok E, Schleicher L, Seifert J, Steuber J. 2019. Occurrence and function of the $Na^+$-translocating NADH:quinone oxidoreductase in *Prevotella spp*. Microorganisms 7. doi:10.3390/microorganisms7050117.
8. Franke T, Deppenmeier U. 2018. Physiology and central carbon metabolism of the gut bacterium *Prevotella copri*. Mol Microbiol. 109:528–540. doi:10.1111/mmi.14058.
9. Ito T, Gallegos R, Matano LM, Butler NL, Hantman N, Kaili M, Coyne MJ, Comstock LE, Malamy MH, Barquera B. 2020. Genetic and biochemical analysis of anaerobic respiration in *Bacteroides fragilis* and its importance *in vivo*. mBio 11. doi:10.1128/mBio.03238-19.
10. Steuber J, Vohl G, Casutt MS, Vorburger T, Diederichs K, Fritz G. 2014. Structure of the *V. cholerae* $Na^+$-pumping NADH:quinone oxidoreductase. Nature 516:62–67. doi:10.1038/nature14003.
11. Steuber J, Vohl G, Muras V, Toulouse C, Claußen B, Vorburger T, Fritz G. 2015. The structure of $Na^+$-translocating of NADH:ubiquinone oxidoreductase of *Vibrio cholerae*: implications on coupling between electron transfer and $Na^+$ transport. Biol Chem. 396:1015–1030. doi:10.1515/hsz-2015-0128.
12. Casutt MS, Nedielkov R, Wendelspiess S, Vossler S, Gerken U, Murai M, Miyoshi H, Möller HM, Steuber J. 2011. Localization of ubiquinone-8 in the $Na^+$-pumping NADH:quinone oxidoreductase from *Vibrio cholerae*. J Biol Chem. 286:40075–40082. doi:10.1074/jbc.M111.224980.
13. Lancaster CRD. 2002. *Wolinella succinogenes* quinol:fumarate reductase—2.2-Å resolution crystal structure and the E-pathway hypothesis of coupled transmembrane proton and electron transfer. Biochim Biophys Acta. 1565:215–231. doi:10.1016/S0005-2736(02)00571-0.
14. Lancaster CR, Simon J. 2002. Succinate:quinone oxidoreductases from ε-proteobacteria. Biochim Biophys Acta.:84–101.
15. Unden G, Steinmetz PA, Degreif-Dünnwald P. 2014. The aerobic and anaerobic respiratory chain of *Escherichia coli* and *Salmonella enterica*: enzymes and energetics. EcoSal Plus 6. doi:10.1128/ecosalplus.ESP-0005-2013.
16. Förster AH, Gescher J. 2014. Metabolic engineering of *Escherichia coli* for production of mixed-acid fermentation end products. Front Bioeng Biotechnol. 2:16. doi:10.3389/fbioe.2014.00016.

17. Berry EA, Trumpower BL. 1985. Isolation of ubiquinol oxidase from *Paracoccus denitrificans* and resolution into cytochrome $bc_1$ and cytochrome $c$-$aa_3$ complexes. J Biol Chem 260:2458–2467. doi:10.1016/S0021-9258(18)89576-X.
18. Melo AMP, Teixeira M. 2016. Supramolecular organization of bacterial aerobic respiratory chains: From cells and back. Biochim Biophys Acta. 1857:190–197. doi:10.1016/j.bbabio.2015.11.001.
19. Davies KM, Blum TB, Kühlbrandt W. 2018. Conserved *in situ* arrangement of complex I and $III_2$ in mitochondrial respiratory chain supercomplexes of mammals, yeast, and plants. PNAS 115:3024–3029. doi:10.1073/pnas.1720702115.
20. Trautmann A, Schleicher L, Deusch S, Gätgens J, Steuber J, Seifert J. 2020. Short-chain fatty acids modulate metabolic pathways and membrane lipids in *Prevotella bryantii* $B_14$. Proteomes 8. doi:10.3390/proteomes8040028.
21. Nowicka B, Kruk J. 2010. Occurrence, biosynthesis and function of isoprenoid quinones. Biochim Biophys Acta. 1797:1587–1605. doi:10.1016/j.bbabio.2010.06.007.
22. Pfenninger-Li XD, Albracht SP, van Belzen R, Dimroth P. 1996. NADH:ubiquinone oxidoreductase of *Vibrio alginolyticus*: purification, properties, and reconstitution of the $Na^+$ pump. Biochemistry 35:6233–6242. doi:10.1021/bi953032l.
23. Muras V, Dogaru-Kinn P, Minato Y, Häse CC, Steuber J. 2016. The $Na^+$-translocating NADH:quinone oxidoreductase enhances oxidative stress in the cytoplasm of *Vibrio cholerae*. J Bacteriol. 198:2307–2317. doi:10.1128/JB.00342-16.
24. Biegel E, Schmidt S, González JM, Müller V. 2011. Biochemistry, evolution and physiological function of the Rnf complex, a novel ion-motive electron transport complex in prokaryotes. Cell Mol Life Sci 68:613–634. doi:10.1007/s00018-010-0555-8.
25. Moparthi VK, Hägerhäll C. 2011. The evolution of respiratory chain complex I from a smaller last common ancestor consisting of 11 protein subunits. J Mol Evol 72:484–497. doi:10.1007/s00239-011-9447-2.
26. Lancaster CR, Kröger A, Auer M, Michel H. 1999. Structure of fumarate reductase from *Wolinella succinogenes* at 2.2 A resolution. Nature 402:377–385. doi:10.1038/46483.
27. Iverson TM, Luna-Chavez C, Cecchini G, Rees DC. 1999. Structure of the *Escherichia coli* fumarate reductase respiratory complex. Science 284:1961–1966. doi:10.1126/science.284.5422.1961.
28. Guimaraes JC, Rocha M, Arkin AP. 2014. Transcript level and sequence determinants of protein abundance and noise in *Escherichia coli*. Nucleic Acids Res 42:4791–4799. doi:10.1093/nar/gku126.
29. Hayashi M, Nakayama Y, Unemoto T. 2001. Recent progress in the $Na^+$-translocating NADH-quinone reductase from the marine *Vibrio alginolyticus*. Biochim Biophys Acta. 1505:37–44. doi:10.1016/S0005-2728(00)00275-9.
30. Cole ST, Condon C, Lemire BD, Weiner JH. 1985. Molecular biology, biochemistry and bionergetics of fumarate reductase, a complex membrane-bound iron-sulfur flavoenzyme of *Escherichia coli*. Biochim Biophys Acta. 811:381–403. doi:10.1016/0304-4173(85)90008-4.
31. Casutt MS, Wendelspiess S, Steuber J, Fritz G. 2010. Crystallization of the $Na^+$-translocating NADH:quinone oxidoreductase from *Vibrio cholerae*. Acta Crystallogr Sect F Struct Biol Cryst Commun. 66:1677–1679. doi:10.1107/S1744309110043125.
32. Vohl G, Nedielkov R, Claussen B, Casutt MS, Vorburger T, Diederichs K, Möller HM, Steuber J, Fritz G. 2014. Crystallization and preliminary analysis of the NqrA and NqrC subunits of the $Na^+$-translocating NADH:ubiquinone oxidoreductase from *Vibrio cholerae*. Acta Crystallogr Sect F Struct Biol Cryst Commun. 70:987–992. doi:10.1107/S2053230X14009881.
33. Kröger A, Biel S, Simon J, Gross R, Unden G, Lancaster CRD. 2002. Fumarate respiration of *Wolinella succinogenes*: enzymology, energetics and coupling mechanism. Biochim Biophys Acta. 1553:23–38. doi:10.1016/S0005-2728(01)00234-1.
34. Fedor JG, Hirst J. 2018. Mitochondrial supercomplexes do not enhance catalysis by quinone channeling. Cell Metab. 28:525-531.e4. doi:10.1016/j.cmet.2018.05.024.
35. Steuber J, Krebs W, Dimroth P. 1997. The $Na^+$-translocating NADH:ubiquinone oxidoreductase from *Vibrio alginolyticus*--redox states of the FAD prosthetic group and mechanism of $Ag^+$ inhibition. Eur J Biochem 249:770–776. doi:10.1111/j.1432-1033.1997.t01-2-00770.x.
36. Nakayama Y, Hayashi M, Yoshikawa K, Mochida K, Unemoto T. 1999. Inhibitor studies of a new antibiotic, korormicin, 2-*n*-heptyl-4-hydroxyquinoline *N*-oxide and $Ag^+$ toward the $Na^+$-translocating NADH-quinone reductase from the marine *Vibrio alginolyticus*. Biol Pharm Bull. 22:1064–1067. doi:10.1248/bpb.22.1064.
37. Hackmann TJ, Ngugi DK, Firkins JL, Tao J. 2017. Genomes of rumen bacteria encode atypical pathways for fermenting hexoses to short-chain fatty acids. Environ Microbiol. 19:4670–4683. doi:10.1111/1462-2920.13929.
38. Madej MG, Nasiri HR, Hilgendorff NS, Schwalbe H, Lancaster CRD. 2006. Evidence for transmembrane proton transfer in a dihaem-containing membrane protein complex. EMBO J. 25:4963–4970. doi:10.1038/sj.emboj.7601361.
39. Simon J, van Spanning RJM, Richardson DJ. 2008. The organisation of proton motive and non-proton motive redox loops in prokaryotic respiratory systems. Biochim Biophys Acta. 1777:1480–1490. doi:10.1016/j.bbabio.2008.09.008.
40. Unden G, Strecker A, Kleefeld A, Kim OB. 2016. $C_4$-dicarboxylate utilization in aerobic and anaerobic growth. EcoSal Plus 7. doi:10.1128/ecosalplus.ESP-0021-2015.

41. Strickler MA, Hall JA, Gaiko O, Pajor AM. 2009. Functional characterization of a $Na^+$-coupled dicarboxylate transporter from *Bacillus licheniformis*. Biochim Biophys Acta. 1788:2489–2496. doi:10.1016/j.bbamem.2009.10.008.
42. Meier T, Polzer P, Diederichs K, Welte W, Dimroth P. 2005. Structure of the rotor ring of F-Type $Na^+$-ATPase from *Ilyobacter tartaricus*. Science 308:659–662. doi:10.1126/science.1111199.
43. McGinn SM, Beauchemin KA, Coates T, Colombatto D. 2004. Methane emissions from beef cattle: Effects of monensin, sunflower oil, enzymes, yeast, and fumaric acid. J Anim Sci. 82:3346–3356. doi:10.2527/2004.82113346x.
44. Vorburger T, Nedielkov R, Brosig A, Bok E, Schunke E, Steffen W, Mayer S, Götz F, Möller HM, Steuber J. 2016. Role of the $Na^+$-translocating NADH:quinone oxidoreductase in voltage generation and $Na^+$ extrusion in *Vibrio cholerae*. Biochim Biophys Acta. 1857:473–482. doi:10.1016/j.bbabio.2015.12.010.
45. Türk K, Puhar A, Neese F, Bill E, Fritz G, Steuber J. 2004. NADH oxidation by the $Na^+$-translocating NADH:quinone oxidoreductase from *Vibrio cholerae*: functional role of the NqrF subunit. J Biol Chem. 279:21349–21355. doi:10.1074/jbc.M311692200.
46. Tao M, Türk K, Diez J, Grütter MG, Fritz G, Steuber J. 2006. Crystallization of the NADH-oxidizing domain of the $Na^+$-translocating NADH:ubiquinone oxidoreductase from *Vibrio cholerae*. Acta Crystallogr Sect F Struct Biol Cryst Commun. 62:110–112. doi:10.1107/S174430910504306X.
47. Walker PA, Leong LE, Ng PW, Tan SH, Waller S, Murphy D, Porter AG. 1994. Efficient and rapid affinity purification of proteins using recombinant fusion proteases. Biotechnology (NY) 12:601–605.
48. Tao M, Casutt MS, Fritz G, Steuber J. 2008. Oxidant-induced formation of a neutral flavosemiquinone in the $Na^+$-translocating NADH:quinone oxidoreductase ($Na^+$-NQR) from *Vibrio cholerae*. Biochim Biophys Acta. 1777:696–702. doi:10.1016/j.bbabio.2008.04.006.
49. Schleicher L, Fritz G, Seifert J, Steuber J. 2020. Anoxic cell rupture of *Prevotella bryantii* by high-pressure homogenization protects the $Na^+$-translocating NADH:quinone oxidoreductase from oxidative damage. Arch Microbiol. doi:10.1007/s00203-019-01805-x.
50. Hein S, Klimmek O, Polly M, Kern M, Simon J. 2017. A class C radical S-adenosylmethionine methyltransferase synthesizes 8-methylmenaquinone. Mol Microbiol. 104:449–462. doi:10.1111/mmi.13638.
51. Juárez O, Athearn K, Gillespie P, Barquera B. 2009. Acid residues in the transmembrane helices of the $Na^+$-pumping NADH:quinone oxidoreductase from *Vibrio cholerae* involved in sodium translocation. Biochemistry 48:9516–9524. doi:10.1021/bi900845y.
52. Geisler V, Ullmann R, Kröger A. 1994. The direction of the proton exchange associated with the redox reactions of menaquinone during electron transport in *Wolinella succinogenes*. Biochim Biophys Acta.:219–226. doi:10.1016/0005-2728(94)90226-7.
53. Kröger A, Innenhofer A. 1976. The function of menaquinone, covalently bound FAD and iron-sulfur protein in the electron transport from formate to fumarate of *Vibrio succinogenes*. Eur J Biochem.:487–495. doi:10.1111/j.1432-1033.1976.tb10933.x.
54. Chance B. 1954. Spectrophotometry of intracellular respiratory pigments. Science 120.
55. Smith PK, Krohn RI, Hermanson GT, Mallia AK, Gartner FH, Provenzano MD, Fujimoto EK, Goeke NM, Olson BJ, Klenk DC. 1985. Measurement of protein using bicinchoninic acid. Anal Biochem. 150:76–85. doi:10.1016/0003-2697(85)90442-7.
56. Paczia N, Nilgen A, Lehmann T, Gätgens J, Wiechert W, Noack S. 2012. Extensive exometabolome analysis reveals extended overflow metabolism in various microorganisms. Microb Cell Fact. 11:122. doi:10.1186/1475-2859-11-122.
57. Shevchenko A, Wilm M, Vorm O, Mann M. 1996. Mass spectrometric sequencing of proteins silver-stained polyacrylamide gels. Anal Chem 68:850–858. doi:10.1021/ac950914h.
58. Olsen JV, Godoy LMF de, Li G, Macek B, Mortensen P, Pesch R, Makarov A, Lange O, Horning S, Mann M. 2005. Parts per million mass accuracy on an Orbitrap mass spectrometer via lock mass injection into a C-trap. Mol Cell Proteomics 4:2010–2021. doi:10.1074/mcp.T500030-MCP200.
59. Keller A, Nesvizhskii AI, Kolker E, Aebersold R. 2002. Empirical statistical model to estimate the accuracy of peptide identifications made by MS/MS and database search. Anal Chem 74:5383–5392. doi:10.1021/ac025747h.
60. Nesvizhskii AI, Keller A, Kolker E, Aebersold R. 2003. A statistical model for identifying proteins by tandem mass spectrometry. Anal Chem 75:4646–4658. doi:10.1021/ac0341261.
61. Leutbecher H, Greiner G, Amann R, Stolz A, Beifuss U, Conrad J. 2011. Laccase-catalyzed phenol oxidation. Rapid assignment of ring-proton deficient polycyclic benzofuran regioisomers by experimental $^1H$-$^{13}C$ long-range coupling constants and DFT-predicted product formation. Org biomol Chem. 9:2667–2673. doi:10.1039/c1ob00012h.
62. Yan L-J, Yang S-H, Shu H, Prokai L, Forster MJ. 2007. Histochemical staining and quantification of dihydrolipoamide dehydrogenase diaphorase activity using blue native PAGE. Electrophoresis 28:1036–1045. doi:10.1002/elps.200600574.
63. Schleicher L, Muras V, Claussen B, Pfannstiel J, Blombach B, Dibrov P, Fritz G, Steuber J. 2018. *Vibrio natriegens* as host for expression of multisubunit membrane protein complexes. Front Microbiol. 9:2537. doi:10.3389/fmicb.2018.02537.
64. Untergasser A, Nijveen H, Rao X, Bisseling T, Geurts R, Leunissen JAM. 2007. Primer3Plus, an enhanced web interface to Primer3. Nucleic Acids Res. 35:W71-4. doi:10.1093/nar/gkm306.

65. Livak KJ, Schmittgen TD. 2001. Analysis of relative gene expression data using real-time quantitative PCR and the 2(-Delta Delta C(T)) Method. Methods 25:402–408. doi:10.1006/meth.2001.1262.

# Supplementary Material

Applied and Environmental Microbiology
Supplementary Data

## A Sodium-Translocating Module Linking Succinate Production to Formation of Membrane Potential in *Prevotella bryantii*

**Lena Schleicher,[a,b] Andrej Trautmann,[a,c] Dennis P. Stegmann,[a,b] Günter Fritz,[a,b] Jochem Gätgens,[e] Michael Bott,[e] Sascha Hein,[d] Jörg Simon,[d] Jana Seifert,[a,c] Julia Steuber[a,b]**

[a] Hohenheim Center for Livestock Microbiome Research, University of Hohenheim, Stuttgart, Germany
[b] Institute of Biology, University of Hohenheim, Stuttgart, Germany
[c] Institute of Animal Science, Unviersity of Hohenheim, Stuttgart, Germany
[d] Microbial Energy Conservation and Biotechnology, Technical University of Darmstadt, Darmstadt, Germany
[e] Institute of Bio- and Geoscience, IBG-1: Biotechnology, Forschungszentrum Jülich, Jülich, Germany

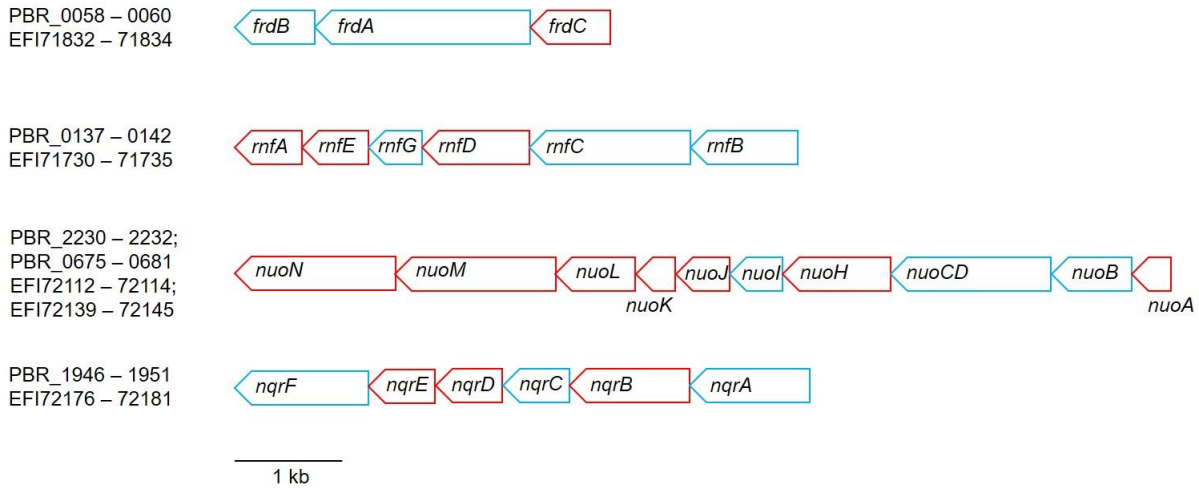


**Figure S1** Predicted operons encoding respiratory complexes of *P. bryantii* b14 with corresponding operon reading frames (ORF). NCBI accession numbers with the prefix EFI are assigned to genes based on ORFs. Subunits of QFR are encoded by *frdC* (686 bp), *frdA* (1979 bp) and *frdB* (758 bp). Subunits of RNF are encoded by *rnfB* (917 bp), *rnfC* (1418 bp), *rnfD* (992 bp), rnfG (572 bp), *rnfE* (626 bp) and *rnfA* (602 bp). The 11-subunit complex related to the Nuo complex (NDH-I, or complex I) is assigned to a gene cluster comprising *nuoA* (350 bp), *nuoB* (764 bp), *nuoCD* (1574 bp), *nuoH* (1094 bp), *nuoI* (281 bp), *nuoJ* (521 bp), *nuoK* (308 bp), *nuoL* (860 bp), *nuoM* (1505 bp), and *nuoN* (1469 bp). Note that genes coding for homologs of NuoE, -F and -G subunits which represent the NADH-oxidizing module in complex I are absent in *P. bryantii*. Subunits of the NQR complex are encoded by *nqrA* (1349 bp), *nqrB* (1157 bp), *nqrC* (632 bp), *nqrD* (629 bp), *nqrE* (626 bp) and *nqrF* (1268 bp). Red, genes coding for membrane bound subunits; blue, genes coding for peripheral subunits.

NqrA

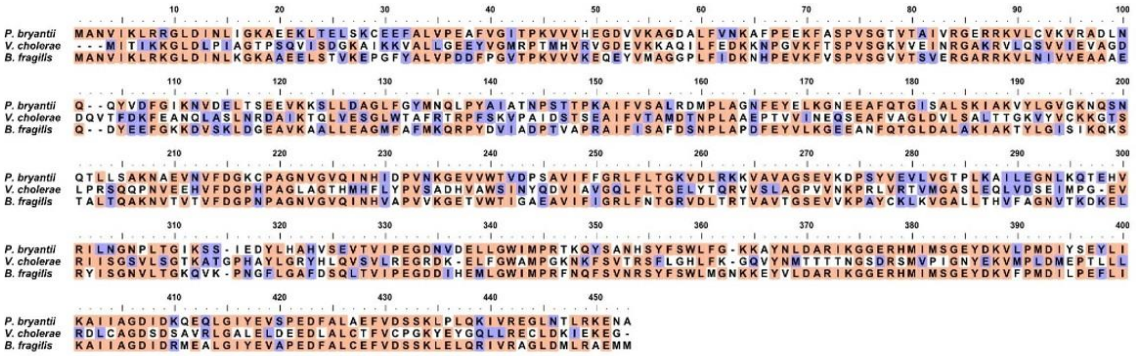


NqrB

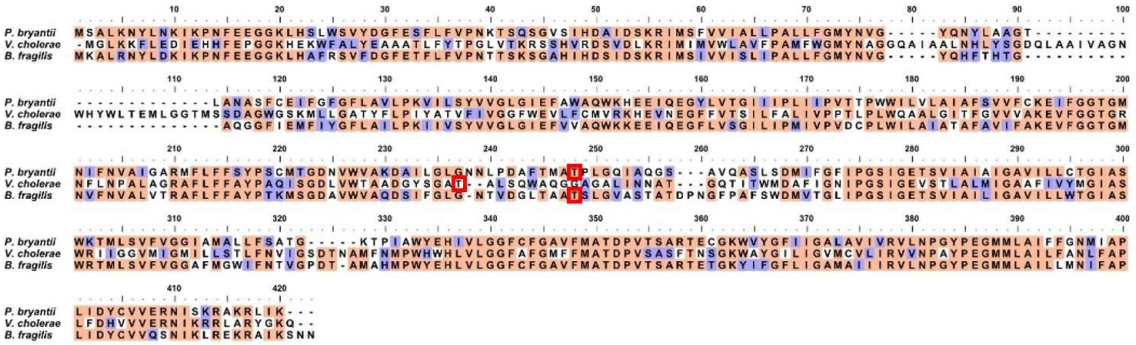


NqrC

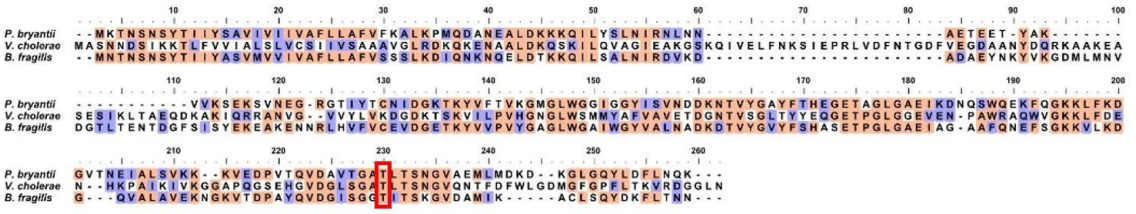


NqrD

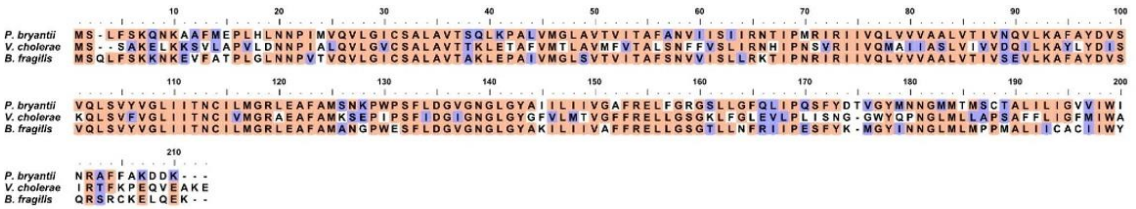


NqrE

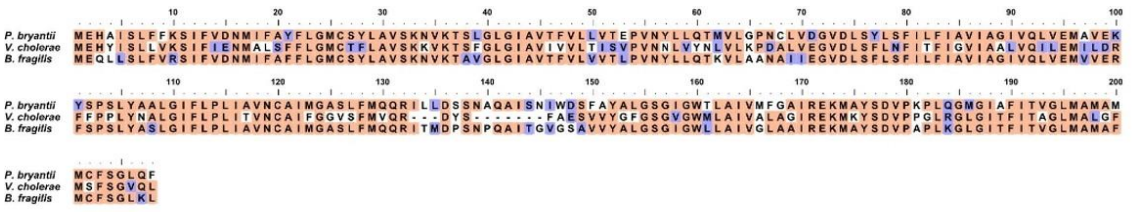

NqrF

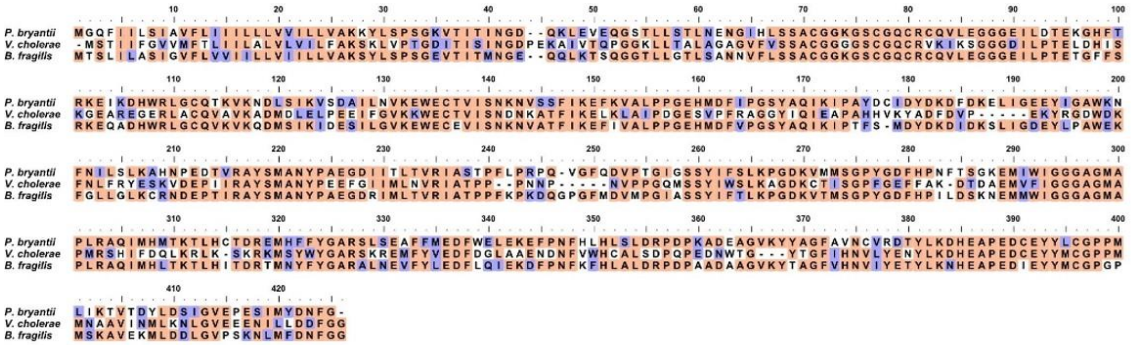


**Figure S2** Protein sequence alignments of the NQR subunits NqrA, NqrB, NqrC, NqrD, NqrE and NqrF from *Prevotella bryantii*, *Vibrio cholerae* and *Bacteroides fragilis*. Orange, identical amino acids; purple, similar amino acids. Conserved amino acids for flavin binding are highlighted in red.

FrdA

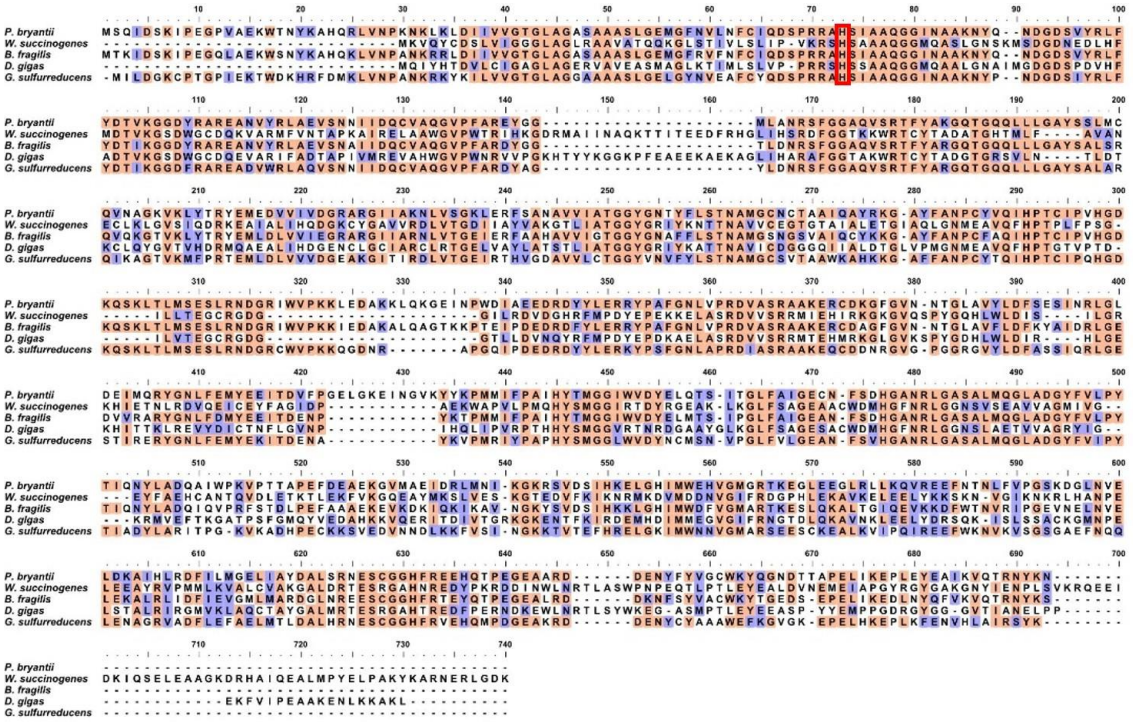


FrdB

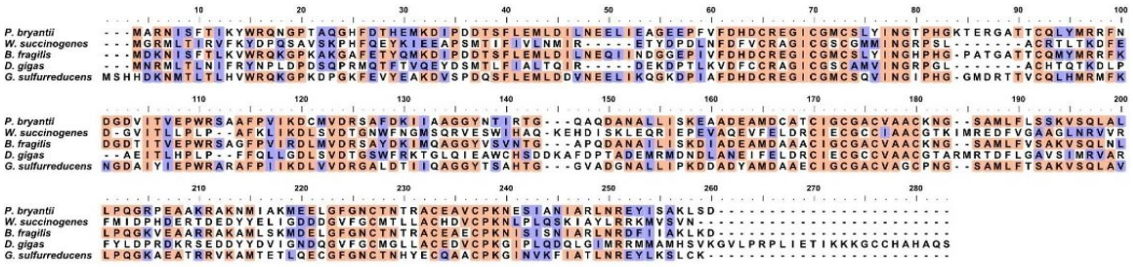


FrdC

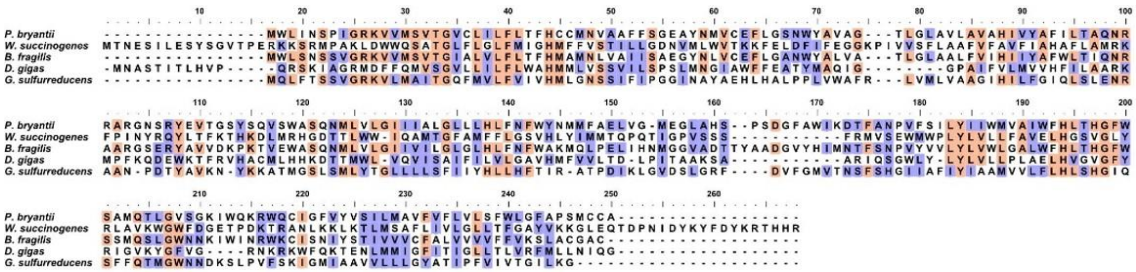


**Figure S3** Protein sequence alignments of the QFR subunits FrdA, FrdB and FrdC from *Prevotella bryantii*, *Wolinella succinogenes*, *Bacteroides fragilis*, *Desulfovibrio gigas* and *Geobacter sulfurreducens* are shown. Orange, identical amino acids; purple, similar amino acids. Conserved amino acids for flavin binding are highlighted in red.

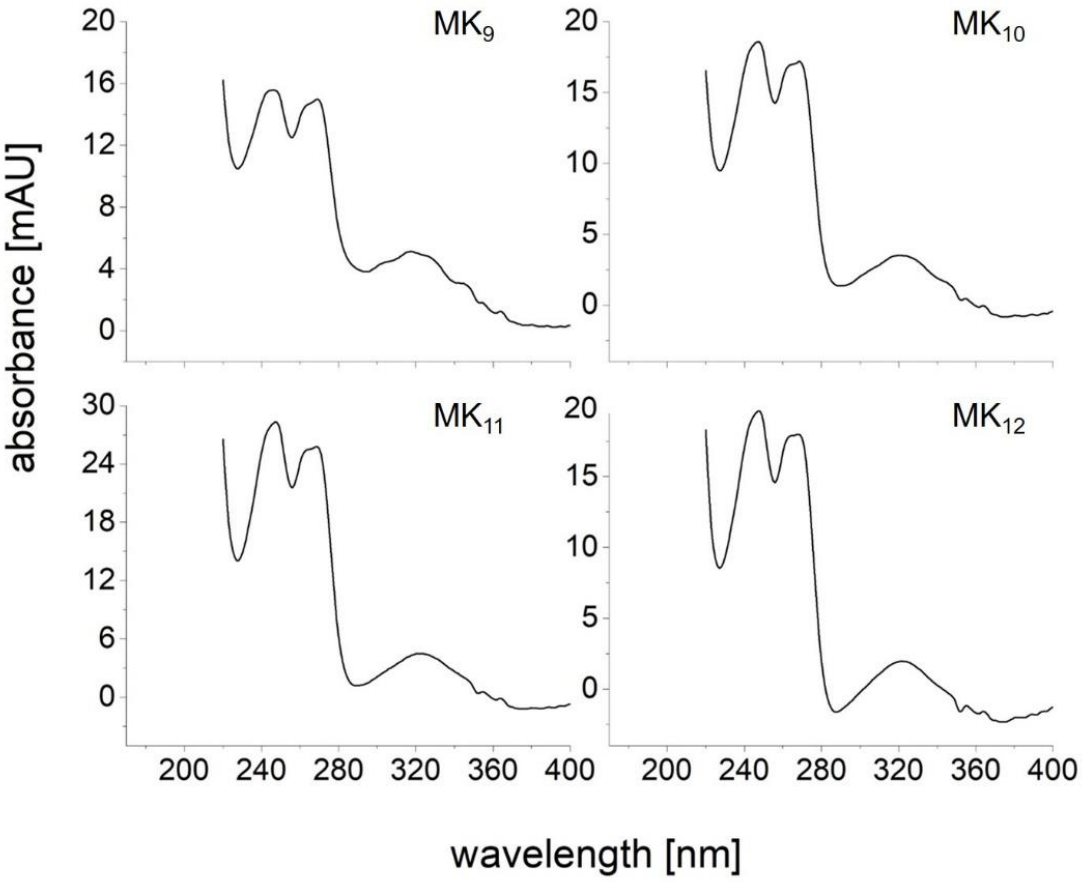


**Figure S4** UV/VIS absorption spectra of menaquinones of *P. bryantii* membranes. Quinones were extracted with organic solvent and separated by HPLC. Fractions assigned to $MK_9$, $MK_{10}$, $MK_{11}$ and $MK_{12}$ by mass spectrometry revealed typical maxima at 246 nm, 264 nm and 329 nm (1).

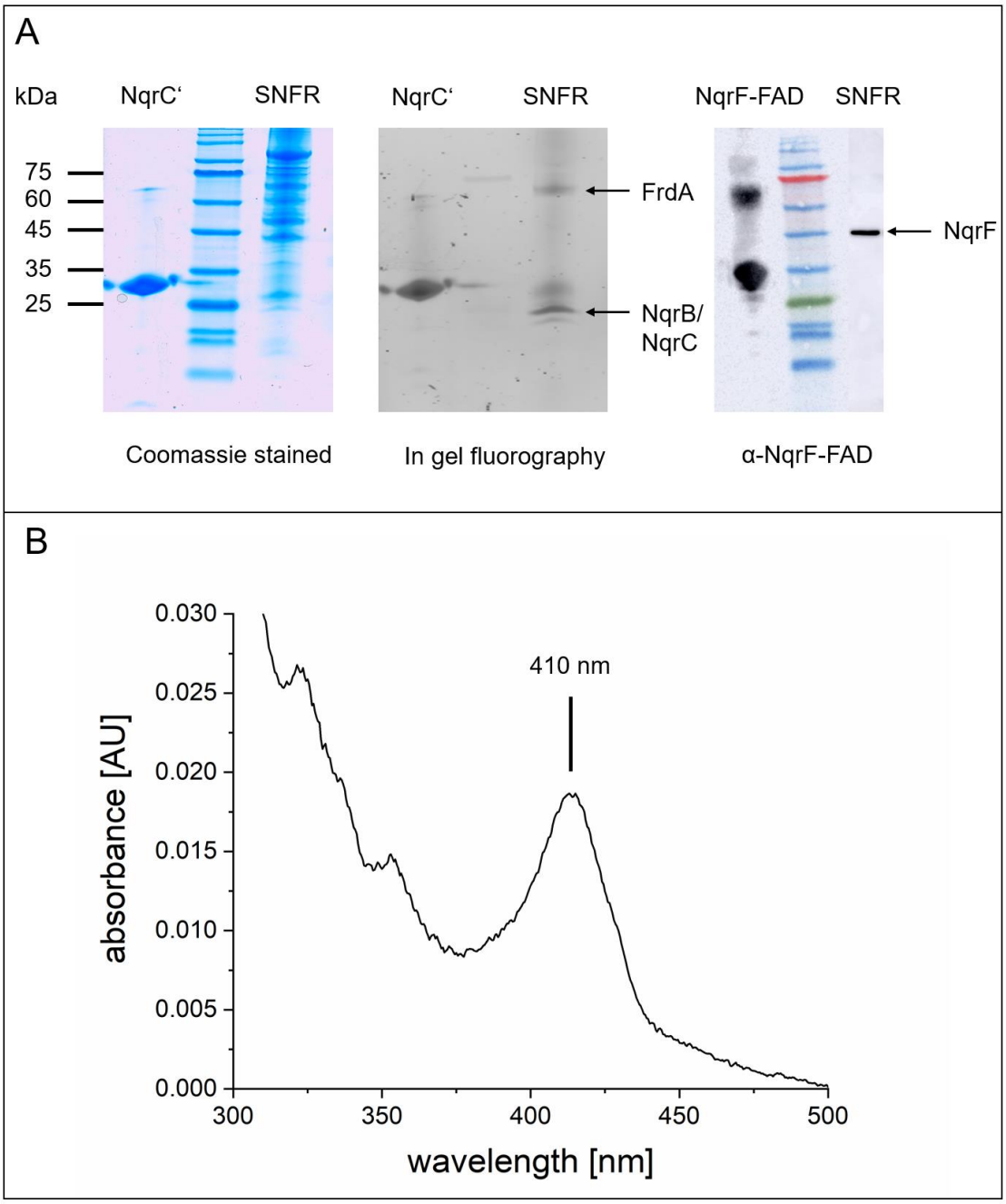


**Figure S5** Characterization of the SNFR complex from size exclusion chromatography. A: Fractions eluting at 49 - 56 mL from the size exclusion column (fig. 4C) were concentrated, and 50 µg were separated by SDS PAGE. Left, after Coomassie staining; middle, fluorography for the detection of flavinylated proteins (with 2 µg flavinylated NqrC´ as positive control); right, Western Blot using anti-NqrF-FAD antibodies with purified NqrF-FAD domain (10 µg) as positive control. B: VIS spectrum of the SNFR (5 µg in 1 mL 20 mM Tris $H_2SO_4$ pH 8.0, 50 mM $K_2SO_4$, 5 % glycerol and 0.03 % DDM) with a maximum at 410 nm.

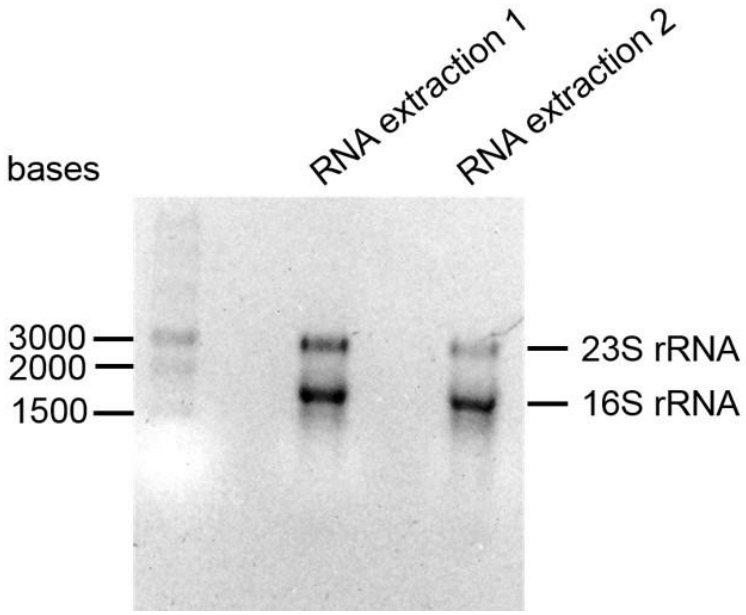


**Figure S6** Total RNA extraction of *P. bryantii* from two biological replicates. Signals obtained from denaturing formaldehyde agarose gels electrophoresis represent the two characteristic ribosomal 23S and 16S rRNAs at 3000 bp and 1500 bp respectively. 2 µl of extracted RNA was mixed with an equal amount of 2x RNA Loading Dye (Thermo Scientific) and incubated for 10 min at 70 °C. Samples were loaded on a 0.75 % agarose TAE (40 mM Tris, 0.05 mM Na2EDTA, 0.1 % acetic acid (v/v)) gel with 20 µl 37 % formaldehyde and 8 µl GelRed. The gel was run in TAE buffer for 1.5 h at 60 V.

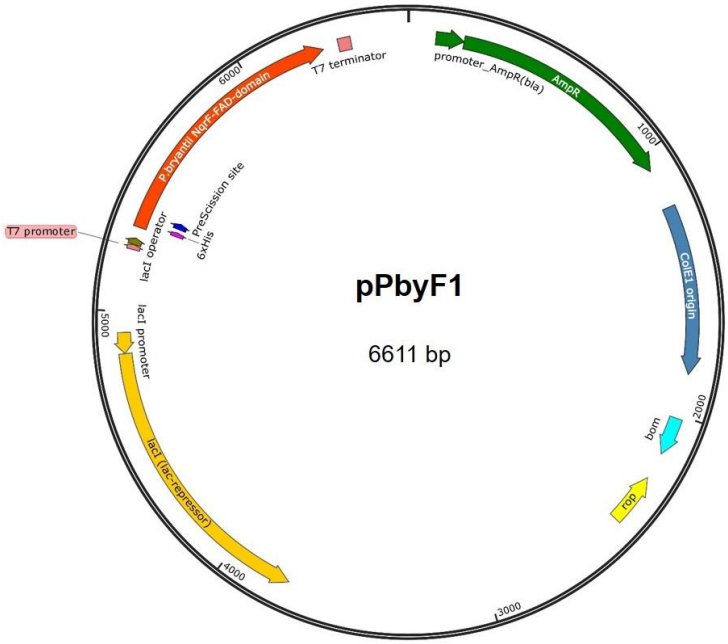


**Figure S7** Schematic map of the expression vector for the P. bryantii NqrF-FAD domain. The ColE1 derived pET15b backbone (Novagen) contains genes for ampicillin resistance, for the lacI repressor protein, and a multiple cloning site (mcs) coupled to a T7-RNA-Polymerase promotor- and terminator-sequence. The codon optimized gene for the NqrF-FAD domain of *P. bryantii* comprising a His-tag and a protease (PreScission) site was inserted into the mcs.

**Table S1** Overall hydrophobicity of subunits of NQR, RNF and QFR. Shown are the amino acid number, molecular mass and hydrophobicity of each subunit. The hydrophobicity was determined with the hydrophobicity index using GRAVY (2). This scale covers the range from - 2 to + 2. Proteins with a hydrophobicity > 0 are hydrophobic and proteins with a hydrophobicity < 0 are hydrophilic.

| | amino acid number | molecular mass [kDa] | hydrophobicity |
|---|---|---|---|
| NQR | | | |
| NqrA | 449 | 49.4 | - 0.115 |
| NqrB | 385 | 41.7 | + 0.739 |
| NqrC | 210 | 23.2 | - 0.297 |
| NqrD | 209 | 22.8 | + 0.912 |
| NqrE | 208 | 22.5 | + 1.023 |
| NqrF | 422 | 47.1 | - 0.129 |
| RNF | | | |
| RnfA | 200 | 21.5 | + 1.217 |
| RnfB | 305 | 31.9 | + 0.114 |
| RnfC | 472 | 50.5 | - 0.044 |
| RnfD | 330 | 35.3 | + 0.721 |
| RnfE | 194 | 20.5 | + 1.069 |
| RnfG | 190 | 19.7 | + 0.013 |
| QFR | | | |
| FrdA | 659 | 73.6 | - 0.376 |
| FrdB | 252 | 27.6 | - 0.239 |
| FrdC | 228 | 25.6 | + 0.864 |

**Table S2** *In silico* tryptic digestion of subunits of NQR, RNF and QFR. Listed are the sequences of the predicted peptides and their expected masses. Only peptides > 500 Da are shown. Peptides identified by mass spectrometry are indicated in red (see also Table S3 and S6).

| | peptide mass [Da] | peptide sequences |
|---|---|---|
| **NQR** | | |
| NqrA | 3721 | SSIEDYLHAHVSEVTVIPEGDNVDELLGWIMPR |
| | 2883 | SLLDAGLFGYMNQLPYAIATNPSTTPK |
| (36 peptides) | 2701 | QEQLGIYEVSPEDFALAEFVDSSK |
| | 1879 | GEVVWTVDPSAVIFFGR |
| | 1875 | CPAGNVGVQINHIDPVNK |
| | 1850 | CEEFALVPEAFVGITPK |
| | 1835 | QYSANHSYFSWLFGK |
| | 1584 | VLPMDIYSEYLIK |
| | 1552 | GNEEAFQTGISALSK |
| | 1527 | DMPLAGNFEYELK |
| | 1517 | DPSYVEVLVGTPLK |
| | 1511 | ADLNQQYVDFGIK |
| | 1405 | FASPVSGTVTAIVR |
| | 1263 | NVDELTSEEVK |
| | 1210 | HMIMSGEYDK |
| | 1204 | NQSNQTLLSAK |
| | 1140 | ILNGNPLTGIK |
| | 1092 | NAEVNVFDGK |
| | 1081 | VVVHEGDVVK |

| | | |
|---|---|---|
| | 943 | GLDINLIGK |
| | 934 | AGDALFVNK |
| | 915 | AIIAGDIDK |
| | 876 | AIFVSALR |
| | 859 | VAVAGSEVK |
| | 857 | AILEGNLK |
| | 822 | AYNLDAR |
| | 802 | EGLNTLR |
| | 769 | QTEHVR |
| | 735 | VYLGVGK |
| | 720 | AFPEEK |
| | 690 | LTELSK |
| | 678 | LFLTGK |
| | 675 | MANVIK |
| | 598 | LPLQK |
| | 561 | VLCVK |
| | 502 | VDLR |
| NqrB | 6887 | DAILGLGNNLPDAFTMATPLGQIAQGSAVQASLS |
| | | DMIFGFIPGSIGETSVIAIAIGAVILLCTGIASWKIMSFVV |
| (16 peptides) | 5375 | IALLPALLFGMYNVGYQNYLAAGTLANA |
| | | SFCEIFGFGFLAVLPK |
| | 4521 | HEEIQEGYLVTGIIIPLIIPVTTPWWILVLAIAFSVV |
| | | FCK |
| | 3473 | VLNPGYPEGMMLAIFFGNMI APLIDYCVVER |
| | 3257 | TPIAWYEHIVLGGFCFGAVF MATDPVTSAR |
| | 2385 | LHSLWSVYDGFESFLFVPNK |
| | 2343 | MFLFFSYPSCMTGDNVWVAK |
| | 2179 | VILSYVVGLGIEFAWAQWK |
| | 2114 | TMLSVFVGGIAMALLFSATGK |
| | 1867 | EIFGGTGMNIFNVAIGAR |
| | 1677 | WVYGFIIGALAVIVR |
| | 1545 | TSQSGVSIHDAIDSK |
| | 1119 | IKPNFEEGGK |
| | 651 | NYLNK |
| | 549 | MSALK |
| | 537 | TECGK |
| NqrC | 3007 | TNSNSYTIIYSAVIVIIVAFLLAFVFK |
| | 2891 | VEDPVTQVDAVTGATLTSNGVAEMLMDK |
| (13 peptides) | 2328 | NTVYGAYFTHEGETAGLGAEIK |
| | 1839 | GMGLWGGIGGYISVNDDK |
| | 1544 | ALKPMQDANEALDK |
| | 1497 | NLNNAETEETYAK |
| | 1396 | GLGQYLDFLNQK |
| | 1246 | DGVTNEIALSVK |
| | 1184 | GTIYTCNIDGK |
| | 1120 | QILYSLNIR |
| | 1034 | DNQSWQEK |
| | 756 | YVFTVK |
| | 661 | SVNEGR |
| NqrD | 5772 | AAFMEPLHLNNPIMVQVLGICSALAVTSQLKPALVMG |
| | | LAVTVITAFANVIISIIR |
| (9 peptides) | 4767 | GSLLGFQLIPQSFYDTVGYMNNGMMTMSCTALILIGV |

| | | |
|---|---|---|
| | | VIWINR |
| | 3737 | LEAFAMSNKPWPSFLDGVGNGLGYAIILIIVGAFR |
| | 2845 | AFAYDVSVQLSVYVGLIITNCILMGR |
| | 2132 | IIVQLVVVAALVTIVNQVLK |
| | 731 | NTIPMR |
| | 712 | MSLFSK |
| | 621 | ELFGR |
| | 583 | AFFAK |
| NqrE<br><br>(6 peptides) | 6822<br><br>4142 | TSLGLGIAVTFVLLVTEPVNYLLQTMVLGPNCLVDGV<br>DLSYLSFILFIAVIAGIVQLVEMAVEK<br>ILLDSSNAQAISNIWDSFAYALGSGIGWTLAIVMFGAIR |
| | 3757 | MAYSDVPKPLQGMGIAFITVGLMAMAMMCFSGLQF |
| | 3459 | YSPSLYAALGIFLPLIAVNCAIMGASLFMQQR |
| | 2619 | SIFVDNMIFAYFLGMCSYLAVSK |
| | 1223 | MEHAISLFFK |
| NqrF<br><br>(33 peptides) | 3620 | IASTPFLPRPQVGFQDVPTG IGSSYIFSLKPGDK |
| | 2966 | MGQFIILSIAVFLIIILLLV VILLVAK |
| | 2757 | LEVEQGSTLLSTLNENGIHL SSACGGK |
| | 2465 | TVTDYLDSIGVEPESIMYDN FG |
| | 2323 | DHEAPEDCEYYLCGPPMLIK |
| | 2170 | VALPPGEHMDFIPGSYAQIK |
| | 2085 | AYSMANYPAEGDIITLTVR |
| | 2062 | EFPNFHLHLSLDRPDPK |
| | 2008 | SLSEAFFMEDFWELEK |
| | 1972 | VMMSGPYGDFHPNFTSGK |
| | 1591 | CQVLEGGGEILDTEK |
| | 1559 | EMIWIGGGAGMAPLR |
| | 1408 | ELIGEEYIGAWK |
| | 1316 | IPAYDCIDYDK |
| | 1263 | YYAGFAVNCVR |
| | 1209 | EWECTVISNK |
| | 1157 | EMHFFYGAR |
| | 1089 | VTITINGDQK |
| | 1038 | AHNPEDTVR |
| | 959 | AQIMHMTK |
| | 958 | VSDAILNVK |
| | 948 | NFNILSLK |
| | 845 | TLHCTDR |
| | 794 | NVSSFIK |
| | 751 | YLSPSGK |
| | 710 | GSCGQCR |
| | 689 | NDLSIK |
| | 689 | ADEAGVK |
| | 649 | LGCQTK |
| | 639 | DTYLK |
| | 617 | GHFTR |
| | 613 | DHWR |
| | 524 | DFDK |
| **RNF** | | |
| RnfA | 6495 | IDTALGMGAAVTFVMTLATIVTFLIQTYVLTPFHLQYL<br>QT LAFILVIAALVQMIEIILK |

| | | |
|---|---|---|
| (7 peptides) | 3589 | MEYLLIFISAIFVNNIVLSQ FLGICPFLGVSK |
| | 3327 | TSPALYQALGVFLPLITTNC AVLGVAILVIQK |
| | 3120 | DYSLLQSVVYAFSTALGFAL ALILFAGIR |
| | 2997 | GMQGMSIVLVTAGLLALAFM GFSGLEGGLR |
| | 817 | EQQALTK |
| | 664 | TLFGLN |
| RnfB (19 peptides) | 3097 | CPVGGDPVMGEVADLLGMAV ANTEPMVAVVR |
| | 2828 | MNFILIAVLVLGAIALVAAV ILYIVSK |
| | 2817 | IAQVVEILPGANCGGCGFAG CGGLAEALVK |
| | 2585 | TCQAMNANGSGETGCGFGCL GCGDCTK |
| | 2416 | ACAFDAIHMNPETGLPEVDE EK |
| | 2031 | FEAITIENNLSYIDFNK |
| | 1831 | SVETVAQPAAASVNEETK |
| | 1249 | CVDECPTGAIIK |
| | 1121 | CNGTCTNRPR |
| | 1045 | GADAGSIEGIR |
| | 1013 | SCTAACIGCGK |
| | 961 | FAVQEDPR |
| | 952 | VYVQCVNK |
| | 936 | IAEYDGLR |
| | 873 | CTSCGACTK |
| | 780 | HIIELR |
| | 703 | VNFPVK |
| | 514 | AQPAK |
| | 504 | VEEK |
| RnfC (33 peptides) | 4083 | MFDQLEQEEVVSCISCGSCQFTCPAHRPLLDNIANGK |
| | 3166 | QVPAPPAIPVNVGAIVQNVGTAYAVYQAVMK |
| | 2467 | VGTLLAEAGGFVSAPVYSSVSGTVAK |
| | 2400 | KPAIIINVDEEDEWEESIDR |
| | 2332 | AEFVIINAVECEPYITSDYR |
| | 2325 | SDTLETLAAHPELTSEEIVNR |
| | 2251 | CVEACPMGLEPYLLATLSVNK |
| | 2192 | MGTPMSQLIEACGGLPDDDNK |
| | 2071 | LMMEHADEILVGVELLMK |
| | 1612 | QAIFMLSQHIGAPAK |
| | 1610 | VAGVTGMGGAGFPTFIK |
| | 1573 | GFIGIEENKPEAIR |
| | 1287 | IDNVYDATGYR |
| | 1192 | EHAGIEVVPLK |
| | 1144 | AVISLDVPVCK |
| | 1079 | IGGVHPEENK |
| | 1075 | GTNAITVLTGK |
| | 960 | VLAGGPMMGK |
| | 956 | QLVDAVVGR |
| | 946 | NPSNFLVR |
| | 903 | NKPLFER |
| | 872 | ITAEIPTK |
| | 826 | LCPPPTAK |
| | 819 | LLTELCK |
| | 816 | GAVMGIIR |
| | 790 | EAQACIR |
| | 778 | YPQGGEK |
| | 769 | YTTVTGK |

| | | |
|---|---|---|
| | 700 | AKPADAK |
| | 656 | VAELPK |
| | 645 | LHTFK |
| | 572 | AVVQR |
| | 547 | AEAEK |
| RnfD<br><br>(12 peptides) | 6402 | IITWHIPVSILCTVFVFSGLMHMINPVYANPVYELLSGG MLGAIFMATDYVTSPMTK |
| | 4693 | NMYGVIIALIPAVLVSLYYFGIGSAVVLLTSVAACVFFE WAIAK |
| | 4311 | TKPQVLDGSAMLTGLLLGMNLPSNLPLWIIILGALIAIG VGK |
| | 3949 | LPDTFTMLLGNPANGMGAGTIGEVCAAALLLGLIYML VK |
| | 3945 | CFLLVSFPAQMTSWPTVGQLGSYLDAQTGATPLSVMK NWGSYPEGMSFAILIMNGFTPLINHYMKPK |
| | 3457 | MSFGGLGNNPFNPALVGR |
| | 1848 | GQLIYGVAIGFLTIVIR |
| | 1833 | LIVSLSPHAHGNDSVER |
| | 1831 | TGDASLLDR |
| | 947 | YMLK |
| | 554 | YGIAK |
| | 551 | |
| RnfE<br><br>(8 peptides) | 5056 | IPVFIVVIAAFVTILQMVMSAYAPDSINQALGLFIPLIVV NCIILGR |
| | 4795 | ENPTFVLTLGMCPTLATTTSAINGFSMGLATMAVLICT |
| | 4427 | NFVISCIK<br>ELLGAGSIFGINLLPETTNILLFILPPGAFITLGYLSAIINK |
| | 2762 | NSPLASIFDGIGIGLGFTGALTLLGCVR |
| | 887 | VLLNGMIK |
| | 831 | ITPDMVR |
| | 755 | AESFACK |
| | 592 | MSNIK |
| RnfG<br><br>(10 peptides) | 3742 | NVMGTNDLQVAEPVNVTETIDGKPVSFTIHATTDK |
| | 3133 | MVLVLVGVSLIIGGLLAYIN HLTEGPIAEK |
| | 2923 | VLVGFNPEGQILGYTILQHA ETPGLGAK |
| | 1679 | TLGAAVESVTGGFGGDLK |
| | 1578 | TGNAVDAITASTITSR |
| | 1257 | AINQAYAVYIK |
| | 1153 | NPADGDLHVSK |
| | 851 | AGDWFQK |
| | 673 | TLAAGIK |
| | 601 | GNIIGK |
| **QFR** | | |
| FrdA<br><br>(51 peptides) | 5257 | YYKPMMIFPAIHYTMGGIWVDYELQTSITGLFAIGECN FSDHGANR |
| | 3721 | FSANAVVIATGGYGNTYFLSTNAMGCNCTAAIQAYR |
| | 3628 | LGASALMQGLADGYFVLPYTIQNYLADQAIWPK |
| | 3607 | LDIIVVGTGLAGASAAASLGEMGFNVLNFCIQDSPR |
| | 2530 | GAYFANPCYVQIHPTCIPVHGDK |
| | 2451 | YGNLFEMYEEITDVFPGELGK |

| | | |
|---|---|---|
| | 2367 | GQTGQQLLLGAYSSLMCQVNAGK |
| | 2273 | GFGVNNTGLAVYLDFSESINR |
| | 2244 | LAEVSNNIIDQCVAQGVPFAR |
| | 1827 | DFILMGELIAYDALSR |
| | 1652 | ELGHIMWEHVGMGR |
| | 1544 | GEINPWDIAEEDR |
| | 1539 | DDENYFYVGCWK |
| | 1482 | EEFNTNLFVPGSK |
| | 1450 | YQGNDTTAPELIK |
| | 1437 | VPTTAPEFDEAEK |
| | 1425 | YEMEDVVIVDGR |
| | 1354 | EEHQTPEGEAAR |
| | 1331 | NYQNDGDSVYR |
| | 1309 | AHSIAAQGGINAAK |
| | 1134 | YPAFGNLVPR |
| | 1092 | EPLEYEAIK |
| | 1075 | LGLDEIMQR |
| | 1050 | LTLMSESLR |
| | 1010 | EYGGMLANR |
| | 1006 | NESCGGHFR |
| | 1002 | DGLNVELDK |
| | 939 | IPEGPVAEK |
| | 908 | SFGGAQVSR |
| | 902 | EGLEEGLR |
| | 890 | GVMAEIDR |
| | 885 | LFYDTVK |
| | 858 | DYYLER |
| | 808 | MSQIDSK |
| | 785 | SVDSIHK |
| | 751 | EANVYR |
| | 711 | WTNYK |
| | 659 | EINGVK |
| | 642 | IWVPK |
| | 629 | TFYAK |
| | 618 | LMNIK |
| | 617 | NLVSGK |
| | 609 | AIHLR |
| | 575 | LEDAK |
| | 570 | LVNPK |
| | 567 | GGDYR |
| | 552 | LYTR |
| | 547 | DVASR |
| | 511 | AHQR |
| | 503 | VQTR |
| | 501 | GIIAK |
| FrdB<br><br>(20 peptides) | 3967 | DIPDDTSFLEMLDILNEELI EAGEEPFVFDHDCR |
| | 2206 | EAADEAMDCATCIGCGACVA ACK |
| | 1880 | EGICGMCSLYINGTPHGK |
| | 1798 | QNGPTAQGHFDTHEMK |
| | 1678 | VSQLALLPQGRPEAAK |
| | 1548 | FNDGDVITVEPWR |
| | 1472 | MEELGFGNCTNTR |
| | 1430 | TGQAQDANALLISK |
| | 1155 | NGSAMLFLSSK |

| | | |
|---|---|---|
| | 1149 | IIAAGGYNTIR |
| | 1143 | GATTCQLYMR |
| | 987 | NESIANIAR |
| | 832 | SAAFPVIK |
| | 822 | NISFTIK |
| | 820 | ACEAVCPK |
| | 738 | DCMVDR |
| | 710 | EYISAK |
| | 576 | NMIAK |
| | 567 | SAFDK |
| | 524 | YWR |
| FrdC<br><br>(6 peptides) | 7550 | VVMSVTGVCLILFLTFHCCMNVAAFFSGEAYNMVCEF<br>LGSNWYAVAGTLGLAVLAVAHIVYAFILTAQNR |
| | 6965 | YEVTGSYSQVSWASQNMLVLGIIIALGLLLHLFNFWY<br>NMMFAELVGMEGLAHSPSDGFAWIK |
| | 4484 | DTFANPVFSILYIIWMVAIWFHLTHGFWSAMQTLGVS<br>GK |
| | 3848 | WQCIGFVYVSILMAVFVFLVLSFWLGFAPSMCCA |
| | 1187 | MWLINSPIGR |
| | 574 | IWQK |

**Table S3** Subunits of the NQR, QFR and RNF identified from *P. bryantii* membranes solubilized with 2.5 % DDM or 5 % Triton X-100 identified by mass spectrometry. Bands were excised from Coomassie stained 1D BN PAGE as indicated in fig. 2C. Identified subunit, total number of identified peptides, and peptide sequences are presented.

| **Box number** | **Identified protein** | **Peptide number** | **Peptide sequences** |
|---|---|---|---|
| **1** | FrdA | 29 | SQIDSKIPEGPVAEK; IPEGPVAEK; IPEGPVAEKWTNYK; RAHSIAAQGGINAAK; AHSIAAQGGINAAK; NYQNDGDSVYR; LFYDTVK; LAEVSNNIIDQCVAQGVPFAR; EYGGMLANR; SFGGAQVSR; YEMEDVVIVDGR; NLVSGKLER; LTLMSESLR; GEINPWDIAEEDR; RYPAFGNLVPR; YPAFGNLVPR; LGLDEIMOR; VPTTAPEFDEAEK; VPTTAPEFDEAEKGVMAEIDR; ELGHIMWEHVGMGR; TKEGLEEGLR; EGLEEGLR; QVREEFNTNLFVPGSK; EEFNTNLFVPGSK; DGLNVELDK; NESCGGHFREEHQTPEGEAAR; DDENYFYVGCWK; YQGNDTTAPELIKEPLEYEAIK |
| | NqrA | 19 | RGLDINLIGK; GLDINLIGK; GLDINLIGKAEEK; AEEKLTELSK; CEEFALVPEAFVGITPK; VVVHEGDVVK; AGDALFVNK; ADLNQQYVDFGIK; NVDELTSEEVK; NVDELTSEEVKK; DMPLAGNFEYELK; VYLGVGK; NQSNQTLLSAK; NAEVNVFDGK; CPAGNVGVQINHIDPVNK; DPSYVEVLVGTPLK; HMIMSGEYDK; VLPMDIYSEYLIK; EGLNTLR |
| | FrdB | 14 | NISFTIK; QNGPTAQGHFDTHEMK; GATTCQLYMR; RFNDGDVITVEPWR; FNDGDVITVEPWR; SAAFPVIK; SAAFPVIKDCMVDR; |

| | | | |
|---|---|---|---|
| | | | SAFDKIIAAGGYNTIR; IIAAGGYNTIR; TGQAQDANALLISK; NGSAMLFLSSK; VSQLALLPQGRPEAAK; MEELGFGNCTNTR; NESIANIAR |
| | RnfC | 10 | QAIFMLSQHIGAPAK; IDNVYDATGYR; VAGVTGMGGAGFPTFIK; GFIGIEENKPEAIR; LLTELCK; EHAGIEVVPLK; QLVDAVVGR; HIKNPSNFLVR; GTNAITVLTGK |
| | NqrF | 7 | VTITINGDQK; VSDAILNVK; NVSSFIK; NFNILSLK; VMMSGPYGDFHPNFTSGK; EMIWIGGGAGMAPLR; YYAGFAVNCVR |
| | NqrC | 7 | ALKPMQDANEALDK; KQILYSLNIR; QILYSLNIR; NLNNAETEETYAK; GTIYTCNIDGK; DGVTNEIALSVKK; GLGQYLDFLNQK |
| | RnfG | 5 | TLGAAVESVTGGFGGDLK; AGDWFQK; NPADGDLHVSK; NPADGDLHVSKDDK; AINQAYAVYIK |
| | NqrB | 2 | TSQSGVSIHDAIDSK; TSQSGVSIHDAIDSKR |
| | RnfD | 2 | LIVSLSPHAHGNDSVER; TGDASLLDR |
| **2** | NqrA | 28 | RGLDINLIGK; GLDINLIGK; GLDINLIGKAEEK; AEEKLTELSK; CEEFALVPEAFVGITPK; VVVHEGDVVK; AGDALFVNK; FASPVSGTVTAIVR; ADLNQQYVDFGIK; NVDELTSEEVK; VDELTSEEVKK; SLLDAGLFGYMNQLPYAIATNPSTTPK; AIFVSALR; DMPLAGNFEYELK; GNEEAFQTGISALSK; VYLGVGK; NQSNQTLLSAK; NAEVNVFDGK; CPAGNVGVQINHIDPVNK; KVAVAGSEVKDPSYVEVLVGTPLK; VAVAGSEVKDPSYVEVLVGTPLK; DPSYVEVLVGTPLK; ILNGNPLTGIK; AYNLDAR; HMIMSGEYDK; VLPMDIYSEYLIK; EGLNTLR; EGLNTLRK |
| | FrdA | 18 | IPEGPVAEK; AHSIAAQGGINAAK; NYQNDGDSVYR; LFYDTVK; LAEVSNNIIDQCVAQGVPFAR; EYGGMLANR; YEMEDVVIVDGR; RYPAFGNLVPR; LGLDEIMOR; VPTTAPEFDEAEK; VPTTAPEFDEAEKGVMAEIDR; TKEGLEEGLR; DGLNVELDK; NESCGGHFREEHQTPEGEAAR; YQGNDTTAPELIKEPLEYEAIK |
| | RnfC | 14 | IGGVHPEENKITAEIPTK; QAIFMLSQHIGAPAK; VGTLLAEAGGFVSAPVYSSVSGTVAK; SDTLETLAAHPELTSSEIVNR; VAGVTGMGGAGFPTFIK; VDKGFIGIEENKPEAIR; LLTELCK; EHAGIEVVPLK; QLVDAVVGR; HIKNPSNFLVR; VLAGGPMMGK; GTNAITVLTGK; GAVMGIIR |
| | NqrF | 12 | VTITINGDQK; CQVLEGGGEILDTEK; VSDAILNVK; VALPPGEHMDFIPGSYAQIK; IPAYDCIDYDK; IPAYDCIDYDKDFDK; ELIGEEYIGAWK; AYSMANYPAEGDIITLTVR; VMMSGPYGDFHPNFTSGK;EMIWIGGGAGMAPLR; |

| | | | |
|---|---|---|---|
| | | | EMHFFYGAR; YYAGFAVNCVR |
| | NqrC | 11 | ALKPMQDANEALDK; ALKPMQDANEALDKK; KQILYSLNIR; QILYSLNIR; NLNNAETEETYAK; GTIYTCNIDGK; TKYVFTVK; DGVTNEIALSVKK; DGVTNEIALSVK; DKGLGQYLDFLNQK; GLGQYLDFLNQK |
| | FrdB | 10 | NISFTIK; QNGPTAQGHFDTHEMK; GATTCQLYMR; SAAFPVIK; IIAAGGYNTIR; TGQAQDANALLISK; NGSAMLFLSSK; VSQLALLPQGRPEAAK; MEELGFGNCTNTR; NESIANIAR |
| | RnfG | 6 | TLGAAVESVTGGFGGDLK; AGDWFQK; NPADGDLHVSK; GNIIGKNPADGDLHVSK; NPADGDLHVSKDDK; AINQAYAVYIK |
| | NqrB | 3 | IKPNFEEGGK; TSQSGVSIHDAIDSK; TSQSGVSIHDAIDSKR |
| | RnfD | 3 | LIVSLSPHAHGNDSVER; TGDASLLDR; MSFGGLGNNPFNPALVGR |
| | NqrD | 1 | ITPDMVR |
| | NqrE | 1 | MEHAISLFFK |
| **3** | FrdA | 26 | SQIDSKIPEGPVAEK; RAHSIAAQGGINAAK; AHSIAAQGGINAAK; NYQNDGDSVYR; LFYDTVK; LAEVSNNIIDQCVAQGVPFAR; EYGGMLANR; SFGGAQVSR; YEMEDVVIVDGR; NLVSGKLER; LTLMSESLR; GEINPWDIAEEDR; RYPAFGNLVPR; YPAFGNLVPR; LGLDEIMOR; VPTTAPEFDEAEK; GVMAEIDR; TKEGLEEGLR; EGLEEGLR; EEFNTNLFVPGSK; DGLNVELDK; NESCGGHFREEHQTPEGEAAR; DDENYFYVGCWK; YQGNDTTAPELIKEPLEYEAIK; YQGNDTTAPELIK |
| | NqrA | 23 | RGLDINLIGK; GLDINLIGK; GLDINLIGKAEEK; AEEKLTELSK; VVVHEGDVVK; AGDALFVNK; FASPVSGTVTAIVR; ADLNQQYVDFGIK; NVDELTSEEVK; NVDELTSEEVKK; DMPLAGNFEYELK; GNEEAFQTGISALSK; VYLGVGK; NQSNQTLLSAK; NAEVNVFDGK; CPAGNVGVQINHIDPVNK; VAVAGSEVKDPSYVEVLVGTPLK; VAVAGSEVK; DPSYVEVLVGTPLK; AYNLDAR; HMIMSGEYDK; VLPMDIYSEYLIK; EGLNTLR |
| | FrdB | 13 | NISFTIK; QNGPTAQGHFDTHEMK; GATTCQLYMR; FNDGDVITVEPWR; SAAFPVIK; SAAFPVIKDCMVDR; SAFDKIIAAGGYNTIR; IIAAGGYNTIR; TGQAQDANALLISK; NGSAMLFLSSK; VSQLALLPQGRPEAAK; MEELGFGNCTNTR; NESIANIAR |
| | NqrF | 9 | VTITINGDQK; CQVLEGGGEILDTEK; VSDAILNVK; NVSSFIK; VMMSGPYGDFHPNFTSGK; EMIWIGGGAGMAPLR; EMHFFYGAR; YYAGFAVNCVR |
| | NqrC | 9 | ALKPMQDANEALDK; ALKPMQDANEALDKK; KQILYSLNIR; QILYSLNIR; NLNNAETEETYAK; GTIYTCNIDGK; TKYVFTVK; DGVTNEIALSVKK; DGVTNEIALSVK |
| | RnfC | 7 | IDNVYDATGYR; LLTELCK; EHAGIEVVPLK; |

| | | | |
|---|---|---|---|
| | | | QLVDAVVGR; NPSNFLVR; GTNAITVLTGK; GAVMGIIR |
| | RnfG | 4 | TLGAAVESVTGGFGGDLK; NPADGDLHVSK; NPADGDLHVSKDDK; AINQAYAVYIK |
| | NqrB | 3 | IKPNFEEGGK; TSQSGVSIHDAIDSK;TSQSGVSIHDAIDSKR |
| | RnfD | 1 | TGDASLLDR |
| **4** | NqrA | 25 | RGLDINLIGK; GLDINLIGK; GLDINLIGKAEEK; AEEKLTELSK; VVVHEGDVVK; AGDALFVNK; FASPVSGTVTAIVR; ADLNQQYVDFGIK; NVDELTSEEVK; NVDELTSEEVKK; AIFVSALR; DMPLAGNFEYELK; GNEEAFQTGISALSK; VYLGVGK; NQSNQTLLSAK; NAEVNVFDGK; CPAGNVGVQINHIDPVNK; VAVAGSEVKDPSYVEVLVGTPLK; VAVAGSEVK; DPSYVEVLVGTPLK; ILNGNPLTGIK; HMIMSGEYDK; VLPMDIYSEYLIK; EGLNTLR; EGLNTLRK |
| | FrdA | 18 | IPEGPVAEK; AHSIAAQGGINAAK; NYQNDGDSVYR; LFYDTVK; EYGGMLANR; SFGGAQVSR; YEMEDVVIVDGR; NLVSGKLER; LTLMSESLR; YPAFGNLVPR; LGLDEIMOR; VPTTAPEFDEAEK; GVMAEIDR; TKEGLEEGLR; EEFNTNLFVPGSK; DGLNVELDK; YQGNDTTAPELIK |
| | NqrF | 12 | VTITINGDQK; CQVLEGGGEILDTEK; VKNDLSIK; EWECTVISNK; NVSSFIK; IPAYDCIDYDK; NFNILSLK; AYSMANYPAEGDIITLTVR; VMMSGPYGDFHPNFTSGK; EMIWIGGGAGMAPLR; EMHFFYGAR; YYAGFAVNCVR |
| | NqrC | 9 | ALKPMQDANEALDK; ALKPMQDANEALDKK; KQILYSLNIR; QILYSLNIR; NLNNAETEETYAK; GTIYTCNIDGK; TKYVFTVK; DGVTNEIALSVKK; DGVTNEIALSVK |
| | FrdB | 7 | NISFTIK; IIAAGGYNTIR; TGQAQDANALLISK; NGSAMLFLSSK; VSQLALLPQGRPEAAK; MEELGFGNCTNTR; NESIANIAR |
| | RnfC | 7 | ITAEIPTK; IDNVYDATGYR; LLTELCK; EHAGIEVVPLK; NPSNFLVR; GTNAITVLTGK; GAVMGIIR |
| | RnfG | 4 | AGDWFQK; NPADGDLHVSK; NPADGDLHVSKDDK; AINQAYAVYIK |
| | NqrB | 3 | IKPNFEEGGK; TSQSGVSIHDAIDSK; TSQSGVSIHDAIDSKR |
| | RnfD | 1 | TGDASLLDR |

**Table S6** Mass spectrometric analyses of NQR, QFR and RNF subunits identified from *P. bryantii* membranes solubilized with 2.5% DDM. Solubilisate was separated first on BN PAGE. The corresponding lane was further separated by 2D SDS PAGE. Spots exhibiting in gel fluorography were cut out and subjected to mass spectrometry (fig. 4B). Identified subunit, total number of identified peptides, and peptide sequences are presented.

| Box number | Identified protein | Peptide number | Peptide sequences |
|---|---|---|---|
| **5** | FrdA | 27 | SQIDSKIPEGPVAEK; IPEGPVAEK; IPEGPVAEKWTNYK; RAHSIAAQGGINAAK; AHSIAAQGGINAAK; NYQNDGDSVYR; LFYDTVK; EYGGMLANR; SFGGAQVSR; YEMEDVVIVDGR; NLVSGKLER; LTLMSESLR; RYPAFGNLVPR; YPAFGNLVPR; LGLDEIMOR; VPTTAPEFDEAEK; GVMAEIDR; GVMAEIDRMNIK; TKEGLEEGLR; EGLEEGLR; QVREEFNTNLFVPGSK; EEFNTNLFVPGSK; DGLNVELDK; YQGNDTTAPELIKEPLEYEAIK |
| | FrdB | 10 | QNGPTAQGHFDTHEMK; GATTCQLYMR; FNDGDVITVEPWR; SAAFPVIK; SAAFPVIKDCMVDR; TGQAQDANALLISK; NGSAMLFLSSK; VSQLALLPQGRPEAAK; MEELGFGNCTNTR; NESIANIAR |
| | NqrA | 5 | AGDALFVNK; GNEEAFQTGISALSK; VYLGVGK; NQSNQTLLSAK; NAEVNVFDGK |
| | RnfC | 5 | ITAEIPTK; IDNVYDATGYR; QLVDAVVGR; NPSNFLVR; GTNAITVLTGK |
| | NqrF | 4 | CQVLEGGGEILDTEK; VSDAILNVK; EMIWIGGGAGMAPLR; YYAGFAVNCVR |
| | NqrC | 1 | NLNNAETEETYAK |
| | NqrB | 1 | TSQSGVSIHDAIDSK |
| **6** | FrdA | 22 | SQIDSKIPEGPVAEK; IPEGPVAEK; RAHSIAAQGGINAAK; AHSIAAQGGINAAK; NYQNDGDSVYR; LFYDTVK; LFYDTVKGGDYR; EYGGMLANR; SFGGAQVSR; YEMEDVVIVDGR; RYEMEDVVIVDGR; YGNLFEMYEEITDVFPGELGK; VPTTAPEFDEAEK; TKEGLEEGLR; EGLEEGLR; EEFNTNLFVPGSK; DGLNVELDK; NESCGGHFREEHQTPEGEAAR; YQGNDTTAPELIKEPLEYEAIK |
| | NqrA | 22 | RGLDINLIGK; GLDINLIGKAEEK; VVVHEGDVVK; AGDALFVNK; FASPVSGTVTAIVR; VRADLNQQYVDFGIK; ADLNQQYVDFGIK; NVDELTSEEVK; NVDELTSEEVKK; AIFVSALR; DMPLAGNFEYELK; VYLGVGK; VYLGVGKNQSNQTLLSAK; NQSNQTLLSAK; NAEVNVFDGK; VAVAGSEVKDPSYVEVLVGTPLK; VAVAGSEVK; AILEGNLKQTEHVR; ILNGNPLTGIK; AYNLDAR; HMIMSGEYDK; EGLNTLRKENA |
| | RnfC | 17 | IGGVHPEENKITAEIPTK; ITAEIPTK; ITAEIPTKVAELPK; QAIFMLSQHIGAPAK; |

| | | | |
|---|---|---|---|
| | | | VKVAGVTGMGGAGFTPFIK; VAGVTGMGGAGFTPFIK; VDKGFIGIEENKPEAIR; GFIGIEENKPEAIR; LLTELCK; EHAGIEVVPLK; QLVDAVVGR; HIKNPSNFLVR; AVISLDVPVCK; GTNAITVLTGK; GTNAITVLTGKDAHRK; GAVMGIIR |
| | NqrF | 7 | VTITINGDQK; VSDAILNVK; NVSSFIK; AYSMANYPAEGDIITLTVR; VMMSGPYGDFHPNFTSGK; EMIWIGGGAGMAPLR; YYAGFAVNCVR |
| | NqrC | 6 | KQILYSLNIR; QILYSLNIR; NLNNAETEETYAK; TKYVFTVK; DGVTNEIALSVKK |
| | FrdB | 4 | IIAAGGYNTIR; TGQAQDANALLISK; MEELGFGNCTNTR; LNREYISAK |
| | NqrB | 3 | IKPNFEEGGK; TSQSGVSIHDAIDSK; TSQSGVSIHDAIDSKR |
| **7** | FrdA | 8 | IPEGPVAEK; NYQNDGDSVYR; SFGGAQVSR; YEMEDVVIVDGR; LTLMSESLR; LGLDEIMQR; TKEGLEEGLR; EGLEEGLR |
| | FrdB | 5 | IIAAGGYNTIR; TGQAQDANALLISK; NGSAMLFLSSK; MEELGFGNCTNTR; NESIANIAR |
| | NqrA | 3 | VVVHEGDVVK; VYLGVGK; NQSNQTLLSAK |
| | NqrC | 3 | ALKPMQDANEALDK; NLNNAETEETYAK; GTIYTCNIDGK |
| | NqrB | 2 | SALKNYLNK; IKPNFEEGGK |
| | NqrF | 1 | VSDAILNVK |
| | RnfD | 1 | TGDASLLDR |
| **8** | FrdA | 8 | NYQNDGDSVYR; NLVSGKLER; LTLMSESLR; LGLDEIMQR; VPTTAPEFDEAEK; TKEGLEEGLR; DGLNVELDK |
| | NqrC | 3 | ALKPMQDANEALDK; NLNNAETEETYAK; GTIYTCNIDGK |
| | NqrA | 3 | AGDALFVNK; VYLGVGK; NQSNQTLLSAK |
| | FrdB | 1 | IIAAGGYNTIR |
| | RnfD | 1 | TGDASLLDR |

For table S4, S5 and S7 see: https://journals.asm.org/doi/10.1128/AEM.01211-21?url_ver=Z39.88-2003&rfr_id=ori:rid:crossref.org&rfr_dat=cr_pub%20%200pubmed#pill-references (18.10.2021).

# References

1. Hein S, Klimmek O, Polly M, Kern M, Simon J. 2017. A class C radical S-adenosylmethionine methyltransferase synthesizes 8-methylmenaquinone. Mol Microbiol. 104:449–462. doi:10.1111/mmi.13638.
2. Chang KY, Yang J-R. 2013. Analysis and prediction of highly effective antiviral peptides based on random forests. PLoS ONE 8:e70166. doi:10.1371/journal.pone.0070166

# Chapter 4 – Central carbon metabolism, sodium-motive electron transfer, and ammonium formation by the vaginal pathogen *Prevotella bivia*

**Lena Schleicher[1,2], Sebastian Herdan[1,2], Günter Fritz[1,2], Andrej Trautmann[2,3], Jana Seifert[2,3] and Julia Steuber[1,2,*]**

[1] Institute of Biology, University of Hohenheim, Garbenstraße 30, 70599 Stuttgart, Germany;lena.schleicher@uni-hohenheim.de (L.S.); sebastian.herdan@uni-hohenheim.de (S.H.); guenter.fritz@uni-hohenheim.de (G.F.)

[2] HoLMiR- Hohenheim Center for Livestock Microbiome Research, University of Hohenheim, Leonore-Blosser-Reisen-Weg 3, 70599 Stuttgart, Germany; anderj.trautmann@uni-hohenheim.de (A.T.); seifert.jana@uni-hohenheim.de (J.S.)

[3] Institute of Animal Science, University of Hohenheim, Emil-Wolff-Straße 8, 70599 Stuttgart, Germany

* Correspondence: julia.steuber@uni-hohenheim.de, +49-711-459-222-28

International Journal of *Molecular Sciences*

MDPI

*Article*

# Central Carbon Metabolism, Sodium-Motive Electron Transfer, and Ammonium Formation by the Vaginal Pathogen *Prevotella bivia*

**Lena Schleicher [1,2], Sebastian Herdan [1,2], Günter Fritz [1,2], Andrej Trautmann [2,3], Jana Seifert [2,3] and Julia Steuber[1,2,*]**

1 Institute of Biology, University of Hohenheim, Garbenstraße 30, 70599 Stuttgart, Germany; lena.schleicher@uni-hohenheim.de (L.S.); sebastian.herdan@uni-hohenheim.de (S.H.); guenter.fritz@uni-hohenheim.de (G.F.)

2 HoLMiR-Hohenheim Center for Livestock Microbiome Research, University of Hohenheim, Leonore-Blosser-Reisen-Weg 3, 70599 Stuttgart, Germany; andrej.trautmann@uni-hohenheim.de (A.T.); seifert.jana@uni-hohenheim.de (J.S.)

3 Institute of Animal Science, University of Hohenheim, Emil-Wolff-Straße 8, 70599 Stuttgart, Germany

* Correspondence: julia.steuber@uni-hohenheim.de; Tel.: +49-711-459-222-28

**Citation:** Schleicher, L.; Herdan, S.; Fritz, G.; Trautmann, A.; Seifert, J.; Steuber, J. Central Carbon Metabolism, Sodium-Motive Electron Transfer, and Ammonium Formation by the Vaginal Pathogen *Prevotella bivia*. *Int. J. Mol. Sci.* **2021**, *22*, 11925. https://doi.org/10.3390/ijms222111925

**Academic Editors:** Rosa María Martínez-Espinosa and Carmen Lucía Pire-Galiana

**Received:** 13 October 2021

**Accepted:** 28 October 2021

**Published:** 3 November 2021

**Publisher's Note:** MDPI stays neutral with regard to jurisdictional claims in published maps and institutional affiliations.



**Abstract** Replacement of the *Lactobacillus* dominated vaginal microbiome by a mixed bacterial population including *Prevotella bivia* is associated with bacterial vaginosis (BV). To understand the impact of *P. bivia* on this microbiome, its growth requirements and mode of energy production were studied. Anoxic growth with glucose depended on $CO_2$ and resulted in succinate formation, indicating phosphoenolpyruvate carboxylation and fumarate reduction as critical steps. The reductive branch of fermentation relied on two highly active, membrane-bound enzymes, namely the quinol:fumarate reductase (QFR) and $Na^+$-translocating NADH:quinone oxidoreductase (NQR). Both enzymes were characterized by activity measurements, in-gel fluorography, and VIS difference spectroscopy, and the $Na^+$-dependent build-up of a transmembrane voltage was demonstrated. NQR is a potential drug target for BV treatment since it is neither found in humans nor in *Lactobacillus*. In *P. bivia*, the highly active enzymes L-asparaginase and aspartate ammonia lyase catalyze the conversion of asparagine to the electron acceptor fumarate. However, the by-product ammonium is highly toxic. It has been proposed that *P. bivia* depends on ammonium-utilizing *Gardnerella vaginalis*, another typical pathogen associated with BV, and provides key nutrients to it. The product pattern of *P. bivia* growing on glucose in the presence of mixed amino acids substantiates this notion.

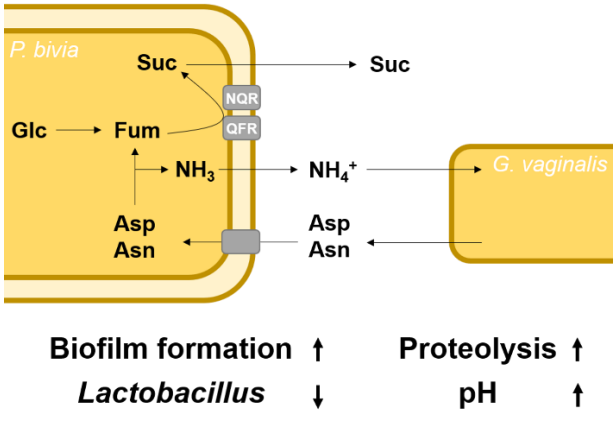


**Keywords** bacterial vaginosis; *Prevotella bivia*; $Na^+$-translocating NADH:quinone oxidoreductase; fumarate reductase; amino acid degradation

## Introduction

The most commonly reported microbiological syndrome among women in reproductive age is bacterial vaginosis (BV) [1]. This infection is associated with a variety of health issues, such as increased susceptibility to sexual transmitted pathogens, higher risk of pelvic inflammatory disease, or preterm births [1]. BV is characterized by a drastic change of the vaginal microbiome [2]. A healthy vagina is dominated by Gram-positive *Lactobacillus*, which maintain a vaginal pH of ~4.5 due to the degradation of sugars to lactic acid [3,4]. In BV, the vaginal microbiota is dominated by opportunistic pathogens such as *Gardnerella vaginalis* (earlier *Haemophilus vaginalis*), *Prevotella bivia*, or *Peptostreptococcus anaerobuis* [3,5,6].

*P. bivia* is a Gram-negative obligate anaerobic bacterium which, together with other *Prevotella* sp., accounts for up to 44% of bacterial species identified in BV patients [7]. It has the ability to invade the human cervix [8] and cause intrauterine infections [9]. *G. vaginalis* is another marker strain for BV and both *G. vaginalis* [10] and *P. bivia* [11] trigger BV phenotypes in mice models. It was proposed that amino acids released by *G. vaginalis* are metabolized by *P. bivia*, leading to a rise in ammonium concentration in a biofilm established by *G. vaginalis* and *P. bivia*. This increases the pH and might promote the formation of a microbial community characteristic for BV [2,12].

Recent studies with *P. copri* [13] and *P. bryantii* [14] reveal important catabolic roles of the $Na^+$-translocating NADH:quinone oxidoreductase (NQR) and the quinol:fumarate oxidoreductase (QFR) in these Prevotella species found in the intestinal tract. Here, we study growth, membrane potential formation, and ammonia production by *P. bivia*. It is demonstrated that the energy metabolism of *P. bivia* relies on NQR and QFR for the recycling of $NAD^+$ during growth on glucose. *P. bivia* readily converts asparagine to ammonium, providing endogenous fumarate as an electron sink. The relevance of these findings for the vaginal microenvironment is discussed.

## Results

**$CO_2$-Dependent Succinate Formation by *P. bivia.*** *P. bivia* was grown in a synthetic, carbonate-buffered medium (pH 7.5) containing short-chain fatty acids (SCFA's), glucose, and mixed amino acids (tryptone) [15]. Searching the genome of *P. bivia* DSM 20514 (NCBI accession number: NZ_AJVZ00000000) revealed a putative metabolic route for glucose fermentation involving phosphoenolpyruvate (PEP) carboxykinase and pyruvate oxidoreductase (POR), ultimately leading to succinate and acetate. To test this assumption, *P. bivia* was cultivated and, at indicated times (t = 0, 5, 18, and 48 h), aliquots were retrieved for metabolite analysis by 1D $^1$H NMR. During two days of growth, cell density increased to an $OD_{600}$ of 1.4 ± 0.2 and the glucose concentration decreased from 13 mM to 5 mM (Figure 1), indicating that glucose (8 mM) was utilized as a carbon source by *P. bivia*. Notably, growth during the first 5 h was not accompanied by a decrease in glucose concentration. As previously reported for *P. bivia* grown in vaginal defined medium [16], succinate (6 mM) was formed as a major product together with malate (5 mM). This indicated a metabolic pathway leading from PEP to oxaloacetate, malate, fumarate, and, finally, succinate.

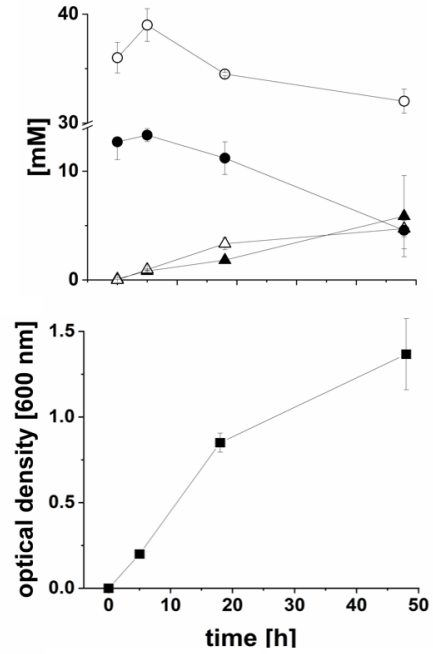


**Figure 1** Consumption of glucose and formation of carboxylic acids during anaerobic growth of *P. bivia*. Upper panel: concentrations of glucose (closed circles), acetate (open circles), succinate (closed triangles), and malate (open triangles). Lower panel: optical density at 600 nm. Average and standard deviations of three biological replicates are shown.

Short-chain fatty acids including acetate are important growth supplements of *P. bryantii* [15] and were also added to the synthetic growth medium used here. The acetate concentration at the timepoint of inoculation was 36 mM. We observed an increase of acetate by 3 mM during the first 5 h of growth, followed by a decrease to a concentration of 32 mM acetate after 2 d when the cells approached the stationary phase (Figure 1, upper panel). This indicated an initial formation and later an uptake as well as consumption of acetate by *P. bivia*. Formation of acetate starts from PEP, which is converted to pyruvate. Oxidation of pyruvate to acetyl-CoA, conversion to acetyl phosphate, and its reaction with ADP leads to ATP and acetate. Degradation of acetate requires its activation to acetyl-CoA. In *E. coli* [17], this is achieved with the help of the AMP forming acetyl-CoA synthase. A homolog of this

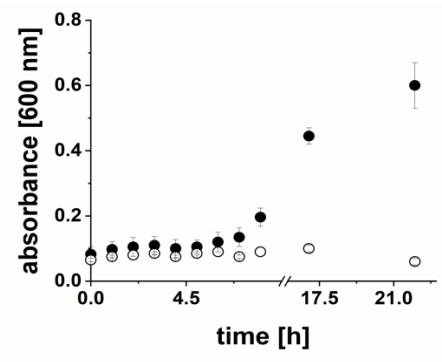


**Figure 2** Growth of *P. bivia* is dependent on $CO_2$. Cells of *P. bivia* were cultivated in medium prepared with $CO_2$ (back circles) or with $N_2$ (white circles). Average and standard deviation of three biological replicates are shown.

enzyme is found in *P. bivia* (Supplementary Table S1).

*P. bivia* did not grow in the medium prepared with $N_2$ instead of $CO_2$ (Figure 2). This indicates that glucose utilization by *P. bivia* critically depends on carboxylation of PEP by PEP carboxykinase. This $CO_2$-dependent step yields oxaloacetate, which is further converted in consecutive steps to malate and fumarate. Fumarate is then reduced to succinate by quinol:fumarate reductase (QFR), as described below. PEP conversion to succinate is a major route in glucose degradation by *P. bivia*. Enzymes catalyzing these reactions, as predicted by genome analysis, are listed with their UNIPROT accession numbers in the electronic Supplementary Material (Table S1).

**Ammonia Formation from L-Asparagine by *P. bivia.*** Another important metabolic reaction in *P. bivia* is the conversion of amino acids. A genome search suggested that *P. bivia* might degrade L-asparagine to ammonia with the help of L-asparaginase and aspartate ammonia lyase (Supplementary Material Table S1). L-asparaginase converts L-asparagine into $NH_3$ and L-aspartate, and the latter is converted to fumarate and $NH_3$ by the aspartate ammonia lyase. High activities of both enzymes were detected in the soluble fraction of *P. bivia*, exhibiting L-asparaginase activity of 951.4 ± 22.3 nmol $min^{-1}$ $mg^{-1}$ and aspartate ammonia lyase activity of 994.9 ± 5.6 nmol $min^{-1}$ $mg^{-1}$.

The effect and conversion of L-asparagine (50 mM) was also studied with growing *P. bivia* cells in medium that was adjusted to pH 5.0, 6.0, and 7.0 at the timepoint of inoculation. In the controls, asparagine was omitted (Figure 3 and Table 1). The highest growth yield and lowest doubling time was observed at neutral pH without added L- asparagine, with $OD_{600}$ of 1.8 ± 0.2 and 8 h. The addition of Asn had a moderate effect on the final yield ($OD_{600}$ of 1.6 ± 0.4) and doubling time (10 h). This was in marked contrast to the growth at pH 6.0, where the Asn addition led to a decrease in the final yield from $OD_{600}$ = 1.1 ± 0.4 to $OD_{600}$ = 0.4 ± 0.1, and to an increase in doubling time from 13 h to 17 h (Table 1). Very low yield ($OD_{600}$ = 0.5 ± 0.1) and high doubling time (101 h) was observed at pH 5. Here, the Asn addition had no significant effect (Table 1) and yields did not increase further when cells were incubated for two additional days (Figure S1).

Considering all pH conditions tested, the net formation of ammonium ($NH_4^+$) when 50 mM of asparagine was added to the medium was ~83 mM at pH 7, 75 mM at pH 6, and 48 mM at pH 5 after 7 days (Table 1). Note that at neutral and acidic pH, $NH_4^+$ was the dominant species (>99%). When biomass was taken into account, the highest ammonium formation rate of cells (416.4 ± 31.4 nmol $min^{-1}$ $mg^{-1}$) was observed at pH 6, followed by 265.7 ± 24.1 nmol $min^{-1}$ $mg^{-1}$ at pH 5 and 119.1 ± 2.5 nmol $min^{-1}$ $mg^{-1}$ at pH 7. Without asparagine added, the ammonium concentration in the cultures increased by ~21 mM (pH 7) and ~13 mM (pH 6 and pH 5), suggesting the conversion of amino acids such as asparagine from tryptone, which is a component of the medium.

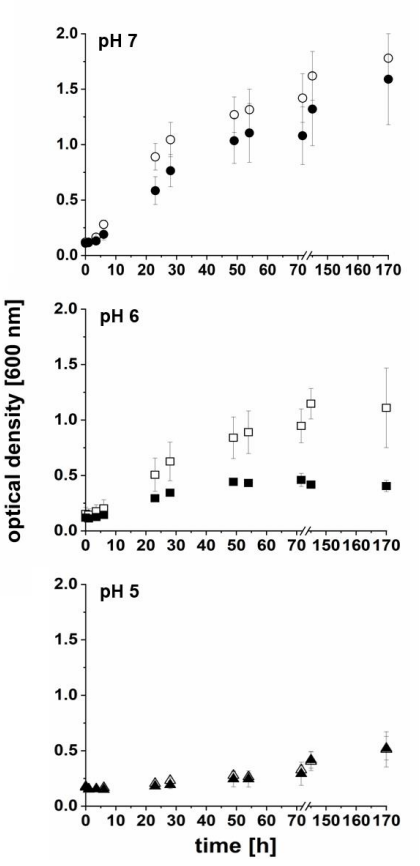


**Figure 3** Effect of L-asparagine on the growth of *P. bivia* at varying pH. *P. bivia* was cultivated in medium with (black symbols) or without (white symbols) supplementation of 50 mM of L-asparagine. The initial pH of the medium was 7.0 (circles; top panel), 6.0 (squares; middle panel), and 5.0 (triangles; lower panel). Average and standard deviations of three biological replicates are shown.

**Table 1** Effect of pH and L-asparagine on the growth and formation of ($NH_3$ + $NH_4^+$) by *P. bivia*. $OD_{600}$ and [$NH_3$ + $NH_4^+$] were determined in the stationary phase (t = 7 d) of *P. bivia* cultures grown at pH 5, 6, or 7 with or without supplementation of 50 mM of L-asparagine.

| Growth Condition | $OD_{600}$ (t = 7 d) | Doubling Time (h) | $NH4^+$ (mM; t = 0) | $NH4^+$ (mM; t = 7) | Net ($NH_3$ + $NH_4^+$) Formed (mM) | Rate of Net ($NH_3$ + $NH_4^+$) Formation (nmol $min^{-1}$ $mg^{-1}$) |
|---|---|---|---|---|---|---|
| pH 5 + Asn | 0.5 ± 0.1 | 91 | 14.7 ± 0.2 | 62.9 ± 0.8 | 48.2 ± 4.4 | 265.7 ± 24.1 |
| pH 5 − Asn | 0.5 ± 0.1 | 101 | 14.8 ± 0.1 | 27.9 ± 0.2 | 13.1 ± 0.1 | 59.7 ± 0.4 |
| pH 6 + Asn | 0.4 ± 0.1 | 17 | 16.9 ± 2.1 | 92.4 ± 1.1 | 75.5 ± 5.6 | 416.4 ± 31.4 |
| pH 6 − Asn | 1.1 ± 0.4 | 13 | 12.1 ± 0.5 | 25.5 ± 0.2 | 13.1 ± 0.6 | 21.7 ± 2.1 |
| pH 7 + Asn | 1.6 ± 0.4 | 10 | 18.1 ± 0.8 | 101.5 ± 0.5 | 83.4 ± 4.1 | 119.1 ± 2.5 |
| pH 7 − Asn | 1.8 ± 0.2 | 8 | 16.5 ± 0.7 | 37.6 ± 0.03 | 21.1 ± 0.25 | 25.2 ± 0.5 |

We speculated that the observed reduction of growth at pH 7 and pH 6 in the presence of L-asparagine was caused by the intoxication of cells with $NH_3/NH_4^+$ [18] formed by *P. bivia*. To test this, *P. bivia* was cultivated at pH 6.0 in the standard growth medium containing 7 mM $(NH_4)_2SO_4$ or 80 mM $(NH_4)_2SO_4$. At high (160 mM) $NH_4^+$ concentration, the final cell yields decreased by approximately 50% compared with the cells grown in the presence of 14 mM $NH_4^+$ (Figure 4).

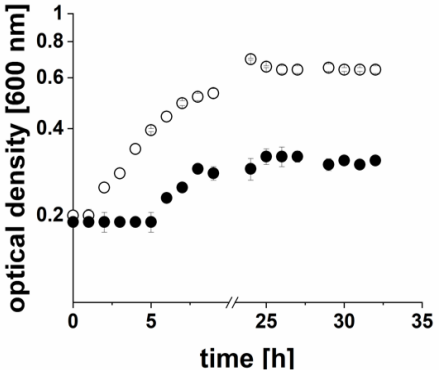


**Figure 4** Effect of $(NH_4)_2SO_4$ on the growth of *P. bivia*. Cells were cultivated with 7 mM of $(NH_4)_2SO_4$ (white circles) or 80 mM of $(NH_4)_2SO_4$ (black circles) at pH 6. Average and standard deviations of three biological replicates are shown.

This finding supports the notion that a reduced growth was observed with asparagine at pH 7 and 6, which is caused by the ammonia/ammonium formed from L-asparagine. Notably, asparagine did not influence growth behavior at pH 5.0, although the ammonium formation rate (per mg of cell protein) was higher than at pH 7 (Table 1).

The concentration of succinate in cell-free supernatants from cultures (pH 7.5) in stationary phase (t = 170 h) with and without supplementation of 50 mM of L-asparagine was determined. With 50 mM of L-asparagine added, 38.2 ± 1.5 mM succinate was formed, corresponding to a formation rate of 241.1 ± 9.6 nmol $min^{-1}$ $mg^{-1}$. Without L-asparagine added, 16.1 ± 0.8 mM of succinate was formed, corresponding to a formation rate of 81.1 ± 4.1 nmol $min^{-1}$ $mg^{-1}$. These results indicated that the L-asparagine present in the medium was taken up by *P. bivia* and converted to fumarate, which acted as an electron acceptor by QFR under the formation of succinate.

**Membrane-Bound Electron Transfer Complexes in *P. bivia.*** The analysis of the *P. bivia* growth medium revealed that succinate is a major product under the chosen conditions, suggesting a reduction of fumarate under the participation of a membrane-bound QFR. The genome of *P. bivia* encodes the FrdABC complex, which is related to the QFR, found in fumarate-respiring anaerobes such as *Wolinella succinogenes* (Figure 5 and Figure S2 in the electronic Supplementary Material). The hydrophilic FrdA subunit is comprised of the fumarate catalytic site and contains one covalently bound FAD [19]. Subunit FrdB, which, similar to FrdA, is oriented towards the cytoplasm, harbors three iron–sulfur centers and interacts with the membrane-bound, quinol-binding FrdC subunit containing two b hemes [19]. Electrons from quinol are transferred from FrdC via FrdB to FrdA, which reduces fumarate to succinate. In-gel fluorography and the subsequent mass spectrometric analysis confirmed the presence of flavinylated FrdA, with an apparent molecular mass of

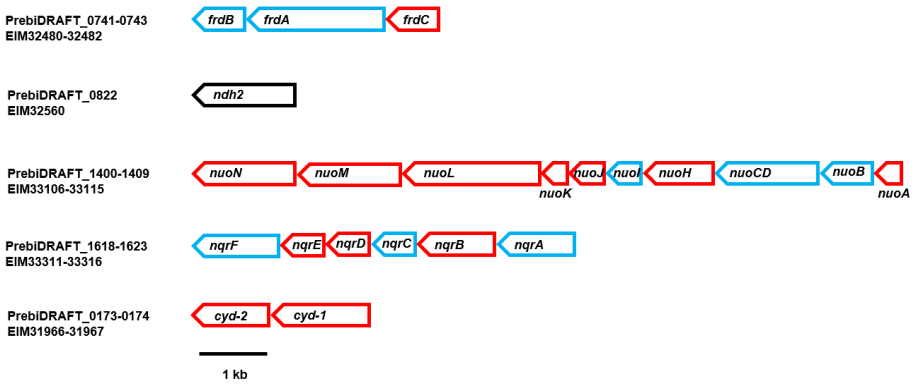


**Figure 5** Genes coding for membrane-bound electron transfer complexes of *P. bivia*. ORF (PrebiDRAFT) and NCBI accession numbers (EIM) are given on the left. The fumarate reductase (QFR) was encoded by *frdA* (1983 bp), *frdB* (675 bp), and *frdC* (756 bp). The non-electrogenic NADH dehydrogenase (Ndh2) is a membrane-associated enzyme encoded by *ndh2* (1308 bp; black frame). The *nuoA* (351 bp), *nuoB* (906 bp), *nuoCD* (1578 bp), *nuoH* (1098 bp), *nuoI* (534 bp), *nuoJ* (534 bp), *nuoK* (309 bp), *nuoL* (2061 bp), *nuoM* (1512 bp), and *nuoN* (1440 bp) genes are similar to the genes coding for the corresponding subunits of the 11-subunit complex related to the NUO complex. The $Na^+$-translocating NADH:quinone oxidoreductase (NQR) was encoded by *nqrA* (1359 bp), *nqrB* (1161 bp), *nqrC* (714 bp), *nqrD* (633 bp), *nqrE* (627 bp), and *nqrF* (1263 bp). The cytochrome *bd* quinol oxidase was encoded by *cyd-2* (1143 bp) and *cyd-1* (1536 bp). Red frames correspond to genes coding for hydrophobic (membrane-bound) subunits. Blue frames correspond to genes coding for hydrophilic (peri or cytoplasmatic) subunits.

ca. 75 kDa in membranes, and DDM-solubilized membranes of *P. bivia* (Figure 6 and Supplementary Material Tables S2 and S3). Besides flavins, hemes assigned to QFR and the cytochrome *bd* quinol oxidase were detected in the VIS redox difference spectrum (dithionite-reduced minus air-oxidized) of solubilized membranes of *P. bivia* (Figure 7). Based on sequence comparison (Figure S2), the FrdC subunit of QFR was predicted to contain two *b* hemes with absorption maxima at 560 nm, 527 nm, and 427 nm in the reduced state. These typical maxima were detected in the solubilized membranes of *P. bivia*. The maximum at 630 nm (Figure 7) was assigned to heme d of cytochrome *bd* quinol oxidase [20].

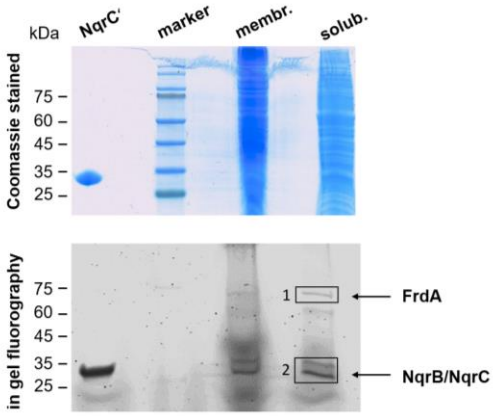


**Figure 6** Detection of flavinylated subunits from QFR and NQR in *P. bivia* membranes. Membranes (100 µg; membr.) and membranes solubilized with DDM (100 µg; solub.) of *P. bivia* were separated by SDS PAGE. Proteins were stained with Coomassie (upper panel) and analyzed by in-gel fluorography (lower panel) to detect flavinylated proteins. NqrC' (25 kDa), the FMN-containing domain of subunit NqrC from *V. cholerae* NQR, served as the control (2 µg). Black boxes (1 and 2) indicate bands subjected to tryptic digestion and mass spectrometry analysis.

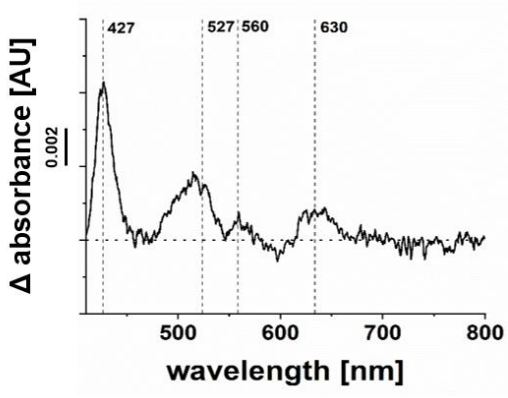


**Figure 7** Detection of hemes b and d in solubilized membranes of *P. bivia*. VIS difference spectrum of dithionite-reduced minus air-oxidized DDM solubilisates (0.8 mg protein/mL) with the maxima of reduced heme *b* (560 nm, 527 nm, and 427 nm) and heme *d* (630 nm). A typical trace from three biological replicates is presented.

**NADH:Quinone and Quinol:Fumarate Oxidoreduction Activities of *P. bivia* Membranes.** As expected from succinate formation and in accord with redox cofactor analyses of membrane proteins, native and DDM-solubilized membranes of *P. bivia* exhibited

fumarate reduction activities of 30 ± 2 nmol $min^{-1}$ $mg^{-1}$ and 101 ± 14 nmol $min^{-1}$ $mg^{-1}$, respectively. This raised the question for the redox enzyme providing quinol to QFR. The related *P. bryantii* operates the $Na^+$-translocating NADH:quinone oxidoreductase (NQR), feeding redox equivalents from NADH to the quinone pool [14,21]. The NQR is a membrane-bound protein complex composed of six subunits (NqrABCDEF) harboring one FAD, two iron– sulfur centers, one riboflavin, and two covalently bound FMNs [22,23]. The *P. bivia* NQR encoded by the nqr operon (Figure 5) is related to the enzyme from *V. cholerae* (electronic Supplementary Material, Figure S3). In-gel fluorography of *P. bivia* solubilisates revealed two flavinylated proteins running at ~25 kDa (Figure 6). These proteins were assigned to subunits NqrB and NqrC of NQR by mass spectroscopic analysis of the corresponding bands (Tables S2 and S3, Supplementary Material).

*P. bivia* NqrC and NqrB subunits exhibit 50% and 55% sequence identity to the corresponding subunits from *V. cholerae* NQR, including the conserved threonine residues Thr209 (NqrC) and Thr204 (NqrB, *P. bivia* numbering) for covalent attachment of FMNs [24]. *P. bivia* membranes exhibited specific activities of 170 ± 5 nmol $min^{-1}$ $mg^{-1}$ NADH oxidation and 74 ± 6 nmol $min^{-1}$ $mg^{-1}$ ubiquinone-1 (Q1) reduction. DDM-solubilized membranes of *P. bivia* exhibited specific activities of 244 ± 4 nmol $min^{-1}$ $mg^{-1}$ NADH oxidation and 106 ± 20 nmol $min^{-1}$ $mg^{-1}$ Q1 reduction. *P. bivia* harbors genes coding for enzymes that are required for menaquinone synthesis (Men pathway, [25]) but lacks the pathway for ubiquinone synthesis. With 2,3-dimethyl-1,4-naphthoquinone (DMN) as an electron acceptor, *P. bivia* membranes exhibited specific activities of 150 ± 4 nmol $min^{-1}$ $mg^{-1}$ NADH oxidation and 28 ± 10 nmol $min^{-1}$ $mg^{-1}$ DMN reduction. DDM-solubilized membranes of *P. bivia* exhibited specific activities of 287 ± 7 nmol $min^{-1}$ $mg^{-1}$ (NADH oxidation) and 40 ± 1 nmol $min^{-1}$ $mg^{-1}$ (DMN reduction). In *P. bivia*, ORFs assigned to *nuo* genes suggested the presence of the 11-subunit complex related to the NUO complex (NADH dehydrogenase I, or complex I; Figure 5) [26]. The 11-subunit complex of *P. bivia* lacks the NADH-oxidizing part of the bona fide NUO complex and does not catalyze NADH oxidation. In contrast, the non-electrogenic NADH dehydrogenase (NDH2) [27] encoded by *ndh2* (Figure 5) exhibits NADH:Q oxidoreduction activity. To estimate the contribution of NQR and NDH-2 to the overall NADH oxidation activity, the effects of $Ag^+$ (an inhibitor of NQR) [14,28] and $Na^+$ (the coupling cation of NQR) [23] on NADH:Q oxidoreduction activity were studied. Half-maximal inhibition of NADH oxidation activity was observed at 1 µM $Ag^+$, which is reminiscent of the inhibition profile observed with membrane-bound NQR from *Vibrio alginolyticus* [28,29].

NADH:Q oxidoreduction activity was stimulated by $Na^+$, whereas the addition of $K^+$ did not lead to increased activity (Figure 8). It is concluded that respiratory NADH oxidation in *P. bivia* is predominantly catalyzed by the $Na^+$-translocating NQR. This raised the question regarding whether the formation of a membrane potential in *P. bivia* is stimulated by $Na^+$.

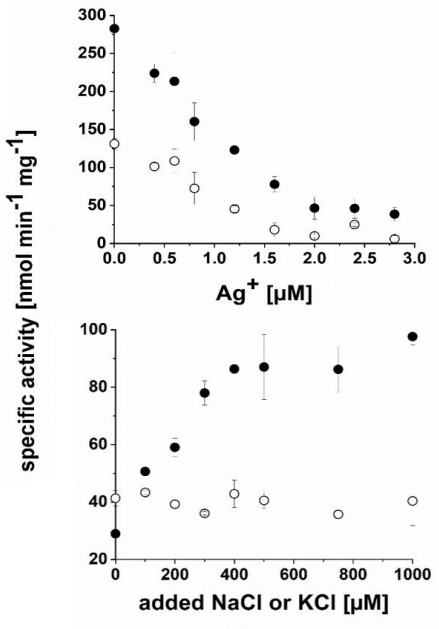


**Figure 8** The $Na^+$ -translocating NADH:quinone oxidoreductase is the major membrane-bound NADH dehydrogenase in *P. bivia*. Assays were performed with solubilized membranes (50 µg of protein). Upper panel: NADH dehydrogenase activity at increasing [$Ag^+$] in chloride-free assay buffer. Lower panel: Q1 reduction activities at increasing [$K^+$] (open circles) or [$Na^+$] (closed circles). Residual $Na^+$ concentration of buffer was at ~10 µM. Average and standard deviations from two technical replicates are shown.

**Sodium Dependent Membrane Potential in *P. bivia*.** The membrane potential (ΔΨ, inside negative) was estimated using the fluorescent dye $DiOC_2$ (3,3`-diethyloxacarbocyanine iodide), which exhibits increased emission at 635 nm in cells with high ΔΨ. The membrane potential established by *P. bivia* was strongly diminished when cells were depleted for $Na^+$ by repeated washing with $K^+$ (Figure 9). The sodium ionophore monensin, the protonophore carbonyl cyanide mchlorophenylhydrazone (CCCP), and $NH_4^+$ diminished the membrane potential with decreasing efficiency. This indicates that *P. bivia* maintains an electrochemical $Na^+$ gradient (sodium motive force (SMF)). In addition, an electrochemical proton potential (proton motive force (PMF)) was established in *P. bivia*, as indicated by the partial dissipation of the membrane potential by a protonophore, specifically CCCP. In *P. bivia*, ammonium (10 mM) acted as uncoupling agent. This was unexpected given that ammonium in the millimolar concentration range is usually added as a nitrogen source

the to bacterial growth media. These findings were in line with the observed reduced growth when Asn or $NH_4^+$ was added to *P. bivia* cultures.

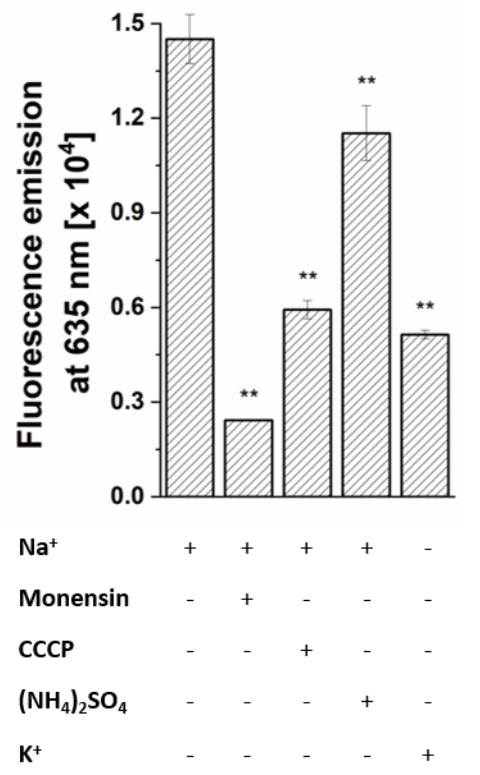


**Figure 9** Effect of $Na^+$ and uncouplers on the membrane potential of *P. bivia*. The fluorescence emission of cells incubated under the indicated conditions was corrected by the emission of fluorophore in buffer. CCCP, carbonyl cyanide m-chlorophenylhydrazone. Mean values and averages from four technical replicates are shown. Asterisks (**) indicate significant differences from cells incubated with $Na^+$ in the absence of inhibitors with $p < 0.05$.

**Cytochrome *bd* Quinol Oxidase of *P. bivia*.** Absorbances in the VIS difference spectrum assigned to heme d and the presence of both cyd-1 and cyd-2 genes suggested the presence of cytochrome *bd* quinol oxidase in *P. bivia*. This was analyzed by monitoring the peroxidase activity of this enzyme. Solubilized membranes catalyzed the oxidation of the $DMNH_2$ with $H_2O_2$ as an electron acceptor with a specific activity of 0.6 nmol $min^{-1}$ $mg^{-1}$. Solubilized membranes from *P. bryantii*, which lack the *bd* quinol oxidase, exhibited only residual $DMNH_2$ oxidation activity at rates similar to protein-free controls (Figure 10).

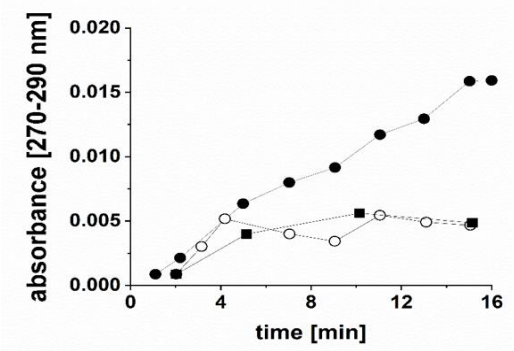


**Figure 10** Cytochrome *bd* quinol oxidase activity of *P. bivia*. Oxidation of $DMNH_2$ in the presence of $H_2O_2$ (peroxidase activity) was followed with solubilized membranes from *P. bivia* (closed circles) or *P. bryantii* (open circles). The control reaction was performed in the absence of solubilized membranes (closed squares).

## Discussion

Key metabolic features of *P. bivia* are succinate production, the generation of an electrochemical sodium gradient, the operation of a terminal oxidase, and the conversion of asparagine under the formation of ammonium. From the genome, *P. bivia* is predicted to operate both the typical and atypical Embden-Meyerhoff-Parnas (EMP) pathways, yielding PEP as a central intermediate [30] (Figure S4). The $CO_2$-dependent growth indicates that carboxylation of PEP to oxaloacetate by the carboxykinase is crucial for *P. bivia*. This reaction ultimately provides endogenous fumarate, acting as an acceptor for an electron transport chain, which generates a membrane potential (Figure 11). Fumarate is reduced to succinate by the membrane-bound quinol:fumarate oxidoreductase (QFR), which uses menaquinol as a substrate. The product pattern observed with *P. bivia* compares favourably with the results of a transcriptome study of the vaginal microbiota of BV patients, which identified pathways leading to succinate and short-chain fatty acids [31].

Besides QFR, *P. bivia* operates a membrane-bound NADH:quinone oxidoreductase (NQR), which provides menaquinol for the fumarate reduction and regenerates the $NAD^+$ required for glycolysis. The similarity of *P. bivia* NQR to the $Na^+$-translocating *V. cholerae* NQR [23] and the stimulation of NADH:quinone oxidoreduction activity by $Na^+$ indicate that the *P. bivia* NQR acts as a $Na^+$ pump. In accordance with this notion, the membrane potential established by *P. bivia* cells critically depends on $Na^+$ and collapses in the presence of the sodium ionophore monensin. It is proposed that the build-up of a membrane potential by the $Na^+$ -translocating NQR is crucial for the energy conservation

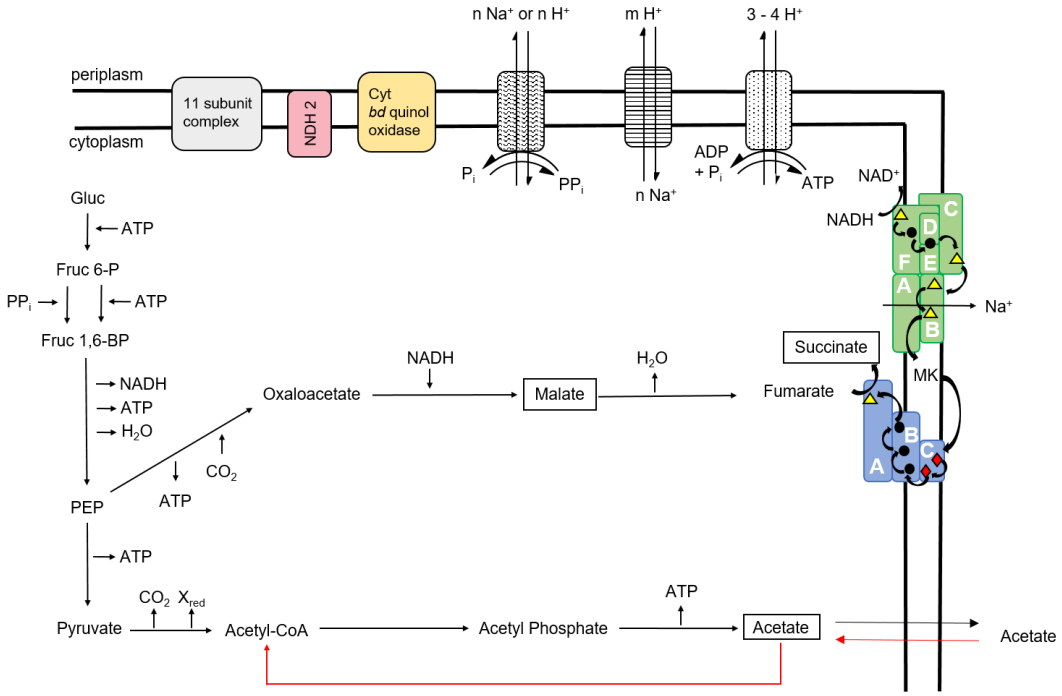


**Figure 11** Energy-converting complexes and central carbon metabolism of *P. bivia*. Important products are highlighted by black boxes. Red arrows indicate reactions for the assimilation of acetate. Gluc = glucose; Gluc 6-P = glucose 6phosphate; and PEP = phosphoenolpyruvate. Blue = fumarate reductase (QFR); green = $Na^+$-translocating NADH:quinone oxidoreductase (NQR); dotted = $F_1F_O$ ATPase; striped = $Na^+/H^+$ antiporter; wavy = pyrophosphatase; yellow = cytochrome *bd* quinol oxidase; red = NDH2; and grey = 11-subunit complex related to NDHI (complex I). Subunits of NQR (A–F) and QFR (A–C) are indicated. Colored symbols in the protein complexes represent cofactors. Yellow triangle = flavin; black circle = iron-sulfur center; red diamond = heme *b*; and MK = menaquinone. UNIPROT numbers of proteins are listed in Table S1 (electronic Supplementary Material).

in *P. bivia*. NQR is widely distributed in *Prevotella* sp. [14] but it is neither found in the *Lactobacilli* of the vaginal microbiota, nor in the human host. This makes NQR an attractive target for the development of antibacterial compounds, as demonstrated for the case of *Chlamydia trachomatis* [32].

Partial dissipation of the transmembrane voltage by the protonophore CCCP indicates that *P. bivia* also establishes a PMF, probably with the help of the $F_1F_O$ ATPase. Considering critical, conserved residues in the cation-binding site [33], the $F_1F_O$ ATPase of *P. bivia* is a proton rather than a sodium-dependent enzyme. To regulate cytoplasmic proton and $Na^+$ concentrations, *P. bivia* operates $Na^+/H^+$ antiporters related to NhaA and NhaD (Supplementary Material Table S1; Figure 11).

The formation of $H_2O_2$ and other reactive oxygen species by *Lactobacilli* colonizing the vaginal epithelium [34] prohibits the growth of strict anaerobes, which typically lack enzymes protecting against oxidative stress. *P. bivia* is an exception since it operates a superoxide dismutase [35] and possesses an active bd oxidase utilizing quinol as an electron donor for the reduction of $O_2$ or $H_2O_2$. Moreover, *P. bivia* exhibits robust growth at acidic pH, producing ammonium from asparagine. Thus, it is capable of thriving in a vaginal environment dominated by *Lactobacilli.*

BV is characterized by a biofilm [36] established by a microbial consortium, with *Gardnerella vaginalis* and *Prevotella bivia* as prominent strains. In metabolic cross-feeding, ammonium released by *P. bivia* was utilized by *G. vaginalis* [12], followed by the degradation of the vaginal mucus layer by sialidases and adherence of other BV-associated bacteria [37]. *G. vaginalis* lacks metabolic routes for amino acid synthesis with the exception of pathways for the synthesis of L-aspartate and L-asparagine [38]. *P. bivia* possesses L-asparaginase and aspartate ammonia lyase, producing $[NH_3 + NH_4^+]$ at high rates in vitro and in vivo. $NH_4^+$ (160 mM) inhibited the growth of *P. bivia*, most likely due to the partial dissipation of the membrane potential. This is in marked contrast to the situation in *E. coli*, where no detrimental effect on growth was observed up to 500 mM $NH_4^+$ [18]. In a consortium with *G. vaginalis* consuming ammonium, high turnover of Asn by *P. bivia* under the formation of fumarate is possible and *P. bivia* will benefit from fumarate acting as an electron acceptor. This could facilitate the colonization of the vaginal epithelium by *G. vaginalis* and *P. bivia* at an early stage of BV.

## Materials and Methods

**Bacterial Strains and Growth Conditions.** *Prevotella bivia* DSM 20514 and *Prevotella bryantii* $B_1$4 were cultivated anaerobically at 39 °C in a synthetic medium composed of 1% tryptone (w/v), 13 mM of glucose, 50 mM of $NaHCO_3$, 15% (by volume) mineral solution 1 (17 mM $K_2HPO_4$), 15% (by volume) mineral solution 2 (17 mM $KH_2PO_4$, 45 mM of $(NH_4)_2SO_4$, 100 mM of NaCl, 5 mM of $MgSO_4$, and 5.4 mM $CaCl_2$), and 0.44 µM of resazurin (sodium salt). The redox potential was adjusted with 8 mM of L-Cysteine HCl. In addition, the medium contained (by volume) 0.17% acetic acid, 0.01% n-valeric acid, 0.01% iso-valeric acid, 0.03% n-butyric acid, 0.01% iso-butyric acid, and 0.06% propionic acid [15]. Hungate tubes (7 mL volume) and serum bottles (0.1 L or 1 L volume) with gas-tight caps were used.

**Isolation and Solubilization of Membranes.** Cells were harvested at an $OD_{600}$ of 1.5–2.0 (*P. bivia*) or at an $OD_{600}$ of 2.5–3.0 (*P. bryantii*) by centrifugation at 9000× *g* for 30 min (4 °C). The cells were washed twice in 20 mM of Tris-$H_2SO_4$ (pH 7.5) and 50 mM of $K_2SO_4$. Cells (10 g wet weight) were resuspended in 30 mL of 20 mM Tris-$H_2SO_4$ (pH 7.5) containing 50 mM of $K_2SO_4$, 5 mM of $MgSO_4$, 1 mM of dithiothreitol, 1 mM of phenylmethyl sulfonylfluoride (PMSF), 0.1 mM of diisopropyl fluorophosphate, and traces of DNase I (Roche Diagnostics GmbH, Mannheim, Germany). The suspension was passed three times through an EmulsiFlex®-C3 high-pressure homogenizer (Avestin Europe GmbH, Mannheim, Germany) at 20,000 psi. Cell debris and unbroken cells were removed by centrifugation at 27,000 g for 30 min at 4 °C. Membranes were collected by ultracentrifugation (50,000 rpm, Beckman Ti70 rotor; Beckman Coulter GmbH, Krefeld, Germany) for 90 min at 4 °C; washed once in 20 mM of Tris-$H_2SO_4$ (pH 7.5), 50 mM of $K_2SO_4$, and 5% (*v*/*v*) glycerol; and resuspended in the same buffer. The membrane suspension (5–10 mg protein/mL) was frozen by pipetting aliquots of 30 µL into liquid $N_2$. The frozen droplets were collected and stored in liquid $N_2$ until further use. For the solubilization of the membranes, protein and n-dodecyl-ß-D-maltoside (DDM; 7.5 µM final concentration) were incubated in a 1:3.75 (protein:detergent) ratio in a buffer containing 20 mM of Tris-$H_2SO_4$ (pH 7.5), 50 mM of $K_2SO_4$, and 5% (*v*/*v*) glycerol, with a total volume of 1.5 mL, for 2 h at 6 °C under gentle shaking (350 rpm). The membrane suspensions were ultracentrifuged (50,000 rpm, Beckman Ti70 rotor; Beckman Coulter GmbH, Krefeld, Germany) for 45 min at 4 °C. Supernatants containing solubilized membrane proteins were frozen and stored in liquid $N_2$ as described above.

**Bacterial Growth.** Growth was followed in Hungate tubes with 7 mL of medium inoculated with 500 µL of *P. bivia* overnight culture grown at pH ~7. Turbidity of the cultures in tubes was measured with a cell density meter (WPA biowave CO8000, Biochrom Ltd., Cambridge, UK) at 600 nm. To analyze the $CO_2$ dependency of the growth of *P. bivia*, triplicate growth experiments with medium prepared with $CO_2$ [15] were conducted. In the controls, $CO_2$ was replaced with $N_2$. To analyze the medium during growth under a chosen condition, six tubes per experiment were inoculated at t = 0 h and turbidity was monitored in parallel. At indicated times, the culture from one tube was retrieved. To study the effect of pH on the growth of *P. bivia*, the growth medium was adjusted to pH 5, 6, or 7 by adding NaOH. Growth was monitored for 7 days (pH 6 and pH 7) or 9 days (pH 5) in triplicate experiments. At indicated times, cells were harvested by centrifugation at 16,000 g for 5 min at 4 °C and both pH and ammonium concentration of supernatants were determined. In parallel growth experiments, the media contained 50 mM of L-asparagine. To study the effect of $NH_4^+$ on growth, medium (pH 6.0) was supplemented with 7 mM of $(NH_4)_2SO_4$ and 14 mM of $K_2SO_4$, or with 80 mM of $(NH_4)_2SO_4$ and 20 mM of $K_2SO_4$. To identify and quantify organic compounds in cultures by $^1$H-NMR, experiments in Hungate tubes were performed in triplicates. After 5 h, 18 h, and 48 h of growth, the ODs were determined and one culture was harvested by centrifugation at 16,000 g for 5 min at 4 °C to obtain supernatants for NMR analysis.

**Analytical Methods.** The protein concentration was determined with the bicinchoninic acid method [39] using the reagent from Pierce™ (ThermoFisher Scientific, Waltham, MA, USA). To determine the protein content of the cell suspensions, cells from 1 mL of culture were washed in 300 mM of sucrose. The cell pellet was resuspended in 5% (*v*/*v*) trichloroacetic acid and heated (100 °C) for 10 min [40]. [$NH_3$ + $NH_4^+$] in supernatants of cell cultures was determined spectrophotometrically with the Nessler's reagent [41]. Ammonium sulfate was used as the standard.

Glucose, acetate, succinate, and malate in cultures of *P. bivia* were determined by 1D $^1$H NMR spectroscopy. Supernatants from cell cultures were dried with a vacuum concentrator (program V-AQ; Eppendorf SE, Hamburg, Germany,). The pellets were resuspended in 50 mM of $Na_2HPO_4$ (pH 7) in $D_2O$ containing 5 mM of 3-trimethylsilyl propionic-2,2,3,3 acid sodium salt (TSP) as an internal reference for the $^1$H chemical shift calibration and the suspensions were filled into NMR tubes. 1D $^1$H NMR spectra were recorded using a Bruker Avance III HD NMR 600 MHz spectrometer equipped with a 5 mm BBO Prodigy cryo-probe (Bruker BioSpin GmbH, Ettlingen, Germany). For structural identification of the metabolites, 1D $^1$H heteronuclear NMR experiments (*g*HSQC and *g*HMBC) [42] were recorded at 298 K. For acquisition, processing, and evaluation of NMR spectra, the software TopSpin 3.5pl7 (Bruker BioSpin GmbH, Ettlingen, Germany) was used. To quantify succinate in medium, to which 50 mM of L-asparagine was added at the start of the growth, cells were cultivated for 50 h in Hungate tubes. Cell-free

supernatants were analyzed using the Sigma -Aldrich™ Succinate Assay Kit (Merck KGaA, Darmstadt, Germany).

Denaturing polyacrylamide gel electrophoresis (SDS-PAGE) was performed with a 12% polyacrylamide gel [43]. Protein and membrane suspensions were diluted in 5x SDS sample buffer (500 mM of DTT; 1 M of Tris-HCl, pH 6.8; 5% SDS; and 28.8% glycerol (*w*/*v*), bromophenol blue) and boiled for 5 min before loading on the gel. In-gel fluorescence of covalently bound flavins in NqrB, NqrC, and FrdA, separated by SDS-PAGE, was detected using the ImageQuant LAS 4000 imager ($\lambda_{excitation}$ = 460, emission filter = Y515 CyTM2; Cytiva, Marlborough, MA, USA). As a positive control, the purified NqrC' subunit was used. This protein is a truncated variant of the NqrC subunit of the *V. cholerae* NQR comprising the covalently attached FMN but lacking the N-terminal transmembrane helix [44]. The molecular mass of NqrC' was 25.38 kDa. Proteolysis of proteins separated by SDS-PAGE, followed by mass spectrometric analysis of the peptides, was performed as described previously [21].

**UV/Vis Difference Spectra of Redox Cofactors in *P. bivia*.** The absorption spectrum of dithionite-reduced redox cofactors in solubilized membranes of *P. bivia* was compared with an aliquot of the same sample with cofactors in their air-oxidized state using a double-beam UV/VIS spectrophotometer (UV-2600i; Shimadzu GmbH, Berlin, Deutschland). Light is split by a half mirror passing separately through the reference sample (beam 1) and through the test sample (beam 2). The light intensities passing through the sample and reference were compared. The range of 220–800 nm was monitored with an interval of 0.5 nm and with medium scan speed. The difference in absorbance of beam 2 minus beam 1 at a given wavelength was calculated using the software LabSolutions UV-Vis (Shimadzu GmbH, Berlin, Deutschland). DDM-solubilized membranes of *P. bivia* were analyzed at a concentration of ~0.8 mg of protein per mL in 20 mM of potassium phosphate buffer, pH 7.5. Beam 1 contained air-oxidized solubilisate, whereas in beam 2, an aliquot of solubilisate mixed with a few crystals of sodium dithionite was analyzed. The difference spectrum of dithionite-reduced minus air-oxidized membranes was recorded.

**Enzymatic Assays.** NADH oxidation and quinone reduction activities were monitored simultaneously in a quartz cuvette (d = 1 cm) in a total volume of 1 mL at 25 °C using a Hewlett Packard 8452A diode-array spectrophotometer (Agilent Technologies, Santa Clara, CA, USA). NADH oxidation was followed at 340 nm ($\varepsilon_{NADH}$ = 6.22 $mM^{-1}$ $cm^{-1}$) and ubiquinone-1 (Q1) or 2,3-dimethyl-1,4-naphthoquinone (DMN) reduction at 280 nm ($\varepsilon_{Q1}$ = 14.5 $mM^{-1}$ $cm^{-1}$ and $\varepsilon_{DMN}$ = 15.2 $mM^{-1}$ $cm^{-1}$) [45]. Solubilized membranes of *P. bivia* (50 µg of protein in 20 mM of Tris-$H_2SO_4$, pH 7.5; 50 mM of $K_2SO_4$; 5% (*v*/*v*) glycerol; and 7.5 µM of DDM) were incubated with varying amounts of $AgNO_3$ (0–3.0 µM) for 5 min at 4 °C and were added to a cuvette with buffer (20 mM of Tris $H_2SO_4$, pH 7.5; 100 mM of $Na_2SO_4$; 100 µM of NADH; and 100 µM of Q1) to start the enzymatic reaction. In buffers, chloride was replaced with sulfate to avoid precipitation of AgCl. To study the effect of $Na^+$ on NADH dehydrogenase activity of solubilized membranes (50 µg), NaCl (0–1000 µM) or corresponding amounts of KCl (0–1000 µM) were added to the assay buffer (20 mM of Tris $H_2SO_4$, pH 7.5; 100 µM of NADH; and 100 µM of Q1). The residual $Na^+$ concentration in the assay without the added NaCl was ~10 µM, as determined by atomic absorption spectroscopy (AA240, Agilent Technologies, Santa Clara, CA, USA).

Quinol:fumarate oxidoreductase (QFR) activity was determined with anoxic materials and buffer (20 mM of potassium phosphate, pH 7.5) containing benzyl viologen (~0.5 mM) in the anaerobic chamber. Benzyl viologen was reduced by adding sodium dithionite crystals to achieve an absorbance of 1 at 564 nm [46]. Then, 100–200 µg of protein was added. The reaction was started by adding 10 mM of fumarate. Decrease in absorbance of benzyl viologen was monitored at 564 nm ($\varepsilon$ = 19.5 $mM^{-1}$ $cm^{-1}$) in a cuvette at 20 °C using a diode array spectrophotometer (Black-comet, StellarNet Inc., Tampa, FL, USA). The cuvette holder was placed inside the anaerobic chamber. The detector and light source (SL5 UV + VIS lamp, StellarNet Inc., Tampa, FL, USA) were placed outside of the anaerobic chamber and the components were connected with fiber optic cables.

The cytochrome quinol *bd* oxidase activity in solubilized membranes was determined by following the oxidation of quinol with $H_2O_2$ [47]. 2,3-dimethyl-1,4-naphthoquinol ($DMNH_2$), obtained as described in [48], was used as an electron donor. $DMNH_2$ oxidation with $H_2O_2$ as an electron acceptor was monitored from the formation of DMN ($\varepsilon_{DMN}$ = 15.2 $mM^{-1}$ $cm^{-1}$) [49] under anoxic conditions by recording difference spectra over 16 min in a double-beam photometer (Lambda 16, PerkinElmer, Waltham, MA, USA). Buffers and reagents were made anoxic by flushing with $N_2$ and were mixed in cuvettes inside the anaerobic chamber. Cuvettes were sealed gas-tight and difference spectra were recorded immediately outside of the chamber. In beam 1, the reference cuvette was analyzed, containing 1 mL of assay solution (180 µg of solubilized membrane protein from *P. bivia* or *P. bryantii*; 50 mM of MOPS, pH 7.0; 100 mM of NaCl; 0.1% *v*/*v* DDM; and 200 µM of $DMNH_2$). A cuvette with 1 mL of assay solution mixed with 10 µL of 30% (by volume) $H_2O_2$ was placed in beam 2. To calculate the rates of $DMNH_2$ oxidation, the difference in absorbance from 270 nm to 290 nm obtained by subtraction of the spectrum of beam 1 from the spectrum of beam 2 at a given timepoint was determined. In the control, $H_2O_2$ was omitted.

For L-asparaginase and aspartate lyase activity determinations, the soluble protein fraction of *P. bivia*

was obtained by ultracentrifugation of crude cell extracts. L-asparaginase activity was determined as described in [41]. Aspartate ammonia lyase activity was determined as described in [50] and modified as follows. After incubation at 30 °C for 30 min, the assay solution (1 mL) was heated at 80 °C for 5 min to stop the reaction. The ($NH_3$ + $NH_4^+$) concentration was determined photometrically with the Nessler's reagent [51].

**Membrane Potential.** Membrane potential of *P. bivia* was estimated with the BacLight™ Bacterial Membrane Potential Kit ((ThermoFisher Scientific, Waltham, MA, USA)) using a Infinite F200 Pro plate reader (Tecan Deutschland GmbH, Crailsheim, Germany) [52]. *P. bivia* cells were cultivated in Hungate tubes until an $OD_{600}$ of 0.6 was reached. The following steps were performed in the anaerobic chamber. Cells were harvested, diluted in sodium buffer (10 mM of sodium buffer, pH 7.4, and 145 mM of NaCl) or potassium buffer (10 mM of potassium buffer, pH 7.4, and 145 mM of KCl), and adjusted to $OD_{600}$ = 0.25. Cells in 800 µL of this suspension were sedimented by centrifugation (16,000 g, 5 min), washed twice, and resuspended in 800 µL of the corresponding buffer. To analyze the effect of ionophores on the membrane potential, 2.5 µM of carbonylcyanid-m-chlorphenylhydrazon (CCCP), 2.5 µM of monensin, or 5 mM of $(NH_4)_2SO_4$ were added to cell suspensions, as indicated. After incubation for 10 min (20 °C), the fluorescence dye $3,3^0$-diethyloxacarbocyanine iodide ($DiOC_2$, 15 µM) was added and cells were further incubated for 60 min in the dark. Outside of the anaerobic chamber, three aliquots (200 µM) of each sample were applied to a black, flat-bottom 96-well plate (polysterene; 4titude Ltd., Berlin, Germany). To determine red fluorescence intensities, excitation was set to 480 nm (band width, 9 nm) and emission to 635 nm (band width, 20 nm; gain, 117). To determine green fluorescence intensities, the emission was changed to 535 nm (band width, 25 nm; gain, 107). Fluorescence emission intensities were in the linear range of the fluorescence detector. Background fluorescence intensities of buffer with dye and of cell suspensions were determined for background corrections. As expected, an increase of red fluorescence intensity, indicating a transmembrane voltage, was accompanied by a decrease in green fluorescence intensity. Mean values of red fluorescence intensities are presented.

## Supplementary Materials

Supplementary Materials are available online at https://www.mdpi.com/article/10.3390/ijms222111925/s1.

## Author Contributions

Conceptualization, J.S. (Julia Steuber) and L.S.; methodology, L.S. and G.F.; software, L.S.; validation, L.S. and A.T.; formal analysis, L.S. and A.T.; investigation, L.S. and S.H.; resources, J.S. (Julia Steuber) and J.S. (Jana Seifert); data curation, L.S.; writing—original draft preparation, L.S.; writing—review and editing, J.S. (Julia Steuber), J.S. (Jana Seifert), A.T. and L.S.; visualization, L.S.; supervision, J.S. (Julia Steuber); project administration, J.S. (Julia Steuber) and J.S. (Jana Seifert); funding acquisition, J.S. (Julia Steuber) and J.S. (Jana Seifert). All authors have read and agreed to the published version of the manuscript.

**Funding** This research study was funded by the Deutsche Forschungsgemeinschaft to J. Seifert and J. Steuber (project number 327953272).

## Data Availability Statement

Additional data are provided in the Supplementary Materials.

**Acknowledgements** We thank Johannes Günther, Jens Pfannstiel, and Berit Würtz of the Core Facility University of Hohenheim for their support in the NMR spectroscopy and mass spectrometry.

## Conflicts of Interest

The authors declare no conflict of interest.

## References

1. Onderdonk, A.B.; Delaney, M.L.; Fichorova, R.N. The human microbiome during bacterial vaginosis. *Clin Microbiol Rev*. **2016**; 29(2):223–238. doi:10.1128/CMR.00075-15
2. Muzny, C.A.; Taylor, C.M.; Swords, W.E.; Tamhane, A.; Chattopadhyay, D.; Cerca, N.; Schwebke, J.R. An updated conceptual model on the pathogenesis of bacterial vaginosis. *J Infect Dis*. **2019**; 220(9):1399–1405. doi:10.1093/infdis/jiz342
3. Ravel, J.; Gajer, P.; Abdo, Z.; Schneider, G.M.; Koenig, S.S.K.; McCulle, S.L.; Karlebach, S.; Gorle, R.; Russell, J.; Tacket, C.O.; Brotman, R.M.; Davis, C.C.; Ault, K.; Peralta, L.; Forney, L.J. Vaginal microbiome of reproductive-age women. *PNAS*. **2011**; 108 Suppl 1:4680–4687. doi:10.1073/pnas.1002611107
4. Nunn, K.L.; Clair, G.C.; Adkins, J.N.; Engbrecht, K.; Fillmore, T.; Forney, L.J. Amylases in the human vagina. *mSphere*. **2020**; 5(6). doi:10.1128/mSphere.00943-20
5. Zozaya-Hinchliffe, M.; Lillis, R.; Martin, D.H.; Ferris, M.J. Quantitative PCR assessments of bacterial species in women with and without bacterial vaginosis. *J Clin Microbiol*. **2010**; 48(5):1812–1819. doi:10.1128/JCM.00851-09
6. Delaney, M. Nugent score related to vaginal culture in pregnant women. *Obstet Gynecol*. **2001**; 98(1):79–84. doi:10.1016/S0029-7844(01)01402-8
7. Aroutcheva, A.; Ling, Z.; Faro, S. *Prevotella bivia* as a source of lipopolysaccharide in the vagina. *Anaerobe*. **2008**; 14(5):256–260. doi:10.1016/j.anaerobe.2008.08.002
8. Strömbeck, L.; Sandros, J.; Holst, E.; Madianos, P.; Nannmark, U.; Papapanou, P.; Mattsby-Baltzer, I. *Prevotella bivia* can invade human cervix epithelial (HeLa) cells.

*APMIS*. **2007**; 115(3):241–251. doi:10.1111/j.1600-0463.2007.apm_512.x
9. Mikamo, H.; Kawazoe, K.; Sato, Y.; Imai, A.; Tamaya, T. Preterm labor and bacterial intra-amniotic infection: arachidonic acid liberation by phospholipase A2 of *Prevotella bivia*. *Anaerobe*. **1998**; 4(5):209–212. doi:10.1006/anae.1998.0165
10. Gilbert, N.M.; Lewis, W.G.; Lewis, A.L. Clinical features of bacterial vaginosis in a murine model of vaginal infection with *Gardnerella vaginalis*. *PLoS One*. **2013**; 8(3):e59539. doi:10.1371/journal.pone.0059539
11. Gilbert, N.M.; Lewis, W.G.; Li, G.; Sojka, D.K.; Lubin, J.B.; Lewis, A.L. *Gardnerella vaginalis* and *Prevotella bivia t*rigger distinct and overlapping phenotypes in a mouse model of bacterial vaginosis. *J Infect Dis*. **2019**; 220(7):1099–1108. doi:10.1093/infdis/jiy704.
12. Pybus, V.; Onderdonk, A.B. Evidence for a commensal, symbiotic relationship between *Gardnerella vaginalis* and *Prevotella bivia* involving ammonia: potential significance for bacterial vaginosis. *J Infect Dis*. **1997**; 175(2):406–413. doi:10.1093/infdis/175.2.406
13. Franke, T.; Deppenmeier, U. Physiology and central carbon metabolism of the gut bacterium *Prevotella copri*. *Mol Microbiol*. **2018**; 109(4):528–540. doi:10.1111/mmi.14058
14. Deusch, S.; Bok, E.; Schleicher, L.; Seifert, J.; Steuber, J. Occurrence and function of the $Na^+$-translocating NADH:quinone oxidoreductase in *Prevotella spp*. *Microorganisms*. **2019**; 7(5). doi:10.3390/microorganisms7050117
15. Trautmann, A.; Schleicher, L.; Deusch, S.; Gätgens, J.; Steuber, J.; Seifert, J. Short-chain fatty acids modulate metabolic pathways and membrane lipids in *Prevotella bryantii* $B_14$. *Proteomes*. **2020**; 8(4). doi:10.3390/proteomes8040028
16. Pybus, V.; Onderdonk, A.B. The effect of pH on growth and succinate production by *Prevotella bivia*. *Microb Ecol Health Dis*. **1996**; 9(1):19–25. doi:10.3109/08910609609167725
17. Wolfe, A.J. The acetate switch. *Microbiol Mol Biol Rev*. **2005**; 69(1):12–50. doi:10.1128/MMBR.69.1.12-50.2005
18. Müller, T.; Walter, B.; Wirtz, A.; Burkovski, A. Ammonium toxicity in bacteria. *Curr Microbiol*. **2006**; 52(5):400–406. doi:10.1007/s00284-005-0370-x
19. Lancaster, C.D. *Wolinella succinogenes* quinol:fumarate reductase—2.2-Å resolution crystal structure and the E-pathway hypothesis of coupled transmembrane proton and electron transfer. *Biochim Biophys Acta*. **2002**; 1565(2):215–231. doi:10.1016/s0005-2736(02)00571-0
20. Borisov, V.B.; Gennis, R.B.; Hemp, J.; Verkhovsky, M.I. The cytochrome *bd* respiratory oxygen reductases. *Biochim Biophys Acta*. **2011**; 1807(11):1398–1413. doi:10.1016/j.bbabio.2011.06.016
21. Schleicher, L.; Trautmann, A.; Stegmann, D.P.; Fritz, G.; Gätgens, J.; Bott, M.; Hein, S.; Simon, J.; Seifert, J.; Steuber, J. A sodium-translocating module linking succinate production to formation of a membrane potential in *Prevotella bryantii*. *Appl Environ Microbiol*. **2021**; AEM0121121. doi:10.1128/AEM.01211-21
22. Steuber, J.; Vohl, G.; Casutt, M.S.; Vorburger, T.; Diederichs, K.; Fritz, G. Structure of the *V. cholerae* $Na^+$-pumping NADH:quinone oxidoreductase. *Nature*. **2014**; 516(7529):62–67. doi:10.1038/nature14003
23. Steuber, J.; Vohl, G.; Muras, V.; Toulouse, C.; Claußen, B.; Vorburger, T.; Fritz, G. The structure of $Na^+$-translocating of NADH:ubiquinone oxidoreductase of *Vibrio cholerae*: implications on coupling between electron transfer and $Na^+$ transport. *Biol Chem*. **2015**; 396(9-10):1015–1030. doi:10.1515/hsz-2015-0128
24. Casutt, M.S.; Wendelspiess, S.; Steuber, J.; Fritz, G. Crystallization of the $Na^+$-translocating NADH:quinone oxidoreductase from *Vibrio cholerae*. *Acta Crystallogr Sect F Struct Biol Cryst Commun*. **2010**; 66(Pt 12):1677–1679. doi:10.1107/S1744309110043125
25. Nowicka, B.; Kruk, J. Occurrence, biosynthesis and function of isoprenoid quinones. *Biochim Biophys Acta*. **2010**; 1797(9):1587–1605. doi:10.1016/j.bbabio.2010.06.007
26. Moparthi, V.K.; Hägerhäll, C. The evolution of respiratory chain complex I from a smaller last common ancestor consisting of 11 protein subunits. *J Mol Evol*. **2011**; 72(5-6):484–497. doi:10.1007/s00239-011-9447-2
27. Heikal, A.; Nakatani, Y.; Dunn, E.; Weimar, M.R.; Day, C.L.; Baker, E.N.; Lott, J.S.; Sazanov, L.A.; Cook, G.M. Structure of the bacterial type II NADH dehydrogenase: a monotopic membrane protein with an essential role in energy generation. *Mol Microbiol*. **2014**; 91(5):950–964. doi:10.1111/mmi.12507
28. Steuber, J.; Krebs, W.; Dimroth, P. The $Na^+$-translocating NADH:ubiquinone oxidoreductase from *Vibrio alginolyticus*--redox states of the FAD prosthetic group and mechanism of $Ag^+$ inhibition. *Eur J Biochem*. **1997**; 249(3):770–776. doi:10.1111/j.1432-1033.1997.t01-2-00770.x
29. Asano, M.; Hayashi, M.; Unemoto, T.; Tokuda, H. $Ag^+$ -sensitive NADH dehydrogenas in the $Na^+$ -motive respiratory chain of the marine bacterium *Vibrio alginolyticus*. *Agric Biol Chem*. **1985**; 49(9):2813–2817. doi:10.1080/00021369.1985.10867173
30. Hackmann, T.J.; Ngugi, D.K.; Firkins, J.L.; Tao, J. Genomes of rumen bacteria encode atypical pathways for fermenting hexoses to short-chain fatty acids. *Environ Microbiol.*

**2017**; 19(11):4670–4683. doi:10.1111/1462-2920.13929
31. Macklaim, J.M.; Fernandes, A.D.; Di Bella, J.M.; Hammond, J.; Reid, G.; Gloor G.B. Comparative meta-RNA-seq of the vaginal microbiota and differential expression by *Lactobacillus iners* in health and dysbiosis. *Microbiome*. **2013**; 1(1):12. doi:10.1186/2049-2618-1-12
32. Dibrov, P.; Dibrov, E.; Maddaford, T.G.; Kenneth, M.; Nelson, J.; Resch, C.; Pierce, G.N. Development of a novel rationally designed antibiotic to inhibit a nontraditional bacterial target. *Can J Physiol Pharmacol*. **2017**; 95(5):595–603. doi:10.1139/cjpp-2016-0505
33. Meier, T.; Polzer, P.; Diederichs, K.; Welte, W.; Dimroth, P. Structure of the rotor ring of F-Type $Na^+$-ATPase from *Ilyobacter tartaricus*. *Science*. **2005**; 308(5722):659–662. doi:10.1126/science.1111199
34. Amabebe, E.; Anumba, D.O.C. The vaginal microenvironment: the physiologic role of *Lactobacilli*. *Front Med*. **2018**; 5:181. doi:10.3389/fmed.2018.00181
35. Schleicher, L.; Fritz, G.; Seifert, J.; Steuber, J. Anoxic cell rupture of *Prevotella bryantii* by high-pressure homogenization protects the $Na^+$-translocating NADH:quinone oxidoreductase from oxidative damage. *Arch Microbiol*. **2020**; 202(5):1263–1266. doi:10.1007/s00203-019-01805-x
36. Jung, H.; Ehlers, M.M.; Lombaard, H.; Redelinghuys, M.J.; Kock, M.M. Etiology of bacterial vaginosis and polymicrobial biofilm formation. *Crit Rev Microbiol*. **2017**; 43(6):651–667. doi:10.1080/1040841X.2017.1291579
37. Schwebke, J.R.; Muzny, C.A.; Josey, W.E. Role of *Gardnerella vaginalis* in the pathogenesis of bacterial vaginosis: a conceptual model. *J Infect Dis*. **2014**; 210(3):338–343. doi:10.1093/infdis/jiu089
38. Harwich, M.D.; Alves, J.M.; Buck, G.A.; Strauss, J.F.; Patterson, J.L.; Oki, A.T.; Girerd, P.H.; Jefferson, K.K. Drawing the line between commensal and pathogenic *Gardnerella vaginalis* through genome analysis and virulence studies. *BMC Genomics*. **2010**; 11:375. doi:10.1186/1471-2164-11-375
39. Smith, P.K.; Krohn, R.I.; Hermanson, G.T.; Mallia, A.K.; Gartner, F.H.; Provenzano, M.D.; Fujimoto, E.K.; Goeke, N.M.; Olson, B.J.; Klenk, D.C. Measurement of protein using bicinchoninic acid. *Anal Biochem*. **1985**; 150(1):76–85. doi:10.1016/0003-2697(85)90442-7
40. Ito, M.; Cooperberg, B.; Krulwich, T.A. Diverse genes of alkaliphilic *Bacillus firmus* OF4 that complement $K^+$-uptake-deficient *Escherichia coli* include an *ftsH* homologue. *Extremophiles*. **1997**; 1(1):22–28. doi:10.1007/s007920050011
41. Mohamed, S.A.; Elshal, M.F.; Kumosani, T.A.; Aldahlawi, A.M. Purification and characterization of asparaginase from *Phaseolus vulgaris* seeds. *Evid Based Complement Alternat Med*. **2015**; 2015:309214. doi:10.1155/2015/309214
42. Leutbecher, H.; Greiner, G.; Amann, R.; Stolz, A.; Beifuss, U.; Conrad, J. Laccase-catalyzed phenol oxidation. Rapid assignment of ring-proton deficient polycyclic benzofuran regioisomers by experimental $^{1}H$-$^{13}C$ long-range coupling constants and DFT-predicted product formation. *Org Biomol Chem*. **2011**; 9(8):2667–2673. doi:10.1039/c1ob00012h
43. Schägger, H.; von Jagow, G. Tricine-sodium dodecyl sulfate-polyacrylamide gel electrophoresis for the separation of proteins in the range from 1 to 100 kDa. *Anal Biochem*. **1987**; 166(2):368–379. doi:10.1016/0003-2697(87)90587-2
44. Vohl, G.; Nedielkov, R.; Claussen, B.; Casutt, M.S.; Vorburger, T.; Diederichs, K.; Möller, H.M.; Steuber, J.; Fritz, G. Crystallization and preliminary analysis of the NqrA and NqrC subunits of the $Na^+$-translocating NADH:ubiquinone oxidoreductase from *Vibrio cholerae*. *Acta Crystallogr Sect F Struct Biol Cryst Commun*. **2014**;70(Pt 7):987–992. doi:10.1107/S2053230X14009881
45. Juárez, O.; Athearn, K.; Gillespie, P.; Barquera, B. Acid residues in the transmembrane helices of the $Na^+$-pumping NADH:quinone oxidoreductase from *Vibrio cholerae* involved in sodium translocation. *Biochemistry*. **2009**; 48(40):9516–9524. doi:10.1021/bi900845y
46. Kroger, A.; Innerhofer, A. The function of menaquinone, covalently bound FAD and iron-sulfur protein in the electron transport from formate to fumarate of *Vibrio succinogenes*. *Eur J Biochem*. **1976**; 69(2):487–495. doi:10.1111/j.1432-1033.1976.tb10933.x
47. Al-Attar, S.; Yu, Y.; Pinkse, M.; Hoeser, J.; Friedrich, T.; Bald, D.; de Vries, S. Cytochrome *bd* displays significant quinol peroxidase activity. *Sci Rep*. **2016**; 6:27631. doi:10.1038/srep27631
48. Trumpower, B.L.; Edwards, C.A. Purification of a reconstitutively active iron-sulfur protein (oxidation factor) from succinate cytochrome *c* reductase complex of bovine heart mitochondria. *J Biol Chem*. **1979**; 254(17):8697–8706.
49. Geisler, V.; Ullmann, R.; Kröger, A. The direction of the proton exchange associated with the redox reactions of menaquinone during electron transport in *Wolinella succinogenes*. *Biochim Biophys Acta*. **1994**; 1184(2-3):219–226. doi:10.1016/0005-2728(94)90226-7
50. Blasco, L.; Kahala, M.; Tupasela, T.; Joutsjoki, V. Determination of aspartase activity in dairy *Propionibacterium strains*. *FEMS microbiol Lett*. **2011**; 321(1):10–13. doi:10.1111/j.1574-6968.2011.02299.x
51. Bzura, J.; Koncki, R. A mechanized urease activity assay. *Enzyme Microb Technol*. **2019**;

123:1–7. doi:10.1016/j.enzmictec.2019.01.001

52. Vorburger, T.; Nedielkov, R.; Brosig, A.; Bok, E.; Schunke, E.; Steffen, W.; Mayer, S.; Götz, F.; Möller, H.M.; Steuber, J. Role of the $Na^+$-translocating NADH:quinone oxidoreductase in voltage generation and $Na^+$ extrusion in *Vibrio cholerae*. *Biochim Biophys Acta*. **2016**;1857(4):473–482. doi:10.1016/j.bbabio.2015.12.010

## Supplementary Material

International Journal of Molecular Science
Supplementary Data

# Central carbon metabolism, sodium-motive electron transfer, and ammonium formation by the vaginal pathogen *Prevotella bivia*

**Lena Schleicher[1,2], Sebastian Herdan[1,2], Günter Fritz[1,2], Andrej Trautmann[2,3], Jana Seifert[2,3] and Julia Steuber[1,2,*]**

[1] Institute of Biology, University of Hohenheim, Garbenstraße 30, 70599 Stuttgart, Germany;lena.schleicher@uni-hohenheim.de (L.S.); sebastian.herdan@uni-hohenheim.de (S.H.); guenter.fritz@uni-hohenheim.de (G.F.)
[2] HoLMiR- Hohenheim Center for Livestock Microbiome Research, University of Hohenheim, Leonore-Blosser-Reisen-Weg 3, 70599 Stuttgart, Germany; anderj.trautmann@uni-hohenheim.de (A.T.); seifert.jana@uni-hohenheim.de (J.S.)
[3] Institute of Animal Science, University of Hohenheim, Emil-Wolff-Straße 8, 70599 Stuttgart, Germany
* Correspondence: julia.steuber@uni-hohenheim.de, +49-711-459-222-28

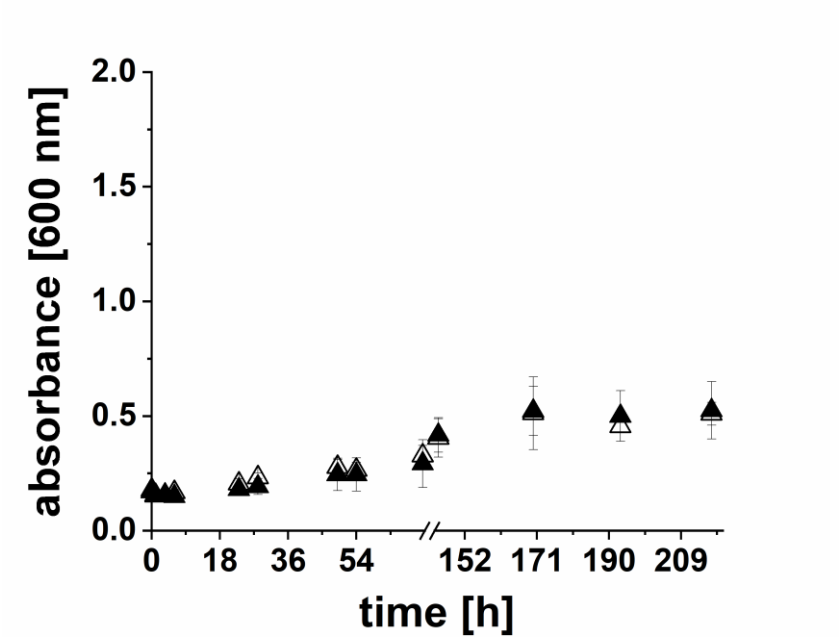


**Figure S1** Growth of *P. bivia* at pH 5.0 with (black triangles) or without (white triangles) 50 mM L-asparagine added. Average and standard deviations of three biological replicates are shown.

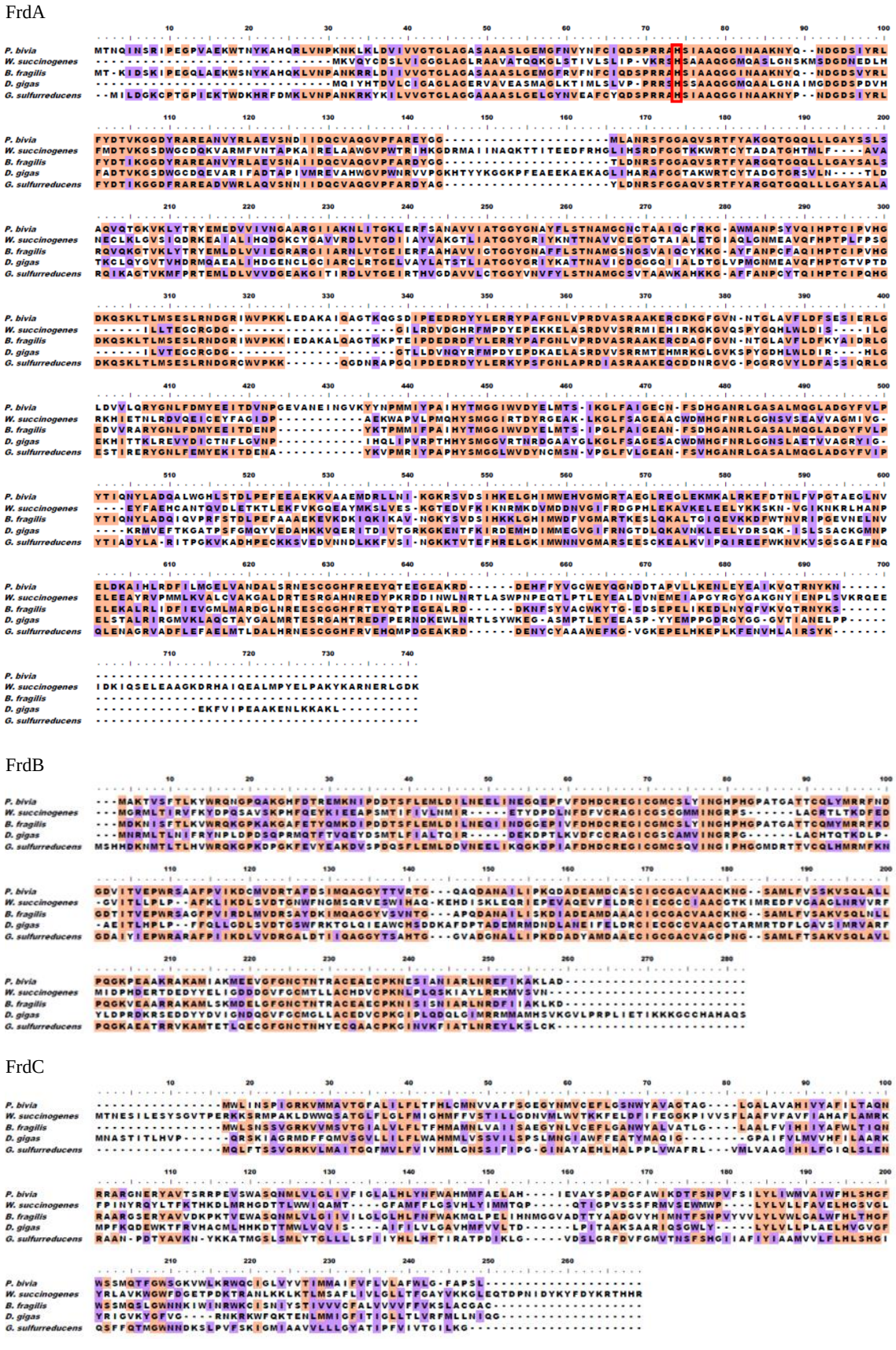


**Figure S2** Protein sequence alignments of the QFR subunits FrdA, FrdB and FrdC form *Prevotella bivia*, *Wolinella succinogenes*, *Bacteroides fragilis*, *Desulfovibrio gigas* and *Geobacter sulfurreducens*. Orange, identical amino acids; purple, similar amino acids. Conserved amino acids for flavin binding are highlighted in red.

NqrA

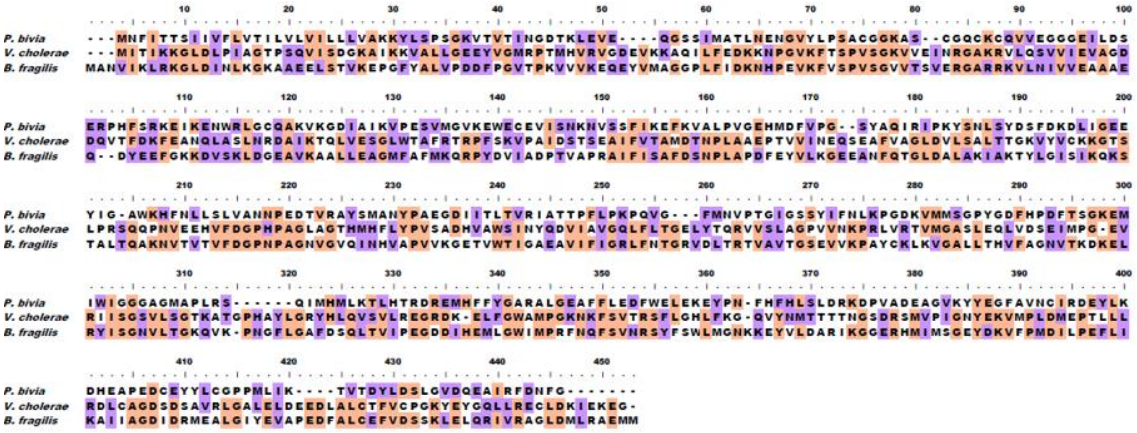


NqrB

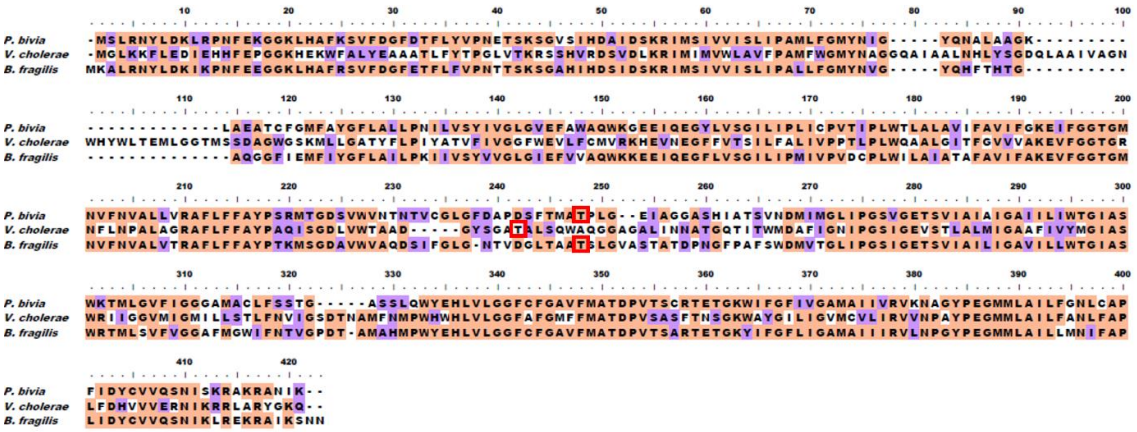


NqrC


NqrD

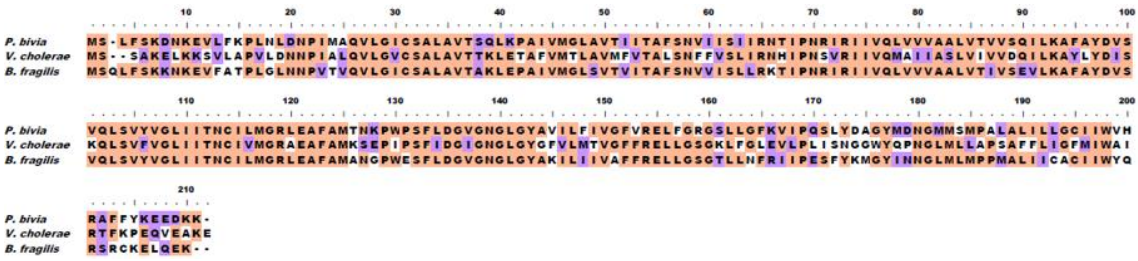

NqrE

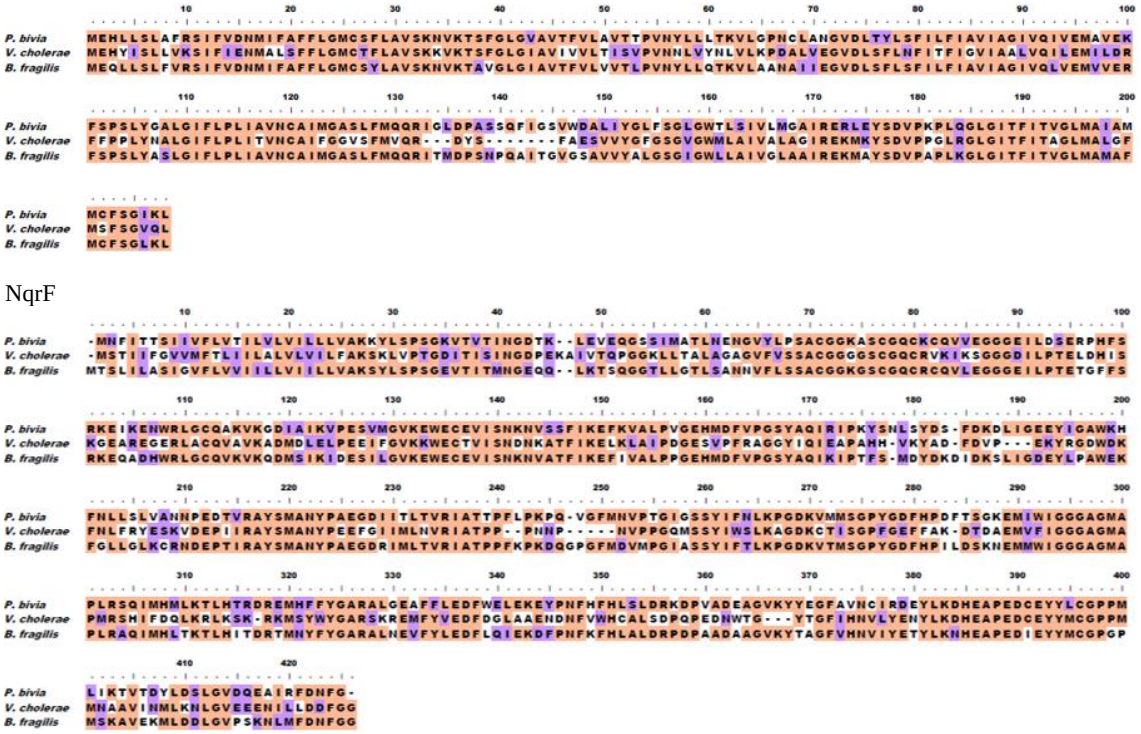


NqrF




**Figure S3** Protein sequence alignments of the NQR subunits NqrA, NqrB, NqrC, NqrD, NqrE and NqrF form *Prevotella bivia*, *Vibrio cholerae* and *Bacteroides fragilis*. Orange, identical amino acids; purple, similar amino acids. Conserved amino acids for flavin binding are highlighted in red.

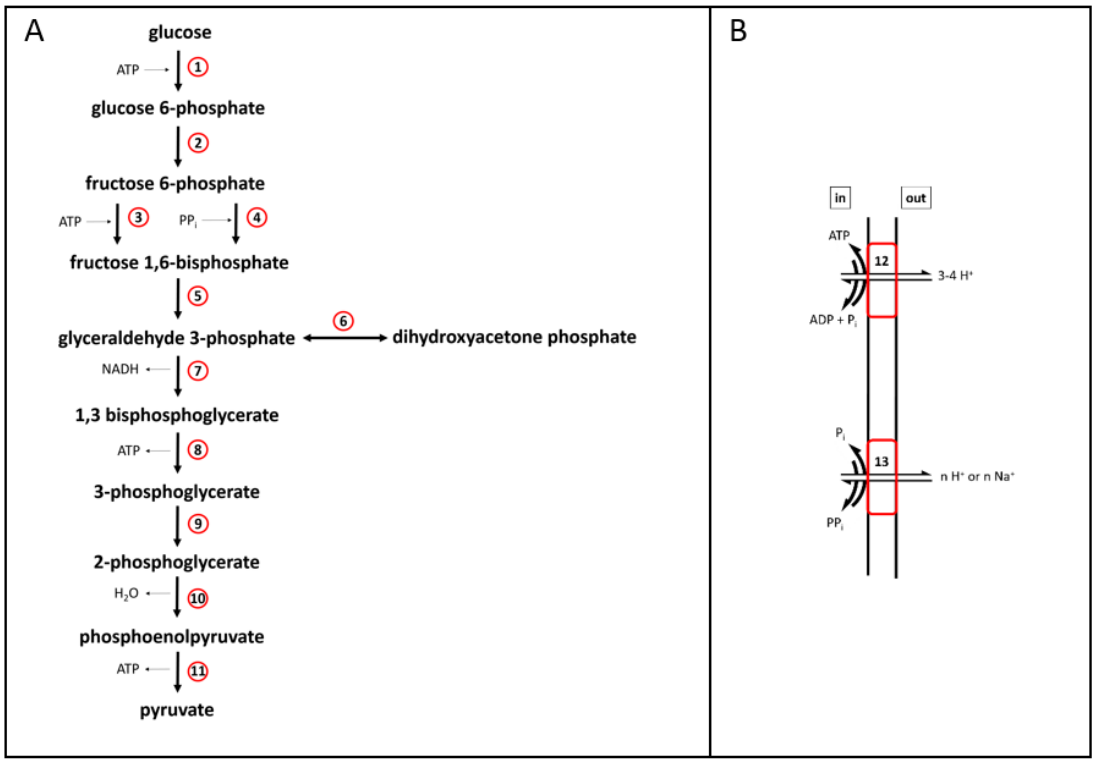


**Figure S4** Predicted pathways for glycolysis, and enzymes for regeneration of ATP or $PP_i$ in *Prevotella bivia*. A: Conversion of glucose to pyruvate. Glucokinase (1); glucose 6-phosphate isomerase (2); ATP-dependent phosphofructokinase (3); $PP_i$-dependent phosphofructokinase (4); aldolase (5); triose-phosphate isomerase (6); glyceraldehyde dehydrogenase (7); phosphoglycerate kinase (8); phosphoglycerate mutase (9); enolase (10); pyruvate kinase (11). B: Regeneration of ATP or $PP_i$ by the $F_1F_O$ ATPase (12) or the pyrophosphatase (13) is driven by electrochemical $H^+$ - or $Na^+$ -gradients.

**Table S1** Enzymes involved in glycolysis and energy conversion of *P. bivia* DSM 20514. Functional assignments are based on the genome information (NCBI accession number; NZ_AJVZ00000000). Corresponding UNIPROT accession numbers and predicted catalytic activities are listed.

| Enzyme | UNIPROT acccession number | Reaction |
|---|---|---|
| L-asparaginase | I4ZB31 | L-asparagine + $H_2O$ → L-aspartic acid + $NH_3$ |
| Aspartate ammonia lyase | I4ZB31 | L-aspartic acid ⇌ fumarate + $NH_3$ |
| Glucokinase | I4Z6R6 | glucose + ATP → glucose 6-phosphate + ADP + $P_i$ |
| Glucose 6-phosphate isomerase | I4Z9B5 | glucose 6-phosphate ⇌ fructose 6-phosphate |
| ATP-dependent phosphofructokinase | I4ZBC7 | fructose 6-phosphate + ATP → fructose 1,6-bisphosphate + ADP + $P_i$ |
| $PP_i$-dependent phosphofructokinase | I4Z6W8 | fructose 6-phosphate + $PP_i$ → fructose 1,6-bisphosphate + $P_i$ |
| Aldolase | I4Z941 | fructose 1,6-bisphosphate → glyceraldehyde 3-phosphate + dihydroxyacetone phosphate |
| Triose-phosphate isomerase | I4ZC94 | dihydroxyacetone phosphate ⇌ glyceraldehyde 3-phosphate |
| Glyceraldehyde dehydrogenase | I4ZAB6 | glyceraldehyde 3-phosphate + $NAD^+$ + $P_i$ ⇌ 1,3-bisphosphoglycerate + NADH + $H^+$ |
| Phosphoglycerate kinase | I4ZC16 | 1,3-bisphosphoglycerate + ADP + $P_i$ ⇌ 3-phosphoglycerate + ATP |
| Phosphoglycerate mutase | I4Z8T9 | 3-phosphoglycerate ⇌ 2-phosphoglycerate |
| Enolase | I4ZCE6 | 2-phosphoglycerate ⇌ phosphoenolpyruvate + $H_2O$ |

| | | |
|---|---|---|
| Pyruvate kinase | I4ZA98 | phosphoenolpyruvate + ADP → pyruvate + ATP |
| $F_1F_O$ ATP synthase (proton-dependent) | I47BC8+9<br>I4ZBD1-6 | ATP + (3-4) $H^+_{in}$ ⇌ ADP + $P_i$ + (3-4) $H^+_{out}$ |
| Pyrophosphatase | I4Z7F1 | $PP_i$ + $H_2O$ + n $Na^+_{in}$ / n $H^+_{in}$ ⇌ 2 $P_i$ + n $Na^+_{out}$ / n $H^+_{out}$ |
| PEP carboxykinase | I4Z866 | phosphoenolpyruvate + NDP + $P_i$ + $CO_2$ ⇌ oxaloacetate + NTP |
| Malate dehydrogenase | I4Z8Y0 | oxaloacetate + NADH ⇌ malate + $NAD^+$ |
| Fumarase | I4ZA21 | malate ⇌ fumarate + $H_2O$ |
| Pyruvate oxidoreductase | I4ZAL7 | Pyruvate + CoA + $X_{ox}$ ⇌ acetyl-CoA + $CO_2$ + $X_{red}$ |
| Phosphate acetyltransferase | I4Z807 | acetyl-CoA + phosphate ⇌ acetyl phosphate + CoA |
| Acetate kinase | I4Z808 | acetyl phosphate + ADP + $P_i$ ⇌ acetate + ATP |
| AMP-forming acetyl-CoA synthase | A0A137T148 | acetate + ATP + CoA → acetyl-CoA + AMP + $PP_i$ |
| Quinol:fumarate oxidoreductase | I4Z8D8+9<br>I4Z8E0 | $QH_2$ + fumarate ⇌ Q + succinate |
| $Na^+$ -translocating NADH:quinone oxidoreductase | I4ZAR9<br>I4ZAS0-4 | NADH +$H^+$ + Q + 2 $Na^+_{in}$ → $NAD^+$ + $QH_2$ + 2 $Na^+_{out}$ |
| 11-subunit complex (related to Nuo complex) | I4ZA64-73 | unknown |
| NADH dehydrogenase 2 (non-electrogenic) | I4Z8L8 | NADH +$H^+$ + Q → $NAD^+$ + $QH_2$ |
| Cytochrome *bd* quinol oxidase | I4Z6X4-5 | $QH_2$ + ½ $O_2$ → Q + $H_2O$ |
| NhaA | I4ZAA4 | $Na^+_{in}$ + 2 $H^+_{out}$ ⇌ $Na^+_{out}$ + 2 $H^+_{in}$ |
| NhaD | I4Z742 | n $Na^+_{in}$ + m $H^+_{out}$ ⇌ n $Na^+_{out}$ + m $H^+_{in}$<br>n $Li^+_{in}$ + m $H^+_{out}$ ⇌ n $Li^+_{out}$ + m $H^+_{in}$ |

**Table S2** Flavinylated subunits of the NQR and QFR in *P. bivia* membranes solubilized with 2.5 % DDM. Fluorescent bands indicating flavinylated proteins were excised from the SDS gel (see corresponding boxes highlighted in fig. 6), subjected to proteolysis, and analyzed by mass spectrometry. Total number of identified peptides and peptide sequences of FrdA, NqrB and NqrC are presented.

| **Box** | **Protein** | **Peptide number** | **Peptide sequence** |
|---|---|---|---|
| 1 | FrdA | 31 | IPEGPVAEK; IPEGPVAEKWTNYK; RAHSIAAQGGINAAK; AHSIAAQGGINAAK; NYQNDGDSIYR; LAEVSNDIIDQCVAQGVPFAR; EYGGMLANR; SFGGAQVSR; GQTGQQLLLGAYSSLSAQVQTGK; LYTRYEMEDVVIVNGAAR; YEMEDVVIVNGAAR; NLITGKLER; LTLMSESLR; QGSDIPEEDRDYYLER; RYPAFGNLVPR; YPAFGNLVPR; GFGVNNTGLAVFLDFSESIER; LGLDVVLQR; YGNLFDMYEEITDVNPGEVANEINGVK; GLFAIGECNFSDHGANR; LGASALMQGLADGYFVLPYTIQNYLADQALWGHLSTDLPEFEEAEK; ELGHIMWEHVGMGR; TAEGLREGLEK; KEFDTNLFVPGTAEGLNVELDK; EFDTNLFVPGTAEGLNVELDK; DFILMGELVANDALSR; EEYQTEEGEAK; EEYQTEEGEAKR; ENLEYEAIK; ENLEYEAIKVQTR |
| 2 | NqrB | 4 | SVFDGFDTFLYVPNETSK; SGVSIHDAIDSKR; SGVSIHDAIDSK; AFLFFAYPSR |
| | NqrC | 10 | QILFALNQDR; QILFALNQDRDMTNPQAEK; DMTNPQAEK; EIITADDIINADGQVTTSGK; QGGIEAGFK; TVFGAYFNHESETAGLGAEIKDNK; KLFAAGDEK; LFAAGDEK; KIALSVMK; GSLQPYVK |

# Chapter 5 – Structural models of the NQR and QFR

## 5.1 Introduction

Results presented in this thesis shed a light on the function of two electron transfer complexes from the rumen model organism *P. bryantii*, namely the NQR and QFR. The NQR is a sodium-translocating NADH:quinone oxidoreductase and a key player in the anaerobic energy conservation of *P. bryantii*. It is embedded into the inner bacterial membrane and comprises six subunits (NqrABCDEF). The homologous NQR of *V. cholerae* harbors six cofactors: one FAD in NqrF, two FeS centers in NqrF and NqrD/E, one riboflavin in NqrB, and two covalently bound FMNs in NqrB and NqrC (1). The QFR is a quinol:fumarate reductase, oxidizing menaquinol and reducing fumarate to succinate. It is composed of three subunits (FrdABC), with FrdA containing one FAD, FrdB harboring three FeS centers and FrdC comprising two hemes *b* (2). Together, these enzymes form a supercomplex in the membrane of *P. bryantii* (3) and represent an important energy-generating module. This supercomplex intimately connects NADH-driven sodium ion translocation to an important step in sugar degradation by *P. bryantii*, namely, the formation of succinate.

3D structures of the NQR and QFR from *P. bryantii* are the basis for a detailed, mechanistic understanding of these enzymes, and of the supercomplex. However, experimentally verified 3D protein structures, especially from mulitsubunit membrane complexes or supercomplexes, are not easily achieved. Thus, structural models of the *P. bryantii* NQR and QFR were generated based on the 3D structures of the highly related enzymes from *V. cholerae* and *D. gigas.* The quality of the models was assessed with a main focus on the cofactor binding sites and overall architecture.

## 5.2 Material and Methods

Amino acid sequences of Pb-NQR and Pb-QFR subunits (queries) were retrieved from Uniprot. Selection of a suitable template (protein with known structure) for modelling and the actual building of a structural model was done with the software Phyre2. Four consecutive core methods are used by Phyre2 for homology modelling (4): In the first stage, the query amino acid sequence is scanned against a sequence database by the software HHblits, resulting in an evolutionary sequence profile. Furthermore, a secondary structure of the protein is predicted with the software PSPI-Pred16 (4). These results are used in the second stage by Phyre2 to create a hidden Markov model (HMM). The HMM is a stochastic model, describing different states of a system and the probabilities of their transitions. In this case, the HMM invokes different states (positions) of the amino acids in the structure of the query protein. Every state has an occurrence probability and a transition probability, which indicates the probability of moving from one state to another (5). Phyre2 scans the generated HMM against a pre-compiled database (fold library) of HMMs from proteins with an experimentally determined protein structure, resulting in a list of structural based query-template alignments (HMM-HMM matching). This matching process allows the prediction of significant protein sequence similarities and their positions in the modelled structure, including insertions and deletions along the alignment (6). HMM-HMM matching is also used to predict secondary structure types and transmembrane regions (7). Consequently, these alignments are the basis to create crude backbone models. In the third stage, a library of fragments and the (CCD)17 algorithm are used to correct insertions or deletions in the crude model. Finally, sidechain fitting to the backbone is performed using R3 protocol20 (4). For every model, different factors (confidence value, coverage, sequence identity, TM score) are calculated, depending on the used template, allowing estimation of the quality of the model. These calculations are based on the alignments of the HMM-HMM matchings and thus, not only the amino acid sequences are taken into consideration, but also the amino

acid positioning in the 3D model (6). The coverage value gives the percentage of coverage between the query and the template. The sequence identity is the proportion of the protein residues, which correspond to identical template residues in the generated alignment (4). With a structure derived sequence identity > 30%, the model has a high accuracy, and the side chain conformations of conserved residues exhibit the same orientations. The confidence value represents the probability (from 0 to 100%) that the query and the template are homologous (4), but it is no direct measure for the accuracy of the model. However, a model with > 90% confidence indicates that the query structure is very likely to adopt to the overall fold of the template structure. Moreover, it suggests that the core of the protein is modelled at high accuracy. The template modelling (TM) score (from 0-1) is a measure of similarity between the modelled protein and the template structure (4). Identical structures score 1.0, whereas a score < 0.2 indicates a similarity no better than random.

Next to these basic informations of the modelled structure quality, Phyre2 gives more detailed information about the secondary structure and the different domains. Here, the ProQ2 assessment, clash analysis, rotamer analysis, Ramachandran analysis and the alignment confidence are shown. The results of these analyses are all presented in color-coded structures of the modelled protein, allowing local qualification of the structure. ProQ2 is a model quality assessment algorithm, predicting and visualizing local as well as global structural model correctness (color code: from red, good, to blue, bad) (8). By clash analysis, atoms in residues are identified, which may lie to close to one another in the model. A large number of clashes could indicate bad sidechain placement or an incorrect backbone in this region (color code: from blue, good, to red, bad). The Rotamer analysis shows side chains, which may have not been modelled ideally (stage 4 of protein modelling by Phyre2; color code: blue, good; red, bad). The Ramachandran analysis asks, if residues in the model lie in electrostatically favorable, allowed or disallowed regions. Thus, it addresses the stereochemistry and geometry of the modelled structure (color code: blue, good; green,

allowed; red, bad). The alignment confidence shows the reliability of the pairwise query-template alignment of the HMM-HMM matching (color code: from red, good, to blue, bad).

## 5.3 Results and Discussion

### 5.3.1 Model of the structure of *Prevotella bryantii* NQR and comparison with the *Vibrio cholerae* NQR

The Pb-NQR subunits were modelled using the corresponding subunits of the NQR from *V. cholerae*. Considering the factors describing model quality, reliable models with a high confidence, coverage, identity and TM score were built (table 5.1).

**Table 5.1** Quality of the 3D models of *P. bryantii* NQR. Homology modelling of the NQR from *P. bryantii* was performed with Phyre2. Given are the templates for modelling, which were selected by Phyre2, as well as the confidence, coverage, identity and template modelling (TM) score.

| | | template | Confidence [%] | Coverage [%] | Identity [%] | TM score |
|---|---|---|---|---|---|---|
| **NQR** | NqrA | NqrA from *V. cholerae* | 100 | 88 | 32 | 1.0 |
| | NqrB | NqrB from *V. cholerae* | 100 | 84 | 45 | 1.0 |
| | NqrC | NqrC from *V. cholerae* | 100 | 98 | 29 | 1.0 |
| | NqrD | NqrD from *V. cholerae* | 100 | 85 | 56 | 1.0 |
| | NqrE | NqrE from *V. cholerae* | 100 | 90 | 57 | 1.0 |
| | NqrF | NqrF from *V. cholerae* | 100 | 95 | 49 | 1.0 |

Figure 5.1 shows the model of the structure of the *P. bryantii* NQR complex. The NQR is composed of six subunits: NqrA (green), NqrB (red), NqrC (yellow), NqrD (magenta), NqrE (orange) and NqrF (blue). Importantly, the Vc-NQR harbors six cofactors, which were included in the model of Pb-NQR. NqrF comprises one FAD and one [2Fe-2S] cluster,

NqrD/E contain a Fe site, NqrC harbors one FMN and NqrB comprises one FMN and one riboflavin. A detailed comparison of the cofactor binding sites in the model with the structure of the Vc-NQR is crucial to assess the quality of the Pb-NQR structural model. To this end, a structural alignment of the Pb-NQR model with the Vc-NQR structure was performed, with special emphasis on amino acid residues participating in the binding of cofactors.

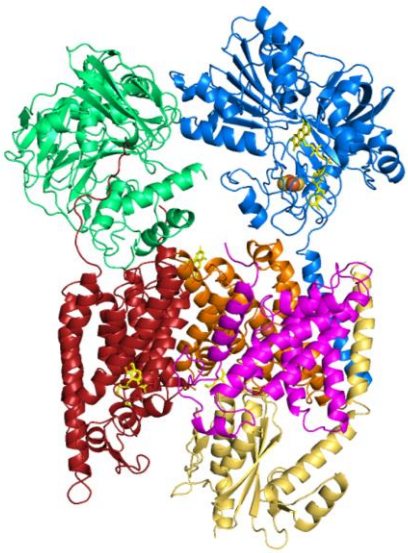

**Figure 5.1** Modelled structure of *P. bryantii* NQR. The NQR is composed of six subunits: NqrA (green), NqrB (red), NqrC (yellow), NqrD (magenta), NqrE (orange) and NqrF (blue). Note that the positions of cofactors reflect the assumed positions in the Vc-NQR. These are one FAD and one [2Fe-2S] in NqrF, one site for Fe binding formed by NqrD and NqrE, one FMN in NqrC, one FMN and one riboflavin in NqrB. Flavin structures are indicated in yellow, iron atoms are shown as orange spheres, sulfur atoms as yellow spheres and the membrane is indicated with dashed lines. Pb-NQR structure was modelled with Phyre2 and the structure was drawn with PyMOL version 2.5.

Vc-NqrF catalyzes the initial step of respiration by oxidizing NADH under transfer of hydride to FAD, and stepwise electron transfer from the flavin to the [2Fe-2S] cluster. Therefore, it harbors a NADH binding pocket in proximity to one non-covalently bound FAD in the C-terminal FAD-binding region (1, 9). The crucial amino acids for NADH binding are poorly characterized until now, but it is known from other enzymes that a nucleotide binding site is typically formed by two α-helices flanking parallel β-sheets (10). This so-called Rossmann fold is observed in Vc-NqrF, and it is also present in the model of Pb-NQR (fig. 5.2, panel A). The position of amino acid residues critical for this NADH

binding site are highly conserved. In close proximity, the FAD is coordinated by three amino acid residues in Vc-NqrF: Tyr212, Ser213 and Phe406 (9) (fig. 5.2, panel B). In the modelled Pb-NqrF structure, these amino acids are also present (Tyr216, Ser217, Phe421), assuming very similar orientations. In the overlay, the model and the experimentally determined structure essentially exhibit identical features, here shown with emphasis on the Pb-NqrF model depicted in blue (fig. 5.2, panel B). The same applies to the amino acid residues coordinating the [2Fe-2S] cluster in the N-terminal ferredoxin domain of NqrF. This cluster is coordinated in Vc-NqrF by the sulfur residues of the four cysteines Cys70, Cys76, Cys79 and Cys111 (1, 9) (fig 5.2, panel C). These cysteine residues exhibit very similar positions in the modelled Pb-NqrF structure (Cys69, Cys75, Cys78, Cys110).

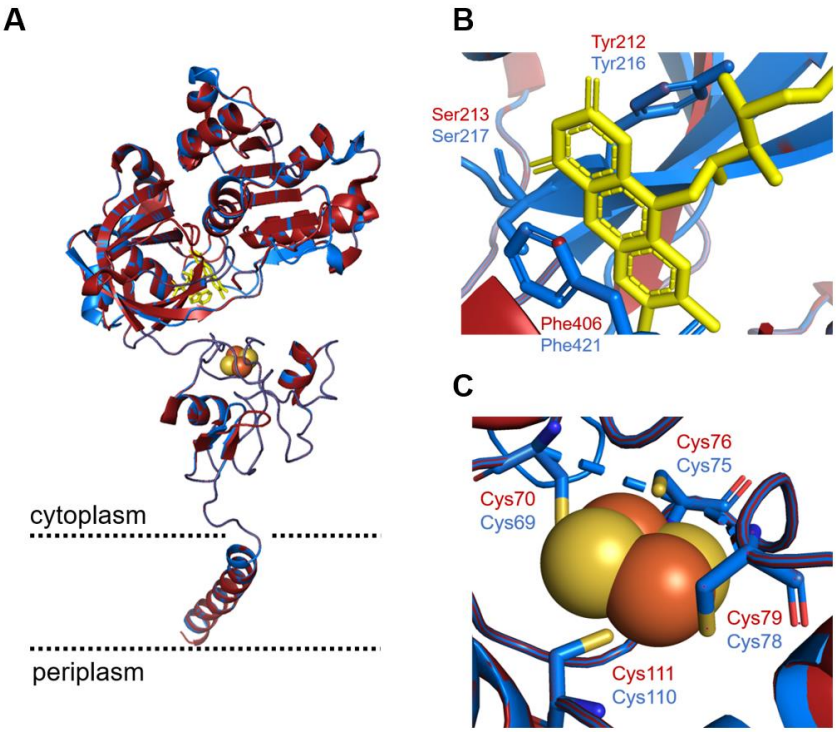


**Figure 5.2** Structural alignment of the NqrF from *P. bryantii* (blue) and *V. cholerae* (red). A: Subunit NqrF with two cytoplasmic domains harboring the FAD and [2Fe-2S] cofactors, respectively. B: Close-up view of the FAD binding domain. The conserved amino acids Tyr212, Ser213 and Phe406 in Vc-NqrF and Tyr216, Ser217 and Phe421 in Pb-NqrF coordinate the non-covalently bound FAD. C: Close-up view of the [2Fe-2S] coordination. Four cysteines (Cys70, Cys76, Cys79 and Cys111 in Vc-NqrF; Cys69, Cys75, Cys78 and Cys110 in Pb-NqrF) coordinate the FeS cluster with their sulfur residues (yellow colored sticks). FAD is indicated in yellow, iron atoms are shown as orange spheres and sulfur atoms as yellow spheres. The dashed line in C represents an unmodelled loop. The coordinates of the Vc-NqrF structure were obtained from the protein data bank (PDB 4P6V) and the Pb-NqrF structure was modelled with Pyhre2. The structures were aligned and drawn with PyMOL version 2.5.

The Fe site between NqrD and NqrE is crucial for the electron transport from NqrF to NqrC. The structural alignment shows that the modelled Pb-NqrDE structures are highly similar to the Vc-NqrDE subunits (fig. 5.3, panel A). Four cysteine residues (Cys29 and Cys112 from NqrD; Cys26 and Cys120 from NqrE) in Vc-NqrDE coordinate the Fe via their thiol groups (53) (fig. 5.3, panel B). In Pb-NqrDE these cysteines are also present (Cys30 and Cys113 from NqrD; Cys26 and Cys120 from NqrE) (fig. 5.3, panel B).

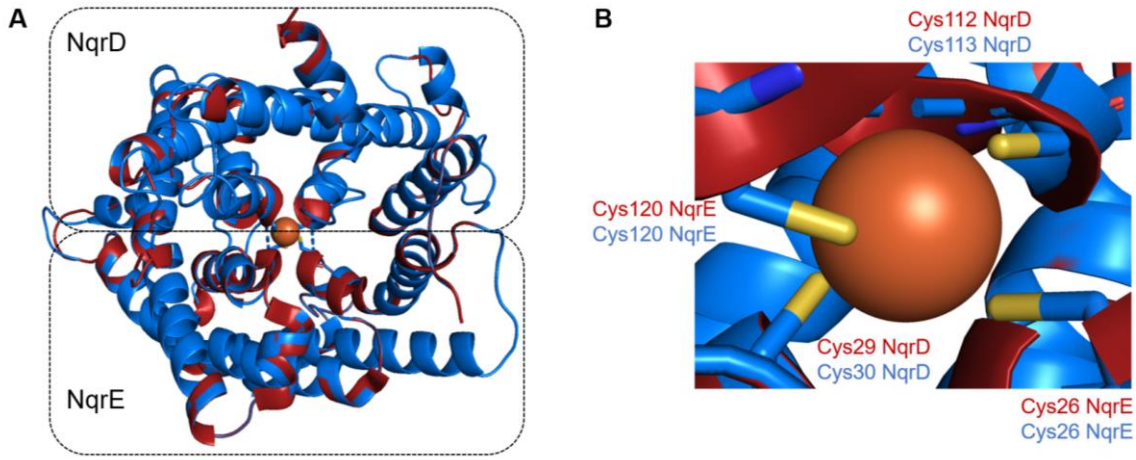


**Figure 5.3** Structural alignment of the NqrD and NqrE subunits from *P. bryantii* (blue) and *V. cholerae* (red). A: Subunits NqrD and NqrE each provide two cysteine residues for coordination of a Fe site located at the interface of the two subunits. B: Close-up view of the Fe site. The thiol groups (yellow) of the four cysteines (Cys29, Cys112 in Vc-NqrD and Cys26, Cys120 in Vc-NqrE; Cys30, Cys113 in Pb-NqrD and Cys26, Cys120 in Pb-NqrE) coordinate the Fe (orange sphere). The coordinates of the Vc-NqrD and NqrE structures were obtained from the protein data bank (PDB 4P6V) and the Pb-NqrD and NqrE structures were modelled with Phyre2. The structures were aligned and drawn with PyMOL version 2.5.

From the Fe site, electrons are transferred to covalently bound FMNs. Closest to the Fe site is the FMN located in Vc-NqrC, with Thr225 forming a phosphodiester bond to the flavin (fig 5.4, panel A) (11, 12). In Pb-NqrC the conserved threonine (Thr183) adopts a similar position (fig. 5.4, panel A). Another FMN is found in Vc-NqrB, where it is bound *via* a phosphodiester bond to threonine 236 (fig. 5.4, panel B) (13, 14). The conserved Thr221 in Pb-NqrB is found in a similar position. It is therefore reasonable to assume that Thr183 and Thr221 in Pb-NqrC and Pb-NqrB each are covalently linked to FMN (fig. 5.4, panel B). This is supported by the finding that NqrC and NqrB contain both covalently linked flavins (3).

It was suggested that the reduction of FMN in Vc-NqrB is coupled to the translocation of $Na^+$ ions through a channel in NqrB (1). In this study, critical amino acid residues, participating either directly or indirectly to $Na^+$ transport, were proposed. These are Val161, Ile164, Leu168, Phe338, Phe342 and Asp346 in Vc-NqrB. In the structural model of Pb-NqrB, a putative channel was observed with prominent, conserved amino acid residues (Val135, Ile138, Leu142, Phe309, Phe313, Asp317) at similar positions as observed in Vc-NQR (1). Notably, the position of Ile138 in Pb-NqrB (Ile164 in Vc-NqrB) in close proximity to the FMN located adjacent to the predicted channel (1) is also observed in the modelled structure of Pb-NqrB.

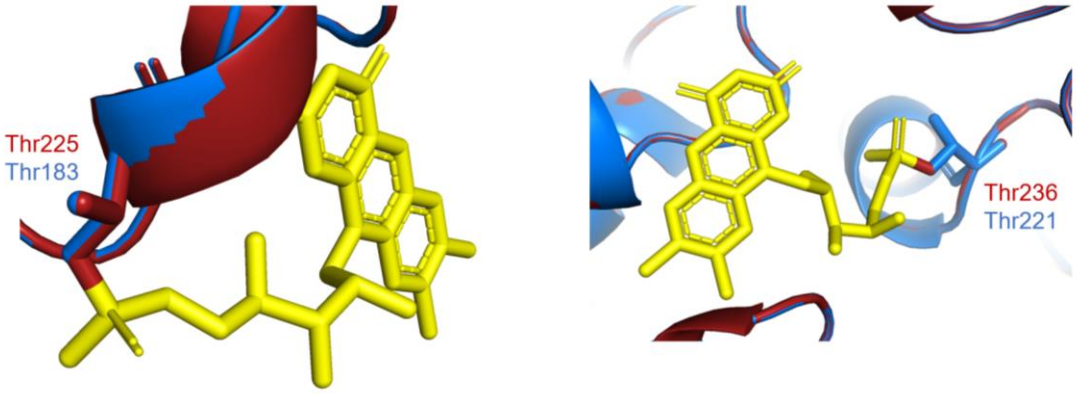


**Figure 5.4** Structural alignments of the NqrB and NqrC subunits from *P. bryantii* (blue) and *V. cholerae* (red). A: Close-up view of the FMN binding site in NqrC with Thr225 (Vc-NqrC) and Thr183 (Pb-NqrC). B: Close-up view of the FMN binding site in NqrB with Thr236 (Vc-NqrB) and Thr221 (Pb-NqrB). The coordinates of the Vc-NqrB and NqrC structures were obtained from the protein data bank (PDB 4P6V) and the Pb-NqrB and NqrC structures were modelled with Phyre2. The structures were aligned and drawn with PyMOL version 2.5.

In Vc-NQR, electron transport from FMN on NqrB to quinone proceeds *via* riboflavin (15-17). In the crystallographic structure of Vc-NQR, the position of the riboflavin could not be assigned unambiguously (1). A similar problem is encountered with the binding site(s) for ubiquinone. Vc-NQR binds ubiquinone-8 (18) and there is evidence that quinone interacts with NqrA (18, 19) and NqrB (20, 21). Therefore, putative binding sites for riboflavin and quinone cannot be predicted yet. In this context, it should be noted that the Pb-NQR utilizes menaquinone rather than ubiquinone, since *P. bryantii* exclusively relies on menaquinone

for respiration (3). Still, the model of Pb-NQR presented here represents a good starting point for further functional studies.

### 5.3.2 Model of the structure of *Prevotella bryantii* QFR and comparison with the *Wolinella succinogenes* QFR

Based on the primary sequences of the Pb-QFR subunits, the enzyme belongs to the class of type B succinate:quinone oxidoreductase, which includes the QFRs of *W. succinogenes* (22) and *D. gigas* (23). Accordingly, the Pb-QFR is composed of three subunits and its transmembrane FrdC subunit contains two hemes *b* participating in electron transfer from menaquinol to fumarate. The 3D crystallographic structure of the Dg-QFR served as template for model building of Pb-QFR by Pyhre2. Here, a high confidence, coverage and TM score were calculated, but only moderate identities, especially with FrdC, were observed (Table 5.2). Therefore, a more detailed analysis of the secondary structure quality of the modelled QFR structure was done with Phrye2.

**Table 5.2** Quality of the 3D model of *P. bryantii* QFR. Homology modelling of the QFR subunits from *P. bryantii* was performed with Phyre2. Given are the templates for modelling, which were selected by Phyre2, as well as the confidence, coverage, identity and template modelling (TM) score.

| | | template | Confidence [%] | Coverage [%] | Identity [%] | TM score |
|---|---|---|---|---|---|---|
| **QFR** | FrdA | FrdA from *D. gigas* | 100 | 95 | 28 | 1.0 |
| | FrdB | FrdB from *D. gigas* | 100 | 98 | 23 | 1.0 |
| | FrdC | FrdC from *D. gigas* | 100 | 86 | 17 | 1.0 |

The ProQ2 assessment indicates a good quality of the core structures, illustrated by yellow and orange colored cores of the modelled protein structures (fig. 5.5, first row). Blue color indicates regions where the quality of the model is lower, which is frequently observed in loops or other connecting protein domains. Still, the clash analysis indicates that only a few domains in the modelled structures exhibit unfavorable positions of amino acid side chains. Thus, an overall correct positioning of side chains in the models is assumed (fig 5.5, second row). Furthermore, only a few domains reveal incorrect modelling in terms of rotamer analysis (fig. 5.5, third row). Ramachandran analysis revealed only a few disallowed regions near or in the loop domains in the modelled FrdABC structures (fig. 5.5, fourth row). Nevertheless, the overall stereochemistry and geometry of the models are adequate. Finally, the alignment confidence shows that the cores of the modelled structures have a high confidence, whereas the loop regions have a bad confidence (fig. 5.5, fifth row).

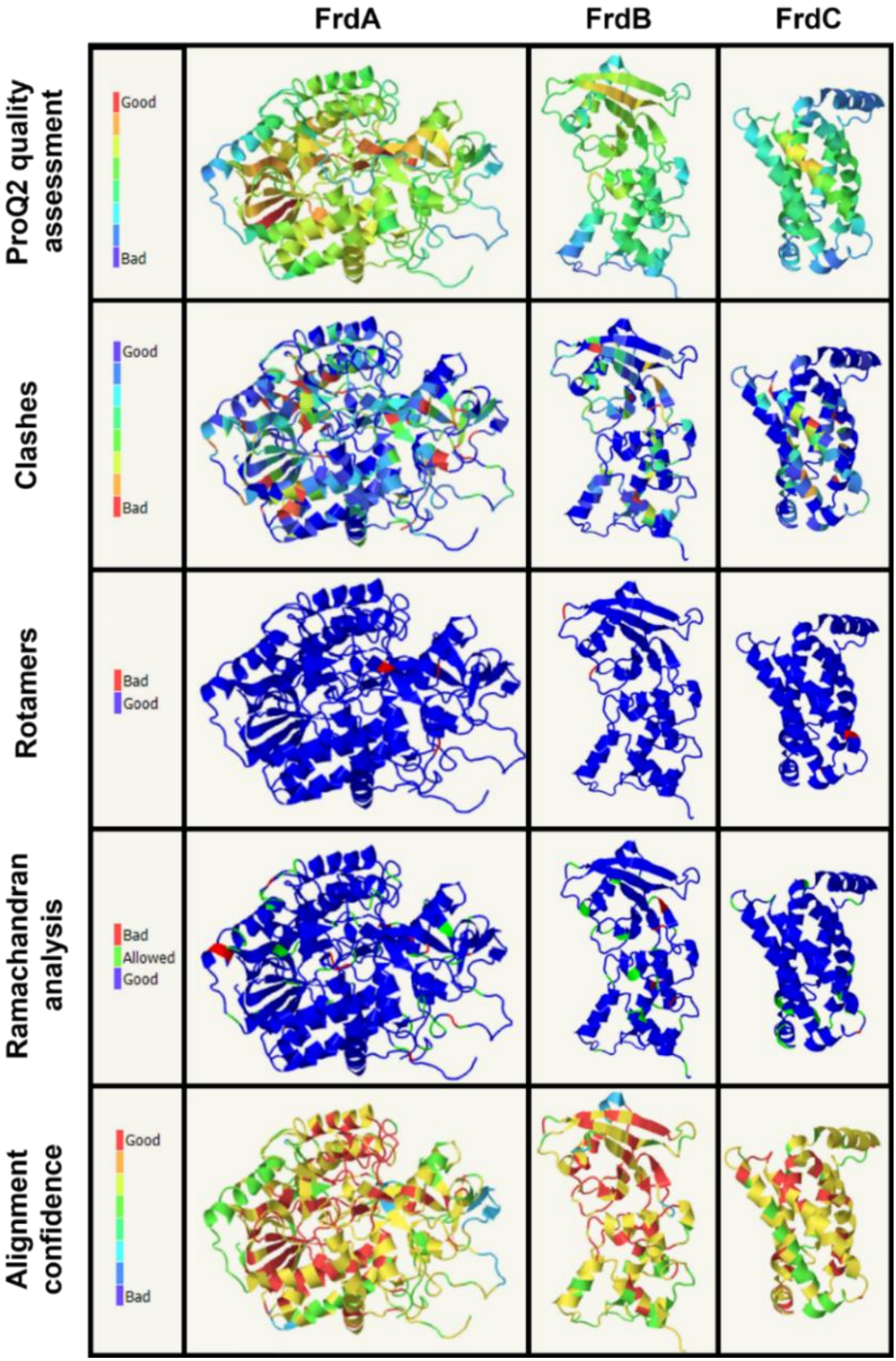


**Figure 5.5** Homology modelling of the FrdA (second column), FrdB (third column) and FrdC (fourth column) subunits from *P. bryantii* performed by Phyre2, using the *D. gigas* QFR subunits as templates. Shown are the ProQ2 quality assessment (first row), clash analyses (second row), rotamer analyses (third row), Ramachandran analyses (fourth row) and alignment confidence (fifth row). The results of the different analyses are color-coded (first column).

Considering all the factors for model quality, the modelled structures of the Pb-QFR subunits are not as reliable as observed with the Pb-NQR. This should be taken into account in subsequent studies. However, the model of Pb-QFR (fig.5.6) includes three subunits, namely FrdA (red), FrdB (green) and FrdC (yellow), and six cofactors known from the *D. gigas* enzyme, which could be placed at corresponding positions into the Pb-QFR structural model. FrdA contains one covalently bound FAD, FrdB comprises three FeS clusters and FrdC harbors two hemes *b*. Since the *W. succinogenes* enzyme is the best studied QFR, the Pb-QFR structural model, based on the Dg-QFR crystallographic structure, was compared with the crystallographic structure of the Ws-QFR. Based on the structure-function studies performed with the Ws-QFR (22, 24), we asked if critical amino acid residues conserved in QFRs from *W. succinogenes* and *D. gigas* are likely to play important roles in the Pb-QFR.

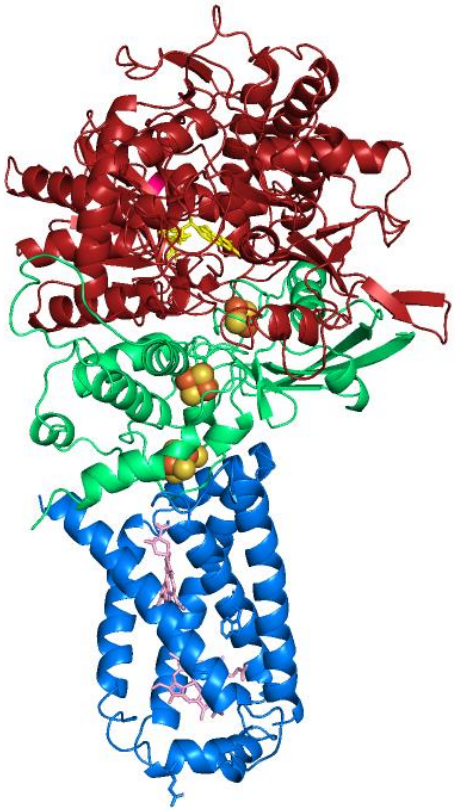

**Figure 5.6** Modelled structure of *P. bryantii* QFR. The QFR is composed of 3 subunits: FrdA (red), FrdB (green) and FrdC (blue). Cofactors were positioned according to their localization in the *D. gigas* QFR. These are one FAD in FrdA, three FeS clusters in FrdB and two hemes *b* in FrdC. Flavins are indicated as yellow sticks, iron atoms are shown as orange spheres and sulfur atoms as yellow spheres, hemes *b* are represented as pink sticks. The Pb-NQR structure was modelled with Phyre2, using the *D. gigas* crystallographic structure as template, and drawn with PyMOL version 2.5.

During fumarate respiration in *W. succinogenes*, $MKH_2$ is oxidized in a catalytic site in FrdC. The quinone binding site in Ws-QFR is suggested to be near the distal heme in FrdC, with Glu66 playing an essential role for $MKH_2$ oxidation (24) (Fig. 5.7, panel A). In the modelled Pb-FrdC, a glutamate is found in this region (Glu47) but at a position shifted by three amino acid residues (fig. 5.7, panel A). Still, the corresponding Glu47 from Pb-FrdC is predicted to be located in a cavity leading to the periplasm, as observed with Glu66 in Ws-FrdC. Glu47 is located in a putative loop region of Pb-FrdC, which exhibits only low sequence similarity to the corresponding region in the FrdC from *D. gigas*, according to the Phyre2 qualification analysis of the modelled Pb-FrdC structure (fig. 5.5). In *W. succinogenes* FrdC, Glu66 plays a crucial role in $MKH_2$ oxidation since it accepts protons from quinol and releases them to the periplasm (24). Considering the structural model of Pb-FrdC, the same function is predicted for Pb-Glu47. Electrons from $MKH_2$ are transferred to the distal heme *b*, which is coordinated by His44 and His143 in Ws-FrdC (fig. 5.7, panel B) (2). A second, proximal heme *b* in Ws-FrdC enables electron transfer from the FrdC to the FrdB subunit, facilitated by its location towards the cytoplasmic surface of the membrane and thus to the iron-sulfur clusters of Ws-FrdB. This proximal heme *b* is also coordinated by two histidines (His93, His182) (fig. 5.7, panel C) (2). The modelled Pb-FrdC structure comprises five transmembrane helices, containing these four histidines in the modelled core structure at the very same positions with the same orientations (His27 and His118 for distal heme *b*; His68 and His171 for proximal heme *b*) (fig. 5.7, panel B and C).

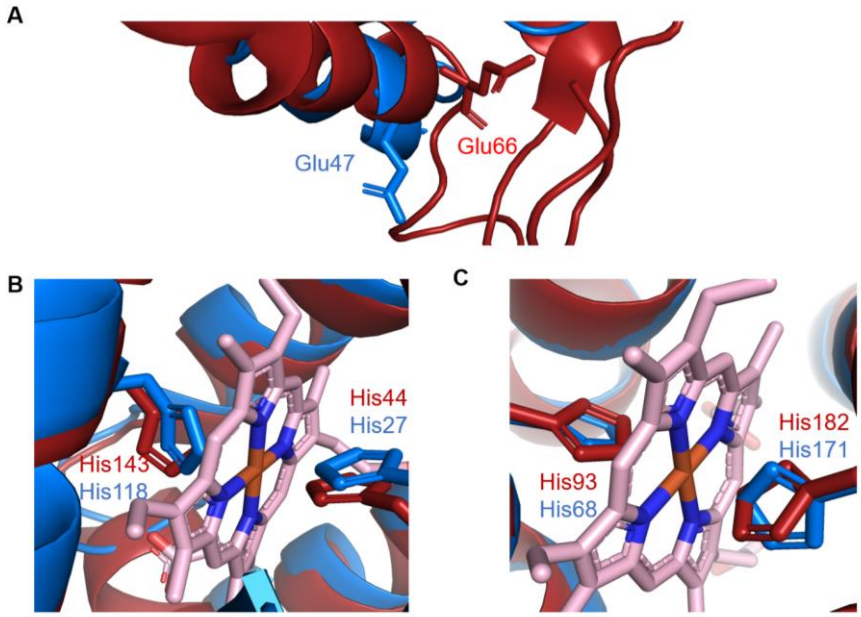


**Figure 5.7** Structural alignment of FrdC from *P. bryantii* (blue) and *W. succinogenes* (red). The Pb-QFR structural model, based on the Dg-QFR crystallographic structure, was compared with the crystallographic structure of the Ws-QFR. A: Close-up view of the menaquinol oxidation site, with Glu66 from Ws-FrdC and Glu47 from Pb-FrdC, which may be part of a proton wire towards the periplasm. B: Close-up view of distal heme *b*, coordinated by His44 and His143 in Ws-FrdC, and by His27 and His118 in Pb-FrdC. C: Coordination of proximal heme *b* in a close-up view. His93 and His182 are responsible for heme *b* coordination in Ws-FrdC. His 68 and His171 function as heme *b* ligands in Pb-FrdC. Heme *b* structures are indicated in pink. The coordinates of the Ws-FrdC structure were obtained from the protein data bank (PDB 2BS2) and the Pb-FrdC, based on the *D. gigas* crystallographic structure, was modelled with Phyre2. The structures were aligned and drawn with PyMOL version 2.5.

The electrons from $MKH_2$ are transferred through Ws-FrdB *via* three FeS clusters (fig. 5.8, panel A) (2). The [3Fe-4S] cluster, proximal to hemes *b*, is coordinated by the thiol groups of the three cysteines Cys161, Cys208 and Cys214 (fig. 5.8, panel B). These amino acid residues are located in a domain, which is in contact with the FrdC subunit. The [3Fe-4S] cluster accepts electrons from the proximal heme *b* and passes them to the [4Fe-4S], which is ligated by four cysteine residues (Cys151, Cys154, Cys157, Cys218) (fig. 5.8, panel C). Electron transfer proceeds via [2Fe-2S] cluster, located between the [4Fe-4S] cluster and the Ws-FrdA subunit. The [2Fe-2S] cluster is coordinated by four cysteine residues (Cys57, Cys62, Cys65, Cys77) (fig. 5.8, panel D). In the model of Pb-FrdB, all cysteine residues required for the coordination of the three FeS centers are present and oriented in a manner, which would permit Fe ligation by the thiol groups (fig. 5.8). Thus, it can be predicted that

Cys174, Cys219 and Cys225 are responsible for [3Fe-4S] coordination (fig. 5.8, panel B), and that Cys164, Cys167, Cys170 and Cys229 ligate the [4Fe-4S] (fig. 5.8, panel C). The [2Fe-2S] cluster is predicted to be coordinated by Cys62, Cys67, Cys70 and Cys89 (fig. 5.8, panel D).

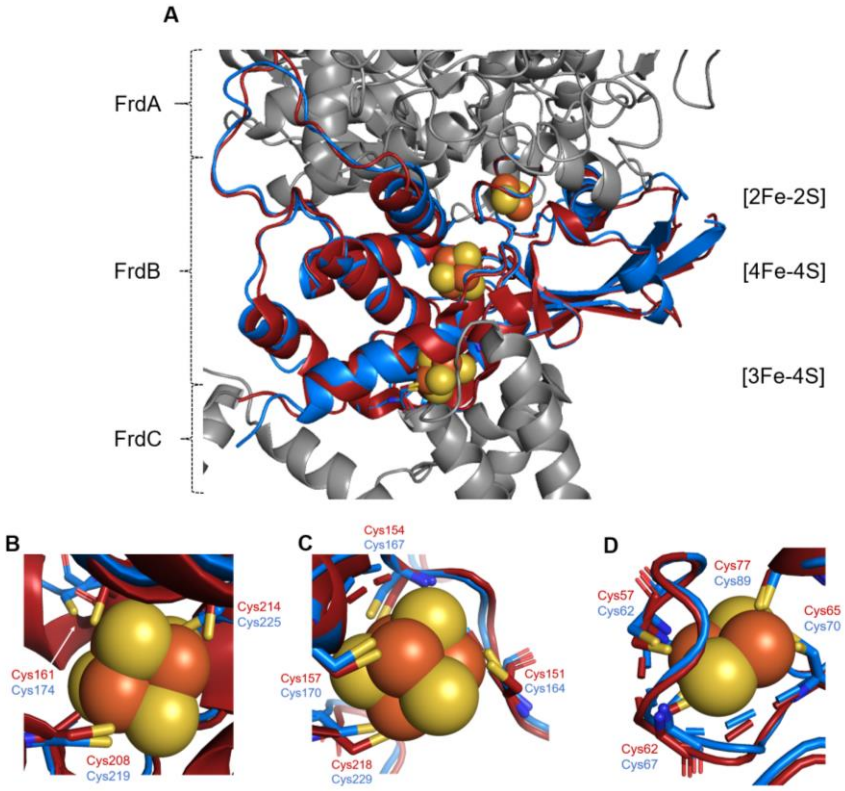


**Figure 5.8** Structural alignment of FrdB from *P. bryantii* (blue) and *W. succinogenes* (red). The Pb-QFR structural model, based on the Dg-QFR crystallographic structure, was compared with the crystallographic structure of the Ws-QFR. A: FrdB is located between FrdA and FrdC, and harbors three FeS-clusters ([3Fe-4S], [4Fe-4S], [2Fe-2S]). B: Close-up view of the [3Fe-4S] cluster. In Ws-FrdC it is coordinated by Cys161, Cys208 and Cys214. In Pb-FrdC it is predicted to be ligated by Cys174, Cys219, Cys225. C: Close-up view of the [4Fe-4S] cluster. In Ws-FrdC the residues of Cys151, Cys154, Cys157 and Cys218 are responsible for FeS ligation. In Pb-FrdC Cys164, Cys167, Cys170 and Cys229 are predicted to coordinate the FeS cluster. D: Close-up view of the [2Fe-2S] cluster with Cys57, Cys62, Cys65 and Cys77 acting as ligands in Ws-FrdC. Cys62, Cys67, Cys70 and Cys89 are predicted to coordinate the [2Fe-2S] cluster in Pb-FrdB. Fe atoms are indicated as orange spheres, sulfur atoms as yellow spheres and thiol groups of cysteines as yellow sticks. The coordinates of the Ws-FrdB structure were obtained from the protein data bank (PDB 2BS2) and the Pb-FrdB, based on the *D. gigas* crystallographic structure, was modelled with Phyre2. The structures were aligned and drawn with PyMOL version 2.5.

From Ws-FrdB, electrons are transferred to a covalently bound FAD in Ws-FrdA. This FAD is linked by its 8α-methyl group to the histidine His43 (fig. 5.9, panel A) (2). The modelled Pb-FrdB structure predicts with a high confidence also a histidine (His73) at the same position with the same orientation. The Ws-FrdA subunit also comprises a dicarboxylate-

binding site, responsible for fumarate binding and reduction. This binding site is formed mainly by the isoalloxazine ring of the FAD and four crucial amino acid residues (Phe141, Arg301, His369, Arg404) (fig. 5.9, panel B) (2). Analyzing the modelled Pb-FrdA structure, these four residues can also be observed (Phe148, Arg338, His420, Arg454) in a region with a high predicted quality (fig. 5.9, panel B).

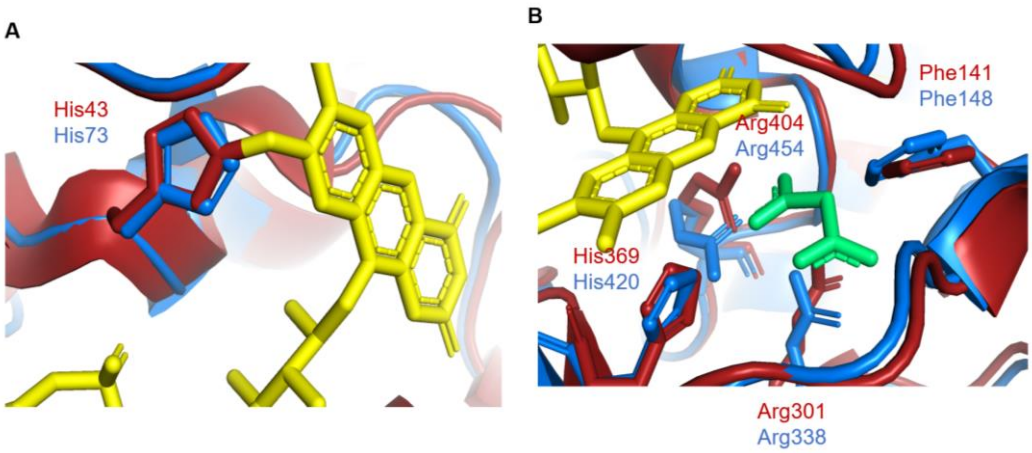


**Figure 5.9:** Structural alignment of FrdA from *P. bryantii* (blue) and *W. succinogenes* (red). The Pb-QFR structural model, based on the Dg-QFR crystallographic structure, was compared with the crystallographic structure of the Ws-QFR. A: Close-up view of FAD binding site with His43 responsible for covalent attachment of FAD in *W. succinogenes* FrdA. The corresponding His73 in the model of Pb-FrdA adopts a very similar position. B: Close-up view of the dicarboxylate- binding site, formed by Phe141, Arg301, His369 and Arg404 in Ws-FrdA, and by Phe148, Arg338, His420 and Arg454 in the model of Pb-FrdA. FAD is indicated in yellow and fumarate as a green structure. The coordinates of the Ws-FrdA structure were obtained from the protein data bank (PDB 2BS2) and the Pb-FrdA structure, based on the *D. gigas* crystallographic structure, was modelled with Phyre2. The structures were aligned and drawn with PyMOL version 2.5.

The modelled structure of Pb-QFR is in accordance with experimental data (3) confirming the existence of a *P. bryantii* QFR composed of three subunits (FrdABC), with similar catalytic functions as described for *W. succinogenes* (24-26). Although some domains of the modelled Pb-QFR structure only have a moderate quality (fig. 5.5), the structural data presented here revealed core regions for binding of cofactors and substrates with a high degree of conservation among QFRs from *D. gigas* and *W. succinogenes*. This supports the assumption that *P. bryantii* operates a quinol:fumarate reductase belonging to the type B of succinate:quinone oxidoreductases. The Pb-QFR model substantiates the biochemical studies (3) and provides a starting point for further mechanistic studies on Pb-QFR.

# 5.4 References


1. Steuber J, Vohl G, Casutt MS, Vorburger T, Diederichs K, Fritz G. 2014. Structure of the *V. cholerae* $Na^+$-pumping NADH:quinone oxidoreductase. Nature 516:62–67. doi:10.1038/nature14003.
2. Lancaster CR, Kröger A, Auer M, Michel H. 1999. Structure of fumarate reductase from *Wolinella succinogenes* at 2.2 A resolution. Nature 402:377–385. doi:10.1038/46483.
3. Schleicher L, Trautmann A, Stegmann D, Fritz G, Gätgens J, Bott M, Hein S, Simon J, Seifert J, Steuber J. 2021. A sodium-translocating module linking succinate production to formation of a membrane potential in *Prevotella bryantii*. Appl Environ Microbiol:AEM0121121. doi:10.1128/AEM.01211-21.
4. Kelley LA, Mezulis S, Yates CM, Wass MN, Sternberg MJE. 2015. The Phyre2 web portal for protein modeling, prediction and analysis. Nat Protoc 10:845–858. doi:10.1038/nprot.2015.053.
5. Eddy SR. 2004. What is a hidden Markov model? Nat Biotechnol. 22:1315–1316. doi:10.1038/nbt1004-1315.
6. Söding J. 2005. Protein homology detection by HMM-HMM comparison. Bioinformatics 21:951–960. doi:10.1093/bioinformatics/bti125.
7. Bystroff C, Krogh A. 2008. Hidden Markov Models for prediction of protein features. Methods Mol Biol 413:173–198. doi:10.1007/978-1-59745-574-9_7.
8. Ray A, Lindahl E, Wallner B. 2012. Improved model quality assessment using ProQ2. BMC Bioinformatics 13:224. doi:10.1186/1471-2105-13-224.
9. Türk K, Puhar A, Neese F, Bill E, Fritz G, Steuber J. 2004. NADH oxidation by the $Na^+$-translocating NADH:quinone oxidoreductase from *Vibrio cholerae*: functional role of the NqrF subunit. J Biol Chem 279:21349–21355. doi:10.1074/jbc.M311692200.
10. Rossmann MG, Moras D, Olsen KW. 1974. Chemical and biological evolution of nucleotide-binding protein. Nature 250:194–199. doi:10.1038/250194a0.
11. Barquera B, Häse CC, Gennis RB. 2001. Expression and mutagenesis of the NqrC subunit of the NQR respiratory $Na^+$ pump from *Vibrio cholerae* with covalently attached FMN. FEBS Lett 492:45–49. doi:10.1016/S0014-5793(01)02224-4.
12. Casutt MS, Schlosser A, Buckel W, Steuber J. 2012. The single NqrB and NqrC subunits in the $Na^+$-translocating NADH: quinone oxidoreductase ($Na^+$-NQR) from *Vibrio cholerae* each carry one covalently attached FMN. Biochim Biophys Acta. 1817:1817–1822. doi:10.1016/j.bbabio.2012.02.012.
13. Nakayama Y, Yasui M, Sugahara K, Hayashi M, Unemoto T. 2000. Covalently bound flavin in the NqrB and NqrC subunits of $Na^+$ -translocating NADH-quinone reductase from *Vibrio alginolyticus*. FEBS Lett 474:165–168. doi:10.1016/S0014-5793(00)01595-7.
14. Casutt MS, Huber T, Brunisholz R, Tao M, Fritz G, Steuber J. 2010. Localization and function of the membrane-bound riboflavin in the $Na^+$-translocating NADH:quinone oxidoreductase ($Na^+$-NQR) from *Vibrio cholerae*. J Biol Chem 285:27088–27099. doi:10.1074/jbc.M109.071126.
15. Barquera B, Zhou W, Morgan JE, Gennis RB. 2002. Riboflavin is a component of the $Na^+$-pumping NADH-quinone oxidoreductase from *Vibrio cholerae*. Proc Natl Acad Sci USA 99:10322–10324. doi:10.1073/pnas.162361299.
16. Juárez O, Nilges MJ, Gillespie P, Cotton J, Barquera B. 2008. Riboflavin is an active redox cofactor in the $Na^+$-pumping NADH: quinone oxidoreductase ($Na^+$-NQR) from *Vibrio cholerae*. J Biol Chem 283:33162–33167. doi:10.1074/jbc.M806913200.
17. Tao M, Casutt MS, Fritz G, Steuber J. 2008. Oxidant-induced formation of a neutral flavosemiquinone in the $Na^+$-translocating NADH:Quinone oxidoreductase ($Na^+$-NQR) from *Vibrio cholerae*. Biochim Biophys Acta 1777:696–702. doi:10.1016/j.bbabio.2008.04.006.
18. Casutt MS, Nedielkov R, Wendelspiess S, Vossler S, Gerken U, Murai M, Miyoshi H, Möller HM, Steuber J. 2011. Localization of ubiquinone-8 in the $Na^+$-pumping NADH:quinone oxidoreductase from *Vibrio cholerae*. J Biol Chem 286:40075–40082. doi:10.1074/jbc.M111.224980.
19. Ito T, Murai M, Ninokura S, Kitazumi Y, Mezic KG, Cress BF, Koffas MAG, Morgan JE, Barquera B, Miyoshi H. 2017. Identification of the binding sites for ubiquinone and inhibitors in the $Na^+$-pumping NADH-ubiquinone oxidoreductase from *Vibrio cholerae* by photoaffinity labeling. J Biol Chem 292:7727–7742. doi:10.1074/jbc.M117.781393.
20. Tuz K, Li C, Fang X, Raba DA, Liang P, Minh DDL, Juárez O. 2017. Identification of the catalytic ubiquinone-binding site of *Vibrio cholerae* sodium-dependent NADH dehydrogenase: A novel ubiquinone-binding motif. J Biol Chem 292:3039–3048. doi:10.1074/jbc.M116.770982.
21. Juárez O, Neehaul Y, Turk E, Chahboun N, DeMicco JM, Hellwig P, Barquera B. 2012. The role of glycine residues 140 and 141 of subunit B

in the functional ubiquinone binding site of the $Na^+$-pumping NADH:quinone oxidoreductase from *Vibrio cholerae*. J Biol Chem 287:25678–25685. doi:10.1074/jbc.M112.366088.

22. Lancaster CD. 2002. *Wolinella succinogenes* quinol:fumarate reductase—2.2-Å resolution crystal structure and the E-pathway hypothesis of coupled transmembrane proton and electron transfer. Biochim Biophys Acta 1565:215–231. doi:10.1016/S0005-2736(02)00571-0.
23. Guan H-H, Hsieh Y-C, Lin P-J, Huang Y-C, Yoshimura M, Chen L-Y, Chen S-K, Chuankhayan P, Lin C-C, Chen N-C, Nakagawa A, Chan SI, Chen C-J. 2018. Structural insights into the electron/proton transfer pathways in the quinol:fumarate reductase from *Desulfovibrio gigas*. Sci rep 8:14935. doi:10.1038/s41598-018-33193-5.
24. Lancaster CR, Gross R, Haas A, Ritter M, Mäntele W, Simon J, Kröger A. 2000. Essential role of Glu-C66 for menaquinol oxidation indicates transmembrane electrochemical potential generation by *Wolinella succinogenes* fumarate reductase. Proc Natl Acad Sci USA 97:13051–13056. doi:10.1073/pnas.220425797.
25. Lancaster CRD. 2013. The di-heme family of respiratory complex II enzymes. Biochim Biophys Acta 1827:679–687. doi:10.1016/j.bbabio.2013.02.012.
26. Lancaster CRD, Sauer US, Gross R, Haas AH, Graf J, Schwalbe H, Mäntele W, Simon J, Madej MG. 2005. Experimental support for the "E pathway hypothesis" of coupled transmembrane $e^-$ and $H^+$ transfer in dihemic quinol:fumarate reductase. Proc Natl Acad Sci USA 102:18860–18865. doi:10.1073/pnas.0509711102.

# Chapter 6 – Discussion

## 6.1 Phylogenetic distribution of QFR and NQR

Succinate:quinone oxidoreductases are divided into the four types A-D. Type A harbors two hydrophobic subunits with two hemes *b* (1). Here, succinate is oxidized and thermoplasma-quinone is reduced in the membrane. Succinate:quinone oxidoreductases belonging to type B harbor three subunits, containing two hemes *b*. This type of enzyme is known to operate in both directions with MK as electron acceptor/donor (2). Succinate:quinone oxidoreductases belonging to type C, with two membranous subunits and one heme *b* (3), also operate in both directions, but exclusively use UQ as substrate (1). Type D enzymes represent QFRs with two hydrophilic subunits, which lack heme cofactors (1, 4). The four types of succinate:quinone oxidoreductases are further divided into three functional classes, based on their quinone specificity and their *in vivo* function (5). Subclass 1 represents SQRs, oxidizing succinate and reducing high potential quinones, such as ubiquinone. QFRs couple fumarate reduction to the oxidation of a low potential quinol and belong to subclass 2. Enzymes belonging to subclass 3 represent SQRs, which oxidize succinate and reduce low potential quinones (5). Focusing on the distribution of isoprenoid quinones in the five main bacterial phyla Bacteroidetes, Proteobacteria, Chlorobi, Firmicutes and Actinobacteria, low potential quinones are the dominant quinone species in phyla with mainly obligate anaerobic members (Bacteroidetes, Chlorobi, Firmicutes, Actinobacteria) (6). Since similar primary sequences of the SQOR subunits can be observed in enzymes of archaea, eukaryotes and bacteria, it is suggested that a homolog of SQOR was present in the last universal ancestor (2). However, it should be noted that this SQR related enzyme was not necessarily catalyzing a fumarate reduction or succinate oxidation. Hägerhäll proposed two scenarios, how the two SQOR classes 1 and 2 could have been evolved out of class 3 (2). In the first scenario, the early role of the SQR related to class 3 enzyme was to catalyze the thermodynamically

unfavorable reaction of succinate oxidation and MK reduction. In the course of evolution, some organisms shifted to high potential quinones or used the enzyme in the reversed reaction for a thermodynamically more favored reaction. In the second scenario, the ancestral SQOR was not catalyzing the conversion of succinate or quinone, but rather acted as an energy coupling enzyme, e.g. a proton translocator. In the course of evolution, this early, energy-transducing enzyme lost the function in organisms acquiring enzymes related to the Complex I family. Hägerhäll and co-workers further suggested that the proton-translocating capacity of the early SQOR was retained in organisms, which do not operate a Complex I-type of enzyme. Doubtlessly, the evolution of SQORs in the bacterial kingdom is highly speculative and most likely not monophyletic (2).

We analyzed the distribution of the different SQOR types in the bacterial phyla (table 6.1). QFRs, oxidizing low potential quinols and reducing fumarate, are present in the phyla Chlorobi, Bacteroidetes, Actinobacteria and Proteobacteria. Here, the QFR is composed of three subunits and contains two hemes *b*. Among Proteobacteria, this QFR type is only present in δ- and ε-Proteobacteria classes. Bacteria from the other classes all contain UQ as dominant quinone species. Thus, SQRs oxidizing succinate and reducing high potential quinones are present in these groups. Interestingly, among the γ- Proteobacteria some groups (*Enterobacteriales, Pasteurelalles*) comprise both, UQ and MK, enabling the organism to utilize either succinate or fumarate prevalent under different environmental conditions with adequate catalytic pathways. Consequently, these organisms encode both SQR and QFR, which are expressed differentially. Typically, their QFRs are D enzymes (harboring two hydrophilic domains but no heme), oxidizing low potential quinols and reducing fumarate (2). Bacteria belonging to the Firmicutes operate SQRs, which oxidize succinate and reduce low potential quinones. In summary, different SQORs are broadly distributed through the bacterial kingdom, most likely due to their high variability in terms of substrate specificity

and energy conversion. This makes SQORs ideally suited to participate in different catabolic reactions, which are critical for aerobic and anaerobic respiration, or fermentation (7).

*Prevotella bryantii* and *Prevotella bivia* belong to the family *Prevotellaceae*, which is assigned to the phylum Bacteroidetes (8). These bacteria are obligate anaerobic bacteria and contain MK as dominant quinone species. They comprise a QFR with three subunits and two hemes *b*, which preferentially oxidizes $MKH_2$ under reduction of fumarate *in vivo*.

Unlike SQORs, the NQR is not present in archaea or eukaryotes, but is formed exclusively in the bacterial kingdom (9). The distribution among the different bacterial phyla suggests, that the NQR was not present in the last bacterial ancestor, since it occurs only in Chlorobi, Bacteroidetes and Proteobacteria (9). Notably, organisms belonging to the class of ε-Proteobacteria do not contain the *nqr* operon in their genomes. Interestingly, the NQR is evolutionary related to the electrogenic ferredoxin:$NAD^+$ oxidoreductase RNF, which catalyzes the oxidation of ferredoxin and reduction of $NAD^+$, generating a SMF or PMF (10). This catalytic property can be reversed, depending on the metabolic adaptations of the bacteria (10). The RNF comprises six subunits (RnfABCDEG), of which RnfACDEG are homologous to the NQR subunits NqrEABDC, but the electron input models of the NQR (NqrF) and RNF (RnfB) do not share significant sequence similarities with any RNF/NQR subunit (11). In contrast to the *nqr* operon, the *rnf* operon can be found in a more broad range of bacterial classes and also in the kingdom of archaea (11). Thus, it is suggested that the RNF might have been the enzymatic ancestor of the NQR. The duplication of the *rnf* operon in basal bacterial classes, and the loss of the *rnfB* gene in the duplicate triggered this evolutionary process (11). The *nqrF* gene evolved most likely from the recruitment of a new gene, which descended from the reductase subunit of an aromatic monooxygenase. This evolutionary event was accompanied by a switch in electron acceptor (from ferredoxin to NADH) and donor (from $NAD^+$ to quinone). By horizontal gene transfer events, this new *nqr* operon was spread to other bacterial lineages (11).

Taken together, only organisms of the phylum Bacteroides and Chlorobi, and members of the δ-Proteobacteria contain both, NQR and QFR (subclass 2). The interplay between QFR and NQR, as demonstrated for *P. bryantii* (12) and *P. bivia* (13) is likely to be of relevance for the anaerobic energy conservation in these phyla and classes in general. The coupling of NQR and QFR is mediated by MK, which is the main quinone found in these taxonomic groups. It seems likely that other anaerobes containing both NQR and QFR (table 6.1) also utilize both enzymes to re-oxidize NADH concomitant with the build-up of transmembrane voltage as shown for *P. bryantii* (12). This, however, awaits experimental verification in the future.

**Table 6.1** SQRs and QFRs of typical bacteria of the phyla Firmicutes, Actinobacteria, Bacteriodetes, Chlorobi and Proteobacteria. Specific growth conditions as chosen in the corresponding study cited were either aerobic or anaerobic. The proposed directionality of the enzymatic reaction (succinate oxidation, SQR; fumarate reduction, QFR) is indicated. Subunits (SU) are listed with Uniprot accession numbers and calculated molecular weights, as well as the heme content in subunits C and D, and the SQOR type (A-D classification). The dominant quinone species at the indicated growth condition is also listed. Subunits marked with "?" are present as shown by experimental data, but no hit in the Uniprot data base could be found. This could be due to erroneous annotation, or incomplete genome information. Subunits of *C. mediatlanticus* TB-2 do not have Uniport accession numbers. NCBI nomenclature is used instead. *B. subtilis, Bacillus subtilis; A. viscosus, Actinomyces viscosus; B. fragilis, Bacteroides fragilis; C. marinum, Cyclobacterium marinum; F. canadensis, Flexibacter canadensis; F. succinicans, Flavobacterium succinicans; P. bryantii, Prevotella bryantii; P. bivia, Prevotella bivia; R. marinus, Rhodothermus marinus; C. jejuni, Campylobacter jejuni; C. mediatlanticus, Caminibacter mediatlanticus; D. gigas, Desulfovibrio gigas; E. coli, Escherichia coli; G. sulfurreducens, Geobacter sulfurreducens; H. influencea, Haemophilus influencea; H. pylori, Helicobacter pylori; N. meningitidis, Neisseria meningitidis; P. aeruginosa, Pseudomonas aeruginosa; P. denitrificans, Paracoccus denitrificans; V. cholerae, Vibrio cholerae; W. succinogenes, Wolinella succinogenes.*

| phyla/organism | specific growth condition | proposed reaction *in vivo* (SQR or QFR) | SU A | SU B | SU C | SU D | number of hemes *b* | subclass | quinone type | references |
|---|---|---|---|---|---|---|---|---|---|---|
| **Firmicutes** | | | | | | | | | | |
| *B. subtilis* strain 168 | aerobic | SQR | P08065 65 kDa | P08066 28 kDa | P08064 23 kDa | - | 2 | 3 | MK | (14) |
| **Actinobacteria** | | | | | | | | | | |
| *A. viscosus* C505 | anaerobic | QFR | F2V166 75 kDa | F2V167 28 kDa | F2V165 28 kDa | - | 2 | 2 | MK | (15) |
| **Bacteriodetes** | | | | | | | | | | |
| *B. fragilis* | anaerobic | QFR | Q7X479 72 kDa | Q7X478 27 kDa | Q7X480 26 kDa | - | 2 | 2 | MK | (16) |
| *C. marinum* ATCC 25205 | aerobic | SQR | G0J4L1 72 kDa | G0J4L0 27 kDa | G0J4L2 25 kDa | - | 2 | 3 | MK | |
| *F. canadensis* ATCC 29591 | aerobic | SQR | H8KMG8 74 kDa | H8KMG7 27 kDa | H8KMG9 26 kDa | - | 2 | 3 | MK | |
| *F. succinicans* | anaerobic | QFR | A0A199XQQ8 74 kDa | A0A199XPJ3 28 kDa | A0A199XPU1 25 kDa | - | 2 | 2 | MK | (17) |
| *P. bryantii* $b_1$4 | anaerobic | QFR | D8DXM6 73 kDa | D8DXM5 28 kDa | D8DXM7 26 kDa | - | 2 | 2 | MK | (12) |
| *P. bivia* DSM 20514 | anaerobic | QFR | I4Z8D9 73 kDa | I4Z8E0 27 kDa | I4Z8D8 25 kDa | - | 2 | 2 | MK | (13) |

| | | | | | | | | | | |
|---|---|---|---|---|---|---|---|---|---|---|
| **Chlorobi** | | | | | | | | | | |
| *R. marinus* ATCC 43812 | aerobic | SQR | D0MD06 65 kDa | D0MD07 27 kDa | D0MD05 19 kDa | - | 2 | 3 | MK | (18) |
| **Proteobacteria** | | | | | | | | | | |
| *C. jejuni* ATCC 700819 | anaerobic | QFR | Q0PBA1 74 kDa | Q0PBA0 28 kDa | Q0PBA2 30 kDa | - | 2 | 2 | MK | (19) |
| *C. mediatlanticus* TB-2 | anaerobic | QFR | WP_1383 23656.1 63 kDa | WP_0074 73051 37 kDa | ? | - | 2 | 2 | MK | (20) |
| *D. gigas* ATCC 19364 | anaerobic | QFR | T2GB49 69 kDa | T2G9X8 30 kDa | T2GAT5 25 kDa | - | 2 | 2 | MK | (21) |
| *E. coli* K12 | aerobic | SQR | P0AC41 64 kDa | P07014 27 kDa | P69054 14 kDa | P0AC44 13 kDa | 1 | 1 | UQ | (22) |
| *E. coli* K12 | anaerobic | QFR | P00363 66 kDa | P0AC47 27 kDa | P0A8Q0 15 kDa | P0A8Q3 13 kDa | - | 2 | MK | (22) |
| *G. sulfurreducens* ATCC 51573 | anaerobic | QFR | Q74DY8 71 kDa | Q74DY7 28 kDa | Q74DY9 24 kDa | - | 2 | 2 | MK | (23) |
| *H. influencae* ATCC 51907 | aerobic | SQR | ? | ? | ? | ? | 1 | 1 | UQ | (24) |
| *H. influencae* ATCC 51907 | anaerobic | QFR | P44894 66 kDa | P44893 29 kDa | P44892 15 kDa | P44891 13 kDa | - | 2 | MK | (2) |
| *H. pylori* ATCC 700824 | anaerobic | QFR | Q9ZMP0 80 kDa | Q9ZMP1 28 kDa | Q9ZMN9 29 kDa | - | 2 | 2 | MK | (25) |
| *N. meningitidis* MC58 | aerobic | SQR | Q9JZP8 65 kDa | Q7DDK2 27 kDa | Q7DDK3 14 kDa | Q9JZP9 13 kDa | 1 | 1 | UQ | (26) |
| *P. aeruginosa* ATCC 15692 | aerobic | SQR | Q9I3D5 64 kDa | Q9I3D4 26 kDa | Q9I3D7 14 kDa | Q9I3D6 14 kDa | 1 | 1 | UQ | (27) |
| *P. denitrificans* | aerobic | SQR | Q59661 66 kDa | Q59662 30 kDa | Q596659 14 kDa | Q59660 14 kDa | 1 | 1 | UQ | (28) |
| *V. cholerae* M66-2 | aerobic | SQR | C3LS85 66 kDa | C3LS86 28 kDa | C3LS87 15 kDa | C3LS88 14 kDa | 1 | 1 | UQ | (29) |
| *W. succinogenes* ATCC 29543 | anaerobic | QFR | P17412 73 kDa | P17596 27 kDa | P17413 30 kDa | - | 2 | 2 | MK | (30) |

## 6.2. Energy conservation utilizing di-heme containing QFRs

In fumarate respiration, two protons are liberated by oxidation of $MKH_2$ and two protons are consumed by reduction of fumarate to succinate. The overall reaction contributes to the built-up of an electrochemical proton gradient, if protons from $MKH_2$ are released at the periplasmic aspect of the membrane. If protons liberated during oxidation of $MKH_2$ are released at the cytoplasmic side, QFR operates in electroneutral manner. For QFR of *W. succinogenes*, quinol:fumarate oxidoreduction in principle could be associated with the generation of a transmembrane electrochemical proton potential because protons are released into the periplasm, with an essential role for Glu66 acting as proton acceptor during $MKH_2$ oxidation. Glu66 is located in a cavity connected to the periplasmic aqueous phase (31). However, in *W. succinogenes* it was shown that the QFR reaction is electroneutral (32). In a counterbalanced mechanism of $H^+$ movement, two protons are transferred from the periplasm into the cytoplasm in concert with the two electrons passing from $MKH_2$ *via* the two heme groups to fumarate (fig. 6.1, panel A) (32). For *W. succinogenes* QFR, it was shown that Glu180 plays a crucial role in this transmembrane proton transport (33). Now the question rises, if the QFR of *P. bryantii* also catalyzes transmembrane proton transport from the periplasm to the cytoplasm. In Pb-QFR, protons from $MKH_2$ oxidation are likely to be released into the periplasm, considering the high degree of similarity to the Ws-QFR regarding primary sequences, and in view of the 3D structural model of Pb-QFR (fig. 5.7, Chapter 5). The question of the mode of Pb-QFR action (electroneutral *versus* electrogenic) requires experimental validation. The modelled structure of Pb-FrdC does not confirm a similar position of Glu180 in Pb-FrdC and Ws-FrdC, therefore, an obvious $H^+$ acceptor/donor identified in the E-pathway of Ws-FrdC is absent in the modelled Pb-FrdC structure (fig. 6.1, panel C). Other charged amino acid residues in Pb-FrdC could participate in a proton wire, notably Glu90 positioned at the cytoplasmic side of the transmembrane

helix. Also, proton-bound water molecules could participate in proton translocation. Furthermore, a tyrosine (Tyr41) near the distal heme and the Glu46 in Pb-FrdC are reminiscent to amino acid residues observed in the 3D structure of *Desulfovibrio gigas* FrdC (Tyr63) (21). Note that QFR of *D. gigas* is predicted to operate the E-pathway, with Tyr63 acting as initial proton acceptor (21). In Ws-FrdC, the carboxylic group of the propionate side chain of ring C from the distal heme is considered to act as proton donor/acceptor during proton transport via the E-pathway (34). In the modelled Pb-FrdC structure, the propionate side chain of the distal heme assumes a very similar position (fig. 5.7, Chapter 5). In summary, it seems feasible that Pb-QFR does not contribute to the generation of an electrochemical gradient. As a consequence, energy generation by membrane bound electron transfer complexes demonstrated for *P. bryantii* (12) is achieved in the dehydrogenase segment of the electron transport chain, for example by the $Na^+$ -translocating NADH:quinone oxidoreductase (12) as outlined in the following chapter. However, one must consider there is no counterflow of protons in Pb-QFR, as observed with the di-heme menaquinol:fumarate oxidoreductase (SQR) of *B. subtilis* (35). Interestingly, the *B. subtilis* enzyme shows a similar architecture and cofactor content as Ws-QFR, but mainly operates as succinate:menaquinone oxidoreductase. Due to the midpoint potentials of the succinate/fumarate ($E^{0'}$ = +30 mV) and the $MKH_2$/MK ($E^{0'}$ = -80 mV) redox couples, the reduction of MK by succinate is strongly endergonic ($\Delta G^{0'}$ = +21.2 kJ/mol). Thus, MK reduction by succinate needs energy input and in this case, it is driven by the proton motive force ($\Delta p$) (36). This force is defined as (equation 6.1):

$$\Delta p = \frac{\Delta \mu H^+}{F} = -\Delta\Psi + \frac{2.3\ RT}{F}\ \Delta pH \qquad (6.1)$$

Where $\Delta\mu H^+$ is the electrochemical proton gradient (kJ/mol), F the Faraday constant (95.5 kJ $V^{-1}$ $mol^{-1}$), $\Delta\Psi$ the membrane potential (V), R the gas constant (8.3 J $K^{-1}$ $mol^{-1}$), T the

absolute temperature (298 K) and ΔpH the pH difference between the cytoplasm and periplasm (37).

Thus, Δ*p* is given in voltage (V) and combines the membrane voltage and the electrochemical gradient. In bacteria, Δ*p* is approximately -160 mV, of which around -140 mV are provided by the membrane potential (38). For *B. subtilis* this Δ*p* is essential for SQR activity (36). In previous studies it was shown, that the *B. subtilis* SQR is also capable to catalyze the oxidation of $MKH_2$ and reduction of fumarate under formation of a Δ*p* with the help of the so-called redox loop in concert with a dehydrogenase (fig. 6.1, panel B) (35). In a redox loop, two respiratory enzymes work together so that the reduction reaction on the cytoplasmatic side of the energy-transducing membrane is associated with proton binding, and the oxidation reaction by the second enzyme leads to proton release at the periplasmic side. In *B. subtilis*, the SQR is predicted to operate together with a NADH dehydrogenase in a respiratory chain, coupling the generation of Δ*p* by fumarate reduction with NADH *via* oxidation/reduction of MK. MK reduction by the NADH dehydrogenase is accompanied by proton consumption, taken up from the cytoplasm. These protons are liberated at the periplasmic side upon $MKH_2$ oxidation by the SQR. Furthermore, two protons are consumed in the cytoplasm upon fumarate reduction (35, 39). It should be noted that this is some discussion, if this proposed generation of Δ*p* associated with the *B. subtilis* SQR is energetically possible *in vivo* (40). Studies performed with the related SQR of *Bacillus licheniformis* did not reveal evidence for generation of Δ*p* using the quinones DMN and 2-ethyl-3-methyl-1,4-naphthoquinone (EMN) (39), which exhibit a similar midpoint potential (approx. -40 mV) as MK (33). Quinones with a lower midpoint potential (approx. -130 mV) allowed generation of Δ*p* across the membrane *in vitro*, as expected from the large difference in oxidation/reduction potentials with regard to the succinate/fumarate couple (39). With the small oxidation/reduction potential difference of the succinate/fumarate and $MK/MKH_2$ redox couples ($\Delta E^{0'}$ = 110 mV) the reaction is under standard conditions exergonic ($\Delta G^{0'}$ =

+21.2 kJ/mol), but still theoretically not enough to translocate protons across the membrane against the transmembrane potential. With a ΔpH of -1.2 and a ΔΨ of -72 mV, which was determined for *B. licheniformis* grown under anaerobic conditions (39), 24 kJ/mol is needed to translocate a proton from the cytoplasm into the periplasm. Using a quinone with a lower midpoint potential (e.g. -130 mV), $\Delta G^{0'}$ of fumarate reduction and $QH_2$ oxidation increases to 30.5 kJ/mol. Thus, it is expected that the compensatory E-pathway is essential and present in all di-heme QFRs enzymes working with menaquinone (41).

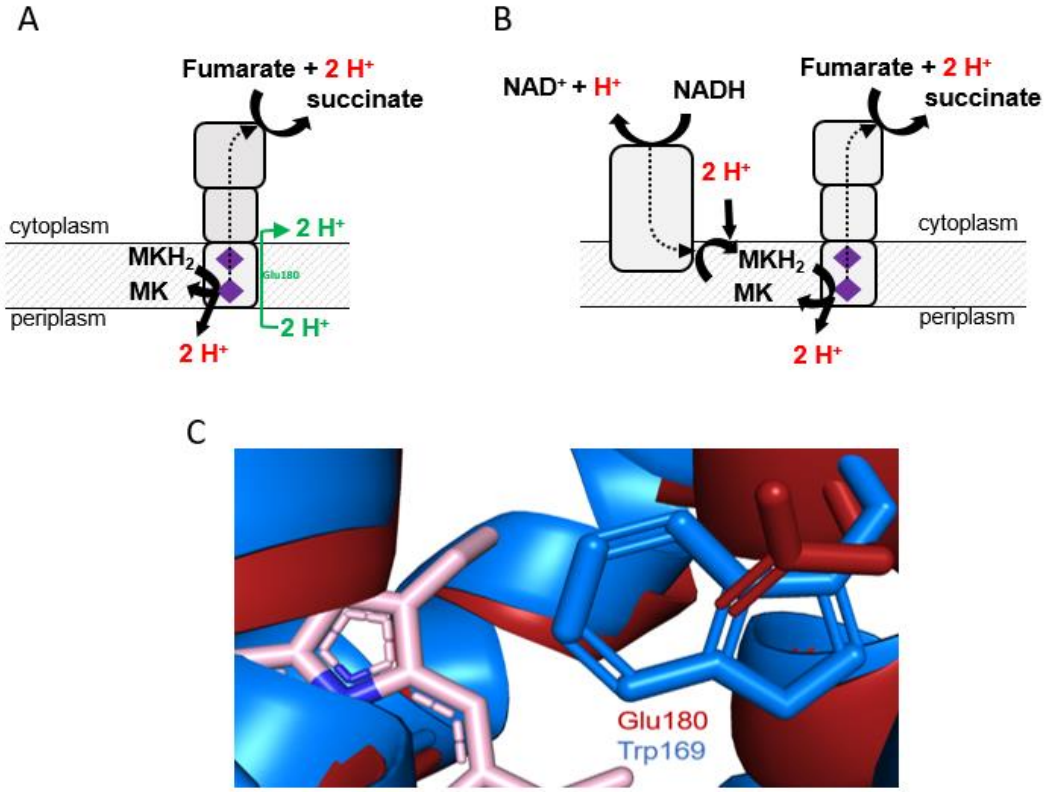


**Figure 6.1** Operation modes of quinol:fumarate oxidoreduction by di-heme containing QFRs. A: Electroneutral quinol:fumarate oxidoreduction, due to a counterbalanced proton transport from the periplasm into the cytoplasm. This so-called E-pathway is indicated in green. The inner bacterial membrane is indicated with grey stripes. Upper part represents the cytoplasm, lower part represents the periplasm. Hemes in FrdC are indicated as purple diamonds. MK, menaquinone; $MKH_2$, menaquinol. Figure was adapted from (33) B: Electrogenic quinol:fumarate oxidoreduction in *B. subtilis* by the redox loop mechanism. Figure was adapted from (35). The inner bacterial membrane is indicated with grey stripes. Upper part represents the cytoplasm, lower part represents the periplasm. Hemes in FrdC are indicated as purple diamonds. MK, menaquinone; $MKH_2$, menaquinol. C: Close-up view of the FrdC region comprising the Glu180 in *W. succinogenes* (red) and Trp169 of *P. bryantii* (blue). The coordinates of the Ws-FrdC structure were obtained from the protein data bank (PDB 2BS2) and the Pb-FrdC structure, based on the *D. gigas* crystallographic structure, was modelled with Phyre2. The structures were aligned and drawn with PyMOL version 2.5.

## 6.3. Respiratory coupling of QFR and dehydrogenases

Respiratory electron transfer chains operating a NADH dehydrogenase in the first segment and a QFR as second, terminal segment are found in many anaerobic bacteria, with *E. coli* as prominent example (42). In *E. coli*, NADH dehydrogenase I (NDH-I or Nuo) provides quinol for QFR under anaerobic growth conditions in the presence of fumarate added to the medium, or provided by endogenous reactions. Fumarate reduction is coupled to the overall generation of a PMF because NADH is oxidized by NDH-I, a primary proton pump (7). Studies with organisms of the phylum Bacteroidetes point to the existence of respiratory chains composed of NQR and QFR, although the interaction of other NADH dehydrogenases such as NDH-I and the non-electrogenic NDH-II with QFR should also be considered. For example, *Bacteroides fragilis* contains three NADH dehydrogenases (NDH-I, NDH-II, NQR), which could provide $MKH_2$ for fumarate reduction (43). Based on genome analyses, fermentative and respiratory pathways utilizing NQR and QFR in different *Prevotella* species were predicted (44). Franke and Deppenmeier (45) presented evidence for the activity of the NQR and QFR in *P. copri*. To confirm respiratory electron transfer with fumarate as terminal electron acceptor in *Prevotella* species, a detailed study combining *in vivo* and *in vitro* approaches revealed a physical interaction and efficient electron exchange of NQR and QFR in *P. bryantii* (12). This electron transfer from NADH to fumarate *via* NQR and QFR is coupled to the transport of sodium ions from the cytoplasm into the periplasm by NQR, generating a SMF (12). Notably, fumarate is formed as endogenous substrate during the fermentation of glucose by *P. bryantii*. *P bryantii* provides the basis for an additional energy-generating step, namely the reduction of fumarate by NQR plus QFR under built-up of a transmembrane potential. At the same time, $NAD^+$ is regenerated (12).

### 6.3.1 Energy conservation in *Prevotella bryantii*

*P. bryantii* ferments roughly 1 mol glucose to 1 mol acetate and 1 mol succinate (12) (fig. 6.2). Theoretically, this is accompanied with the net generation of 1 mol NADH, 3 mol ATP and 1 mol of an unknown electron carrier, acting as electron acceptor for pyruvate oxidoreductase. Based on sequence comparisons focusing on the cation-transporting c-subunits of the $F_1F_0$ ATP synthase, it was proposed that $H^+$ is the preferred coupling cation of ATP synthase from *P. bryantii* (12). The question arises how much electron transfer from NADH to fumarate will contribute to overall ATP formation in *P. bryantii* degrading glucose. The number of c-subunits in the c-ring of a given ATP synthase determines the $H^+$/ATP ration (46) of the enzyme *in vivo*. The transport mechanism of ATP synthases from *Prevotella* species has not been studied yet. For $H^+$-translocating, bacterial ATP synthases stoichiometries of 8-15 protons transported per 3 molecules of ATP synthesized were reported (46, 47). An overall $Na^+/e^-$ stoichiometry of 1:2 is assumed in the following consideration. Studying the expression levels of putative, energy generating electron transfer complexes predicted from the genome of *P. bryantii*, Schleicher and co-workers (12) presented evidence that NQR and QFR represent the major respiratory complexes in cells growing on glucose as sole carbon source. It was also demonstrated, that these respiratory complexes form a supercomplex, namely the sodium translocating NADH:fumarate oxidoreductase (SNFR) supercomplex (12). Assuming that QFR does not contribute to the built-up of $\Delta p$ (fig. 6.1, panel A), *P. bryantii* largely depends on NQR for establishing a SMF, in accord with the observed dissipation of $\Delta p$ by the $Na^+$ -selective ionophore monensin (12). The main catabolic route for glucose degradation in *P. bryantii* leads to 1 molecule succinate and 1 molecule acetate formed per molecule glucose (12) (fig. 6.2). In the course of this overall reaction, 2 molecules NADH are formed and re-oxidized. Out of these, 1 molecule of NADH is used for the final reduction step yielding succinate, which is catalyzed by a respiratory module composed of NQR and QFR. With an assumed exchange

of 2 $Na^+$ per 1 $H^+$ by antiporters (48, 49), the contribution of NQR to overall ATP formation would be moderate, with roughly 0.25 molecules ATP formed in addition to 3 molecules of ATP formed by substrate-level phosphorylation (fig. 6.2). However, the contribution of NQR will be strongly affected by the transport modes of the prevalent $Na^+/H^+$ antiporters (electrogenic *versus* electroneutral) under a given growth condition. For example, at acidic pH, electroneutral $Na^+/H^+$ antiporters working in concert with a primary $Na^+$ pump, which efficiently decreases intracellular [$Na^+$] would be advantageous for *P. bryantii* to maintain cytoplasmic pH in the neutral range.

It should be noted that the proposed pathway for glucose degradation to succinate and acetate (fig. 6.2) is incomplete when considering the overall redox balance, because the electron acceptor for pyruvate oxidation has not been identified yet. Flavodoxins and different types of FeS proteins are expected to operate in *P. bryantii* as predicted from the genome (https://bacteria.ensembl.org/Prevotella_bryantii_b14_gca_000179055/Info/Index?db=core;g=PBR_2023;r=contig_108:13080-134398;t=EFI72250; 01.12.2021). They might undergo reduction by the pyruvate oxidoreductase (UNIPROT accession number: D8DWJ0_PREBR) and deliver electrons in different redox potential ranges to other cellular compounds and proteins. Notably, *P. bryantii* harbors a RNF complex and a 11-subunit complex related to Nuo (12). The catalytic properties and function of the latter are unknown so far. The RNF complex catalyzes oxidation of ferredoxin ($E^{0'}$ = -450 to -500 mV) and reduction of $NAD^+$ ($E^{0'}$ = -320 mV) under generation of $\Delta p$ (50). In the reversed reaction, RNF catalyzes reverse electron transfer, e.g. the oxidation of NADH and reduction of ferredoxin driven by an electrochemical gradient (50). It seems unlikely that RNF works in concert with the NQR and QFR during degradation of glucose (12). Reduction of $NAD^+$ by RNF provided by the NQR was proposed by Hackmann and co-workers (44). This is not compatible with the product pattern (12) (fig. 6.2), because $NAD^+$ is required as acceptor in the initial reactions of glucose oxidation (12). Still, the re-generation of the electron acceptor

for pyruvate oxidoreduction is an important and essential step to allow for acetate production, which next to succinate is a major fermentative route (12). It is proposed that electron carriers operating in more positive redox ranges are used, such as flavodoxin (-60 mV for $Fld/Fld^-$) (51) or rubredoxin (from -100 to +200 mV) (52), which are not suitable as electron donors for the RNF operating as electrogenic pump under reduction of $NAD^+$ (-320 mV). Although it cannot be excluded that RNF contributes to the built-up of an electrochemical gradient in *P. bryantii*, this scenario is considered very unlikely during growth on glucose. Importantly, RT-qPCR studies with cells grown under these conditions revealed that the amount of NQR and QFR clearly exceeds the amount of RNF (12), in accord with a prominent role for the NQR in *P. bryantii* energy conservation (fig. 6.2). The 11-subunit complex is homologous to the NADH:quinone oxidoreductase I (NDH-I or Nuo), but it is lacking the catalytic domains for NADH oxidation (53). The 11-subunit complex is not uncommon in bacteria, but its physiological function remains unclear until now. It was suggested that this complex with several FeS centers interacts with yet unknown redox partners and contributes to the build-up of electrochemical gradients (53). It is unlikely that the 11-subunit complex plays a major role in anaerobic growth of *P. bryantii* on glucose since RT-qPCR revealed low mRNA levels when compared to NQR (12). In summary, growth of *P. bryantii* on glucose leads to succinate and acetate as major fermentative end-products. During acetate generation, pyruvate oxidoreductase delivers electrons to an unknown electron carrier under oxidative decarboxylation of pyruvate to acetyl-CoA and $CO_2$. The formation of succinate from fumarate represents the reductive branch, which is critical for the regeneration of $NAD^+$, and the NADH:fumarate oxidoreduction is catalyzed by NQR and QFR. To provide fumarate for this energy-generating redox reaction, *P. bryantii* operates PEP carboxylase, which requires $CO_2$ to form oxaloacetate. The importance of this step is reflected by the $CO_2$ dependency of *P. bryantii* growth on glucose.

This pathway of glucose degradation in *P. bryantii* reflects the ruminal environment, which is rich in starch, cellulose, hemicellulose and $CO_2$ (54). Complex polysaccharides are degraded and converted to soluble monosaccharides, volatile fatty acids or gases by several microorganisms of the ruminal microbiome (54, 55). In the rumen, *P. bryantii* is predicted to extrude mainly acetate and succinate as fermentative end-products, which are metabolized by other organisms to propionate. Acetate and propionate are nutrients for the host (56), since the uptake of glucose from the gastrointestinal tract of the ruminant is limited (56, 57). Propionate is an important nutrient for the ruminant since it enters the pathway of gluconeogenesis, yielding glucose. However, propionate may also be degraded by ruminal bacteria specialized in decarboxylation phosphorylation (chapter 1.3.4) (58).

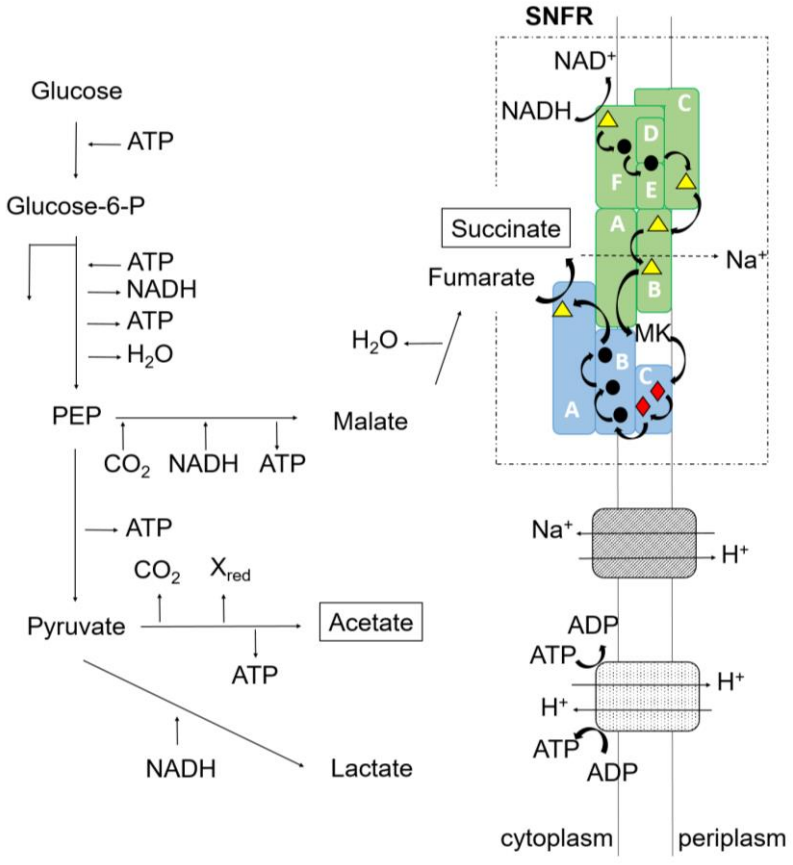


**Figure 6.2** The SNFR supercomplex represents the major charge-separating module in *P. bryantii*. Major end products are shown in black boxes. Blue, fumarate reductase (QFR); green, $Na^+$-translocating NADH:quinone oxidoreductase (NQR); hatching, $Na^+/H^+$ antiporter; stippling, $F_1F_o$ ATPase/ATP synthase. Subunits of NQR (lettered A to F) and QFR (lettered A to C) are indicated. Colored symbols in the protein complexes represent cofactors. Yellow triangle, flavin; black circle, iron-sulfur center; red diamond, heme b. NQR and QFR form a sodium-translocating NADH:fumarate oxidoreductase (SNFR) supercomplex (dashed box) (12).

### 6.3.2 Energy conservation in *Prevotella bivia*

*Prevotella bivia* is an inhabitant of the human vaginal milieu and it is involved in bacterial vaginosis, the most commonly reported syndrome among women in reproductive age (59, 60). Like *P. bryantii*, *P. bivia* harbors a QFR and NQR as major respiratory enzymes in its membrane (13). Besides succinate and acetate, high amounts of malate are extruded during anaerobic growth on glucose (13). *P. bivia* converts 1.5 mol glucose into 1 mol acetate, 1 mol malate and 1 mol succinate (fig. 6.3, panel A). This is accompanied with the formation of 4 mol ATP, 1 mol $CO_2$ and 1 mol unknown reduced electron carrier (13). The reduction of fumarate under oxidation of NADH by QFR and NQR contributes to the overall energetic yield, since NQR in *P. bivia* generates a SMF (13). Next to NQR, *P. bivia* harbors the 11-subunit complex (Nuo homolog) but no RNF. This is in marked contrast to *P. bryantii*. Unlike *P. bryantii, P. bivia* contains the cytochrome *bd* quinol oxidase (13). This quinol oxidase does not act as a proton pump (61) but it would be beneficial for *P. bivia*. *P. bivia* colonizes the microaerophilic vaginal milieu, where small amounts of oxygen are present. This was shown before for the strict anaerobic *Bacteroides fragilis* (62). Furthermore, *P. bivia* operates a superoxide dismutase, disproportionating two molecules of superoxide ($O_2^-$) to one molecule $O_2$ and one molecule $H_2O_2$, which is a typical by-product of aerobic metabolism (63).

Next to glycolysis, amino acid degradation leads to endogenous fumarate production in *P. bivia*. L-asparagine and L-aspartate are catabolized by the enzymes L-asparaginase and aspartate ammonia lyase to fumarate and $NH_3$ (13). This is especially important during a BV infection, which is caused by a biofilm community adherent to the vaginal epithelium cells (64). Here, the healthy *Lactobacillus* microbiome is replaced by a community of anaerobes, dominated by *Gardnerella vaginalis* and *P. bivia*. It is suggested that cross-feeding between these two species occurs, which supports BV development and severity of the infection. *P. bivia* releases ammonium during growth, which is utilized by *G. vaginalis* for amino acid

synthesis. Simultaneously, *G. vaginalis* produces L-asparagine and L-aspartate as sole amino acids (65). Growth of *P. bivia* is inhibited by ammonia in the low millimolar range (13), but high turnover of L-asparagine under formation of fumarate and ammonia is possible in a consortium with *G. vaginalis*. This is advantageous for *P. bivia* since fumarate acts as electron sink, recovering $NAD^+$ required for the initial step of glycolysis. The ability of *P. bivia* to recover fumarate from amino acids is beneficial for itself and for *G. vaginalis*. Ammonia released in this process will also increase the pH. In summary, *P. bivia* facilitates colonization of vaginal epithelia at an early stage of BV, hereby promoting biofilm formation, suppressing colonization by *Lactobacilli*, enhancing proteolysis of the vaginal mucus layer and increasing pH (fig. 6.3, panel B).

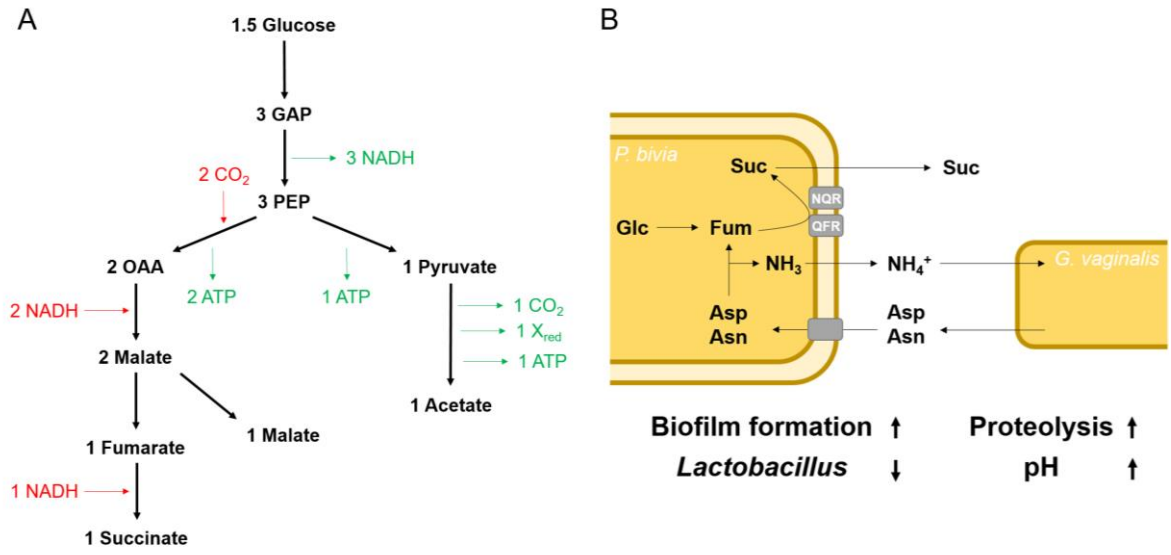


**Figure 6.3** Energy conversion in *P. bivia*. A: Flow of intermediates in the central carbon metabolism of *P. bivia*. It is assumed here that 1.5 mol glucose is converted into 1 mol succinate, 1 mol malate and 1 mol acetate. GAP, glycerinaldehyde; PEP, phosphoenolpyruvate; OAA, oxaloacetate; $X_{red}$, reduced (unknown) electron carrier. B: Overview of energy conservation in *P. bivia* and its interplay with *Gardnerella vaginalis*. Glc, glucose; Fum, fumarate; Suc, succinate; Asn, asparagine: Asp, aspartate.

## 6.4 *Prevotella* spp. as potential pathogens

Although *Prevotella* spp. have been implicated in local and systemic infections, a causative role has rarely been confirmed. Only in few cases, the phenotype of human disease was observed in animal models (153). *Prevotella* spp. associated diseases are often accompanied with microbial imbalance and dysbiosis, and an upregulated inflammatory response. As Gram-negative bacterium, *Prevotella* spp. possesses lipopolysaccharides (LPS), which are the major components of the outer membrane and cover more than 90% of the cell surface (223). LPS are considered as endotoxins, because they are recognized by the host immune system as "pathogen associated molecular patterns" (PAMP), inducing an inflammatory response. Notably, LPS activates mononuclear phagocytes, resulting in an increased phagocytic activity, secretion of pro-inflammatory cytokines (TNF-α, IL-6, interferon-β) and the synthesis of pro-inflammatory proteins (224, 225). In general, the activation of these phagocytes is important to fight invading pathogens. Nevertheless, a prolonged and uncontrolled activation and a resulting systemic and prolonged immune system response can have fatal consequences for the host. An endotoxic shock can lead to death, due to endothelial damage, loss of vascular tone and organ failure. Previous studies demonstrated, that *P. bivia* produces high amounts of LPS (~ 11000 EU/mL) and that the abundance of *P. bivia* in BV patients correlates positively with the LPS level in their vaginal fluid (160). Thus, LPS might represent one virulence factor of *Prevotella* spp. Interestingly, some *Prevotella* strains produce outer membrane vesicles (OMVs). OMVs are nanometer-sized, spherical proteoliposomes formed by the outer membrane of Gram-negative bacteria during bacterial growth (226). They are composed of a phospholipid bilayer with an outer layer of LPS, outer membrane proteins and receptors (227). Specific components may be selectively enriched or depleted from OMVs, indicating a highly regulated secretion mechanism (227–229). Thus, OMVs contribute to pathogenesis by release of LPS into the environment, or

even by carrying virulence factors, such as toxins or adhesins (230, 228). Furthermore, OMVs have an effect on microbial interactions e.g. by promoting nutrient acquisition in bacterial communities (231). Several studies demonstrated that *Prevotella* spp. produce OMVs *in vivo* and *in vitro* (232, 233). Isolated OMVs from *P. melaninogenica*, involved in lung fibrosis, were able to induce cytokine expression and to constantly promote the development of TH17 cells in mouse lungs (233). This strong, persisting immune response was shown to promote pulmonary fibrosis.

In the case of BV, it would be very interesting to investigate, if *P. bivia* does produce OMVs. If so, further investigation on these OMVs would be beneficial to understand BV development. Do these OMVs contain elevated LPS levels and do they promote an inflammatory immune response? Furthermore, the influence of OMVs on the BV microbiome could be investigated. Do these OMVs promote biofilm formation and do they facilitate nutrient acquisition for other BV associated bacteria, such as *G. vaginalis*? Answering these questions would not only help to understand and treat BV, this knowledge could also be applied to other *Prevotella* associated infections.

## 6.5 References


1. Hägerhäll C, Hederstedt L. 1996. A structural model for the membrane-integral domain of succinate:quinone oxidoreductases. FEBS Lett 389:25–31. doi:10.1016/0014-5793(96)00529-7.
2. Hägerhäll C. 1997. Succinate: quinone oxidoreductases. variations on a conserved theme. Biochim Biophys Acta 1320:107–141. doi:10.1016/s0005-2728(97)00019-4.
3. Yankovskaya V, Horsefield R, Törnroth S, Luna-Chavez C, Miyoshi H, Léger C, Byrne B, Cecchini G, Iwata S. 2003. Architecture of succinate dehydrogenase and reactive oxygen species generation. Science 299:700–704. doi:10.1126/science.1079605.
4. Iverson TM, Luna-Chavez C, Cecchini G, Rees DC. 1999. Structure of the *Escherichia coli* fumarate reductase respiratory complex. Science 284:1961–1966. doi:10.1126/science.284.5422.1961.
5. Lancaster CRD. 2004. Respiratory chain Complex II and succinate:quinone oxidoreductases. *In* Lancaster CD (ed), Respiratory chain Complex II and succinate:quinone oxidoreductases, 3rd ed. Elsevier.
6. Collins MD, Jones D. 1981. Distribution of isoprenoid quinone structural types in bacteria and their taxonomic implication. Microbiol Rev 45:316–354.
7. Unden G, Dünnwald P. 2008. The aerobic and anaerobic respiratory chain of *Escherichia coli* and *Salmonella enterica*: enzymes and energetics. EcoSal Plus 3. doi:10.1128/ecosalplus.3.2.2.
8. Avgustin G, Wallace RJ, Flint HJ. 1997. Phenotypic diversity among ruminal isolates of *Prevotella ruminicol*: proposal of *Prevotella brevis* sp. nov., *Prevotella bryantii* sp. nov., and *Prevotella albensis* sp. nov. and redefinition of *Prevotella ruminicola*. Int J Syst Bacteriol. 47:284–288. doi:10.1099/00207713-47-2-284.
9. Reedy CJ, Gibney BR. 2004. Heme protein assemblies. Chem Rev. 104:617–649. doi:10.1021/cr0206115.
10. Biegel E, Schmidt S, González JM, Müller V. 2011. Biochemistry, evolution and physiological

function of the Rnf complex, a novel ion-motive electron transport complex in prokaryotes. Cell Mol Life Sci. 68:613–634. doi:10.1007/s00018-010-0555-8.

11. Reyes-Prieto A, Barquera B, Juárez O. 2014. Origin and evolution of the sodium -pumping NADH: ubiquinone oxidoreductase. PLoS One 9:e96696. doi:10.1371/journal.pone.0096696.
12. Schleicher L, Trautmann A, Stegmann D, Fritz G, Gätgens J, Bott M, Hein S, Simon J, Seifert J, Steuber J. 2021. A sodium-translocating module linking succinate production to formation of a membrane potential in *Prevotella bryantii*. Appl Environ Microbiol:AEM0121121. doi:10.1128/AEM.01211-21.
13. Schleicher L, Herdan S, Fritz G, Trautmann A, Seifert J, Steuber J. 2021. Central carbon metabolism, sodium-motive electron transfer, and ammonium formation by the vaginal pathogen *Prevotella bivia*. Int J Mol Sci 22:11925. doi:10.3390/ijms222111925.
14. Hägerhäll C, Aasa R, Wachenfeldt C von, Hederstedt L. 1992. Two hemes in *Bacillus subtilis* succinate:menaquinone oxidoreductase (complex II). Biochemistry 31:7411–7421. doi:10.1021/bi00147a028.
15. Takahashi N, Kalfas S, Yamada T. 1994. The role of the succinate pathway in sorbitol fermentation by oral *Actinomyces viscosus* and *Actinomyces naeslundii*. Oral Microbiol Immunol 9:218–223. doi:10.1111/j.1399-302x.1994.tb00061.x.
16. Baughn AD, Malamy MH. 2003. The essential role of fumarate reductase in haem-dependent growth stimulation of *Bacteroides fragilis*. Microbiology 149:1551–1558. doi:10.1099/mic.0.26247-0.
17. Callies E, Mannheim W. 1978. Classification of the Flavobacterium-Cytophaga complex on the basis of respiratory quinones and fumarate respiration. Int J Sys Evol Microbiol 28:14–19. doi:10.1099/00207713-28-1-14.
18. Fernandes AS, Pereira MM, Teixeira M. 2001. The succinate dehydrogenase from the thermohalophilic bacterium *Rhodothermus marinus*: redox-Bohr effect on heme $b_L$. J Bioenerg Biomembr 33:343–352. doi:10.1023/a:1010663424846.
19. Weingarten RA, Taveirne ME, Olson JW. 2009. The dual-functioning fumarate reductase is the sole succinate:quinone reductase in *Campylobacter jejuni* and is required for full host colonization. J Bacteriol 191:5293–5300. doi:10.1128/JB.00166-09.
20. Vetriani C, Voordeckers JW, Crespo-Medina M, O'Brien CE, Giovannelli D, Lutz RA. 2014. Deep-sea hydrothermal vent Epsilonproteobacteria encode a conserved and widespread nitrate reduction pathway (Nap). ISME J 8:1510–1521. doi:10.1038/ismej.2013.246.
21. Guan H-H, Hsieh Y-C, Lin P-J, Huang Y-C, Yoshimura M, Chen L-Y, Chen S-K, Chuankhayan P, Lin C-C, Chen N-C, Nakagawa A, Chan SI, Chen C-J. 2018. Structural insights into the electron/proton transfer pathways in the quinol:fumarate reductase from *Desulfovibrio gigas*. Sci rep 8:14935. doi:10.1038/s41598-018-33193-5.
22. Cecchini G, Schröder I, Gunsalus RP, Maklashina E. 2002. Succinate dehydrogenase and fumarate reductase from *Escherichia coli*. Biochim Biophys Acta 1553:140–157. doi:10.1016/s0005-2728(01)00238-9.
23. Butler JE, Glaven RH, Esteve-Núñez A, Núñez C, Shelobolina ES, Bond DR, Lovley DR. 2006. Genetic characterization of a single bifunctional enzyme for fumarate reduction and succinate oxidation in *Geobacter sulfurreducens* and engineering of fumarate reduction in *Geobacter metallireducens*. J Bacteriol 188:450–455. doi:10.1128/JB.188.2.450-455.2006.
24. Othman DSMP, Schirra H, McEwan AG, Kappler U. 2014. Metabolic versatility in *Haemophilus influenzae*: a metabolomic and genomic analysis. Front Microbiol 5:69. doi:10.3389/fmicb.2014.00069.
25. Ge Z, Feng Y, Dangler CA, Xu S, Taylor NS, Fox JG. 2000. Fumarate reductase is essential for *Helicobacter pylori* colonization of the mouse stomach. Microb Pathog 29:279–287. doi:10.1006/mpat.2000.0391.
26. Clark VL, Campbell LA, Palermo DA, Evans TM, Klimpel KW. 1987. Induction and repression of outer membrane proteins by anaerobic growth of *Neisseria gonorrhoeae*. Infect Immun 55:1359–1364. doi:10.1128/iai.55.6.1359-1364.1987.
27. Liang P, Fang X, Hu Y, Yuan M, Raba DA, Ding J, Bunn DC, Sanjana K, Yang J, Rosas-Lemus M, Häse CC, Tuz K, Juárez O. 2020. The aerobic respiratory chain of *Pseudomonas aeruginosa* cultured in artificial urine media: Role of NQR and terminal oxidases. PLoS One 15:e0231965. doi:10.1371/journal.pone.0231965.
28. Hederstedt L. 2002. Succinate:quinone oxidoreductase in the bacteria *Paracoccus denitrificans* and *Bacillus subtilis*. Biochim Biophys Acta 1553:74–83. doi:10.1016/s0005-2728(01)00231-6.
29. Bueno E, Pinedo V, Cava F. 2020. Adaptation of *Vibrio cholerae* to hypoxic environments. Front Microbiol 11:739. doi:10.3389/fmicb.2020.00739.
30. Lancaster CR, Kröger A, Auer M, Michel H. 1999. Structure of fumarate reductase from *Wolinella succinogenes* at 2.2 A resolution. Nature 402:377–385. doi:10.1038/46483.
31. Lancaster CRD, Sauer US, Gross R, Haas AH, Graf J, Schwalbe H, Mäntele W, Simon J, Madej MG. 2005. Experimental support for the "E pathway hypothesis" of coupled transmembrane $e^-$ and $H^+$ transfer in dihemic quinol:fumarate reductase. Proc Natl Acad Sci USA 102:18860–18865. doi:10.1073/pnas.0509711102.
32. Kröger A, Biel S, Simon J, Gross R, Unden G, Lancaster CD. 2002. Fumarate respiration of *Wolinella succinogenes*: enzymology, energetics and coupling mechanism. Biochim Biophys Acta 1553:23–38. doi:10.1016/S0005-2728(01)00234-1.
33. Madej MG, Nasiri HR, Hilgendorff NS, Schwalbe H, Lancaster CRD. 2006. Evidence for transmembrane proton transfer in a dihaem-containing membrane protein complex. EMBO J 25:4963–4970. doi:10.1038/sj.emboj.7601361.
34. Lancaster CR, Gross R, Haas A, Ritter M, Mäntele W, Simon J, Kröger A. 2000. Essential role of

Glu-C66 for menaquinol oxidation indicates transmembrane electrochemical potential generation by *Wolinella succinogenes* fumarate reductase. Proc Natl Acad Sci USA 97:13051–13056. doi:10.1073/pnas.220425797.

35. Schnorpfeil M, Janausch IG, Biel S, Kröger A, Unden G. 2001. Generation of a proton potential by succinate dehydrogenase of *Bacillus subtilis* functioning as a fumarate reductase. Eur J Biochem 268:3069–3074. doi:10.1046/j.1432-1327.2001.02202.x.
36. Schirawski J, Unden G. 1998. Menaquinone-dependent succinate dehydrogenase of bacteria catalyzes reversed electron transport driven by the proton potential. Eur J Biochem 257:210–215. doi:10.1046/j.1432-1327.1998.2570210.x.
37. Muras V, Toulouse C, Fritz G, Steuber J. 2019. Respiratory Membrane Protein Complexes Convert Chemical Energy. Subcell Biochem 92:301–335. doi:10.1007/978-3-030-18768-2_10.
38. Tran QH, Unden G. 1998. Changes in the proton potential and the cellular energetics of *Escherichia coli* during growth by aerobic and anaerobic respiration or by fermentation. Eur J Biochem 251:538–543. doi:10.1046/j.1432-1327.1998.2510538.x.
39. Madej MG, Nasiri HR, Hilgendorff NS, Schwalbe H, Unden G, Lancaster CRD. 2006. Experimental evidence for proton motive force-dependent catalysis by the diheme-containing succinate:menaquinone oxidoreductase from the Gram-positive bacterium *Bacillus licheniformis*. Biochemistry 45:15049–15055. doi:10.1021/bi0618161.
40. Azarkina N, Konstantinov AA. 2002. Stimulation of menaquinone-dependent electron transfer in the respiratory chain of *Bacillus subtilis* by membrane energization. J Bacteriol 184:5339–5347. doi:10.1128/JB.184.19.5339-5347.2002.
41. Lancaster CRD. 2013. The di-heme family of respiratory complex II enzymes. Biochim Biophys Acta 1827:679–687. doi:10.1016/j.bbabio.2013.02.012.
42. Tran QH, Bongaerts J, Vlad D, Unden G. 1997. Requirement for the proton-pumping NADH dehydrogenase I of *Escherichia coli* in respiration of NADH to fumarate and its bioenergetic implications. Eur J Biochem 244:155–160. doi:10.1111/j.1432-1033.1997.00155.x.
43. Ito T, Gallegos R, Matano LM, Butler NL, Hantman N, Kaili M, Coyne MJ, Comstock LE, Malamy MH, Barquera B. 2020. Genetic and biochemical analysis of anaerobic respiration in *Bacteroides fragilis* and its importance *in vivo*. mBio 11. doi:10.1128/mBio.03238-19.
44. Hackmann TJ, Ngugi DK, Firkins JL, Tao J. 2017. Genomes of rumen bacteria encode atypical pathways for fermenting hexoses to short-chain fatty acids. Environ Microbiol. 19:4670–4683. doi:10.1111/1462-2920.13929.
45. Franke T, Deppenmeier U. 2018. Physiology and central carbon metabolism of the gut bacterium *Prevotella copri*. Mol microbiol. 109:528–540. doi:10.1111/mmi.14058.
46. Meier T, Faraldo-Gómez JD, Börsch M. 2011. ATP Synthase – a paradigmatic molecular machine, p. 208–238. *In* Frank J (ed), Molecular Machines in Biology. Cambridge University Press, Cambridge.
47. Pogoryelov D, Klyszejko AL, Krasnoselska GO, Heller E-M, Leone V, Langer JD, Vonck J, Müller DJ, Faraldo-Gómez JD, Meier T. 2012. Engineering rotor ring stoichiometries in the ATP synthase. Proc Natl Acad Sci USA 109:E1599-608. doi:10.1073/pnas.1120027109.
48. Taglicht D, Padan E, Schuldiner S. 1993. Proton-sodium stoichiometry of NhaA, an electrogenic antiporter from *Escherichia coli*. J Biol Chem 268:5382–5387.
49. Padan E, Venturi M, Gerchman Y, Dover N. 2001. $Na^+/H^+$ antiporters. Biochim Biophys Acta 1505:144–157. doi:10.1016/S0005-2728(00)00284-X.
50. Kuhns M, Trifunović D, Huber H, Müller V. 2020. The Rnf complex is a $Na^+$ coupled respiratory enzyme in a fermenting bacterium, *Thermotoga maritima*. Commun Biol. 3:431. doi:10.1038/s42003-020-01158-y.
51. Chowdhury NP, Klomann K, Seubert A, Buckel W. 2016. Reduction of flavodoxin by electron bifurcation and sodium ion-dependent reoxidation by $NAD^+$ catalyzed by ferredoxin-$NAD^+$ reductase (Rnf). J Biol Chem 291:11993–12002. doi:10.1074/jbc.M116.726299.
52. Meyer J. 2008. Iron-sulfur protein folds, iron-sulfur chemistry, and evolution. J Biol Inorg Chem. 13:157–170. doi:10.1007/s00775-007-0318-7.
53. Moparthi VK, Hägerhäll C. 2011. The evolution of respiratory chain complex I from a smaller last common ancestor consisting of 11 protein subunits. J Mol Evol. 72:484–497. doi:10.1007/s00239-011-9447-2.
54. White BA, Lamed R, Bayer EA, Flint HJ. 2014. Biomass utilization by gut microbiomes. Annu Rev Microbiol 68:279–296. doi:10.1146/annurev-micro-092412-155618.
55. Matthews C, Crispie F, Lewis E, Reid M, O'Toole PW, Cotter PD. 2019. The rumen microbiome: a crucial consideration when optimising milk and meat production and nitrogen utilisation efficiency. Gut Microbes 10:115–132. doi:10.1080/19490976.2018.1505176.
56. Yost WM, Young JW, Schmidt SP, McGilliard AD. 1977. Gluconeogenesis in ruminants: propionic acid production from a high-grain diet fed to cattle. J Nutr 107:2036–2043. doi:10.1093/jn/107.11.2036.
57. McAllan AB, Smith RH. 1974. Carbohydrate metabolism in the ruminant. Bacterial carbohydrates formed in the rumen and their contribution to digesta entering the duodenum. Br J Nutr 31:77–88. doi:10.1079/BJN19740010.
58. Dimroth P, Schink B. 1998. Energy conservation in the decarboxylation of dicarboxylic acids by fermenting bacteria. Arch Microbiol 170:69–77. doi:10.1007/s002030050616.
59. Gilbert NM, Lewis WG, Li G, Sojka DK, Lubin JB, Lewis AL. 2019. *Gardnerella vaginalis* and *Prevotella bivia* trigger distinct and overlapping phenotypes in a mouse model of bacterial vaginosis. J Infect Dis 220:1099–1108. doi:10.1093/infdis/jiy704.
60. Randis TM, Ratner AJ. 2019. *Gardnerella* and *Prevotella*: co-conspirators in the pathogenesis of

bacterial vaginosis. J Infect Dis 220:1085–1088. doi:10.1093/infdis/jiy705.
61. Miller MJ, Gennis RB. 1985. The cytochrome *d* complex is a coupling site in the aerobic respiratory chain of *Escherichia coli*. J Biol Chem 260:14003–14008. doi:10.1016/S0021-9258(17)38675-1.
62. Baughn AD, Malamy MH. 2004. The strict anaerobe *Bacteroides fragilis* grows in and benefits from nanomolar concentrations of oxygen. Nature 427:441–444. doi:10.1038/nature02285.
63. Schleicher L, Fritz G, Seifert J, Steuber J. 2020. Anoxic cell rupture of *Prevotella bryantii* by high-pressure homogenization protects the $Na^+$-translocating NADH:quinone oxidoreductase from oxidative damage. Arch Microbiol 202:1263–1266. doi:10.1007/s00203-019-01805-x.
64. Schwebke JR, Muzny CA, Josey WE. 2014. Role of *Gardnerella vaginalis* in the pathogenesis of bacterial vaginosis: a conceptual model. J Infect Dis 210:338–343. doi:10.1093/infdis/jiu089.
65. Harwich MD, Alves JM, Buck GA, Strauss JF, Patterson JL, Oki AT, Girerd PH, Jefferson KK. 2010. Drawing the line between commensal and pathogenic *Gardnerella vaginalis* through genome analysis and virulence studies. BMC Genomics 11:375. doi:10.1186/1471-2164-11-375.
66. Tett A, Pasolli E, Masetti G, Ercolini D, Segata N. 2021. *Prevotella* diversity, niches and interactions with the human host. Nat Rev Microbiol 19:585–599. doi:10.1038/s41579-021-00559-y.
67. Rosenfeld Y, Shai Y. 2006. Lipopolysaccharide (Endotoxin)-host defense antibacterial peptides interactions: role in bacterial resistance and prevention of sepsis. Biochim Biophys Acta 1758:1513–1522. doi:10.1016/j.bbamem.2006.05.017.
68. Dobrovolskaia MA, Vogel SN. 2002. Toll receptors, CD14, and macrophage activation and deactivation by LPS. Microbes Infect 4:903–914. doi:10.1016/s1286-4579(02)01613-1.
69. Rietschel ET, Brade H, Holst O, Brade L, Müller-Loennies S, Mamat U, Zähringer U, Beckmann F, Seydel U, Brandenburg K, Ulmer AJ, Mattern T, Heine H, Schletter J, Loppnow H, Schönbeck U, Flad HD, Hauschildt S, Schade UF, Di Padova F, Kusumoto S, Schumann RR. 1996. Bacterial endotoxin: Chemical constitution, biological recognition, host response, and immunological detoxification. Curr Top Microbiol Immunol 216:39–81. doi:10.1007/978-3-642-80186-0_3.
70. Aroutcheva A, Ling Z, Faro S. 2008. *Prevotella bivia* as a source of lipopolysaccharide in the vagina. Anaerobe 14:256–260. doi:10.1016/j.anaerobe.2008.08.002.
71. Schwechheimer C, Kuehn MJ. 2015. Outer-membrane vesicles from Gram-negative bacteria: biogenesis and functions. Nat Rev Microbiol 13:605–619. doi:10.1038/nrmicro3525.
72. Zingl FG, Kohl P, Cakar F, Leitner DR, Mitterer F, Bonnington KE, Rechberger GN, Kuehn MJ, Guan Z, Reidl J, Schild S. 2020. Outer membrane vesiculation facilitates surface exchange and *in vivo* adaptation of *Vibrio cholerae*. Cell Host Microbe 27:225-237.e8. doi:10.1016/j.chom.2019.12.002.
73. Veith PD, Chen Y-Y, Gorasia DG, Chen D, Glew MD, O'Brien-Simpson NM, Cecil JD, Holden JA, Reynolds EC. 2014. *Porphyromonas gingivalis* outer membrane vesicles exclusively contain outer membrane and periplasmic proteins and carry a cargo enriched with virulence factors. J Proteome Res 13:2420–2432. doi:10.1021/pr401227e.
74. Friedrich V, Gruber C, Nimeth I, Pabinger S, Sekot G, Posch G, Altmann F, Messner P, Andrukhov O, Schäffer C. 2015. Outer membrane vesicles of *Tannerella forsythia*: biogenesis, composition, and virulence. Mol Oral Microbiol 30:451–473. doi:10.1111/omi.12104.
75. Olofsson A, Vallström A, Petzold K, Tegtmeyer N, Schleucher J, Carlsson S, Haas R, Backert S, Wai SN, Gröbner G, Arnqvist A. 2010. Biochemical and functional characterization of *Helicobacter pylori* vesicles. Mol microbiol. 77:1539–1555. doi:10.1111/j.1365-2958.2010.07307.x.
76. Cecil JD, Sirisaengtaksin N, O'Brien-Simpson NM, Krachler AM. 2019. Outer membrane vesicle-host cell interactions. Microbiol Spectr 7. doi:10.1128/microbiolspec.PSIB-0001-2018.
77. Han P, Bartold PM, Salomon C, Ivanovski S. 2021. Salivary outer membrane vesicles and DNA methylation of small extracellular vesicles as biomarkers for periodontal status: a pilot study. Int J Mol Sci 22. doi:10.3390/ijms22052423.
78. Yang D, Chen X, Wang J, Lou Q, Lou Y, Li L, Wang H, Chen J, Wu M, Song X, Qian Y. 2019. Dysregulated lung commensal bacteria drive interleukin-17B production to promote pulmonary fibrosis through their outer membrane vesicles. Immunity 50:692-706.e7. doi:10.1016/j.immuni.2019.02.001.

# Appendix

## Abbreviations

| | |
|---|---|
| ADP | Adenosine diphosphate |
| AMP | Adenosine monophosphate |
| ATP | Adenosine triphosphate |
| DDM | Dodecyl β-D-maltoside |
| *D. gigas* | *Desulfovibrio gigas* |
| DMN | 2,3-demethyl-1,4-naphtoquinone |
| *E. coli* | *Escherichia coli* |
| FAD | Flavin adenine dinucleotide |
| FeS | Iron sulfur cluster |
| FMN | Flavin mononucleotide |
| MK | Menaquinone |
| $MKH_2$ | Menaquinol |
| NADH | Nicotinamide adenine dinucleotide |
| NDH-I | NADH dehydrogenase 1 |
| NDH-II | NADH dehydrogenase 2 |
| NQR | $Na^+$ -translocating NADH:quinone oxidoreductase |
| PEP | Phosphoenolpyruvate |
| $P_i$ | Inorganic phosphate |
| PMF | Proton motive force |
| $PP_i$ | Pyrophosphate |
| Q | Quinone |
| QFR | Quinol:fumarate oxidoreductase |
| $QH_2$ | Quinol |
| RF | Riboflavin |
| RNF | Ferredoxin:$NAD^+$ oxidoreductase |
| SLP | Substrate-level phosphorylation |
| SMF | Sodium motive force |
| SQOR | Succinate:quinone oxidoreductase |
| SQR | Succinate:quinone reductase |
| UQ | Ubiquinone |
| $UQH_2$ | Ubiquinol |
| *V. cholerae* | *Vibrio cholerae* |
| *W. succinogenes* | *Wolinella succinogenes* |

# Authors' Contributions

Results shown in this thesis have been mainly incorporated into publications and manuscripts. Here I describe my own contributions and the contributions of the co-authors.

## Chapter 2

"Anoxic cell rupture of *Prevotella bryantii* by high-pressure homogenization protects the $Na^+$ -translocating NADH:quinone oxidoreductase from oxidative damage"

Lena Schleicher[1], Günter Fritz[1], Jana Seifert[2], Julia Steuber[1*]
[1]Institute of Microbiology, University of Hohenheim, Stuttgart, Germany
[2]Institute of Animal Science, University of Hohenheim, Stuttgart, Germany
* Correspondence: Julia Steuber, julia.steuber@uni-hohenheim.de, +49 711 459 22228

In this work, anoxic membrane isolation of *P. bryantii* was described and its impact on enzymatic activities. Reconstruction of the Emulsiflex was planned and executed with G. Fritz (fig. 1, Chapter 2). All other experimental steps and measurements were performed by me.

## Chapter 3

"A sodium-translocating module linking succinate production to formation of a membrane potential in *Prevotella bryantii"*

Lena Schleicher*†, Andrej Trautmann*‡, Dennis P. Stegmann*†, Günter Fritz*†, Jochem Gätgens¶, Michael Bott¶, Sascha Hein§, Jörg Simon§, Jana Seifert*‡, Julia Steuber*†#
* HoLMiR- Hohenheim Center for Livestock Microbiome Research, University of Hohenheim, Leonore-Blosser-Reisen-Weg 3, 70599 Stuttgart, Germany
† Institute of Biology, University of Hohenheim, Garbenstraße 30, 70599 Stuttgart, Germany
‡ Institute of Animal Science, University of Hohenheim, Emil-Wolff-Straße 8, 70599 Stuttgart, Germany
§ Microbial Energy Conversion and Biotechnology, Department of Biology, Technical University of Darmstadt, Schnittspahnstraße 10, 64287 Darmstadt, Germany
¶ Institute of Bio- and Geosciences, IBG-1: Biotechnology, Forschungszentrum Jülich, 52425 Jülich, Germany
# Correspondence: Julia Steuber, julia.steuber@uni-hohenheim.de, +49 711 459 22228

In this work, glucose fermentation and energy conservation in *P. bryantii* was analyzed with several different methods. A. Trautmann helped with the growth curve and determination of metabolite concentrations (fig. 1, Chapter 3). Furthermore, he prepared the samples for NMR

analyses (fig. 6, Chapter 3). D.P. Stegmann expressed and purified NqrF-FAD of *P. bryantii* for antibody production. These antibodies were used for immune detection of *P. bryantii* NqrF (fig. 4, Chapter 3). G. Fritz helped with SNFR enrichment by size exclusion chromatography (fig. 4, Chapter 3). J. Gätgens conducted GC-ToF experiments (fig. 1, Chapter 3) and S. Hein helped with quinone extraction and identification (fig. 2, Chapter 3). I performed all other experimental steps and measurements.

**Chapter 4**

"Central carbon metabolism, sodium-motive electron transfer, and ammonium formation by the vaginal pathogen *Prevotella bivia*"

Lena Schleicher[1,2], Sebastian Herdan[1,2], Günter Fritz[1,2], Andrej Trautmann[2,3], Jana Seifert[2,3] and Julia Steuber[1,2,*]
[1] Institute of Biology, University of Hohenheim, Garbenstraße 30, 70599 Stuttgart, Germany
[2] Institute of Animal Science, University of Hohenheim, Emil-Wolff-Straße 8, 70599 Stuttgart, Germany
[3] HoLMiR- Hohenheim Center for Livestock Microbiome Research, University of Hohenheim, Leonore-Blosser-Reisen-Weg 3, 70599 Stuttgart, Germany
* Correspondence: Julia Steuber, julia.steuber@uni-hohenheim.de, +49 711 459 22228

This work describes energy conservation in *P. bivia* and its potential contribution to bacterial vaginosis. Solubilized membrane samples of *P. bivia* were prepared with the bachelor student S. Herdan. He did enzymatic measurements and recorded the difference spectra (fig. 7 and 8, Chapter 4). A. Trautmann helped with the growth curves and determination of metabolite concentrations (fig. 1, Chapter 4). All other experimental steps and measurements were performed by me.

Date, Signature Supervisor

# Eidesstattliche Versicherung

Eidesstattliche Versicherung über die eigenständig erbrachte Leistung gemäß § 18 Absatz 3 Satz 5 der Promotionsordnung der Universität Hohenheim für die Fakultäten Agrar-, Natur- sowie Wirtschafts- und Sozialwissenschaften

1. Bei der eingereichten Dissertation zum Thema

   „Energy conservation in anaerobic *Prevotella bryantii* and *Prevotella bivia*: the role of membrane bound electron transfer complexes“

   handelt es sich um meine eigenständig erbrachte Leistung.
2. Ich habe nur die angegebenen Quellen und Hilfsmittel benutzt und mich keiner unzulässigen Hilfe Dritter bedient. Insbesondere habe ich wörtlich oder sinngemäß aus anderen Werken übernommene Inhalte als solche kenntlich gemacht.
3. Ich habe nicht die Hilfe einer kommerziellen Promotionsvermittlung oder -beratung in Anspruch genommen
4. Die Bedeutung der eidesstattlichen Versicherung und der strafrechtlichen Folgen einer unrichtigen oder unvollständigen eidesstattlichen Versicherung sind mir bekannt.

Die Richtigkeit der vorstehenden Erklärung bestätige ich. Ich versichere an Eides Statt, dass ich nach bestem Wissen die reine Wahrheit erklärt und nichts versschwiegen habe.

Ort, Datum

Unterschrift

Lena Schleicher

# Acknowledgement

I would like to express my greatest appreciation to **Prof. Dr. Julia Fritz-Steuber** for the opportunity to work in her lab on this exciting topic and for the supportive guidance throughout the last years. You have always been encouraging and helpful with upcoming questions. Thank you also for your help in reviewing and shaping the manuscripts. A special thank goes **to PD Dr. Günter Fritz**, who enlightened me with scientific discussions and gave me extremely valuable experimental support in the lab. Thanks also for helping me with the structural models for my PhD Thesis.

Many thanks to **Prof. Dr. Jana Seifert**, who gave always good input for scientific discussions and experimental design. Thanks for being part of the PhD committee. I want to thank here also **Andrej Trautmann** for his experimental help and very nice cooperation.

I appreciate the collaboration with **Dr. Simon Deusch**, **Prof. Dr. Jörg Simon, Dr. Sacha Hein, Prof. Dr. Michael Bott, Jochem Gätgens, Dr. Jens Pfannstiel, Berit Würtz** and **Johannes Günther**.

A big thank goes to all the current and former members of 190i. **Dr. Valentin Muras, Dr. Charlotte Toulouse and Dr. Björn Claußen** introduced me to the work of the lab. **Sabrina Knogl-Tritschler, Jessica Breining, Katharina Göbel, Jann-Louis Hau, Jonatan Vering, Shubhangi Agarwal, Melanie Bernt** and **Dennis Stegmann** were always supportive and had an open ear for occurring problems. Thanks for a nice atmosphere in- and outside the lab and the always constructive coffee breaks. I also thank my former bachelor student **Sebastian Herdan** for being a supportive co-worker. For the technical assistant I want to thank **Luise Weber** and **Yasmin Obermaier**.

I want to express my gratitude to my family, especially my parents and Chris, for their infinite support and encouragement since the very beginning.

Finally, I would like to thank the DFG for their financial support.

# Curriculum Vitae

## Lena Schleicher

born in Stuttgart (Germany), 1993-04-25

### Higher Education

| | |
|---|---|
| **Ph.D. Thesis** | **University of Hohenheim** |
| 2017-11 until today | Institute of Biology, Cellular Microbiology, Prof. Dr. Julia Fritz-Steuber |
| **Master of Science** | **University of Hohenheim** |
| 2015-10 until 2017-09 | Master Thesis: Institute of Biology, Cellular Microbiology, Prof. Dr. Julia Fritz-Steuber |
| **Bachelor of Science** | **University of Hohenheim** |
| 2012-10 until 2015-09 | Bachelor Thesis: Institute of Biology, General Virology, Prof. Dr. Artur Pfitzner |

### Fellowships

| | |
|---|---|
| **Herzog-Carl fellowship** | **University of Manitoba, Canada** |
| 2017 | Department of Microbiology, Prof. Dr. Pavel Dibrov |

### Publications

**"Comparative electricity generation by two locally produced corncob pyrochar electrodes and graphite using microbioal fuel cell technology".** 2021. Musa B., Tariq M., Wüst D., Schleicher L., Steuber J., Kruse A. International Journal of Renewable Energy Research. doi: 10.22541/au.162450465.59670411/v1.

**"Central carbon metabolism, sodium-motive electron transfer, and ammonium formation by the vaginal pathogen *Prevotella bivia*".** 2021. Schleicher L., Herdan S., Fritz G., Trautmann A., Seifert J., Steuber S. International Journal of Molecular Science. doi: 10.3390/ijms222111925.

**"$Na^+$-coupled respiration and reshaping of extracellular polysaccharide layer counteract monensin-induced cation permeability in *Prevotella bryantii* $B_1$4".** Trautmann A., Schleicher L., Pfirrmann, J.Boldt C., Steuber J., Seifert J. 2021. International Journal of Molecular Science. doi: 10.3390/ijms221910202.

**"A sodium-translocating module linking succinate production to formation of a membrane potential in *Prevotella bryanti*i".** 2021. Schleicher L., Trautmann A., Stegmann DP., Fritz G., Gätgens J., Bott M., Hein S., Simon J., Seifert J., Steuber J. Applied and Environmental Microbiology. doi: 10.1128/AEM.01211-21.

**"Short-chain fatty acids modulate metabolic pathways and membrane lipids in *Prevotella bryantii* $B_1$4".** 2020. Trautmann A., Schleicher L., Deusch S., Gätgens J., Steuber J., Seifert J. Proteomes. doi: 10.3390/proteomes8040028.

**"Anoxic cell rupture of *Prevotella bryantii* by high-pressure homogenization protects the $Na^+$ -translocating NADH:quinone oxidoreductase from oxidative damage".** 2019. Schleicher L., Fritz G., Seifert J., Steuber J. Archives of Microbiology. doi: 10.1007/s00203-019-01805-x.

**"Occurrence and function of the $Na^+$ -translocating NADH:quinone oxidoreductase in *Prevotella* spp."** 2019. Deusch S., Bok E., Schleicher L., Seifert J., Steuber J. Microorganisms. doi: 10.3390/microorganisms7050117.

**"*Vibrio natriegens* as host for expression of multisubunit membrane protein complexes."** 2018. Schleicher L., Muras V., Claussen B., Pfannstiel J., Blombach B., Dibrov P., Fritz G., Steuber J." 2018. Frontiers in Microbiology. doi: 10.3389/fmicb.2018.02537.

## Conferences

**VAAM Annual Meeting**

| | |
|---|---|
| 2021-03<br>Online | - |
| 2020-03<br>In Leipzig | Anoxic cell rupture of *Prevotella bryantii* by high pressure homogenization protects the $Na^+$ -translocating NADH:quinone oxidoreductase from oxidative damage |
| 2019-03<br>In Mainz | Growth and metabolism of the rumen bacterium *Prevotella bryantii* |
| 2018-04<br>In Wolfsburg | Expression and functional characterization of cation transporters in *Vibrio natriegens* |

**Perspectives in Bioenergetics conference**

| | |
|---|---|
| 2021-09<br>online | Functions of the $Na^+$ -translocating NADH:quinone oxidoreductase and quinol:fumarate oxidoreductase in energy conservation of *Prevotella bryantii* |

Date, Signature